BDNF-PRODUCING B CELLS MEDIATE PLASTICITY

IN THE RECOVERING BRAIN

AFTER STROKE

APPROVED BY SUPERVISORY COMMITTEE

Ann Stowe Ph.D., Supervising Professor

Nancy Monson, Ph.D., Chair

Mark Goldberg, M.D.

Ellen Vitetta, Ph.D.

Lenora Volk, Ph.D.

Anne Satterthwaite, Ph.D.

DEDICATION

I humbly dedicate this work to my closest friends and family. Navigating the challenges of graduate school and life would not have been possible without your motivation and support. I especially dedicate this work to my mom, whose triumphant journey in stroke recovery inspired me to pursue stroke research in hopes of one day making a difference.

BDNF-PRODUCING B CELLS MEDIATE PLASTICITY IN THE RECOVERING BRAIN AFTER STROKE

by

VANESSA TORRES

DISSERTATION

Presented to the Faculty of the Graduate School of Biomedical Sciences

The University of Texas Southwestern Medical Center at Dallas

In Partial Fulfillment of the Requirements

For the Degree of

DOCTOR OF PHILOSOPHY

The University of Texas Southwestern Medical Center at Dallas

Dallas, Texas

Degree Conferral December, 2021

ACKNOWLEDGMENTS

First, I would like to express my gratitude to my mentor, Dr. Ann Stowe. You have taught me how to finesse scientific ideas while always keeping the big picture in mind. I am extremely grateful for the scientific freedom you've given me over the years, especially as your long-distance student. I thank you for your vision for my scientific potential, constant enthusiasm, and the opportunities you've given me to participate in international science. I especially thank you for your all-encompassing mentorship outside of the lab. It has truly been a privilege and one of the best life experiences to have been your graduate student.

To Drs. Mark Goldberg and Nancy Monson, I am extremely thankful for your willingness to co-mentor me with Dr. Stowe. It has been an incredible experience to work with you and this research would not be possible without your support and constant feedback. I am extremely grateful to you both for fostering a strong sense of community and always including me in lab events.

To my dissertation committee, I thank you for your investment in my research success, especially during my mentor's transition to the University of Kentucky. Your dynamic perspectives and continuous guidance have expanded the boundaries of my scientific vision and professional development.

Lastly, to all current and former members of the Stowe (both at UT Southwestern and the University of Kentucky) and Neurorepair labs, please accept my sincerest gratitude for your

support and invaluable friendships. You have helped me persevere through the struggles and failures of science and graduate school and for that, I am incredibly grateful. You have made me a better mentor, scientist, public speaker, and writer. I will forever cherish the conversations and memories we've made in and out of the lab over the years.

ABSTRACT

BDNF-PRODUCING B CELLS MEDIATE PLASTICITY

IN THE RECOVERING BRAIN

AFTER STROKE

Vanessa Torres, Ph.D.

The University of Texas Southwestern Medical Center at Dallas, 2021

Supervising Professors: Ann Stowe, Ph.D., Mark Goldberg, M.D., and Nancy Monson, Ph.D.

Neuronal networks require significant neurotrophic support for functional plasticity after stroke, but the delivery of neurotrophins has failed thus far in clinical trials. Therefore, identifying endogenous mechanisms that could enhance neurotrophic support in the recovering brain after stroke is essential. B cells, a lymphocyte known to infiltrate the post-stroke brain, possess the ability to produce neurotrophins, including brain-derived neurotrophic factor (BDNF). Depleting B cells after stroke results in motor and cognitive deficits that are mediated by specific brain regions (e.g., hippocampus) outside the initial infarct. We propose that B cells migrate to specific brain regions after stroke and respond to local signals that enhance their neurotrophic capacities to promote neuroplasticity. To investigate whether B cells are a potential source of endogenous BDNF support after stroke, we must identify 1.) the spatial distribution of B cells within the post-stroke brain, 2.) the type of neurotrophic support B cells provide to ischemic-injured neurons and 3.) the impact that the post-stroke microenvironment exerts on the neurotrophic capacity of B cells. Using whole brain microscopy, we discovered that B cells migrate to specific remote brain regions areas outside of the initial infarct that regulate motor and cognitive function

after stroke. To understand how B cells support ischemic-injured neurons, we used *ex vivo* electrophysiology and *in vitro* models of ischemic injury to assess functional and structural neuroplasticity in the presence or absence of B cells. We discovered that B cells support synaptic transmission in the dentate gyrus region of the hippocampus after stroke and through the production of BDNF, B cells protect against the ischemic-induced loss of neurons and neuronal dendrites. After stroke, neuronal BDNF production is dependent on glutamate-induced activity of the N-methyl-D-aspartate receptor (NMDAR) downstream of the GluN2A subunit. Given that B cells also express NMDARs, we investigated whether glutamate can similarly upregulate BDNF in B cells downstream of their NMDARs. Using microscopy, flow cytometry and qPCR, we discovered that stroke and glutamate differentially regulate B cell gene and surface expression of GluN2A. Additionally, both mouse and human B cells elicit a functional response to glutamate and can induce autocrine BDNF signaling. Collectively, the data presented in this thesis are the first to demonstrate a glutamate-induced neurotrophic role for B cells in the ischemic brain. Understanding the mechanisms by which neuroinflammation supports neuroplasticity after stroke enables the development of immune-based therapeutics that harness endogenous neurotrophic support from B cells to ameliorate pathology.

TABLE OF CONTENTS

PRIOR PUBLICATIONS

1.) **Torres, V.O.,** Turchan-Cholewo, J., Malone, M.K., *et al.* "B cells elicit a neurotrophic response to extracellular glutamate following ischemic stroke in young male mice." *Submitted for review: Acta Neuropathologica* (2021)

2.) Ortega-Gutierrez, S., Farooqui, M., **Torres, V.O.,** *et al.* "Ictus-induced adaptive immune cell activation during the hyperacute phase of stroke is associated motor function decline and neuropathology." *Submitted for review: JAMA Neurology* (2021)

3.) Miles, D., Stowe, A.M., **Torres, V.O.,** *et al.* "Traumatic brain injury in pediatric patients results in a global and significant immunosuppression of the adaptive immune system." *In preparation* (2021)

4.) Ortega, S.B.*, **Torres, V.O.*,** Latchney, S.E., *et al.* "B cells migrate to remote cortical regions to support functional recovery following stroke in mice." *Proceedings of the National Academy of Sciences,* 117.9 (2020): 49-83-4993. PMID: 32051245 (* co-first authors)

5.) Poinsatte, K.*, Betz, D.*, **Torres, V.O.*,** *et al.* "Visualization and quantification of post-stroke neuroplasticity and neuroinflammation using serial two-photon tomography in the whole mouse brain." *Frontiers in neuroscience* 13 (2019): 1055. PMID: 31636534 (* co-first authors)

6.) Poinsatte, K., Smith, E.E., **Torres, V.O.,** *et al.* "T and B cell subsets differentially correlate with amyloid deposition and neurocognitive function in aMCI patients after one year of physical activity." *Exercise Immunology Review* 25 (2019): 34-49. PMID: 30785868

7.) Ortega S.B, Pandiyan, P., Windsor, J., **Torres, V.O.,** *et al.* "A pilot study identifying brain-targeting adaptive immunity in pediatric Extracorporeal Membrane Oxygenation (ECMO) patients with acquired brain injury." *Critical Care Medicine* 47.3 (2019): e206. PMID: 30640221

8.) Cardona, S.M., Kim, S.V., Church, K.A., **Torres, V.O.,** *et al.* "Role of the fractalkine receptor in CNS autoimmune inflammation: New approach utilizing a mouse model expressing the human CX3CR1 I249/M280 variant." *Frontiers in cellular neuroscience,* 12 (2018): 365. PMID: 30386211

9.) Poinsatte, K., Selvaraj, U.M., **Torres, V.O.,** *et al.* "Heterogeneity of B cell function in stroke-related risk, prevention, injury, and repair." *Neurotherapeutics* 13.4 (2016): 729-747. PMID: 27492770

10.) Cardona, S.M., Mendiola, A.S., Yang, Y-C., Adkins, S., **Torres, V.O.,** *et al.* "Disruption of fractalkine signaling leads to microglial activation and neuronal damage in the diabetic retina." *ASN Neuro* 7.5 (2015): 1759091415608204. PMID: 26514658

LIST OF FIGURES

LIST OF TABLES

LIST OF DEFINITIONS

7-AAD – 7- aminoactinomycin D

aCSF – artificial cerebral spinal fluid

AAALAC – Association for Assessment and Accreditation of Laboratory Animal Care

ANOVA – analysis of variance

Ara-C – cytarabine

ASC – antibody-secreting cell

B10 – interleukin-10-producing B cell

BBB – blood brain barrier

BCA – bicinchoninic acid

BCR – B cell receptor

BD – Becton and Dickinson

BDNF – brain-derived neurotrophic factor

BM – bone marrow

BP – base pair

Breg – regulatory B cell

CD – cluster of differentiation

cLN – cervical lymph node

CMV – cytomegalovirus

CNS – central nervous system

CPG – cytosine phosphate guanosine

Cre – P1 bacteriophage cyclization recombination recombinase gene

CREB – cyclic adenosine monophosphate-response element binding protein

CREM – cyclic adenosine monophosphate-response element modulator

CSF – cerebral spinal fluid

CXCL – chemokine ligand

CXCR – chemokine receptor

D-APV – D-(1)-2-amino-5-phosphonopentanoic acid

DAMP – danger-associated molecular pattern

DCX - doublecortin

ddCT – delta-delta cycle threshold

DG – dentate gyrus

DMSO – dimethyl sulfoxide

EAE – experimental autoimmune encephalomyelitis

EGTA – ethylene glycol-bis (β-aminoethyl ether)-N,N,N',N'-tetra acetic acid

ELISA – enzyme-linked immunosorbent assay

EtOH – ethanol

FACS – fluorescence-activated cell sorting

FCR – fragment crystallizable receptor

FDR – false discovery rate

GCL – granule cell layer

GluN2A – N-methyl-D-aspartate receptor subunit 2 A

GluN2B – N-methyl-D-aspartate receptor subunit 2 B

HMGB1 – high motility group box 1

HRP – horseradish peroxidase

IFN – interferon

Ig – immunolglobulin

IL – interleukin

i.p. – intraperitoneal

i.v. – intravenous

kDa – kilodalton

KO – knock out

L-glu – L-glutamate

LPS – lipopolysaccharide

LTP – long term potentiation

MAP2 – microtubule-associate protein 2

MBP – myelin basic protein

MCA – middle cerebral artery

MHC – major histocompatibility complex

MMP – matrix metalloproteinases

MRI – magnetic resonance imaging

mRNA – messenger ribonucleic acid

MTT – 3-(4,5-dimethlythiazol-2-yl)-2,5-diphenyl-2H-trtrazolium bromide

MyD88 – myeloid differentiation factor 88

NE – N-methyl-D-aspartate excitotoxicity

NF-κB – nuclear factor kappa B

NGF – nerve growth factor

NIH – National Institutes of Health

NMDAR – N-methyl-D-aspartate receptor

NO – novel object

NT – neurotrophin

OGD – oxygen-glucose deprivation

$p75^{NTR}$ – neurotrophin receptor p75

PBMC – peripheral blood mononuclear cells

PBS – phosphate buffered saline

PFA – paraformaldehyde

qPCR – quantitative polymerase chain reaction

R848 – resiquimod 848

ROS – reactive oxygen species

rpm – rotations per minute

s.c. – subcutaneous

TCN 201- 3-chloro-4-fluoro-*N*-[4-[[2

(phenylcarbonyl)hydrazino]carbonyl]benzyl]benzenesulphonamide

TCR – T cell receptor

Th – T helper

TLR – toll-like receptor

tMCAo – transient middle cerebral artery occlusion

TNF – tumor necrosis factor

Treg – regulatory T cell

TrkB – tropomyosin receptor kinase B

SDS-PAGE – sodium dodecyl (lauryl) sulfate-polyacrylamide gel electrophoresis

SGZ – subgranular zone

STPT – serial two-photon tomography

SVZ – subventricular zone

Val66Met – valine-66-methionine brain-derived neurotrophic factor polymorphism

WT – wild type

CHAPTER ONE
Review of the literature and preliminary data

1.1 Introduction

Stroke is responsible for causing widespread disability and is a leading cause of adult morbidity in the United States [1, 2]. Ischemic stroke accounts for ~87% of all strokes and the disruption of blood to the brain results in ischemic injury secondary to the release of oxygen free radicals [3] and glutamate-induced neuronal excitotoxicity [4]. Additionally, thrombolysis and mechanical thrombectomy, currently the two therapies available for ischemic stroke, are only effective if utilized within hours of stroke onset [5]. Functional recovery after stroke, however, is initially rapid and while it slows considerably by 1 to 3 months [6-8], structural plasticity supporting long-term stroke recovery lasts for years after the ischemic insult [9, 10]. Post-stroke plasticity requires significant support from neurotrophins (e.g., brain-derived neurotrophic factor; BDNF), particularly in brain regions experiencing glutamate-induced excitotoxicity. However, sex and age are key factors in stroke risk that impact recovery potentially through changes in neurotrophin production. For example, circulating levels of BDNF decline with age [11] and are significantly lower in women [12]. In fact, post-stroke depression has been linked to low levels of BDNF [13] with increased depression and an overall lower quality of life (i.e., comorbidities [14, 15], cognitive decline [12], disability and mortality [16]) in post-menopausal women [16-18]. Additionally, BDNF polymorphisms, such as Val66Met (expressed in 30-50% of the population [19, 20]), reduce levels of BDNF and limit post-stroke plasticity [21-24], thus hindering functional recovery. Therefore, understanding the mechanisms that support long-term plasticity, such as enhancing endogenous neurotrophic support, could allow for the development

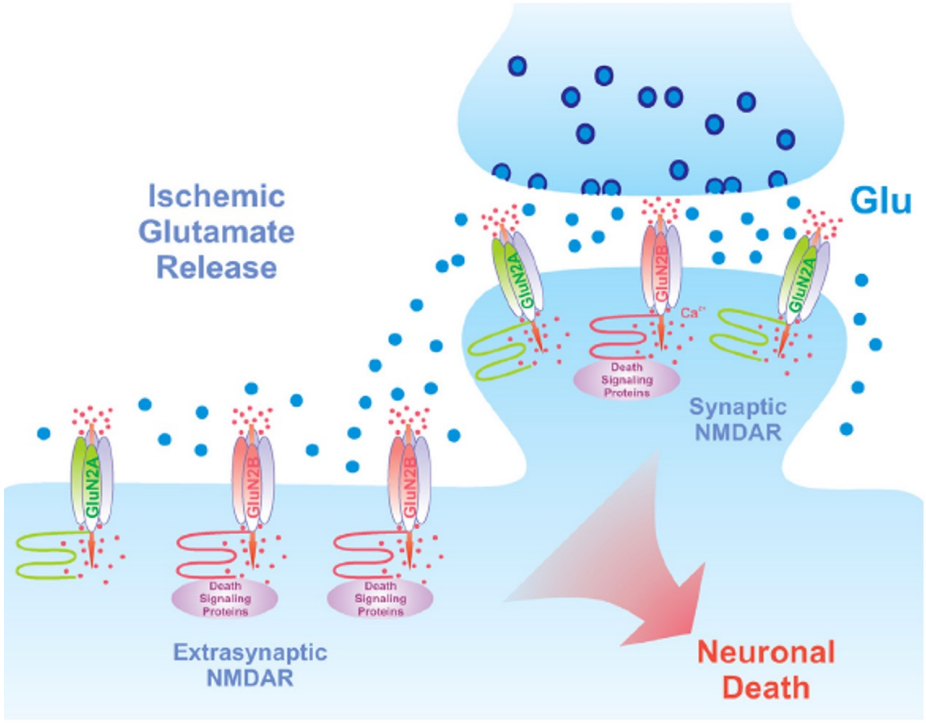

Lai et al., Progress in Neurobiology (2014)

Fig. 1 GluN2B-expressing NMDARs drive glutamate excitotoxicity in neurons after stroke.

of novel neurotherapeutics that augment post-stroke recovery and rehabilitation interventions months to years after onset.

1.2 Glutamate-induced mechanisms of excitotoxicity and plasticity after stroke

1.2A NMDAR-mediated excitotoxicity after stroke

Neuroplasticity occurs under homeostatic conditions throughout life in cortical, subcortical, and cerebellar brain regions (e.g., olfactory areas [25, 26], motor cortex [27, 28], hippocampus [25, 26, 29], and cerebellum [30, 31]). These areas are responsible for brain development, neurogenesis, learning, and memory formation. The N-methyl-D-aspartate receptor (NMDAR) is a glutamate-activated cation channel with high calcium (Ca^{2+}) permeability that

induces robust synaptic plasticity under physiological conditions [32]. The dysregulation of glutamate after stroke primarily stems from excessive neuronal activity and action potentials [33-35] that ensue the loss of oxygen and glucose. The release of glutamate can spill-over and increase extrasynaptic glutamate from neighboring glia [33, 34, 36] and/or neurons [34, 36-39]. As a result, mitochondria fail to regulate glutamate-induced overload of intracellular Ca^{2+} levels and in turn, produce reactive oxygen species (ROS; [40, 41]) and ultimately induce neuronal death [42]. Furthermore, neuronal networks interconnected with the area of infarct are negatively impacted by loss of connectivity [43]. Thus, due to their high Ca^{2+} permeability, extrasynaptic NMDARs are the primary mediators of stroke-induced excitotoxic injury (**Fig. 1**). Interestingly, NMDAR antagonists fail to confer neuroprotection after stroke in clinical trials [44-46], highlighting an additional beneficial role of NMDARs in promoting post-stroke neuronal survival and plasticity.

1.2B NMDAR-mediated plasticity after stroke

Neuronal NMDARs are composed of different subunits and expressed in different brain regions [47-51] and subcellular locations [52-56]. The central dogma suggests that extrasynaptic NMDARs (primarily comprised of GluN2B-containing NMDARs; Fig. 1) reduce pro-survival signaling and drive excitotoxicity following stroke and other neurodegenerative diseases [4]. On the other hand, the activity of synaptic and extrasynaptic GluN2A-containing NMDARs is thought to promote neuronal survival by activating various survival-signaling proteins, including extracellular signal-regulated kinase (ERK) which actives the transcription factor CREB to upregulate BDNF [4], creating a positive feed-forward loop between BDNF production and neuronal stability (**Fig. 2**; [57, 58]). BDNF and its receptor, tropomyosin kinase receptor B

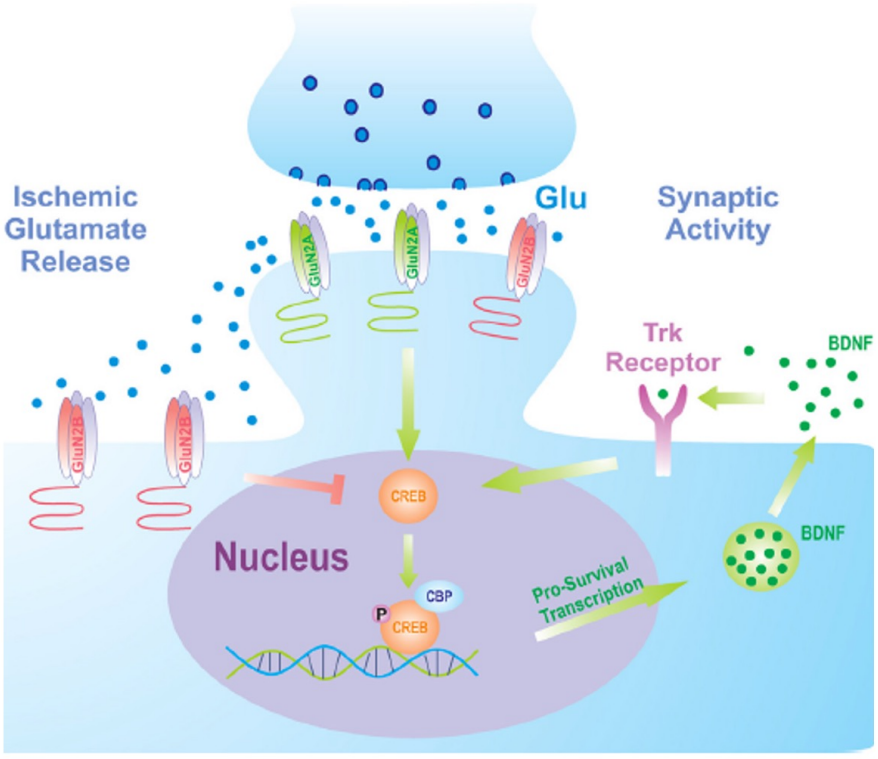

Lai et al., Progress in Neurobiology (2014)

Fig. 2 Glutamate induces BDNF production in neurons downstream of GluN2A-expressing NMDARs.

(TrkB), are widely expressed in the adult brain and are required for basal synaptic transmission and memory formation [59, 60]. In the ischemic-injured brain, BDNF reduces post-stroke neuronal cell death [57, 58, 61, 62] and excitotoxicity [4], enhances behavioral recovery [57, 58, 63], and promotes neurogenesis [64, 65]. However, the exogenous administration of BDNF has failed in clinical trials due to the short half-life of BDNF and limited brain permeability [66-68]. Therefore, understanding mechanisms that could enhance endogenous BDNF production within the post-stroke brain, potentially from GluN2A-containing NMDARs, is essential.

1.3 Inflammatory responses ensuing an ischemic stroke

The post-stroke inflammatory cascade is thought to be a potent, multiphasic process that begins intravascularly immediately following arterial occlusion [69]. Hypoxic injury and the production of ROS triggers the coagulation cascade and subsequently activates complement [70], platelets [71] and endothelial cells [72]. The ensuing activation of resident CNS immune cells and recruitment of peripheral leukocytes into the post-stroke brain are discussed below.

1.3A CNS inflammatory response

Glial cells, particularly microglia and astrocytes, become activated within hours of stroke onset and upregulate cytokines and chemokines that augment the on-going inflammation by recruiting peripheral leukocytes into the central nervous system (CNS) [69]. Microglia, the resident phagocytes of the CNS, make up 10-15% of all glia and constantly survey the CNS through their highly ramified processes [73]. Following ischemic injury, activated microglia exhibit an amoeboid-like morphology and quickly mobilize toward the site of ischemic injury to begin phagocytic removal of dead neurons [74, 75]. Depending on their phenotypic response to the local microenvironment (i.e., ROS [76], cytokines and danger-associated molecular patterns DAMPs [77, 78]), activated microglia can both facilitate blood-brain barrier (BBB) breakdown and mediate neurotoxicity (via release of matrix metalloproteinases (MMPs) [79], cytokines and chemokines [80]), or promote tissue repair and neurogenesis (via synaptic pruning, phagocytosis and release of neurotrophic factors [81]) after stroke [82]. Similarly, the role of astrocytes (which constitute 19-40% of all glia [73]) in post-stroke inflammation is also a double-edged sword. One of the primary functions of astrocytes under homeostatic conditions is to scavenge excess glutamate from the extracellular space and protect neurons from glutamate toxicity [83].

However, the efficiency in glutamate uptake by astrocytes is reduced after stroke, likely as a result of extensive ischemic injury [83]. DAMPs (such as high-mobility group box 1 (HMGB1), heat shock protein (HSP), beta-amyloid and others [69]) released by injured and/or dead neurons rapidly activate astrocytes. Reactive astrocytes, in turn, upregulate glial fibrillary acidic protein (GFAP), proliferate and secrete various pro-inflammatory factors including ROS, cytokines, chemokines and MMPs that exacerbate secondary brain injury by disrupting the BBB further and recruiting peripheral leukocytes [81, 84]. Conversely, astrocytes, like microglia, can also produce neurotrophins that protect stroke-injured neurons and promote recovery [81]. The inflammatory mechanisms mediated by glia after stroke are quite variable and depending on the timepoint after stroke, could be the target for therapeutic interventions.

1.3B Peripheral inflammatory response

Following primary ischemic injury, the integrity of the BBB becomes compromised and the endothelial cells lining the BBB, in addition to microglia and astrocytes, also become activated and express chemokines and adhesion molecules that recruit peripheral immune cells into the post-stroke CNS [85, 86]. Neutrophils and macrophages, both innate immune cells, are the most abundant peripheral leukocytes to infiltrate the ischemic brain within 72 hours (**Fig. 3A**; [85]) and induce tissue damage, cell death and behavioral disfunction [87]. The infiltration of other innate (i.e., natural killer cells and dendritic cells) and adaptive immune cells within the acute window of stroke recovery (i.e., 7 days) also peaks around 72 hours, albeit at cell numbers that are magnitudes lower than neutrophils and macrophages (**Fig. 3B**; [85]). The role of lymphocytes in post-stroke recovery is dynamic and dependent on the lymphocyte subset being evaluated. For example, in the acute phase after stroke, T cell subsets (i.e., cluster of

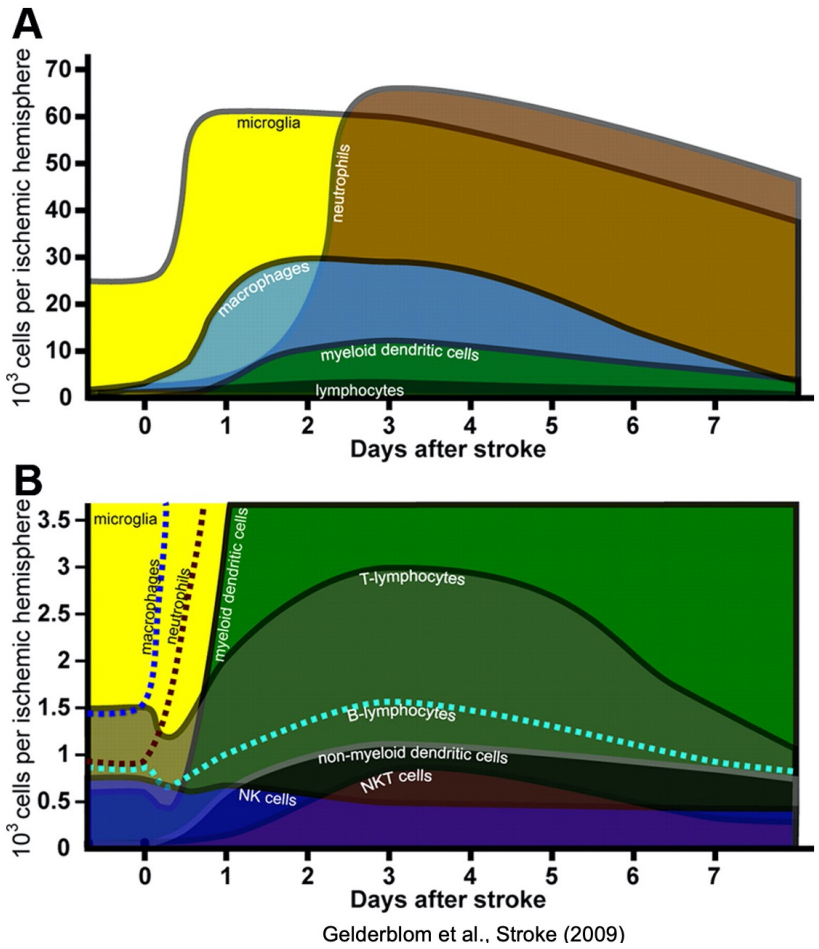

Fig. 3 The number of immune cells found in the post-stroke ischemic brain hemisphere. **(A)** Temporal dynamics of post-stroke inflammation and **(B)** a magnification of the lower part of (A).

differentiation (CD) 4^+ and CD8 T cells) secrete a diversity of pro-inflammatory cytokines (i.e., interleukin (IL)-17, IL-21, IL-23 and interferon gamma (IFNγ)) and/or cytotoxic granules (i.e., perforin and granzyme) that further recruit pro-inflammatory immune cells into the CNS and induce neuronal apoptosis [88]. Recent studies found that $CD8^+$ T cell infiltration into the post-stroke brain persists long after stroke and through their pro-inflammatory and cytotoxic capacities, exacerbate pathology [85, 88-90]. In contrast, $CD4^+$ T cells exert both beneficial and detrimental effects in the chronic phase of stroke. Some studies report that stroke pathology is

inversely correlated with $CD4^+$ T cell infiltration [91] whereas others report a role for $CD4^+$ T cells in supporting B cell-induced cognitive impairment after stroke [92]. In addition to their pro-inflammatory functions, $CD4^+$ T cell also engage anti-inflammatory and immunosuppressive mechanisms after stroke [69, 93, 94]. Regulatory T cells (Tregs) express the transcription factor forkhead box protein 3 (FOX-P3) and exert their anti-inflammatory effects through the secretion of IL-10 and transforming growth factor beta (TGFβ) [95]. As a result, Tregs reduce the activation and cytokine production of peripheral infiltrating immune cells and CNS-resident microglia, thereby ameliorating pathology and promoting functional recovery after stroke [95].

1.4 The role of B cells in non-stroke neurological diseases and stroke recovery

1.4A B cells are multifunctional immune cells

B cells, lymphocytes of the adaptive immune system, develop in the bone marrow and undergo central tolerance (i.e., strong-binding 'self'-antigen-reactive B cells are altered or eliminated to prevent the development of autoimmune diseases) before leaving the bone marrow . Immature, naïve B cells then migrate to secondary lymphoid organs (such as the spleen) where they undergo additional peripheral tolerance (i.e., weak-binding self-reactive B cells are altered, eliminated or made anergic) and mature through their encounter with non-self-antigens, become activated and further differentiate to carry out specific functions [96]. The primary function of B cells is to mount a tailored immune response against pathogens by producing antigen-specific antibodies that effectively and efficiently eliminate the invading pathogen [86]. In addition to producing antibodies, B cells can also become activated to 1.) act as antigen-presenting cells, 2.) clonally expand and/or become memory B cells in response to

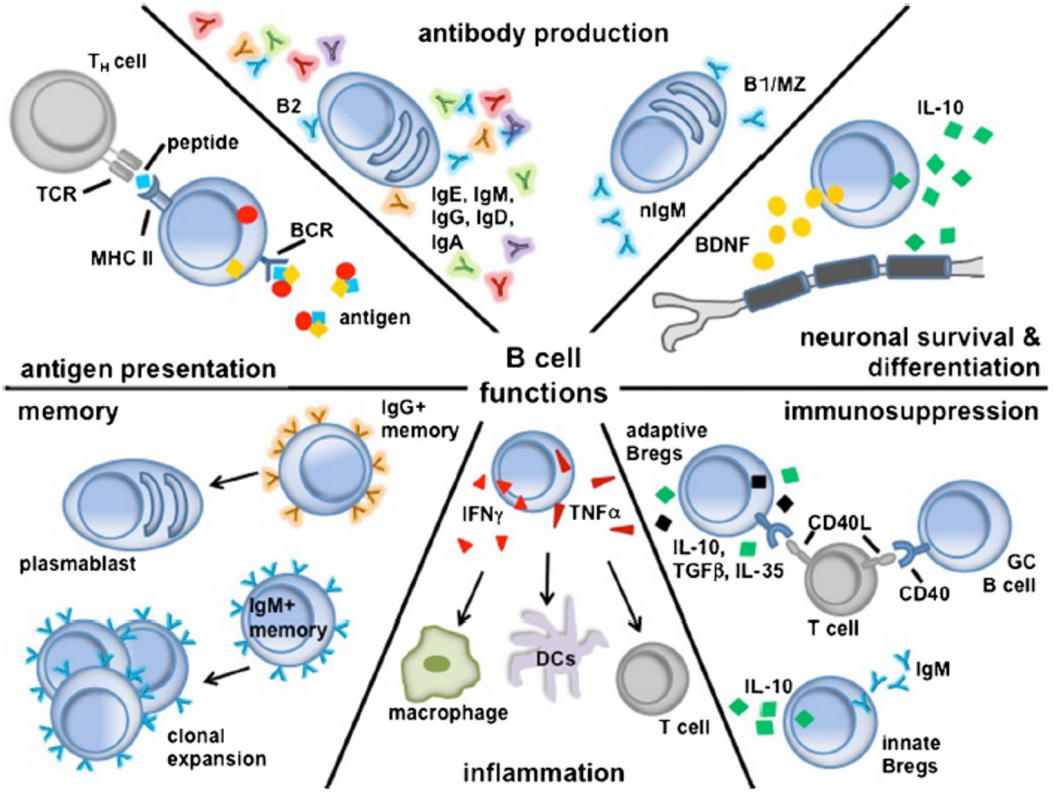

Fig. 4 A summary of B cell functions. TH = T helper; TCR = T cell receptor; MHC = major histocompatibility complex; BCR = B cell receptor; nIgM = natural IgM; MZ = marginal zone; IL = interleukin; BDNF = brain-derived neurotrophic factor; IFN = interferon; TNF = tumor necrosis factor; DC = dendritic cell; Breg = regulatory B cell; TGF = transforming growth factor; GC = germinal center

antigens, 3.) carry out immunoglobulin (IgA, IgG, IgM, IgD, IgE) effector functions and produce cytokines that mediate inflammation, 4.) suppress inflammation via anti-inflammatory cytokines or 5.) produce neurotrophins (**Fig. 4**, [86]). Some activated B cell subsets will remain in the secondary lymphoid organs while other B subsets will egress to other organs, including those in the CNS in either a B cell-specific (e.g., CXCL13 chemokine signaling to the B cell-expressed CXCR4/5 chemokine receptors [97])) or non-B cell-specific (e.g., sphingosine-1-phosphate (S1P) signaling to S1P receptors found on all immune cells [98, 99]) manner. B cells also play an important role in the developing brain by supporting the development and proliferation of

oligodendrocyte precursor cells, and ultimately, mature, myelinating oligodendrocytes [100].

1.4B The role of B cells in non-stroke neurological diseases

In the healthy, developing brain, B cells play a beneficial role in supporting oligodendrogenesis. However, in neuroinflammatory (e.g., multiple sclerosis (MS) and neuromyelitis optica (NMO)), neurodegenerative (e.g., Alzheimer's (AD) and Parkinson's Disease (PD)), and neuropsychiatric (e.g., mood and anxiety disorders) diseases of the CNS, B cells can either exacerbate or mediate pathology depending on the disease state. This subsection will briefly introduce the role of B cells in the non-stroke CNS diseases, however, the role of B cells and the potential for therapeutic targeting will be discussed greater detail in chapter 6.3.

Auto-reactive antibody-secreting B cells play a significant role in exacerbating the pathologies that drive the disease progression of both MS and NMO [101, 102]. Additionally, several dysregulated B cell functions (e.g., increased antigen presentation [103] and proinflammatory cytokine production [104-106] and impaired immunosuppressive activity [107, 108]) apart from autoantibody production are known to exacerbate MS [102] and NMO [109]. The pathological role of B cells in MS and NMO is further demonstrated by ability of B cell depletion to improve MS [110, 111] and NMO [112] pathologies. On the other hand, animal models of AD suggest that antibody-secreting B cells also exacerbate AD progression by migrating into specific CNS regions, secreting antibodies that associate with increased amyloid burden which subsequently induces behavioral and cognitive deficits [113]. The role of B cells in PD is less understood, however, a significant decrease in B cell-related genes (e.g., CD19) *is* associated with increased disease severity and duration [114] which could indicate a potentially beneficial role of B cells in regulating PD pathology. Conversely, the role of the brain-infiltrating

B cells in mood and anxiety disorders (e.g., bipolar disorder (BD)) is not nearly as investigated when compared to neuroinflammatory or neurodegenerative diseases. Nonetheless, BD patients who are in remission[115], or patients undergoing anti-depressant treatment [116] exhibit increased levels of circulating IL-10 which is associated with increased circulating B cells and/or regulatory B cells [115, 117]. These studies, though still in their infancy, indicate a potentially protective effect of peripheral B cells in the regulation of mood disorders.

Collectively, the role of B cells in the pathology of CNS diseases varies depending on the disease state. However, the contrasting roles of B cells in CNS disease may result from subset-specific responses, much like those observed in stroke recovery, which will be discussed in the next subsection.

1.4C The dichotomous role of B cells in acute and long-term stroke recovery

The adaptive immune system is pivotal to stroke recovery, as it can both mediate and ameliorate neuropathology depending on the lymphocyte population, location, and timing of activation [118, 119]. The protective and detrimental mechanisms mediated by B cells in stroke recovery are discussed in detail below.

1.4Ci IL-10-producing B cells ameliorate acute post-stroke pathology

In the last decade, the protective role of IL-10-producing B cells has been well characterized in the acute window after stroke. When compared to wild-type (WT) mice, B cell-deficient mice exhibit increased inflammation (both of activated peripheral and CNS-resident immune cells) in the ipsilesional hemisphere, larger infarct volumes and neurological deficits and increased mortality [120, 121]. These deficits are completely prevented by 48 hours after stroke in B cell-deficient mice that interperitoneally received IL-10-producing B cells [120, 121].

A direct transfer of B cells into the striatum of post-stroke B cell-deficient mice reduces the infarct to a size that is comparable to B cell-deficient mice that received B cells interperitoneally [122]. Additionally, IL-10-producing B cells increase regulatory T cells in B cell-deficient mice which in turn, help reduce the stroke-induced inflammatory cascade in the periphery [121]. Furthermore, IL-10-producing B cells not only reduce inflammation and infarct size in the ipsilesional hemisphere of B cell-sufficient mice 96 hours after stroke, but they also reduce inflammation in the periphery [123]. These studies collectively demonstrate the acute anti-inflammatory and neuroprotective capacities of IL-10-producing B cells and underscore their therapeutic potential after stroke.

Interestingly, a different study argues that B cells do not ameliorate or mediate the acute (i.e., 24-72 hours) neuroinflammatory response (i.e., peripheral immune cell infiltration, local glial activation or neuronal survival) in the post-stroke brain and as a result, do not impact lesion size, motor coordination, or muscle strength after stroke [124]. However, subset-specific roles of B cells in stroke recovery were not investigated and it may be possible that the acute neuroprotective phenotype of IL-10-producing B cells was lost as IL-10-producing B cells only constitute ~28% of stimulated splenic B cells [121] . On the other hand, it may be possible that the role B cells play in stroke recovery is unrelated to inflammation and the impact of that role might manifest itself in remote brain regions beyond the acute window of stroke recovery.

1.4Cii Antibody secreting cells mediate post-stroke cognitive decline

Nearly one-third of all stroke patients suffer cognitive decline or dementia [125], however, the involvement of immune system in cognitive function after stroke is not clearly understood as most investigations focus on acute inflammation. Interestingly, oligoclonal bands

in the cerebral spinal fluid (CSF) of stroke patients months after the initial stroke onset [126] are indicative of active, long-term B cell responses within the CNS. While IL-10-producing B cells reduce inflammation and neurological damage up to 96 hours after stroke, antibody-secreting B cells (ASCs) contribute to long-term post-stroke cognitive deficits and dementia in mice [127]. Activated B cell infiltration into the lesion persists for months after stroke, allowing the formation of ectopic lymphoid structures [92] that may give rise to local isotype-switched ASCs that have been identified in the infarct and peri-infarct areas [127]. Among these ASCs are IgA^+ plasma cells that, unlike IgA^+ plasma cells found in the intestinal mucosa [128], develop in a T cell-independent manner and produce natural IgA antibodies [129]. Nonetheless, the delayed infiltration of B cells and formation of ectopic lymphoid structures (containing both B and T cells) in the post-stroke brain *are* T cell-dependent [92]. Interestingly, the absence of B cells in the CNS (induced directly by pharmacological depletion or genetic deficiency [127], or indirectly, by the depletion of $CD4^+$ T cells [92]) prevents the development of delayed deficits in synaptic plasticity and cognitive function observed in B cell-sufficient WT mice [92, 127]. These mouse studies, along with the presence of B cells and antibodies in post-mortem brain tissue of stroke patients with dementia [127], suggest that ASCs contribute to cognitive impairment after stroke.

Stroke patients exhibit strong T cell and antigen-presenting cell immunoreactivity to neuronal (i.e., microtubule-associated protein 2 (MAP2) and the GluN2A-NMDAR subunit) and myelin (i.e., myelin basic protein (MBP)) antigens in their tonsils and cervical lymph nodes. MAP2 and GluN2A immunoreactivity in stroke patients correlates with smaller infarct size by day 7 and improved functional recovery by 3 months [130]. Conversely, MBP reactivity

correlates with larger infarcts and a decline in functional recovery [130, 131]. In mice, MAP2- and myelin-autoreactive $CD4^+$ and $CD8^+$ T cells (i.e., T cells with increased proliferation and CD25 expression in response to neuronal antigenic peptides) are associated with reduced infarct volumes whereas autoreactivity to GluN2A is associate with larger infarction [132]. These studies suggest that autoreactive T cell responses could significantly impact post-stroke functional recovery but are dependent on species. Notably, neuronal peptide antigens induce what may likely be autoreactive by-stander proliferation of $CD19^+$ B cells from lymph node, but not splenic tissue [132]. Although the autoreactivity of B cells (i.e., the secretion of autoantibodies) to the GluN1-NMDAR subunit have been implicated in neurological and psychiatric deficits that arise as complications of NMDA encephalitis [133, 134], it is unclear whether GluN2A autoantibodies would improve or exacerbate stroke recovery. However, not all myelin and neuronal autoantibodies are pathological [135, 136]. Therefore, it is important to identify the antigenic target(s) and function(s) of ASCs in the post-stroke brain.

1.5 A potential, alternative mechanism by which B cells could exert neuroprotection in stroke recovery

While dichotomous role of B cells in stroke recovery stems from their regulatory- and antibody-secreting capacities (**Fig. 4**), the neurotrophic capacity of B cells in stroke remains unknown. This section of chapter 1 will discuss how glutamate, a neurotransmitter that is significantly dysregulated in the post-stroke brain, may potentiate the neurotrophic capacity of B cells.

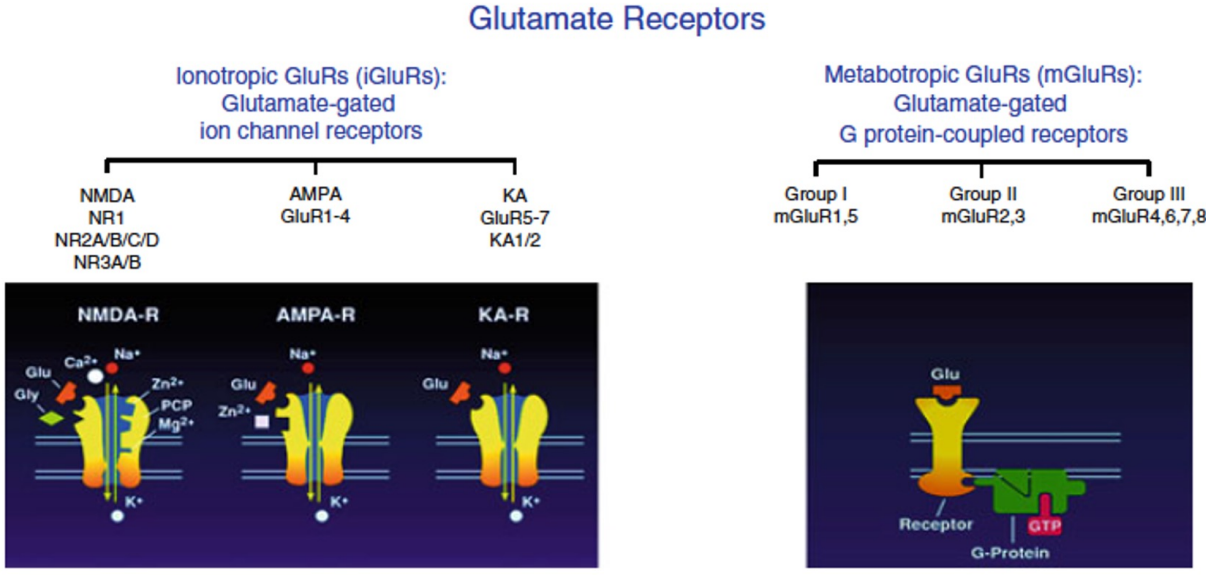

Ganor and Levite, Nerve-Driven Immunity (2012)

Fig. 5 Glutamate receptors expressed in neurons. There are two major classes of glutamate receptors: ionotropic (ion-channels gated by glutamate) and metabotropic (G-coupled proteins) glutamate receptors. Each of class of glutamate receptor is further subdivided in subtypes or groups based on the subunits they express or structure similarity.

1.5A Overview of glutamate receptors

Glutamate receptors are either ionotropic or metabotropic in nature (**Fig. 5**). Ionotropic receptors are sub-categorized into NMDA, alpha-amino-3-hydroxy-5-methylisoxazole-4-propionic acid (AMPA) or 2-carboxy-3-carboxymethyl-4-isopropenylpyrrolidine (Kainate; KA) receptors based on the activating agonist and shared structural and functional properties. NMDARs, as described in chapter 1.2A, are a glutamate-gated cation channel that are highly expressed throughout the CNS and require a two-step process to become activated. First, NMDARs require voltage-dependent activation to depolarize the membrane and remove the Mg^{2+} blockade, thus allowing cation permeability (i.e., Ca^{2+} and Na^{+}). Second, glycine and glutamate, the two natural NMDAR agonists, must bind their respective binding sites on the GluN1 and GluN2 subunits to co-activate the receptor [32]. AMPARs, the most common

glutamate receptor in the CNS, are also cation channels that become activated when 2 of 4 glutamate binding sites are occupied and allow the influx of Ca^{2+} and Na^{+} and K^{+} [137]. Lastly KARs, though not as well characterized as NMDARs and AMPARs, also form a cation channel upon binding glutamate with permeability to Na^{+} and K^{+} ions [138].

Unlike ionotropic glutamate receptors, metabotropic glutamate receptors are glutamate-gated G-coupled protein receptors that require 2 glutamate molecules to become activated and initiate signaling cascades that subsequently impact pre- and post-synaptic transmission [139]. They are sub-categorized into Group I, II or III based on similarities in sequence, intracellular signaling cascades and overall pharmacology. Group I metabotropic receptors (mGluR1 and 5) are predominantly post-synaptic G_q receptors that stimulate phospholipase C [140]. On the other hand, group II (mGluR2 and 3) and group III (mGluR4, 6, 7 and 8) are coupled with G_i/G_0 and primarily function on presynaptic neurons to suppress excitability by inhibiting adenylate cyclase [141].

Ionotropic and metabotropic glutamate receptors are essential for regulating various processes involved in neuronal synaptic transmission and plasticity. One process of particular importance is the upregulation of neurotrophins, such as BDNF, downstream of NMDAR, AMPARs [142], KA, and metabotropic receptors [143, 144]. Interestingly, ionotropic and metabotropic glutamate receptors are also expressed in immune cells and while the production of neurotrophins downstream of these receptors has never been evaluated, glutamate receptors significantly impact immune function as described in the next section.

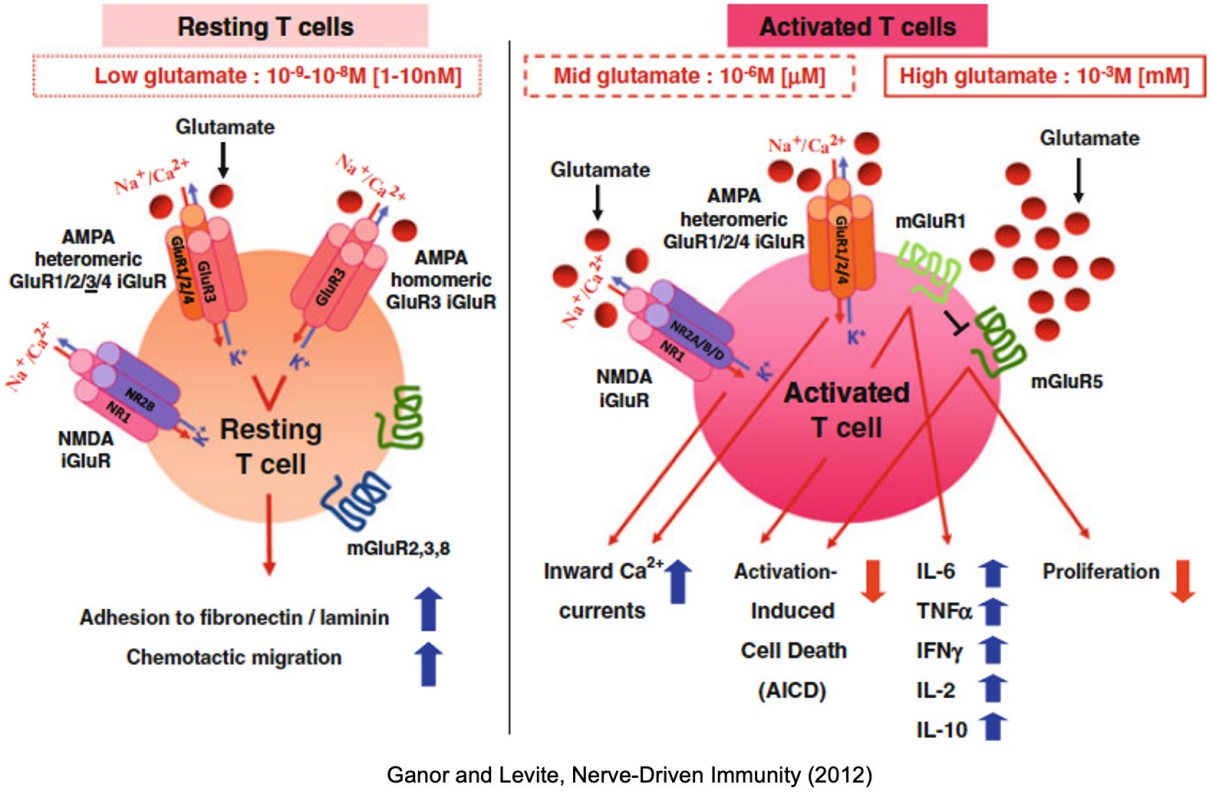

Ganor and Levite, Nerve-Driven Immunity (2012)

Fig. 6 The direct effects of varying glutamate concentrations on T cell function.

1.5B Glutamate receptors expressed on lymphocytes

As reviewed elsewhere [141, 145], the expression and function of glutamate receptors on immune cells has primarily been assessed in general leukocytes, lymphocytes or isolated T cells. These studies suggest that glutamate can differentially affect immune cell function based on glutamate concentration and the receptor that becomes engaged (**Fig. 6**). At low-to-mid glutamate (or glutamate analogue) concentrations (i.e., nM to μM), ionotropic glutamate receptors increase intracellular Ca^{2+} to support the activation and proliferation of lymphocytes [146], whereas metabotropic receptors regulate cytokine secretion (e.g., suppression of IL-6 and enhancement of tumor necrosis factor alpha (TNFα), IFNγ, IL-2 and IL-10 [147]) [145, 148]. Conversely, these studies show that through metabotropic receptors [141, 146, 149], high

glutamate or glutamate analogue concentrations (i.e., mM) decrease intracellular Ca^{2+}, inhibit lymphocyte proliferation, differentially regulate cytokine production, increase ROS production and/or induce necrotic cell death [148]. Although the effect of ionotropic and metabotropic glutamate receptors exert on general leukocyte and T cell function are well-defined, the role of glutamate receptors in B cell function is less understood, particularly in the context of stroke.

There are only two studies that demonstrate the ability for glutamate receptors to promote B cell proliferation and immunoglobulin production (via ionotropic receptors [150]) or induce glutamate concentration-dependent apoptosis (via metabotropic glutamate receptors) in B cells [151]. However, neither study investigated the contribution of NMDARs (or NMDAR subunits) to the glutamate receptor-induced response in B cells. Immune cell NMDARs (identified by GluN1 or general GluN2 expression), much like other non-NMDARs and metabotropic receptors, regulate Ca^{2+} entry and subsequent immune cell activation, proliferation, cytokine production and cell survival. While some studies have investigated the assembly of GluN2 subunits in leukocytes [152] or T cells [153], GluN2 subunits have not yet been specifically investigated in B cells. Given that neuronal GluN2B mediates post-stroke excitotoxicity whereas GluN2A, in contrast, promotes neuronal stability, it is important that we understand the function and assembly of GluN2 subunits in B cells after stroke as these findings could elucidate a mechanism by which B cells exert long-term neuroprotection.

1.5C Neurotrophins produced by lymphocytes

Neurotrophins such as nerve growth factor (NGF) and BDNF are produced by various cells in the post-stroke brain (including neurons, glia and CNS-resident immune cells [154]) and can reduce post-stroke neuronal cell death [57, 58, 61, 62] and excitotoxicity [4], enhance

behavioral recovery [57, 58, 63] and promote neurogenesis [64, 65]. Lymphocytes, including those that infiltrate the post-stroke CNS, have the capacity to produce neurotrophins like NGF and BDNF. While NGF plays a critical role in the development and maintenance of neurons and activity-dependent neuronal function [154, 155], NGF also promotes B cell pro-survival signaling [156], proliferation [157, 158], antigen-specific responses [159] and immunoglobulin production (**Table 1**; [158, 160, 161]). On the other hand, BDNF, which is also integral for neuronal plasticity of the uninjured and post-stroke brain, is required for proper B cell development beyond the Pre-BII stage in the bone marrow (**Table 1**; [162]). The absence of BDNF subsequently reduces B cell, but not T cell numbers in the spleen and blood. BDNF receptors (i.e., TrkB and p75 neurotrophin receptor (NTR)) expressed in bone marrow and splenic B cells increase intracellular Ca^{2+} in response to BDNF. Furthermore, BDNF signaling through its' receptor can protect B cells from stress-induced apoptosis [163], with Pre-B, mature, and antibody-secreting B cells capable of secreting functional BDNF that can induce neurite outgrowth in a non-autonomous manner [163]. Although lymphocytes have the capacity to produce BDNF, B cells are the primary lymphocytic source of BDNF [164, 165]. Therefore, it is a reasonable notion that local upregulation of BDNF within the post-stroke microenvironment could promote the survival of CNS-infiltrating B cells and, as a result, initiate autocrine BDNF signaling that could augment endogenous neurotrophic support in the post-stroke brain.

1.6 Preliminary data (relevant to this thesis): The neuroprotective role of B cells in long-term functional recovery after stroke

Contrary to previous reports demonstrating a detrimental role for antibody-secreting B

cells in long-term stroke recovery of mice and humans, our lab found that B cells play an important neuroprotective role in supporting long-term motor and cognitive function after stroke in young male mice [166]. These findings were also replicated in female mice to determine the role of B cells in female stroke recovery. While estrogen exerts neuroprotective effects following ischemic injury, our studies show that independent of an active estrous cycle, B cell depletion exacerbates motor deficits in females after stroke. However, the role of B cells in female cognitive function after stroke was uninterpretable due to extensive stroke injury. The details of motor and cognitive assessments in both males and females after stroke are discussed below.

1.6A B cell contribute to long-term motor recovery

To determine the role of B cells in motor recovery after stroke, we administered rituximab to $hCD20^+$ or $hCD20^-$ (WT) littermate control mice to deplete B cells prior to inducing stroke, with continuous depletion for 2 weeks (**Fig. 7A**; [166]). Rituximab maintained a successful depletion of B cells in male (**Fig. 7B**) and female (**Fig. 7C**) mice and the infarct volumes between WT and B cell-depleted male (**Fig. 7D**) and female (**Fig. 7E**) mice were similar. Additionally, genotype did not affect motor skill acquisition during rotarod training in males or females (*data not shown*). Male WT mice exhibited a motor deficit at 2 days after stroke ($p<0.001$; **Fig. 8A**) that recovered by 4 days relative to pre-stroke baseline, whereas females exhibited deficits at 2- ($p<0.0001$; **Fig. 8B**) and 7 days ($p<0.05$) after stroke and recovered by day 14 relative to the pre-stroke baseline. In contrast, B cell-depleted males exhibited a significant loss in post-stoke motor function at 2 days ($p<0.01$; **Fig. 8C**), 4 days ($p<0.01$) and 14 days ($p<0.05$) relative to pre-stroke baseline. However, the deficit observed at 2- ($p<0.0001$; **Fig. 8D**), 7- ($p<0.001$) and 14 days ($p<0.001$) after stroke in female mice was a much larger than the

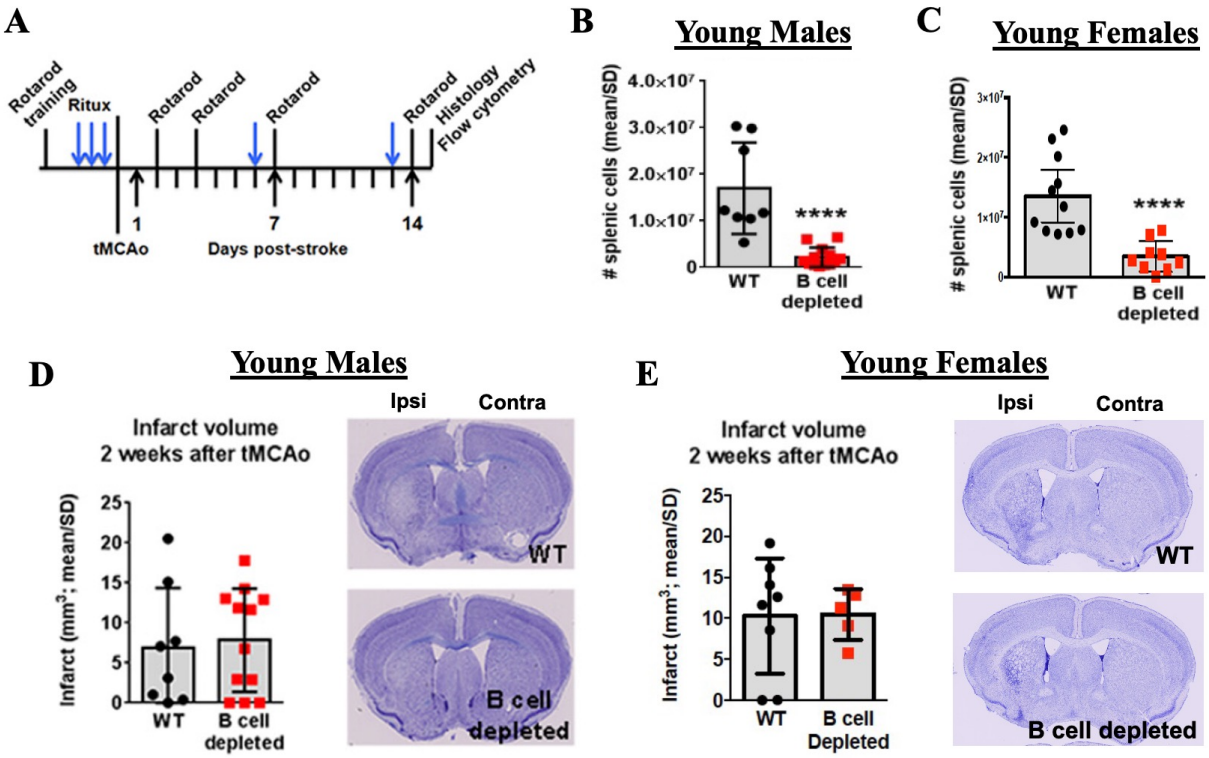

Fig. 7 B cell depletion does not impact infarct volume after stroke. (A) Experimental timeline for motor testing, neurogenesis histology and infarct volume quantification after transient middle cerebral artery occlusion (tMCAo). Rituximab treatment shows successful B cell depletion in wild type (WT; black circles) and B cell-depleted (red squares) young **(B)** male and **(C)** female mice. Infarct volumes were similar between WT and B cell-depleted **(D)** male and **(E)** female mice 14 days after stroke. Representative cresyl violet images for each genotype closest to the mean are shown. Significance determined by Student's *t*-test (****$p<0.0001$ vs. WT control). An (B, D) n=3 or (C, E) n-3 experimental replicates were performed totaling an n=5-12 mice per group.

respective deficit observed in male mice. These data suggest that in absence of B cells, post-stroke motor deficits are exacerbated in females when compared to males, regardless of an active estrus cycle. These data also suggest that B cells may support plasticity (i.e., neuronal networks involved in motor function) in remote brain regions that are critical for motor recovery after stroke [9].

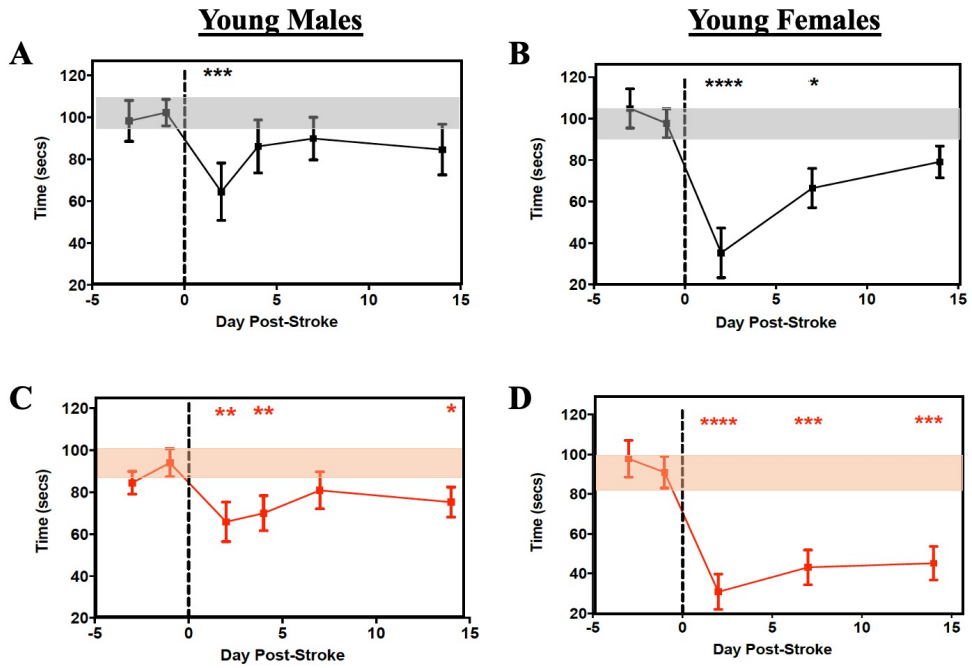

Fig. 8 B cells support motor recovery after stroke. WT **(A)** male and (**B**) female mice exhibited a motor deficit on rotarod 2 days post-stroke when compared to pre-stroke baseline (horizontal gray bar). B cell-depleted (**C**) male and (**D**) female mice exhibited a loss in motor performance at 2, 4 (only in male mice), 7- and 14-days post-stroke compared to the respective pre-stroke baseline (red horizontal bar), an observation independent of infarct volume as shown in Fig. 2. However, when compared to male mice, (**B** and **D**) WT and B cell-depleted female mice exhibited a larger deficit in motor recovery after stroke. Significance determined by repeated measures two-way ANOVA *(*p<0.05, **p<0.01, ***p<0.001, ****p<0.0001* vs. pre-stroke baseline). An (A, C) n=3 or (B, D) n=2 experimental replicates were performed totaling an n=5-12 mice per group.

1.6B B cells support post-stroke neurogenesis

Adult neurogenesis occurs in the sub-ventricular zone (SVZ) and the sub-granular zone (SGZ) of the dentate gyrus, within the hippocampus [25]. Stroke is also a potent inducer of neurogenesis [167, 168] although the mechanism is still poorly understood. We therefore quantified hippocampal neurogenesis 2 weeks after transient middle cerebral artery occlusion (tMCAo) [166]. We used the number of doublecortin-expressing (DCX^+) cells as an index of neurogenesis since immature neuroblasts generated in the inner granular cell layer of the

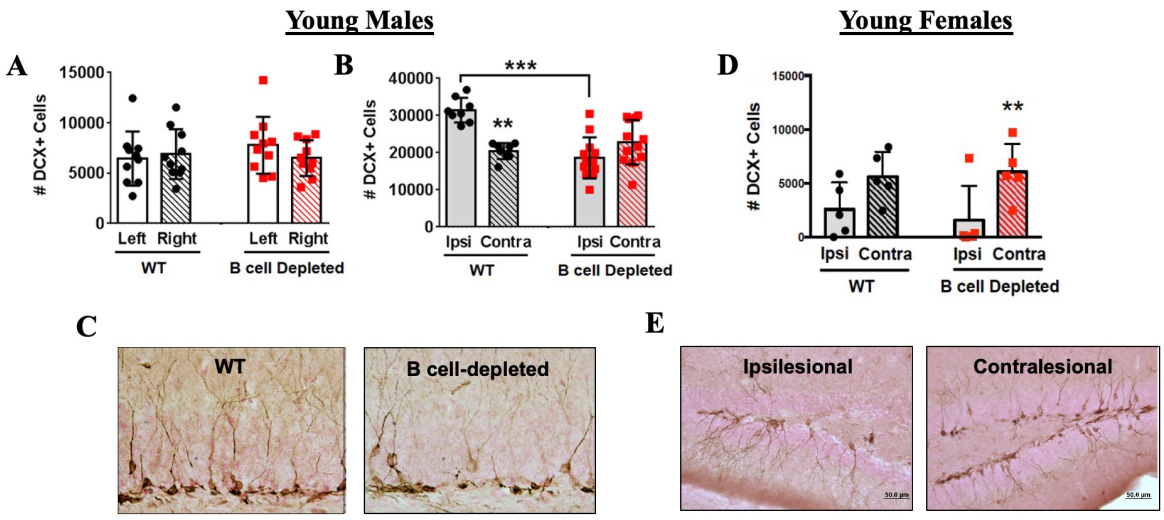

Fig. 9 B cells support post-stroke neurogenesis in young male mice. (A) B cell depletion did not alter basal neurogenesis (i.e., doublecortin (DCX)$^+$ cells) in the dentate gyrus of male mice in the absence of stroke. Stroke-induced neurogenesis was observed in the ipsilesional (ipsi) hemisphere of **(B** and **C)** wild type (WT; black circles), but not B cell-depleted (red squares) male mice 14 days after stroke. However, unlike male mice, ipsilesional neurogenesis in **(D** and **E)** female mice was lower than the contralesional hemisphere, independent of B cell-depletion. Significance was determined by repeated measures two-way ANOVA (***p<0.01, ***p<0.001* vs. ipsilesional hemisphere unless indicated by brackets). An (A-C) n=2-3 or (D, E) n=2 experimental replicates were performed totaling an n=5-12 mice per group.

hippocampal dentate gyrus (DG) express DCX in their cell bodies. In males, two weeks of B cell depletion did not affect DCX$^+$ cell numbers (**Fig. 9A**; [166]). Consistent with other studies [167, 169, 170], WT male mice had more DCX$^+$ neuroblasts in the dentate gyrus of the ipsilesional hemisphere compared to contralesional hemisphere ($p<0.01$; **Fig. 9B, C**) two weeks after stroke [166]. We also confirmed a role for B cells in sustaining post-stroke neuronal cell survival in the hippocampus - an area outside of the ischemic injury (*data not shown).* However, B cell-depleted male mice did not exhibit increased neurogenesis ($p<0.001$ vs. WT) in the ipsilesional DG compared to the contralesional DG [166]. In contrast, stroke-induced ipsilesional neurogenesis did not occur whatsoever in either WT or B cell-depleted female mice (**Fig. 9D, E**). The data stem from extensive injury caused to the hippocampus by a 60-minute tMCAo stroke. The male

data, however, suggest that B cells play an important role in supporting stroke-induced ipsilesional neurogenesis, but not homeostatic neurogenesis in either hemisphere.

1.6C B cell depletion increases spatial memory deficits

Given the role of B cells in supporting post-stroke motor recovery and hippocampal neurogenesis in males 2 weeks after stroke, we sought to investigate whether B cells play a role in supporting cognitive function after stroke. We assessed hippocampal-dependent and -independent forms of learning and memory (using a contextual and cued fear-conditioning paradigm, respectively) 8 weeks after stroke with B cell depletion extended in both uninjured and post-stroke mice (**Fig. 10A**; [166]). As with the 2-week motor recovery cohort shown in Fig. 2C, there was no effect of long-term B cell depletion on infarct volumes (**Fig. 10B**; [166]). During the training phase, there was a significant effect of genotype for both uninjured ($p<0.01$; **Fig. 10C**) and post-stroke male mice ($p<0.001$; **Fig. 10D**; [166]). Post-stroke B cell-depleted male mice froze for longer durations during the second, third (both $p<0.05$) and final ($p<0.05$) tones [166]. The evaluation of contextual hippocampal-dependent memory performed on the following day showed that B cell- depleted post-stroke mice had worse recall compared to WT mice ($p<0.05$; **Fig. 10E**; [166]). In contrast, hippocampal-independent (i.e., amygdala-mediated) cued memory recall was exaggerated in B cell-depleted mice ($p<0.01$; **Fig. 10F**; [166]). These data suggest that long-term B cell depletion independently influences both hippocampal- and amygdala-dependent cognitive functions in male mice after stroke.

1.6D B cell depletion does not affect non-stressful cognitive function, but does increase general anxiety

In addition to learning and memory, we also investigated the role of B cells in non-

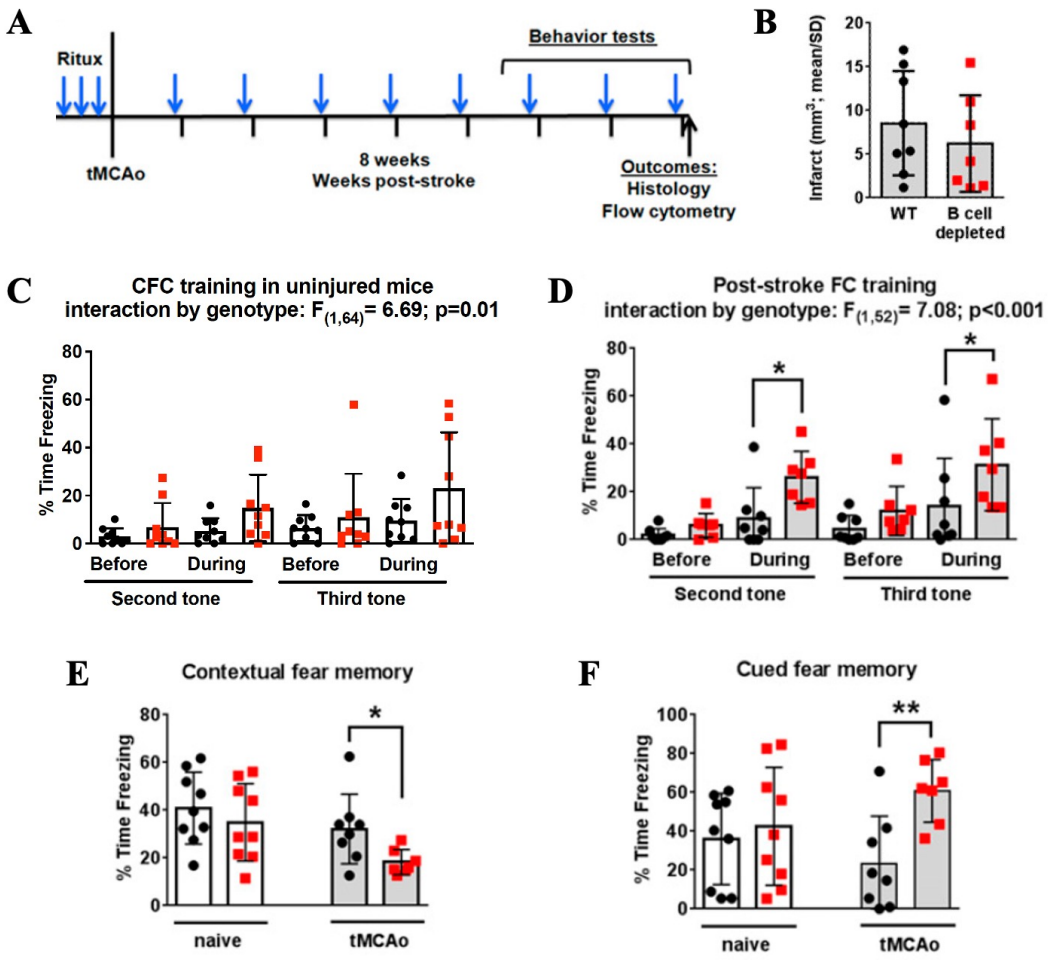

Fig. 10 B cell depletion increases spatial memory deficits independent of infarct volume. **(A)** Experimental timeline for behavior testing in uninjured male mice (white bars) or post-stroke mice 8 weeks after transient middle cerebral artery occlusion (tMCAo; grey bars). **(B)** B cell depletion did not affect infarct volumes. **(C)** On the first day of cued and contextual fear-conditioning, an interaction between the time spent freezing and the genotype of uninjured mice was observed. After stroke, **(D)** B cell-depleted mice exhibited prolonged freezing during the training tones/shocks. **(E)** The next day, post-stroke B cell-depleted mice exhibited deficits in spatial memory as they spent the least amount of time freezing during contextual memory. **(F)** On the last day, post-stroke B cell-depleted mice exhibited more freezing during cued memory. Significance determined by (B) Student's *t*-test, (C, D) repeated measures one-way ANOVA or (E, F) repeated measures two-way ANOVA *(*p<0.05, **p<0.01* vs. (B-D) WT or (E, F) uninjured/naïve control). An n=2-3 experimental replicates were performed totaling an n=7-9 mice per group.

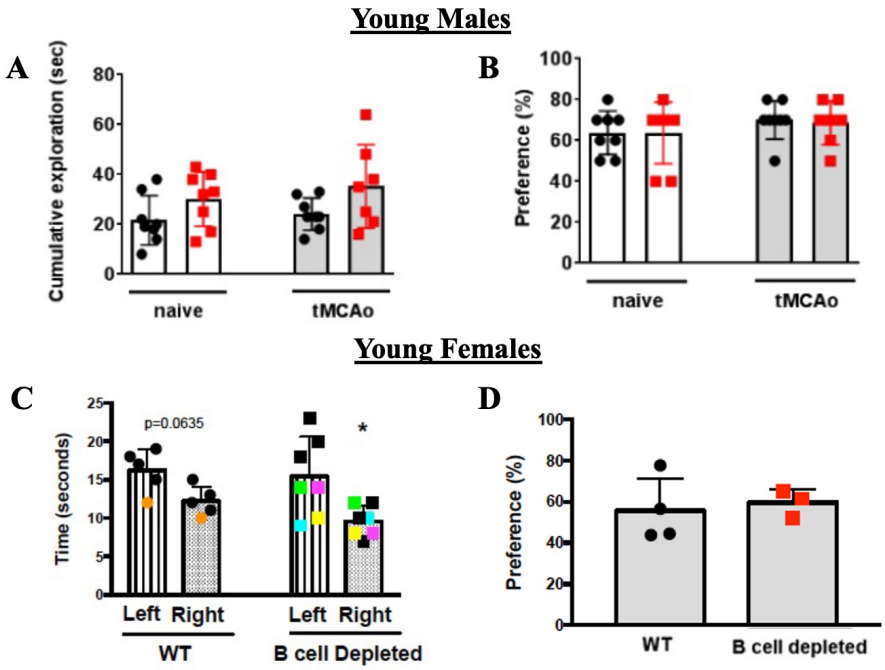

Fig. 11 B cell depletion does not affect non-aversive cognitive function in males. The novel object cognitive test was used to assess non-stressful, long-term cognitive function. There was a similar response in all four male cohorts for (**A**) the amount of time they spent exploring the novel object, as well as **(B)** their preference for the novel object. However, **(C)** female mice exhibit a side bias for the left object during training (colored dots indicate mice that did not meet the training criterion) with (**D**) no significance preference for the novel object. Significance determined by (A-C) repeated measures two-way ANOVA or (D) Student's *t*-test (*$p<0.05$ vs. (C) the left, ipsilesional hemisphere). An (A, B) n=2 or (C, D) n=1 experimental replicates were performed totaling an n=5-8 mice per group.

aversive cognitive function, locomotor activity and anxiety in B cell-depleted male and female mice 8 weeks after stroke. We assessed non-aversive cognitive function using a novel object assessment [171]. Male mice, regardless of stroke injury or B cell-depletion, spent the same amount of time (**Fig. 11A**) and exhibited no preference (i.e., the preference of the novel object was calculated as time spent exploring the novel object or the familiar object in the novel location divided by the cumulative time spent exploring both objects) for the novel object (**Fig. 11B**; [166]). In contrast, female mice exhibited a hemineglect during the training phase of the novel object assessment (**Fig. 11C**) however, no preference for the novel object was observed in

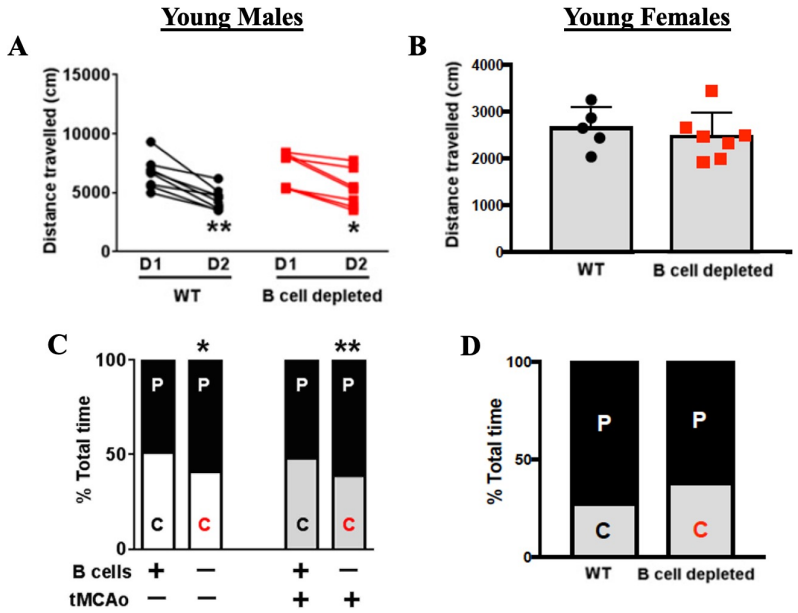

Fig. 12 B cell depletion increases general anxiety in male mice independent of infarct volume. B cell depletion did not affect the total movement of **(A)** male or **(B)** female mice in the open field 8 weeks after stroke (*NOTE: Male data was collected on two separate days in 15-minute assessments, whereas females were assessed once in a 5-minute test*). **(C)** Uninjured B cell-depleted male spent more time in the periphery (P) of the open field compared to the center (C) of the field, which became exacerbated after stroke. However, unlike male mice, the preference to travel along the periphery of the open field was not observed in **(D)** female mice, Significance determined by (A) repeated measures two-way ANOVA, (B) Student's *t*-test or (C, D) two-way ANOVA (**p<0.05, **p<0.01* vs. (A) day 1 or (B-D) WT controls). An (A, C) n=2 or (B, D) n=1 experimental replicates were performed totaling an n=5-8 mice per group.

the female mice that met the novel object training criterion (**Fig. 11D**).

To measure locomotor activity and anxiety, we used an open field assessment and while the total distance travelled decreased on day 2 of open field training in male mice ($p<0.05$; **Fig. 12A**), there was no difference in the distance traveled between WT or B cell-depleted male (**Fig. 12A**; [166]) or female (**Fig. 12B**) mice. B cell-depleted male mice, regardless of injury (e.g., stroke had no significant effect on preference), exhibited a preference to travel in the periphery of the open field (a generalized anxiety phenotype) compared to WT uninjured ($p<0.05$) or post-stroke ($p<0.01$; **Fig. 12C**) male mice [166]. Conversely, B cell depletion did not appear to affect

general anxiety in female mice as there was no significant preference for the periphery of the open field when compared to female mice that had not undergone B cell depletion (**Fig. 12D**). However, it may be possible that additional mice are needed in these cohorts to validate the results. These female data confirm that the injury caused by a 60-minute tMCAo was too extensive to assess the role of B cells in female cognitive function after stroke. Nonetheless, the male data further corroborate a neuroprotective role of B cells in supporting hippocampal cognitive function after stroke.

1.7 Conclusions and hypothesis

Our studies show that long-term, systemic B cell depletion impedes neurogenesis, increases anxiety, and exacerbates memory deficits in male mice after stroke. These post-stroke deficits generally occur in remote brain regions outside the ischemic infarct that can benefit from BDNF to support plasticity to improve function. Additionally, B cells express glutamate receptors [141, 145, 146, 148, 150, 152, 172] that could respond to the post-stroke microenvironment and upregulate BDNF. Despite the critical role of BDNF in the development and function of both neurons and B cells, the role of B cell-derived BDNF in the post-stroke brain has never been evaluated. To investigate whether B cells are a potential source of endogenous BDNF support after stroke, we must identify 1.) the spatial distribution of B cells within the post-stroke brain, 2.) the type of neurotrophic support B cells provide to ischemic-injured neurons and 3.) the impact that the post-stroke microenvironment exerts on the neurotrophic capacity of B cells. The overall goal of this thesis is to investigate the neurotrophic potential of B cells and understand their role in the recovering brain after stroke. We hypothesize

that the post-stroke microenvironment within remote brain regions potentiates the neurotrophic capacity of B cells as a possible mechanism by which B cells in remote, non-ischemic regions of the brain can support functional recovery.

Table 1 – Expression and activity of neurotrophins in healthy B cells

Gene/ protein	Expression	Activity
NGF	Resting and activated human B-cells [105] Higher in memory B-cells [105] and memory-like B-cell line [106]	Proliferation of memory-like B-cell line (CESS) and B lymphocytes in vitro [106, 118] Survival of memory B lymphocytes in vitro and memory-like B-cell line (CESS) [105, 106] Differentiation/IgM production of B lymphocytes in vitro [105, 119] IgG and IgA production from resting and activated B lymphocytes in vitro [119] IL-2R expression by activated B lymphocytes in vitro [120] CD40 expression by B lymphocytes in vitro [120] IgE inhibition in B lymphocytes in vitro [122]
BDNF	Activated human B-cells [105] B-cell lines [107]	Maturation of B-cells in vivo from Pre-BII stage in murine bone marrow [109] Survival of B lymphocytes in vitro with serum deprivation [107] Apoptosis induction (by proBDNF) in a mature B-cell line (BL2) in vitro [107]

Hillis et al., Cell and Molecular Life Sciences (2016)

CHAPTER TWO
Methodology

2.1 Mice

All mice were maintained in accordance with NIH guidelines for the care and use of laboratory animals. UT Southwestern Medical Center and The University of Kentucky approved all procedures according to AAALAC accreditation and current PHS Animal Welfare Assurance requirements. C57BL/6J (WT) mice were purchased from Jackson Laboratory. Transgenic human CD20 (hCD20) and hCD20 tamoxifen-inducible cre (Tg(MS4A1-cre/ERT2)1Mjsk; hCD20-TamCre [173, 174]) mice were obtained from Mark Shlomchik (University of Pittsburgh, Pittsburgh, Pennsylvania). Cre-inducible BDNF floxed mice ($BDNF^{fl/fl}$ [175, 176]) were obtained from Lisa Monteggia (Vanderbilt University, Nashville, Tennessee). Mice were group-housed in cages of 2-4 mice in standard animal housing with cob bedding, a 12/12-hour light cycle with lights on at 6:00 AM, and food and water ad libitum. The desired genotype of offspring was confirmed by PCR (**Table 2**, found at the end of chapter 2 on page 60) and all experimental mice originated within 4 generations of the founding breeders purchased from Jackson Labs.

2.2 B cell depletion

100μg of Rituximab (Micromedex, Greenwood Village, Colorado, U.S.A.) was given intraperitoneally (i.p.) to $hCD20^{+/+}$, $hCD20^{-/-}$ (littermate control), hCD20-$TamCre^{+/+}$ and hCD20-$TamCre^{-/-}$ (littermate control) mice for three consecutive days prior to inducing a 60-minute tMCAo [177]. Following tMCAo, an additional 100μg of Rituximab was administered weekly to

target the turnover of B cells. Splenocytes were isolated at 4 days, 2- or 8 weeks post-tMCAo and stained with a leukocyte antibody flow panel to confirm successful and sustained B cell depletion.

2.3 Stroke surgeries

Mice anesthetized (2% isoflurane/70% NO_2/30%O_2) and maintained at 37ºC body temperature had the left middle cerebral artery (MCA) exposed for transcranial Laser Doppler flowmetry (TSI, Inc) as previously described [97, 132, 166]. A blunted suture (6.0-gauge nylon, 12 mm) was inserted to occlude the MCA (>80% reduction relative to baseline cerebral blood flow) by surgeons blinded to condition, between 8-14:00 hours, with 10 mice/surgeon/day maximum and minimum of 2 duplicate experimental days for each outcome measure. Following MCA occlusion, mice were placed in an incubator (34ºC) and re-anesthetized after 55 minutes to remove the suture. Flowmetry confirmed reperfusion (cerebral blood flow >50% of baseline). Animals were monitored and those not meeting blood flow criteria were removed. Neurological deficit was scored on an established scale of 0-4 (0 = no deficit, 1.0 = limb shake, 2.0 = circling, 2.5 = tight circling, 3.0 = axial twisting) [120, 178]. With the addition of female mice used in the studies discussed in chapter 1, a total of 214 mice were used at 3-8 months of age for experiments, with 132 undergoing tMCAo surgery. A total of 39 tMCAo mice were excluded (70.5% success), including 19 for failure to meet blood flow criteria and 20 for death during or after surgery.

2.4 Behavioral analysis of female B cell-depletion studies (chapter 1)

2.4A Open field and novel object recognition

The novel object (NO) task was comprised of three phases (habituation, familiarization, and testing) on separate days. All phases were performed in a blue-squared open-field box (44 x 44 x 30 cm.) under dim light condition (60 lux.) between 10:00 and 14:00 hours. All female mice tested were acclimated in the testing room 1 hour. prior to testing. In the NO task, each mouse was habituated in the open-field box without objects for 5 minutes for one day (whereas in previous male studies, males were habituated for 15 minutes each day for two days (days 1 and 2)) and locomotor activity was assessed [171]. Female mice were positioned in the center of the box, and then individual total distance moved during the 5 minutes of habituation was automatically recorded using a video tracking system (Noldus Information Technology). In the familiarization phase for NO task, mice were subjected to a 1-minute re-habituation to the empty box and then placed in a holding cage. Immediately after, two identical objects (metal cones) were placed near the corners of the box and ~5 cm from the walls. Mice were returned to the box for familiarization. They were allowed to freely explore until they accumulated a total of 30 seconds. exploring both objects. Exploration was defined as the mouse contacting the object with its whiskers, nose, or front paws. Every mouse was ensured to spend the same amount of time exploring the objects and avoided any bias due to differences in individual levels of exploration by removing the animal from the box once it had explored the objects for a total of 30 seconds. Behaviors such as sitting on the object, looking around, or resting against the object were not counted as exploratory time. Once reaching the 30 seconds. criteria, mice were then removed from the box and returned to their home cages. The mice that did not reach criteria within 5

minutes, were excluded from further testing. In the NO testing phase, mice were subjected to a 1-minute. re-habituation to the empty box and then placed in a holding cage. Immediately after two objects, one of which was novel (doll) and the other was familiar (metal cone), were placed in the same location as during familiarization, mice were reintroduced into the box, and their exploratory behaviors were recorded by video camera for 10 minutes, and manually scored later. The position of the object used as novel or familiar in the NO were counterbalanced across mice.

Fig. 13 Using Rotarod, motor coordination is assessed in young female mice after stroke.

2.4B Rotarod (**Motor Coordination Test)**

The rotarod apparatus (IITC Life Science) consists of 5 semi-enclosed lanes and an elevated metal rod (1.25 inches diameter, 10 inches elevation) with a fine textured finish to enhance grip (**Fig. 13**). For each trial, all female mice were placed on the unmoving rod, allowed to stabilize their posture, and then rod rotation was initiated. Test parameters were as follows: rotation direction, toward investigator to encourage mice to face away while walking; start speed, 4 rotations per minute (rpm); top speed, 44 rpm; acceleration rate, 0.2 rpm/second (200 seconds from start to top speed); max test duration, 300 seconds. Each mouse's trial ended when it either fell from the rod, triggering the fall-detection sensor, or gripped the rod without walking and thereby stayed on the rod for one full rotation (a "passive rotation", in which case the investigator triggered the fall sensor manually). Data was automatically recorded to a computer. Mice that fell within 2 seconds were considered to have been startled by the initial

rotation or “off-balance” at the start of the trial, and this data was excluded. Mice underwent 4 trials/day, and the average time from all 4 trials was taken.

2.5 Tissue isolation and processing

Mice were quickly anesthetized with 100% isoflurane until breathing became deep and shallow. Mice were immediately removed from the anesthesia chamber, placed in a supine position and their abdominal fur was sprayed with 70% EtOH. An incision was made across the abdominal and chest cavities to expose internal organs. For experiments requiring microscopic analysis of CNS tissues, all mice were transcardially perfused with 35-40mL of cold 1x PBS + 1% heparin (5mL/minute for 7-8 minutes on a Ismatec CP 78001-12 perfusion pump) followed by cold 4% PFA. Fixed CNS tissues were dissected and processed as indicated below. For experiments requiring the isolation of fresh cells, and the splenic artery was initially clamped with a hemostat and following a splenic dissection, all mice were perfused only with cold 1x PBS + 1% heparin and desired tissues were dissection. All fresh tissues were stored on ice in EAE media (**Table 3**, page 61) until further processing as described below.

2.5A Spleen

Single-cell spleen suspensions were generated by homogenizing freshly isolated spleens in EAE media atop a 70μm cell strainer with a 3mL syringe plunger. Pelleted cells were resuspended in fresh, pre-warmed EAE media and layered atop pre-warmed Lympholyte separation media. The interphase (containing leukocytes free of red blood cells (RBCs)) of the gradient separation was isolated, immediately washed and resuspended in cold EAE media until further experimental use.

2.5B Cervical lymph nodes

Single-cell cervical lymph node (cLN) suspensions were generated by homogenizing freshly isolated cLNs in EAE media atop a 70μm cell strainer with a 3mL syringe plunger. Cells were immediately washed and resuspended in cold EAE media until further experimental use.

2.5C Bone marrow

Single-cell bone marrow (BM) suspensions were generated by gently flushing out BM from dissected femur and tibia bones using a 25-guage syringe filled with EAE media. The BM was then homogenized atop a 70μm cell strainer with a 3mL syringe plunger. Pelleted cells were resuspended in fresh, pre-warmed EAE media and layered atop pre-warmed Lympholyte separation media. The interphase (containing leukocytes free of RBCs) of the gradient separation was isolated, immediately washed and resuspended in cold EAE media until further experimental use.

2.5D Brain

2.5Di Histology

PFA-perfused brain tissues were post-fixed in 4% PFA at 4°C overnight and transferred to 30% sucrose until tissue sectioning. Coronal brain sections (30μm) spanning the entire hippocampus (-0.9 to -3.7 mm from Bregma) were collected at dry ice temperature on a microtome were obtained using a freezing microtome (Leica) in a 1:6 series to allow for stereological quantification and stored at -20°C in (cryostorage buffer) until further staining.

2.5Dii Electrophysiology

Unperfused anesthetized mice were decapitated, and brain tissue was immediately dissected and sectioned into 390μm-thick sections using a Leica VT1200S vibratome in an ice-

cold oxygenated dissection buffer (**Table 3**, page 61) followed by a 30-minute rest in artificial cerebral spinal fluid (aCSF; **Table 3**, page 61) to allow for tissue stabilization.

2.5E Meninges

The exposed, intact skull (containing undissected brain tissue) of PFA-perfused mice were post-fixed in 4% PFA at 4°C overnight. A previously described [179, 180], the jawbones, lower half of skull beneath auditory canal and brain were dissected from skull cap. The hollow skull cap was post-fixed once again in 4% PFA at 4°C overnight. Following the second post-fixation, the skull cap was placed in a 100% acetone/100% EtOH/4% PFA solution for 15 minutes to stiffen the meninges for dissection. Following the 15-minute incubation, the skull cap was transferred to PBS, placed in a supine position and continuously scored along the edge of the skull to gently remove the meninges. Dissected meninges were washed in 1x PBS and immediately proceeded to immunofluorescent staining.

2.6 Isolation and adoptive transfer of lymphocytes

CD19 B cells and CD8 T cells were isolated from the spleens of hCD20$^{-/-}$ or WT mice, respectively, using magnetic bead separation (Stem Cell Technologies) and the purity of the

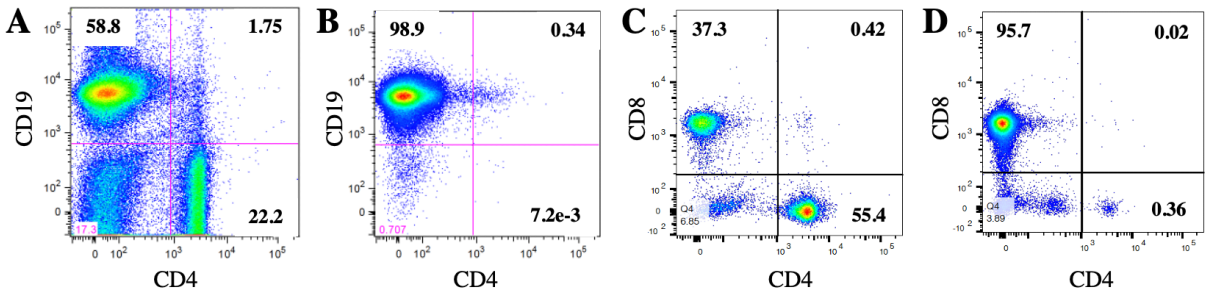

Fig. 14 Purity assessment of isolated lymphocytes. The percentage of CD19^{+} B cells in a splenic sample (**A**) before and (**B**) after CD19 magnetic bead isolation. The percentage of CD8^{+} T cells in a splenic sample (**C**) before and (**D**) after CD8 magnetic bead isolation.

isolated population was verified by flow cytometry (**Fig. 14**) [181]. $hCD20^{-/-}$ $CD19^{+}$ B cells were subsequently labeled with eFluor 450 (e450) proliferation dye and $5x10^{6}$ B cells were transferred intravenously (i.v.) in 0.2mL 0.1M PBS into post-tMCAo $hCD20^{+/+}$ B cell-depleted mice. CD8 T were subsequently labeled with e450 proliferation dye and $3\text{-}5x10^{6}$ CD8 T cells were transferred i.v. in 0.2mL 0.1M PBS into post-tMCAo WT mice.

2.7 Electrophysiology

An n=6 male mice were assigned to each of the 4 experimental groups (i.e., Rituxmab-treated uninjured or post-stroke, $hCD20^{-}$ (WT) or $hCD20^{+}$ (B cell-depleted) mice). Within the uninjured and post-stroke WT groups were 2 $hCD20^{+}$ mice that were unsuccessfully B cell depleted, and thus considered "WT" mice. Mice were anesthetized with isoflurane prior to rapid decapitation. 390µm transverse hippocampal slices (2-4 slices per mouse) were prepared using a Leica VT1200S vibratome following dissection of the hippocampus in ice cold oxygenated (95% O_2/5% CO2) dissection buffer containing. Slices were recovered for at least 2 hours in 30°C aCSF. Field excitatory postsynaptic potentials (fEPSPs and population spikes) were digitally evoked (Cgynus Instruments, Model PG400A) by stimulating the medial performant path with a bipolar platinum/iridium concentric electrode (FHC, Bowdoinham, ME) above the upper blade of the DG cell body layer. Glass recording electrodes filled with aCSF was positioned in the cell body layer approximately 200µm from the stimulating electrode. The signals were amplified by a differential amplifier (Model 1800; A-M Systems), digitized using Axon Instruments Digidata 1550A (Molecular Devices), and monitored using pClamp's Clamp-ex software (Molecular Devices). Recording aCSF and temperature were identical to recovery conditions, with a flow

rate of ~3mL/minute. Input-output curves were obtained by evoking 2-4 responses per stimulation intensity, increasing from 10µA in 5µA increments. Analysis was performed in ClampFit, with all traces from one stimulation intensity averaged to produce a single fEPSP slope or population spike amplitude measurement for each stimulation intensity.

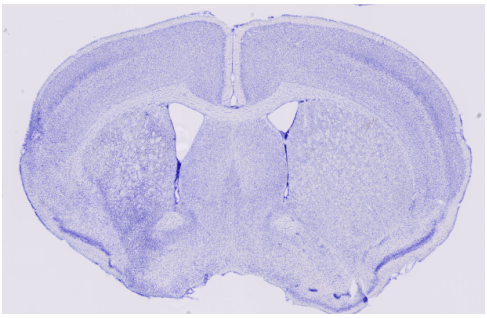

Fig. 15 Brain section from a WT mouse stained with cresyl violet 2 weeks after stroke.

2.8 Infarct volume quantification

2.8A Cresyl violet staining

Brains were extracted and cryoprotected by immersion in 15% sucrose solution for 24 hours followed by immersion in 30% sucrose solution until sectioned into coronal sections (30µm) using a freezing microtome. To visualize the nissl bodies in neurons, pycnotic cells and infarcted tissue (**Fig. 15**), brain sections were mounted onto superfrost-plus slides (Fisher Scientific), washed, dehydrated in 70% EtOH, stained with cresyl violet for 20 minutes at room temperature, followed by continuous dehydration in 95% and 100% EtOH, treated in xylene and cover slipped using DPX (Fluka) [182]. 40x digital images of the slides were obtained using whole slide imaging (Nanozoomer 2.0HT, Hamamatsu Photonics, Hamamatsu-shi, Japan). Infarct volumes were quantified by a blinded observer in Stereo Investigator stereology software (Microbrightfield Biosciences, Williston, VT) using the Cavalieri Estimator Probe, which calculates an estimation of a volume in a user-defined region of interest. Infarcted tissue was defined as areas with pyknotic cells.

2.8B MRI

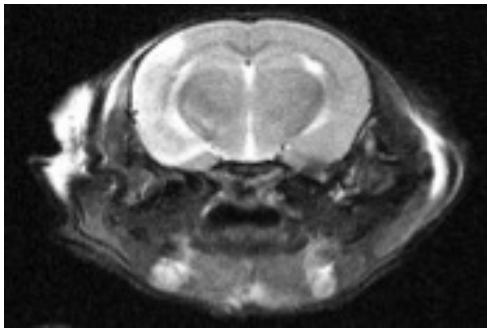

Fig. 16 Brain MRI from a WT mouse 6 days after stroke.

To assess the *in vivo* infarct volume, magnetic resonance imaging (MRI) was conducted using a small animal 7.0 Tesla (16 cm horizontal bore) magnetic resonance scanner with a 400mT/m gradient coil set, a 72 mm volume transmit RF coil and a 4-element receiver array (Bruker BioSpin MRI GmbH, Ettlingen, Germany), run on ParaVision software version 6.0.1. Under anesthesia (2% isoflurane/70% NO_2/30%O_2), each animal was placed supine in the bore of the magnet with a respiratory sensor positioned over its abdomen and a temperature probe placed near the animal, while warm air was blown through the bore to maintain the animal near physiological body temperature. Throughout the imaging session, animal respiration rate and approximate body temperature were monitored with a small animal monitoring system (SA Instruments, Stony Brook, NY). For anatomical brain imaging, high-resolution T2-weighted Rapid Acquisition with Relaxation Enhancement (RARE) axial images of the entire brain volume were acquired. The following imaging parameters were utilized: TR/TE = 6000/12 millisecond, effective TE=36 millisecond, FOV = 19.2 × 19.2 mm, matrix size = 192 × 192, slice thickness = 0.5 mm, in-plane resolution of 100 mm, no gap, 4 averages, RARE factor = 8, and scan time of 9 minutes and 36 seconds. Hyper-intense areas, reflecting high water content, such as edema and dilated/expanded ventricles (**Fig. 16**), were calculated on selected T2-weighted images by manual segmentation using FIJI. The calculated hyper-intense areas were then added together and multiplied by slice thickness (0.5-1mm), for a total of 9-17 slices, based on slice thickness, to obtain total volume of infarct injury.

2.9 Serial two-photon tomography (STPT)

2.9A Sample preparation and imaging

B cell and CD8 T cell migration into the brain was assessed using 3D serial two-photon tomography (STPT) of the entire brain volume (TissueCyte 1000 microscope, TissueVision, Cambridge, MA) [183]. To prepare samples for STPT, a 4.5% (w/v) agarose (Type 1A, low EEO, Sigma Catalog #A0169) solution in 50 mM phosphate buffer was prepared and oxidized by adding 10 mM $NaIO_4$ (Sigma Catalog #S1878) and stirring gently for 2 to 3 hours in the dark. The agarose solution was filtered with vacuum suction and washed 3 times with 50 mM phosphate buffer. The washed agarose was resuspended in the appropriate volume of phosphate buffer to make a 4.5% agarose solution. The oxidized agarose solution was heated to boiling in a microwave, then transferred to a stirring plate and allowed to cool to 60-65 °C. Brains were embedded by filling a cryoembedding mold (VWR Catalog #15560-215) with oxidized agarose, placing the filled mold on a flat ice pack, and then quickly submerging the brain using forceps into the bottom of the block with the cerebellum touching the bottom of the block (olfactory bulbs facing upward). The agarose block was allowed to fully solidify on a frozen ice pack in the dark. Once the agarose blocks were fully hardened, the agarose blocks including the specimens were removed from the molds and placed in small glass jars, where they were treated overnight at 4 °C in the dark in sodium borohydride buffer (50mM sodium borohydride, 50mM borax, 50mM boric acid, pH 9.0-9.5). After overnight crosslinking, the agarose blocks were transferred to phosphate buffer for storage at 4 °C until TissueCyte imaging. In some samples, a pellet of e450-labeled B cells or unlabeled B cells was embedded next to the brain in the same agarose block in order to provide positive and negative control data for image analysis.

On the day of imaging, agarose blocks containing the brain samples were attached to a custom magnetic slide and with superglue then placed on a magnetized stage within an imaging chamber filled with phosphate buffer. STPT imaging is a block-face imaging technique in which 2-dimensional (2D) mosaic images in the coronal plane are formed near the cut surface of the brain (within ~100μm of the surface), followed by physical sectioning with a built-in vibrating microtome to cut away the imaged tissue, preparing a new cut surface for imaging [183]. For this study, 2D mosaic images were taken at 25, 50, and 75 μm from the cut surface, followed by a vibrating microtome cut at 75μm (blade vibration frequency of 70 Hz, advancement velocity 0.5 mm/second). This process produced 570 2D mosaic images and 190 physical sections with a lateral resolution of 0.875μm/pixel (~280 gigabytes of raw data per brain). The excitation laser (MaiTai DeepSee, SpectraPhysics/Newport, Santa Clara, CA) wavelength was 850 nm and was used to excite both YFP and e450. Three image channels of emission fluorescence (pre-set bandpass filters encompassing "red," "green," and "blue" fluorophores) were collected with a predetermined photomultiplier tube voltage of 700 V. Individual tiles were adjusted via flat-field correction and stitched into 2D mosaic images of each imaging plane via custom software ("AutoStitcher," TissueVision) and saved to network-attached storage drives.

2.9B Tissuecyte image analysis

2D coronal images were transferred to a local computing cluster ("BioHPC") via 10Gbit network. Custom software written in MATLAB (MathWorks, Natick, MA) was used to normalize intensity across all image (color) channels, forming a 3-color, 3-dimensional (3D) image of each brain. Image stacks were denoised with a 3D median filter for visualization using

open-source software tools including Vaa3D [184] and ImageJ/FIJI [185]. Additional 3D visualization was facilitated via the ClearVolume plugin [186] for ImageJ/FIJI.

The 3D mouse brain images were registered to Allen Institute for Brain Science Common Coordinate Framework CCF version 3.0, update October 2017) [187]. Specifically, the "red" image channel of each 3D mouse brain image was downsampled to 10μm square lateral voxels, converted to NIFTI format, then registered to the CCF "average template" (10 μm isotropic voxels). Registration was performed using the NiftyReg software package [188, 189] using parameters similar to those used in the "aMAP" image analysis pipeline [190]. Registration involved 3 main steps: (i) affine registration of experimental mouse brain to CCF average template (via the "reg-aladin" function of NiftyReg) (ii) cubic B-spline transformation (via "reg-f3d") and (iii) resampling the transformed brains (via "reg-resample"). All 3 color channels were warped to the CCF using the registration information for the "red" color channel. Registered whole brain images were resampled to match pre-registration voxel sizes and converted to 16-bit .tif format for further analysis. These analysis procedures were partially automated using a "nextflow" workflow implemented on the BioHPC cluster.

Interactive, voxel-based supervised machine learning software ("Ilastik") was used to classify image features across the whole mouse brain, including labeled B cells (chapter 3, **Fig. 23**). In brief, maximum intensity projection images of all full-resolution optical planes and color channels within a physical section were created and downsampled to 1.5μm/pixel lateral resolution (creating a series of 190 3-color images from the 570 optical planes). From these images, 3-5 2D sections spanning the anterior-posterior axis of the brain were chosen for model training. The "Pixel Classification" applet in Ilastik, which implements voxel-based random

forest machine learning, was used to interactively classify voxels belonging to five image features ("labels"): black background, tissue autofluorescence, noise (i.e., bright voxels resulting from imaging microbubbles in the tissue), injured tissue (characterized by dramatic alterations in the autofluorescence signature found in stroke samples) and blue cells (corresponding to labeled B cells). "Blue cell" classification was performed only on samples in which e450-labeled B cells had been injected and were reinforced by training of e450-labeled cell pellets embedded in the agarose adjacent to several samples. "Injured tissue" classification was performed only on tissue that had undergone tMCAo. "Autofluorescence," "black background," and "noise" was trained on sections from all experimental conditions. A unified random forest model based on representative images of all conditions was used to assign "probabilities" that each voxel in the whole brain images belonged to each label (chapter 3, **Fig. 23**), resulting in a 5-channel "probability map" for each "label" for each experimental brain. Each 5-channel probability map was finally warped to CCF coordinates as per the above procedures.

A custom MATLAB script was used to quantify the normalized intensity of voxels within all annotated brain region for each of the 5 channels in the "probability map." Normalization was performed by summing the per-channel intensities in each annotated region, then dividing by the total volume in the annotated region. This produced a matrix of normalized intensities for each channel and each annotated region for both hemispheres of the experimental samples (chapter 3, **Table 6** and **Fig. 24-26**). Because the CCF annotation has variable levels of parcellation depending on brain region, macroscopic brain regions of interest (e.g., striatum, hippocampus) were aggregated for simplicity based on the CCF parent/child hierarchical structure.

2.10 Human peripheral blood isolation and processing

The Institutional Review Board at UT Southwestern and the University of Kentucky approved the collection of venous blood from healthy human donors for the flow cytometry experiments described in section 2.11C. Venous blood was collected into anticoagulated in Acid-Citrate-Dextrose (ACD) vacutainer tubes (BD biosciences). Following the removal of plasma, RBCs were layered atop room temperature Ficoll-Paque PLUS (17-1440-03). The interphase of the gradient separation containing peripheral blood mononuclear cells (PBMCs) was isolated, washed with 1x PBS and cryogenically stored at -120°C in 40% human serum-containing media (40% Human serum, 0.43% 1M HEPES buffer, 0.7% L-Glutamine, 10% DMSO) until Ca^{2+} response assays could be performed.

2.11 Flow cytometry

2.11A Surface protein staining and acquisition

Mouse tissues or human PBMCs were freshly isolated and processed into a single cell suspension. $1x10^6$ cells were used for quantification using fluorescent antibodies specific to leukocytes. Cells were washed with FACS buffer, blocked with an FCR blocking solution for 5-15 minutes at room temperature, stained with an assigned antibody mixture (designed to target surface proteins, **Table 4**, page 64) for 30 minutes at 4°C, and washed with FACS buffer. For experiments assessing surface proteins, surface-stained cells were resuspended in 1% PFA. All

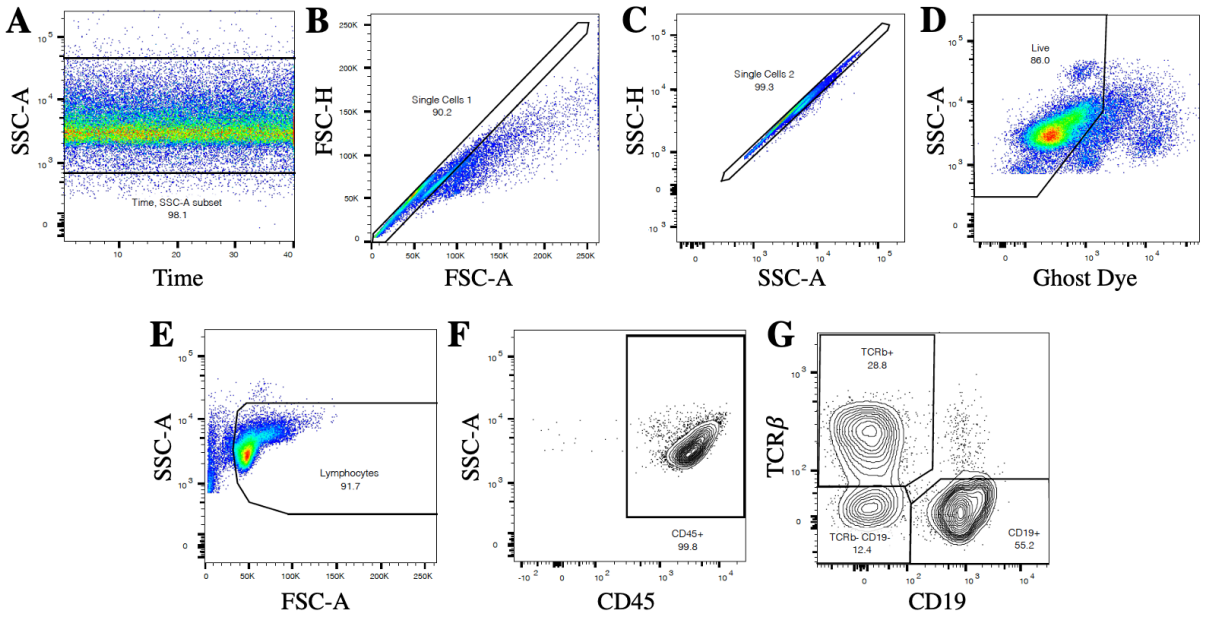

Fig. 17 Gating strategy to identify leukocytes in the spleen of mice. (**A**) Time gate on uniform flow of cells; (**B**) Singlets on forward-scatter properties; (**C**) Singlets on side-scatter properties; (**D**) Ghost dye$^-$ live cells; (**E**) Lymphocytes/leukocytes; (**F**) CD45$^+$ leukocytes; (**G**) CD19$^+$ B cells, TCRβ^+ T cells.

data was acquired on a BD FACS Aria Fusion, BD FACS Aria II, BD FACS Fortessa or BD FACS Symphony and analyzed using FlowJo, Tree Star Inc. to determine population percentages and cell number. The gating strategy for the general leukocyte panel in the spleen is outlined in **Fig.17**.

2.11B Apoptosis assay

Isolated B cells incubated with increasing concentrations of N-methyl-D-aspartate receptor (NMDAR) agonists (glutamate (L-glu) and antagonists (D-APV, ifenprodil or TCN 201) for 6, 12, or 24 hours were stained with annexin V and 7-AAD to assess B cell viability and apoptosis. As described in chapter 2 section 2.9A, 1x10^6 cells were stained with fluorescent surface protein antibodies, washed, and subsequently incubated with an annexin-V binding

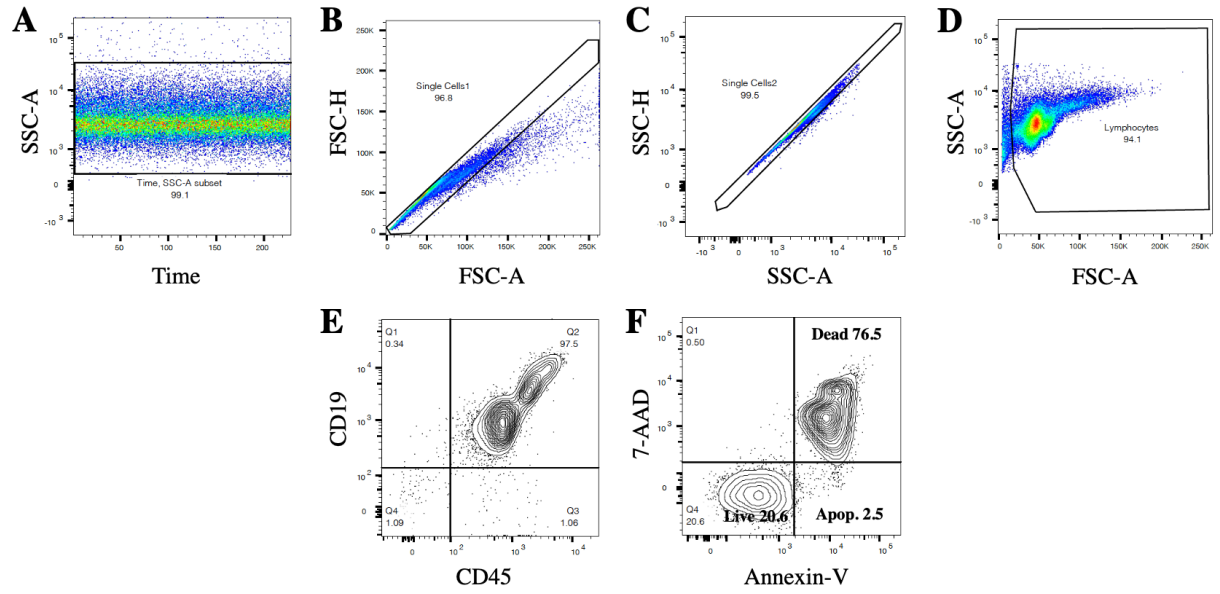

Fig. 18 Gating strategy to identify live, apoptotic and dead B cells. (**A**) Time gate on uniform flow of cells; (**B**) Singlets on forward-scatter properties; (**C**) Singlets on side-scatter properties; (**D**) Lymphocytes/leukocyte; (**E**) $CD45^+$ $CD19^+$ B cells within an isolated B cell population; (**F**) Annexin-V^- 7-AAD- live, annexin-V^+ 7-AAD^- apoptotic and annexin-V^+ 7-AAD^+ dead B cells.

buffer containing a mixture of annexin-V and 7-AAD for 15 minutes at room temperature. B cells were then washed, resuspended in annexin-V binding buffer, and acquired on a flow cytometer within 1 hour of staining. The gating strategy utilized to percentage and cell number of live, apoptotic, and dead cells is outlined in **Fig. 18.**

2.11C Ca^{2+} response assay

Mouse B cells or human PBMCs were stimulated (mouse: 5µg/mL of LPS [191-193], human PBMCs: 10ng/mL of IL-2, IL-6, and IL-21 and 2.5µg/mL of R848 and CPG [194, 195]) for 72 hours at 37°C with 5% CO_2 to activate and expand B cell subsets. Following stimulation, mouse B cells were stained as described in 2.9A to identify live $B220^+$ antibody-secreting cells (ASCs; $CD19^+$ $B220^+$ $CD138^+$), $B220^-$ ASCs ($CD19^+$ $B220^-$ $CD138^+$), naïve ($CD19^+$, $B220^+$,

$CD138^-$, IgM^+, IgD^+), effector ($CD19^+$, $B220^+$, $CD138^-$, $CD5^+$, IgM^+, IgD^-), class-switched ($CD19^+$, $B220^+$, $CD138^-$, $CD5^+$, IgM^+, IgD^-), and regulatory (Bregs; $CD19^+$, $B220^+$, $CD138^-$, $CD5^+$, $CD1d^{high}$) B cells. Human PBMCs were stained to identify live plasmablasts ($CD19^+$ $CD27^+$ $CD38^+$), $CD38^+$ B10 ($CD3^-$ $CD19^+$ $CD27^+$ $CD38^+$ $CD24^{high}$), memory ($CD3^-$ $CD19^+$ $CD27^+$ $CD5^+$ $CD24^+$ $CD1d^{high}$), memory B10 ($CD3^-$ $CD19^+$ $CD27^+$ $CD5^+$ $CD24^{high}$, $CD1d^{high}$), class-switched ($CD3^-$ $CD19^+$ $CD27^+$ IgM^- IgD^-), effector ($CD3^-$ $CD19^+$ $CD27^+IgM^+$ IgD^-), naïve ($CD3^-$ $CD19^+$ $CD27^+$ IgM^+ IgD^+) and naïve B10 ($CD3^-$ $CD19^+$ $CD27^+$ IgM^+ IgD^+ $CD24^{high}$). Cells were washed and loaded with 1.5μM of the Ca^{2+}-indicator Indo-1 in cell-loading media (CLM) for 45 minutes at 37°C. Indo-1-loaded cells were then washed, resuspended in CLM (**Table 3**, page 62), and allowed to de-esterify for 45 minutes at 37°C prior to data acquisitions. Using temperature-controlled UV laser-flow cytometers (BD FACS Aria Fusion, BD FACS Aria II or BD FAC Symphony), cells were maintained at 37°C for the duration of the experiment and the baseline Ca^{2+} activity of the cells in CLM was recorded for 30 seconds. To assess B cell-specific NMDAR activity, B cells previously preincubated with NMDAR antagonists 3-5min preincubation with D-APV (10μM), ifenprodil (30μM) or TCN 201 (10μM)) were immediately treated with glutamate (1μM or 100μM) and a live, 8-minute response was recorded. Each experiment had individual positive (ionomycin (10μg/mL) and negative (8mM EGTA-preincubation followed by 10μg/mL ionomycin stimulus) controls for data normalization. The Ca^{2+} response induced following B cell receptor (BCR) engagement (mouse: 10μg/mL of anti-IgM, human PBMCs: 10μg/mL anti-IgG/IgM)) was also assessed in mouse B cells and human PBMCs. The gating strategies to identify specific B cell subsets in mice and humans are outlined in **Fig. 19 and 20**.

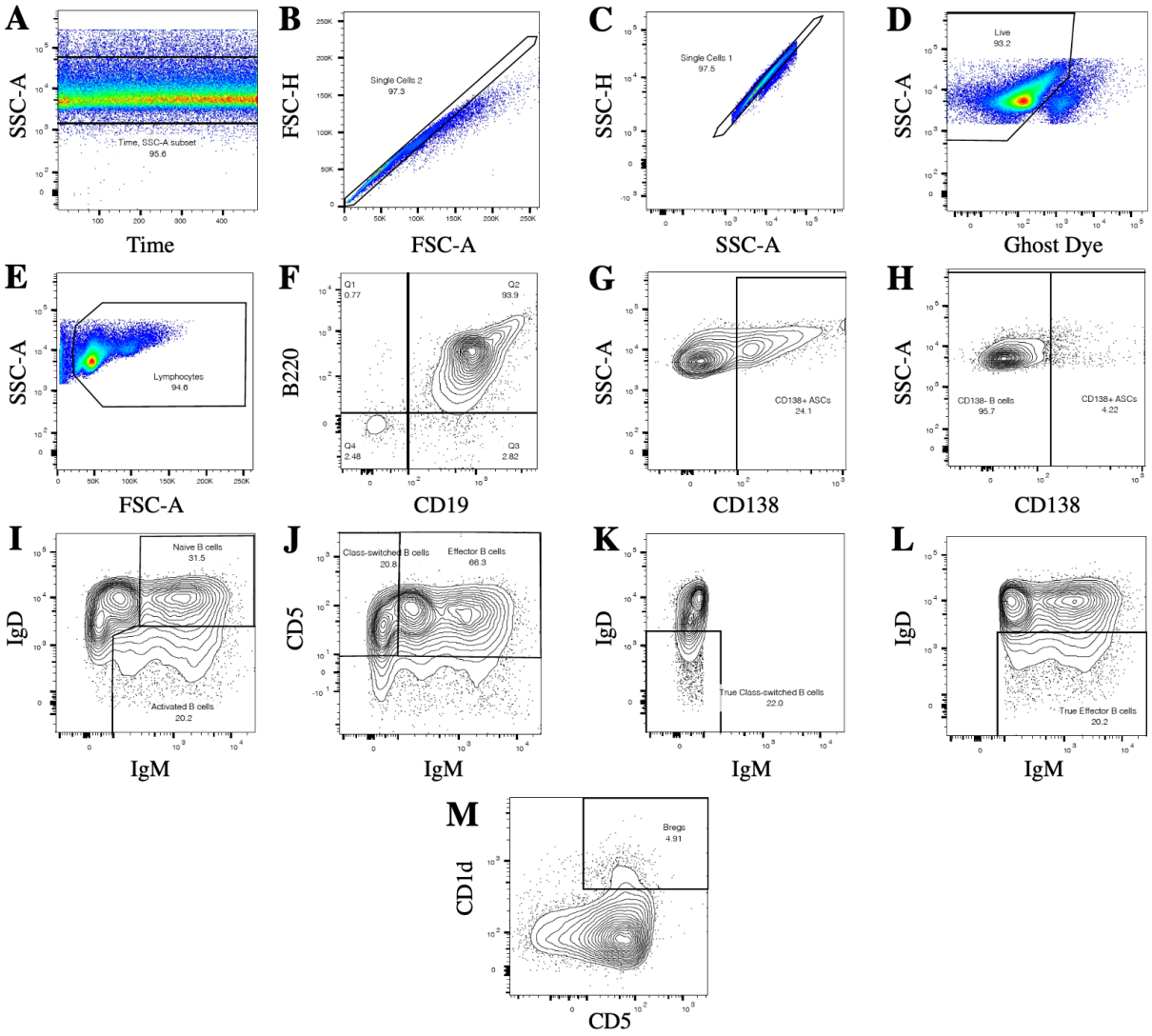

Fig. 19 Gating strategy identifying mouse B cell subsets assessed in Ca^{2+} response assays. (**A**) Time gate on uniform flow of cells; (**B**) Singlets on forward-scatter properties; (**C**) Singlets on side-scatter properties; (**D**) Ghost dye^{-} live cells; (**E**) Lymphocytes/leukocyte; (F) B220^{+} CD19^{+} and B220^{-} CD19^{+} B cells within an isolated B cell population; (**G**) B220^{-} CD138^{+} antibody-secreting cells (ASCs); (**H**) B220^{+} CD138^{+} ASCs and B220^{+} CD138^{-} B cells; (**I**) CD138^{-} IgM^{+} IgD^{+} Naïve B cells; (**J**) CD138^{-} CD5^{+} B cells; (**K**) CD138^{-} CD5^{+} IgM^{-} IgD^{-} class-switched B cells; (**L**) CD138^{-} CD5^{+} IgM^{+} IgD^{-} effector B cells; (**M**) CD138^{-} CD1d^{hi} CD5^{+} regulatory B cells (Bregs).

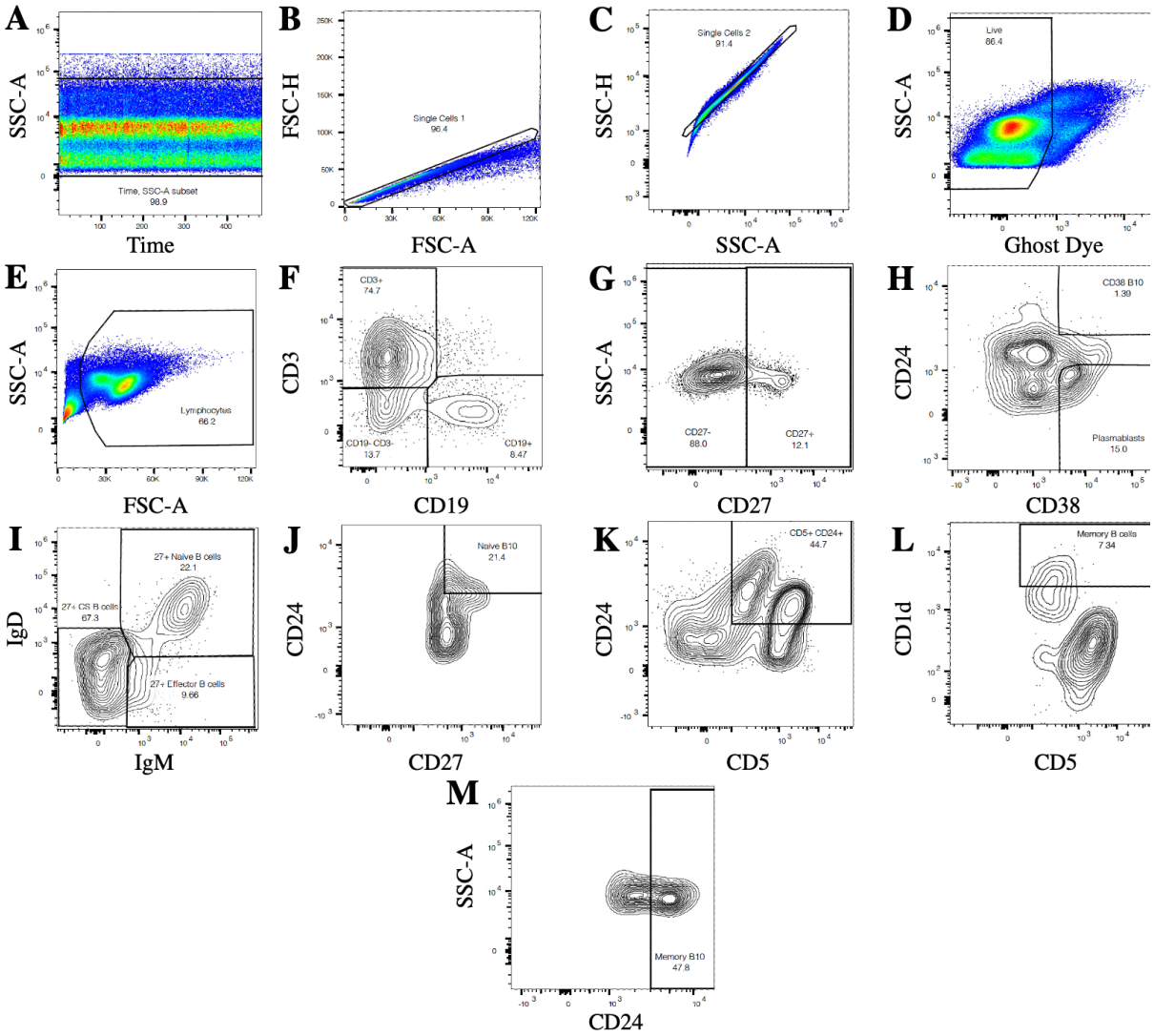

Fig. 20 Gating strategy identifying human B cell subsets assessed in Ca^{2+} response assays. (**A**) Time gate on uniform flow of cells; (**B**) Singlets on forward-scatter properties; (**C**) Singlets on side-scatter properties; (**D**) Ghost dye^{-} live cells; (**E**) Lymphocytes/leukocyte; (**F**) CD3^{-} CD19^{+} B cells within peripheral blood mononuclear cells (PBMCs); (**G**) CD27^{+} B cells; (**H**) CD38^{+} CD24^{-} plasmablasts and CD38^{+} CD24^{hi} B10 B cells; (**I**) CD27^{+} IgM^{+} IgD^{+} Naïve B cells, IgM^{-} IgD^{-} class-switched B cells and IgM^{+} IgD^{-} effector B cells; (**J**) CD27^{+} IgM^{+} IgD^{+} CD24^{hi} Naïve B10 B cells; (**K**) CD27^{+} CD24^{+} CD5^{+} B cells; (**L**) CD27^{+} CD24^{+} CD5^{+} CD1d^{hi} memory B cells; (**M**) CD27^{+} CD24^{+} CD5^{+} CD1d^{hi} CD24^{hi} memory B10 B cells.

2.12 Generation of control BDNF B cells

2.12A BDNF-knock out B cells

Female hCD20-TamCre mice were crossed to $BDNF^{fl/fl}$ male mice for two generations to generate conditional B cell-specific BDNF-KO (hCD20-$TamCre^{+/+}$-$BDNF^{fl/fl}$) and littermate (hCD20-$TamCre^{-/-}$-$BDNF^{fl/fl}$) control mice. Once mice were 3-4 months old, 2mg of tamoxifen (LLC MP Biologicals) dissolved in corn oil (Sigma) was administered i.p. for 3 consecutive days. B cell cellularity and hCD20 expression was assessed by flow cytometry in bone marrow, spleen, and cervical lymph nodes 48 hours after the final tamoxifen injection. The knockout of BDNF was assessed in FACS-sorted $hCD20^{+}$ B cells via PCR and sequencing as seen in chapter 4, **Fig. 33**.

2.12 BDNF-overproducing B cells

A plasmid (e.g., CMV-BDNF-P2A-mCherry) was generated to achieve constitutive BDNF production in B cells. BDNF (ENSMUST00000053317.12, from 109674700 to 109675234 bp) was cloned using infusion-based cloning kits (**Table 3**, page 62) as specified by the manufacturer's protocol and amplified via PCR (Forward primer: 5'-ATGTTCCACCAGGTGAGAAGAGTG-3'; Reverse primer: 5'-CTATCTTCCCCTTTTAATGGTCAGTGTAC-3'). Additional DNA sequences of the plasmid design were then fused to the amplified BDNF product via PCR to complete the CMV-BDNF-P2A-mCherry plasmid construct (chapter 4, **Fig. 34A**). Isolated WT B cells were stimulated with 5μg/mL of LPS at 37°C with 5% CO_2 for 72 hours prior to plasmid transfection. Using a B cell nucleofection kit, 2μg of a CMV-BDNF-P2A-mCherry plasmid (or empty vector plasmid, CMV-P2A-mCherry, where indicated) were transfected into LPS-stimulated B cells. Successful

plasmid transfection was assessed at 24-, 48- and 72-hours post-transfection in B cells via flow cytometry and B cell supernatants via ELISA as specified by the manufacturer (chapter 4, **Fig. 34B-D**).

2.13 Brain cell cultures

2.13A Hippocampal neuronal cultures

As previously described [196], hippocampal tissue from postnatal day 0-2 C57BL/6J pups was digested using papain and DNAse and triturated with a fire-polished Pasteur pipette. Neurons isolated from trituration supernatants were plated ($0.2x10^6$) in plating media in a 24-well culture plate containing poly-L-lysine pre-coated 18mm coverslips and cultured at 37°C with 5% CO_2. 2-4 hours after plating, all plating media was replaced with glial-conditioned feeding media. Ara-C was added on day-in-vitro (DIV) 3 to inhibit astrocytic cell growth and half of the culture media was replaced glial-conditioned feeding media every 4-5 days. Cells were cultured until DIV17 prior to experimental use.

2.13 Mixed cortical cultures

Cortical and hippocampal tissue were isolated from postnatal day 0-2 C57Bl/6J pups and digested using 0.25% Trypsin-EDTA to isolate cells [166]. Mixed cortical cells were plated at $1.8\text{-}2.0x10^6$ per well of a 6-well plate (Corning Primaria) in mixed cortical culture media. A complete media change was done at day-in-vitro (DIV) 3 and cells were cultured at 37°C with 5% CO_2 until confluent (minimum DIV7) prior to experimental use.

2.14 In vitro ischemic injury

2.14A Oxygen-glucose deprivation

All traces of glucose- and serum-containing media were removed from mixed cortical cultured cells by thoroughly washing with serum/glucose-free 1x HBSS. As previously described [166], OGD was induced in DIV7-confluent cells for 2 hours by exposure to 0.1% O_2 in a hypoxic chamber with HBSS. Following OGD, cultures were washed and allowed to recover (± co-cultured B cells) in complete serum/glucose-containing media for 3-4 days prior to assessing metabolic activity via MTT assay and neuronal survivability via immunofluorescent staining (chapter 4, **Fig. 31A**).

2.14Ai MTT assay

Metabolic activity was assessed in OGD-injured mixed cortical cells as an indicator of cell viability after injury. As previously described [197], all culture media was removed and mixed cortical cells were incubated with 0.5mg/mL MTT in fresh media for 3 hours protected from light at 37°C with 5% CO_2 to allow metabolically active cells to convert MTT to formazan crystals. Following the 3h incubation, DMSO was added to dissolve formazan crystals for 15 minutes at 37°C with 5% CO_2 and the absorbance (560nm) and reference (650nm) reads of the dissolved crystals were acquired on a ELISA plate reader (chapter 4, **Fig. 31B**).

2.14B NMDA excitotoxicity

Mixed cortical cultures were thoroughly washed with aCSF followed by a 15-minute incubation with 500μM NMDA at 37°C with 5% CO_2 as previously described [198]. Following the induction of NMDA excitotoxicity, cultures were washed and allowed to recover (± co-

cultured B cells) in complete serum/glucose-containing media for 3-4 days prior to assessing neuronal survivability via immunofluorescent staining as shown in chapter 4, **Fig. 36**.

2.15 Immunohistochemistry and analysis

2.15A Doublecortin (DCX)$^+$ neurons

Hippocampal brain sections were mounted onto coded superfrost-plus slides and were allowed to dry for 2 hours [199, 200]. After drying, sections were first incubated in antigen retrieval solution for 15 minutes. All slides were then incubated in 0.3% H_2O_2 to quench endogenous peroxidases. Nonspecific binding was blocked for 1 hour. All slides were incubated with a primary antibody against DCX overnight at room temperature, washed again, incubated for 2 hours with a biotin-conjugated secondary antibody and lastly, incubated for 90 minutes with ABC. DCX$^+$ cells were visualized with DAB/metal concentrate. After immunostaining, sections were dehydrated with graded ethanol and cover slipped using DPX. Unbiased estimates for DCX cell counts were obtained using stereological quantification on an Olympus BX51 System Microscope with a MicroFIRE A/R camera (Optronics) as previously published [199]. Estimation of total DCX$^+$ cell number was performed using the Optical Fractionator Probe within the Stereo Investigator software (MBF Bioscience) according to previously published stereological methods [201]. An unbiased counting frame superimposed on the region of interest was used to quantify cell number. Counting was performed using a 40x magnification, 0.63 NA lens. At least 250 cells per mouse were counted, and the average number of counting fields per mouse was close to 300. The average number of sections per mouse counted was 10 and representative images can be found in chapter 1, **Fig. 9**.

2.16 Immunofluorescent staining and analysis

2.16A B cell cytospins

B cell cytospins were generated by spinning (Thermo Scientific Cytospin 4) $0.2x10^6$ PFA-fixed B cells onto histology slides. Cytospin pellets were circled with Pap-pen liquid blocker, gently washed, blocked for 1 hour at room temperature and stained for B220 and GluN2A (or GluN2B) in a humidified chamber at 4°C overnight. Cytospins were then washed, incubated with appropriate fluorescent secondary antibodies for 1-2 hours at room temperature, washed again and cover slipped in Fluoromount-G and imaged using confocal microscopy (Zeiss LSM 880 inverted confocal microscope, 40x objective lens zoomed-in to 80-157x magnification). As shown in chapter 5, **Fig. 37**, RGB channels of the z-stack images were used to quantify GluN2A/B subunits and to identify positive B220 expression in FIJI. The z-stacks were split into 2D images and quantified plane-by-plane to identify GluN2A/B subunit clusters. Each cluster of subunits was recorded per cell in view across all planes of the original z-stack to yield a total subunit count. Two images were analyzed per treatment condition, per mouse with an average of 10 B cells counted per image.

2.16B Brain cell cultures

2.16Bi Hippocampal neuronal cultures

DIV17 neuronal coverslips were washed in their wells to remove all non-adherent cells and debris, fixed with 4% PFA for 10-15 minutes at room temperature, blocked for 1-2 hours at room temperature, and incubated with a primary antibody targeting GluN2A or GluN2B overnight on a circular-rotating shaker at 4°C. Coverslips were washed in their wells, incubated with appropriate fluorescent secondary antibodies, washed again, counter stained with DAPI,

gently lifted from their well, and invertedly mounted onto a superfrost-plus histology slide with Fluoromount-G. Neuronal NMDAR subunit expression was then assessed by confocal microscopy (Zeiss LSM 880 inverted confocal microscope, 40x objective lens zoomed-in to 120x magnification) as shown in chapter 5, **Fig. 37A**.

2.16Bii Mixed cortical cultures

Following *in vitro* ischemic injury, neuronal survivability in mixed cortical cultures was assessed at the end of the B cell co-culture recovery period. Culture wells were washed to remove all non-adherent cells and debris, fixed with 4% PFA for 10-15 minutes at room temperature, blocked for 1-2 hours at room temperature, and incubated with a primary antibody targeting the neuronal MAP2 antigen overnight on a horizontal rocker at 4°C. Wells were washed and incubated with a fluorescent secondary antibody, washed again, counterstained with DAPI and cover slipped with Fluoromount-G. Culture plates were imaged on a confocal microscope (Zeiss LSM 880 inverted confocal microscope, 10x magnification, 4 images/well) as shown in chapter 4, **Fig. 31** and $MAP2^{+}$ cells per image were quantified using the counter tool in Photoshop CS6.

2.16C Meninges

Previously fixed meninges were washed, blocked for 2 hours at room temperature, and incubated with primary antibodies targeting Lyve-1 and B220 antigens on a circular-rotating shaker overnight at 4°C. Following the overnight incubation, meninges were then washed, incubated with appropriate fluorescent secondary antibodies for 2 hours at room temperature, washed again, counterstained with DAPI, mounted onto a superfrost-plus histology slide and cover slipped with Fluoromount-G. Confocal images (40x magnification) were acquired on a

Zeiss LSM 880 inverted confocal microscope and representative images can be found in chapter 3, **Fig. 28**.

2.17 qPCR

Naïve or 4 day-post-tMCAo B cells stimulated with 5μg/mL of LPS for 48 hours in the presence or absence of 1μM glutamate (added in final 24hours) were stored in trizol (Invitrogen) until RNA was simultaneously isolated from all samples using RNA isolation kits (Biorad). RNA yield was quantified (Nanodrop, ThermoScientific) and the purity was subsequently assessed (Bioanalyzer 2100, Agilent). RNA was reverse transcribed to cDNA (PerfeCTa SYBR Green Supermix, QuantaBio) followed by quantitative real-time PCR (qPCR; BioRad CFX Connect) to amplify target gene primers. Primers for genes of interest, found in **Table 5** (page 65), were present in mouse brain and splenic cells. Results from samples were compared relative to the standard curve to calculate threshold cycles (CT) in each sample using Bio-Rad CFX Maestro and Real-time PCR (Manager software version 3) software. Using previously described methods [202], the relative quantification of the qPCR data was analyzed using the 2^(-ΔΔCT) method. Briefly, all CT values were normalized to ubiquitin signal (ΔCT = CT(a target gene)−CT(a reference gene)). The ΔCT values were then used for additional data analyses of ΔΔCT (ΔΔCT = ΔCT(a target sample)−ΔCT(a reference sample)) and fold change (2^(-ΔΔCT)).

2.18 Western Blot

2.18A Generation and protein quantification of B cell lysates

Isolated B cells were stimulated with 5μg/mL of LPS at 37°C with 5% CO_2 for 72 hours.

B cells were incubated with brefeldin-A in the final 6 hours. Upon completion of stimulation, B cells were washed and 1-10μL of protease inhibitor cocktail was added to 1-10x10^6 B cells resuspended in a final volume of 125μL of cell lysis reagent. B cells were sonicated on ice (30 seconds, 10-second interval pulses, amplitude 40%) and allowed to rest for 15 minutes. Cell lysates were centrifuged, separated from cell pellets and individual protein concentrations were determined using a BCA protein assay kit.

2.18B Blotting and immunostaining

Following the denaturing (95°C for 5 minutes) of B cell lysates in Laemli buffer, 20μg of denatured lysate was loaded into a 12% SDS-PAGE gel and ran at 250 volts for 30 minutes. Following electrophoresis, the gel protein was transferred to a nitrocellulose membrane as previously described [203]. The membrane was blocked, stained with primary antibodies followed by HRP secondary antibodies, developed in western-blotting substrate and imaged using a BioRad ChemiDoc Imaging System as seen in chapter 5, **Fig. 49**.

2.19 Statistical analysis

Based on previous results and published data [204], power analyses were performed to determine the approximate number of animals to be used per experiment given an expected stroke-induced mortality rate of 30%. All individuals performing experiments were blinded to experimental conditions and all animals were randomly assigned to each group. Using GraphPad Prism 9 (La Jolla, CA), statistical differences were determined through unpaired parametric Student's *t* test, one- or two-way ordinary or repeated-measures ANOVA where appropriate.

Specific analysis details are indicated for each result throughout chapters 1, 3, 4 and 5 and their corresponding figures. Values of $P < 0.05$ were considered significant.

Table 2 - Genotyping Protocol		
Strain	**Primer Sequence**	**Product size**
hCD20	F: 5'-CAT GGT TGA GAG TCA GTG GTC-3' R: 5'-GAT GTT CCT GCT GCC TCT TG-3'	179bp
hCD20-TamCre	F: 5'-CTT GCT CTT GGA CAG GAA CC -3' R: 5'-GCC ATC AGG TGG ATC AAA GT-3'	244bp
fBDNF	F: 5'-TGG GAT TGT GTT TCC GGT GAC-3' R: 5'-GCC TTC ATF CAA CCG AAG TAT G-3'	WT: 420bp Flox: 470bp
PCR reaction mix	All strains used the following reaction mix: 1ul total of all primers (10mM), 10ul Taq DNA Polymerase (Promega M7123), 7ul H_2O and 2ul DNA	
PCR thermal cycler settings	hCD20 and hCD20-TamCre: 1.) 94°C for 4', 2.) 94°C for 30", 3.) 62°C for 45", 4.) 72°C for 1', 5.) repeat steps 2-4 for 39 cycles, 6.) 72°C for 7', 7.) 4°C ∞ fBDNF: 1.) 94°C for 1', 2.) 92°C for 30", 3.) 55°C for 45", 4.) 72°C for 2', 5.) repeat steps 2-4 for 35 cycles, 6.) 72°C for 7', 7.) 4°C ∞	
PCR product electrophoresis	hCD20 and hCD20-TamCre: 1% agarose gel (ThermoFisher 16500-500) (made in 130-150mLs 1x TAE buffer and 8-10uL ethidium bromide (SIGMA E1510), 140V for 50 minutes fBDNF: 2% agarose gel, 70V for 2-3hours	
PCR product gel imaging	Using a BioRad ChemiDoc Imaging System, select 'Ethidium Bromide Gel' application and image the gel with 'optimal exposure' selected.	

Table 3 - Reagents and Buffers		
Method	**Assay/Procedure**	**Reagent/Buffer (catalog number)**
Tissue/cell	Isolation	Perfusion:1x PBS (diluted from FisherScientific BP39920) + 1% heparin (NDC 25021-400-30) Electrophysiology: Dissection buffer ((in mM): 2.6 KCl, 1.25 NaH_2PO_4, 26 $NaHCO_3$, 211 sucrose, 10 glucose, 0.75 $CaCl_2$, 7$MgCl_2$.) and artificial cerebral spinal fluid ((in mM): 125 NaCl, 3.25 KCl, 25$NaHCO_3$,1.25 $NaH_2PO_4 \cdot H_2O$, 11 glucose, 2 $CaCl_2$, 1 $MgCl_2$) Fixation: 4%. PFA (Santa Crux sc-281692)
	Culture	Lymphocytes: EAE media (500mLS RPMI 1640 (Corning 15-040-CV), 50mLs FBS (SIGMA F4135), 5mL pen/strep (Hyclone SV30010), 5mL Glutamax (Gibco 35050-061), 6.25mL HEPES (Corning 25-060-CI), 5mL sodium pyruvate (Gibco 11360-070), 5mL MEM amino acids (cellgro 25-030-CI), 1μL BME (SIGMA M7522)), Lympholyte (CL5030), Percoll (GE Healthcare 17-0891-01) Hippocampal neuronal cultures: Dissecting media (50 mL 10x HBSS (Gibco 14185-052), 5mL pen/strep, 5 mL sodium pyruvate, 5 mL HEPES, 15 m glucose (SIGMA 158968), 420 mL Mill-Q), plating media (neurobasal (Gibco 21103049), 2% B-27 (Gibco 17504044), 1% pen/strep, 1% Glutamax, 5% horse serum (Hyclone SH3007403)), feeding media (neurobasal, 2% B-27, 1% pen/strep, 1% Glutamax), papain (Worthington LS003119), DNAse (SIGMA DN-25), poly-L-lysine (SIGMA P2636), ara-C (SIGMA C-6645)) Mixed cortical cultures: 1x PBS, 0.25% trypsin-EDTA (Hyclone SH30042), mixed cortical culture media (1x DMEM (Corning 10-013-CV), 10% FBS, 1% sodium pyruvate, 100ug/mL Primocin (InvivoGen ant-pm-1))
	Cryostorage	Cryostorage buffer (tissue sections): 30% Glycerol (FisherScientific AA36646K7), 30% Ethylene glycerol (FisherScientific E178-4), 30% water, 10% 10x PBS (FisherScientific BP39920) Lymphocyte freezing media (mouse): 50% FBS, 40% RPMI 1640, 10% DMSO (FisherScientific BP231-1)

In vitro ischemia	OGD	OGD: 1x HBSS (Corning 21-021-CV) Post-OGD culture media: EAE media MTT (Invitrogen M6494)
	NE	NE: 500μM NMDA (Tocris 0114) in ACSF **(**143mM NaCl (SIGMA S5886), 5mM KCl (SIGMA P5405), 10mM HEPES (pH 7.2, ThermoFisher BP310-500), 10mM glucose (SIGMA 158968), 2mM $CaCl_2$ (SIGMA C5670), H_2O)) Post-NE culture media: EAE media
B cell controls	BDNF knock out B cells	20mg/mL tamoxifen (LLC MP Biologicals 156738) reconstituted in corn oil (SIGMA C8267)
	BDNF-overproducing B cells	In-Fusion Snap Assembly Master Mix (Takara 638947)**,** Amaxa Mouse B cell Nucleofector Kit (Lonza VPA-1010), Total BDNF Quantikine ELISA Kit (R&D DBNT00)
Flow cytometry	Surface staining	FACS buffer: 2L 1x PBS, 20g BSA (FisherScientific BP1605-100), 2g NaN_3 (Ricca 7144.8-16) Mouse FC receptor block (Miltenyi 130-092-575), human FC receptor block (Miltenyi 130-059-901), 1% PFA (diluted from Santa Crux sc-281692) + 0.1% EDTA (FisherScientific BP2482)
	Apoptosis assay	AV binding buffer (Tonbo TNB-5000-L050), L-glu (Millipore Sigma G5889), D-APV (Tocris 0106), ifenprodil (Tocris 0545), TCN201 (Tocris 4154)
	Ca^{2+} response assay (mouse and human)	Cell-loading media: RPMI 1640, 2%FBS, 25mM HEPES LPS (SIGMA L6529), anti-IgM (Jackson Labs 115-006-075), IL-2, (ThermoFisher RP-8608), IL-6 (ThermoFisher PHC0064), IL-21 (R&D 8879-il), R848 (Invivogen R848), CPG (Invivogen ODN2006-g5), anti-IgG/IgM (Jackson Labs 109-005-044), EGTA (SIGMA E3889), ionomycin (Millipore 407950), L-glu, D-APV, ifenprodil, TCN201
	STPT	eFluor 450 cell proliferation dye (eBioscience 65-0842-85)
Immunohisto-chemistry	-	Antigen unmasking solution (Vector H-3300), Hydrogen peroxide (ACROS Organics 7722-84-1), ABC Vector Elite Kit (Vector PK-6100), DAB Peroxidase Substrate Kit (Vector SK-4100) Wash buffer: 1x PBS

		Blocking solution: 10% normal rabbit serum (Gemini 100-116) + 0.3% triton-X (SIGMA T9284) +1x PBS Primary antibody solution: 3% normal rabbit serum + 0.3% Tween-20 (BioRad 161-0781) + 1x PBS Secondary antibody solution: 1.5% normal rabbit serum + 1x PBS DPX (Sigma 44581)
Immunofluor-escence	B cell cytospins/hippo-campal neuronal cultures	Wash buffer: 1x PBS Blocking solution: 5% BSA + 0.1% triton X Primary/secondary antibody solution: 1x PBS + 1% BSA Fluoromount-G (SouthernBiotech, 0100-01)
	Mixed cortical cultures/meninges	Wash buffer: 1x PBS + 0.1% triton X Blocking solution: 10% goat serum (Gemini 100-109) + 0.1% triton X Primary/secondary antibody solution: 3% goat serum + 0.05% triton-X + 1% BSA
qPCR	-	Trizol (Invitrogen 15596018), Aurum RNA isolation kit (BioRad 7326830), PerfeCTa Sybr Green Supermix (QuantBio 95054-500)
Western Blot	-	Brefeldin-A (eBioscience 00-4506), Pierce BCA Protein Assay Kit (ThermoFisher 23225), Cell Lytic MT (SIGMA C3228), Protease inhibitor cocktail (SIGMA P8340), Laemli buffer, 12% agarose gel (30% acrylamide (BioRad 161-0156), Tris, SDS, ammonium persulfate, TEMED (BioRad 161-0801)), standard ladder (BioRad 161-0374), running buffer (10x Tris/Glycine/SDS (BioRad 1610732), H_2O), transfer buffer (10x Tris/Glycine (BioRad 1610734), methanol, H_2O), PBS-T, non-fat milk (BioRad 170-6404), Pierce ECL Western Blotting Substrate (ThermoScientific 32106)

Table 4 - Antibodies		
Method	**Panel/Assay**	**Antigen (catalog number)**
Flow cytometry	General leukocytes	1:1000 Ghost dye v450 (Tonbo 13-0863), 1:100 CD45 APC-Cy7 (Biolegend 103116), 1:100 TCRβ BV510 (Biolegend 109234), 1:50 CD19 PE (Tonbo 50-0193)
	Apoptosis assay	1:100 CD45 APC-Cy7, 1:50 CD19 PE, 1:22.5 annexin V FITC (Tonbo 35-6409), 1:22.5 7-AAD (Tonbo 13-6993)
	Mouse Ca^{2+} response assay	1:1000 Ghost dye 780 (Tonbo 13-0865), 1:50 B220 A700 (Tonbo 80-0452), 1:50 CD19 PE-CF594 (BD 562291), 1:50 CD138 PE (BD 553714), 1:50 CD5 APC (BD 550035), 1:50 CD1d FITC (BD 553845), 1:50 IgM BV421 (BD 562595), 1:50 IgD Per-CP-eFluor710 (Invitrogen 46-5993-82), 1.5μM indo-1 (Invitrogen I1223)
	Human Ca^{2+} response assay	1:1000 Ghost dye v450, 1:50 CD45 BUV805 (BD 612891), 1:100 CD3 BV480 (BD 566105), 1:50 IgM APC-Cy7 (Biolegend 314520), 1:50 IgD Alexa Fluor 700 (Biolegend 348229), 1:50 CD1d APC (eBiosciences 17-0016-42), 1:50 CD19 Pe-Cy7 (Tonbo 60-0199), 1:50 CD24 PE-CF594 (BD 555778), 1:50 CD27 PE (Tonbo 50-0279), 1:50 CD5 PerCP-Cy5.5 (eBiosciences 45-0058-42), 1:50 CD38 FITC (BD 340424). 1.5μM indo-1
	BDNF knock out B cells	1:1000 Ghost dye v450, 1:50 CD19 PE-CF594, 1:50 human CD20 PE (BD 560961)
	BDNF-overproducing B cells	1:1000 Ghost dye v450, 1:100 CD45 APC-Cy7, 1:50 CD19 PE
Immuno-histo-chemistry	-	1:200 DCX (Santa Cruz sc-271390), 1:200 B220 (eBioscience 14-0452-81), anti-mouse biotinylated (Vector BP-9200), anti-rat biotinylated (Vector BA-4000)
Immuno-fluoresce-nce	-	1:500 MAP2 (ThermoFisher MA5-12826), 1:200 B220 (eBioscience 14-0452-81), 1:100 GluN2A (NeuroMAB 75-288), 1:100 GluN2B (NeuroMAB 75-101), 1:1000 Lyve-1 (R&D AF2125), 1:500 donkey anti-Rat 488 (Invitrogen A-21208), 1:500 goat anti-mouse 594 (Invitrogen A-11005), 1:500 donkey anti-goat 594 (Invitrogen A-11058), 1:500 donkey anti-goat 647 (Invitrogen A-21447), 1:500 DAPI (Invitrogen D-1306)
Western Blot	-	1:1000 BDNF (abcam ab108319), 1:10,000β-actin (SIGMA A228), 1:500 anti-mouse HRP (Santa Cruz sc-2302), 1:500 anti-rabbit HRP (Santa Cruz sc-2030)

Table 5 - qPCR Gene Primers		
Gene	**Primer Sequence**	**Product size**
Ubiquitin-C	F: 5'- GCC CAG TGT TAC CAC CAA GA -3' R: 5'- CCC ATC ACA CCC AAG AAC A -3'	104bp
BDNF	F: 5'- CTG CCT TGA TGT TTA CTT TGA CAA G -3' R: 5'- GCA ACC GAA GTA TGA AAT AAC CAT AG -3'	106bp
IL-10	F: 5'- TTG GAA TTC CCT GGG TGA GAA -3' R: 5'- GGA GAA ATC GAT GAC AGC GC -3'	68bp
TrkB	F: 5'- GGA AGG ATC AGA GAC AGA TCT CC -3' R: 5'- CTC GTA GTA GAC TCC AGG CCG -3'	59bp
$p75^{NTR}$	F: 5′- CCC TCA AGG GTG ATG GCA ACC TCT -3′ R: 5′- TGT CAG CTC TCT GGA TGC GTC GC -3′	246bp
GluN2A	F: 5'- GAG AAT TTC CGC AAG GGG GA -3' R: 5'- TCC GAG GGA CAT CTC CCA AT -3'	135bp
GluN2B	F: 5’- GTG AGG TGG TCA TGA AGA GG -3’ R: 5’- GCT AGG CAC CGG TTG TAA C -3’	274bp
CREB	F: 5′- TCA GCC GGG TAC TAC CAT TC -3′ R: 5′- TTC AGC AGG CTG TGT AGG AA -3′	196bp
CREM	F: 5'- TTT CCT CTG ATG TGC CTG GT -3' R: 5'- CCC GTG CTA GTC TGA TAT ATG C -3'	119bp

CHAPTER THREE

Results

B CELLS MIGRATE TO BRAIN REGIONS OUTSIDE THE ISCHEMIC INFARCT TO SUPPORT POST-STROKE PLASTICITY

3.1 Introduction

The spinal cord and brain, including the brain regions regulating motor and cognitive function (e.g., olfactory areas [25, 26], motor cortex [27, 28], hippocampus [25, 26, 29], and cerebellum [30, 31]), undergo significant neuroplasticity after stroke to reinnervate injured areas and reorganize neural networks supporting recovery [205-210]. While neuroplasticity occurring within the ipsilesional hemisphere can improve functional outcome [207, 211-213], bi-hemispheric plasticity in the contralesional hemisphere also supports recovery [198, 214-217]. Furthermore, global changes, including angiogenesis, neurogenesis, gliosis, upregulation of growth factors, and neuroinflammation, have a significant impact on post-stroke neuroplasticity [218]. While our understanding of whole-brain neuroplasticity following stroke is ever-evolving, few studies investigate neuroinflammation in reorganizing brain regions.

The adaptive immune system is pivotal to stroke recovery, as it can both mediate and ameliorate neuropathology depending on the lymphocyte population, location, and timing of activation [118, 119]. While antibody-producing B cells contribute to long-term (i.e., months) post-stroke cognitive deficits and dementia in mice [127, 219], an increase of acute interleukin (IL)-10-producing B cells coincides with reduced inflammation and neurological damage up to 96 hours after stroke [120-123]. On the other hand, our studies show that long-term, systemic B

cell depletion impedes neurogenesis, increases anxiety, and exacerbates memory deficits in mice after stroke [166]. Although these deficits generally occur in remote brain regions outside the ischemic infarct, the spatial distribution of B cells within the post-stroke brain has never been investigated.

Many studies that characterize the presence and persistence of immune cells in the post-stroke brain primarily rely on flow cytometry, a technique that requires the dissociation of brain tissue, and therefore, the loss of information on spatial dynamics of immune cell diapedesis. Even studies that use spatially-sensitive techniques, such as immunohistochemistry, often overlook the possibility of recruitment of immune cells into remote brain areas. Given that immune cells can either ameliorate [120-123] or exacerbate stroke-induced neuronal injury through the secretion of cytokines and growth factors [220], it is possible that region-specific immune responses in remote areas of the brain could affect post-stroke plasticity. This highlights the need to understand where plasticity and inflammation occur in the brain after stroke, and whether the two phenomena are interconnected. Moreover, location and timing are particularly relevant as recovery of lost function in stroke patients depends on functional plasticity in areas outside of the infarct (i.e., remote areas) to subsume lost function [9].

To better understand how B cells impact post-stroke plasticity with respect to their migration within the post-stroke brain, male mice were given a transient middle cerebral artery occlusion (tMCAo) and randomly assigned to experimental groups that would either receive serial intravenous (i.v.) tail injections of either PBS or adoptively transferred e450-labeled B cells. The integration of the donor cells within recipient mice was first assessed using flow cytometry. We then used serial two-photon tomography (STPT [183, 187, 221-224]) a block-

face automated imaging technique, to acquire volumetric image datasets of the e450-labeled cells throughout the entire mouse brain. A custom-developed image analysis pipeline incorporating 1.) supervised machine learning-based methods to isolate relevant fluorescent signals of interest, and 2.) registration of the images into the Allen Institute Common Coordinate Framework version 3.0 (CCF 3.0) was then employed to quantify the migration of e450-labeled B within the post-stroke brain. These studies were also replicated using e450-labeled $CD8^+$ T cells, an inflammatory lymphocyte that predominantly migrates into the ischemic core and exacerbates stroke pathology [89-91]. This allowed for the comparison of migration patterns between pro-inflammatory (i.e., $CD8^+$ T cells) and neurotrophic (i.e., B cell) immune cells within the post-stroke brain.

3.2 Results

3.2A Donor lymphocytes successfully integrate into secondary lymphoid organs of post-stroke recipient mice

Prior to assessing the presence and distribution of purified e450-labeled donor $CD19^+$ B cells or $CD8^+$ T cells within the recipient mouse brain, we assessed the presence and viability of either lymphocyte population within secondary lymphoid organs of recipient mice (**Fig. 21A**) [166, 225]. Viable $e450^+$ B cells were identified by flow cytometry in either cohort of mice (i.e., B cell-depleted or B cell-sufficient cohorts) in both the cervical lymph nodes and spleen of B cell-recipient mice 4 days after stroke (**Fig. 21B-E**), confirming the presence of live B cells following adoptive transfer. While the percent of $e450^+$ B cells within the $CD19^+$ B cell population was greatly diminished in the presence of endogenous B cells **(Fig. 21F)**, the cell

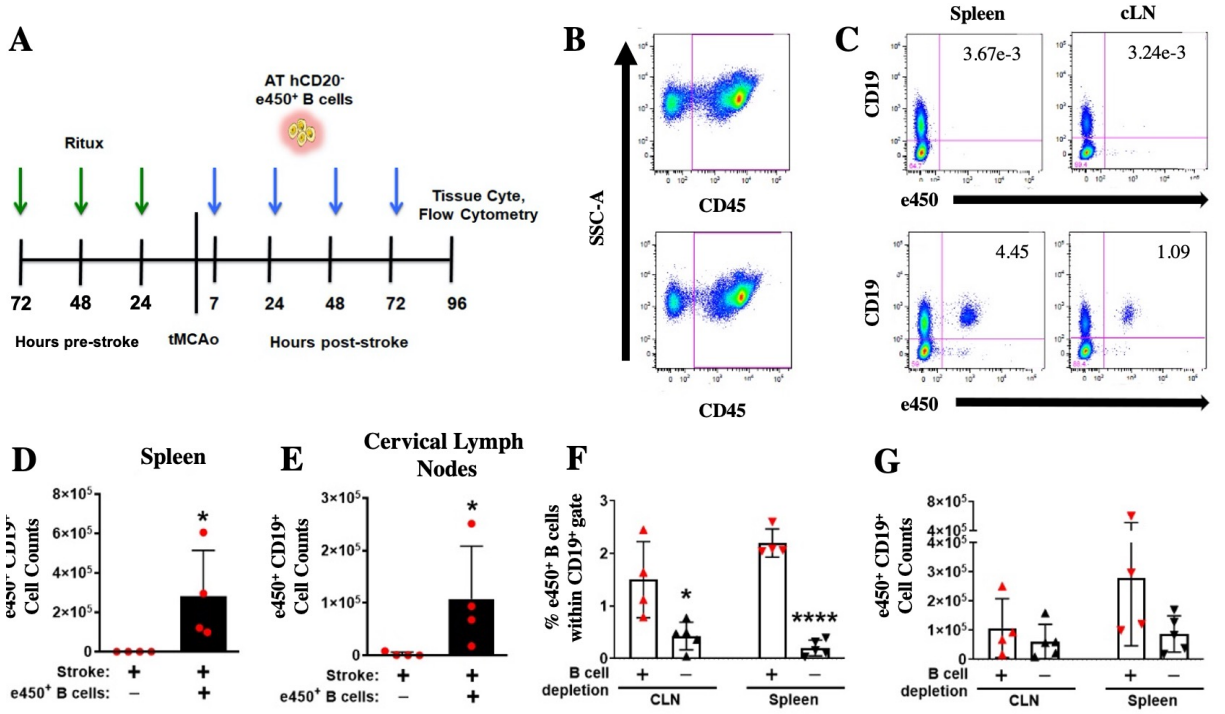

Fig. 21 Verification of live e450-labeled CD19⁺ B cells in recipient mice. (A) Timeline for B cell depletion prior to a transient middle cerebral artery occlusion (tMCAo), with adoptive transfer (AT) of e450-labeled B cells). **(B)** Flow plots of CD45⁺ leukocyte populations originating from a live (Ghost dye⁻) parent gate in PBS-treated (top row) and e450⁺ B cell-treated (bottom row) mice. **(C)** CD19⁺ B cells (y axes) labeled with e450 (x axes) are only in the spleens (left column) and cervical lymph nodes (cLN; right column) of B cell recipients (bottom row) and not PBS recipients (top row). Cell counts for **(D)** splenic and **(E)** CLN e450⁺ B cells in each B cell-depleted recipient mouse (red circles). **(F, G)** Confirmation of e450⁺ B cells in B cell-depleted mice (red triangles) compared to B cell-sufficient mice (black triangles). The **(F)** percent representation and (**G**) cell counts of e450⁺ B cells in the presence or absence of endogenous B cells. Significance determined by Student's *t*-test (**p<0.05*, *****p<0.0001* compared to PBS controls or B cell-depleted cohorts). An n=1 experimental replicate was performed totaling an n=4-5 mice per group.

numbers of e450⁺ B cells in both B cell-depleted and B cell-sufficient recipients, were similar **(Fig. 21G).** Additionally, in pilot experiments where e450-labeled donor B cells were serially injected into the ventricles of the brain instead of intravenously (i.v.) through the tail vein, e450⁺ B cells were also found in the cervical lymph node and spleen tissues of recipient mice 4 days after stroke (*data not shown as cohort analysis is still underway*), demonstrating the ability of B

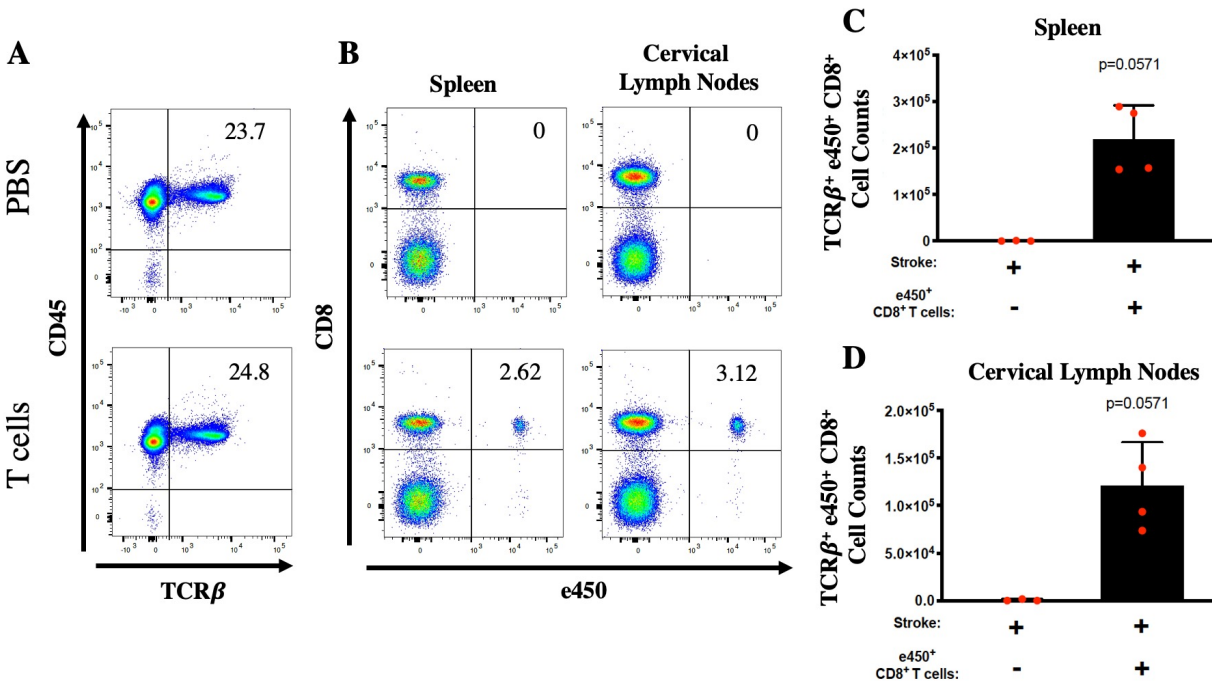

Fig. 22 Verification of live e450-labeled CD8⁺ T cells in recipient mice. Unlike Fig. 16A, CD8⁺ T cell-recipient cohorts did not receive rituximab injections prior to stroke or serial adoptive transfers. (**A**) Flow plots show CD8⁺ T cell populations (x axis) from CD45⁺ leukocyte populations (y axis) for e450⁺ CD8⁺ cell-treated (top row) and PBS-treated (top row) mice. (**B**) CD8⁺ T cells (y axes) labeled with e450 (x axes) are only in the spleens and cervical lymph nodes (CLN) of T cell recipient mice (bottom row). Quantification of cell numbers show e450⁺ CD8⁺ T cells only in the (**C**) spleen and (**D**) cervical lymph nodes in recipient mice (right column). Trending significance determined by Student's *t*-test. An n=1 experimental replicate was performed totaling an n=4-5 mice per group.

cells within the central nervous system (CNS) to migrate outward into the periphery. We also confirmed the presence of viable e450-labeled CD8⁺ T cells in the spleen and cervical lymph nodes of T cell recipient mice (**Fig. 22A, B**), represented both by percentage and cell number (**Fig. 22C, D**).

3.2B STPT identifies a bilateral migration pattern of B cells in the post-stroke brain

We previously observed B cell infiltration into the brain following stroke [97, 182]. Given that B cells support motor and cognitive function after stroke [166], we wanted to determine whether B cells infiltrate brain areas favorable to post-stroke plasticity. We established a custom

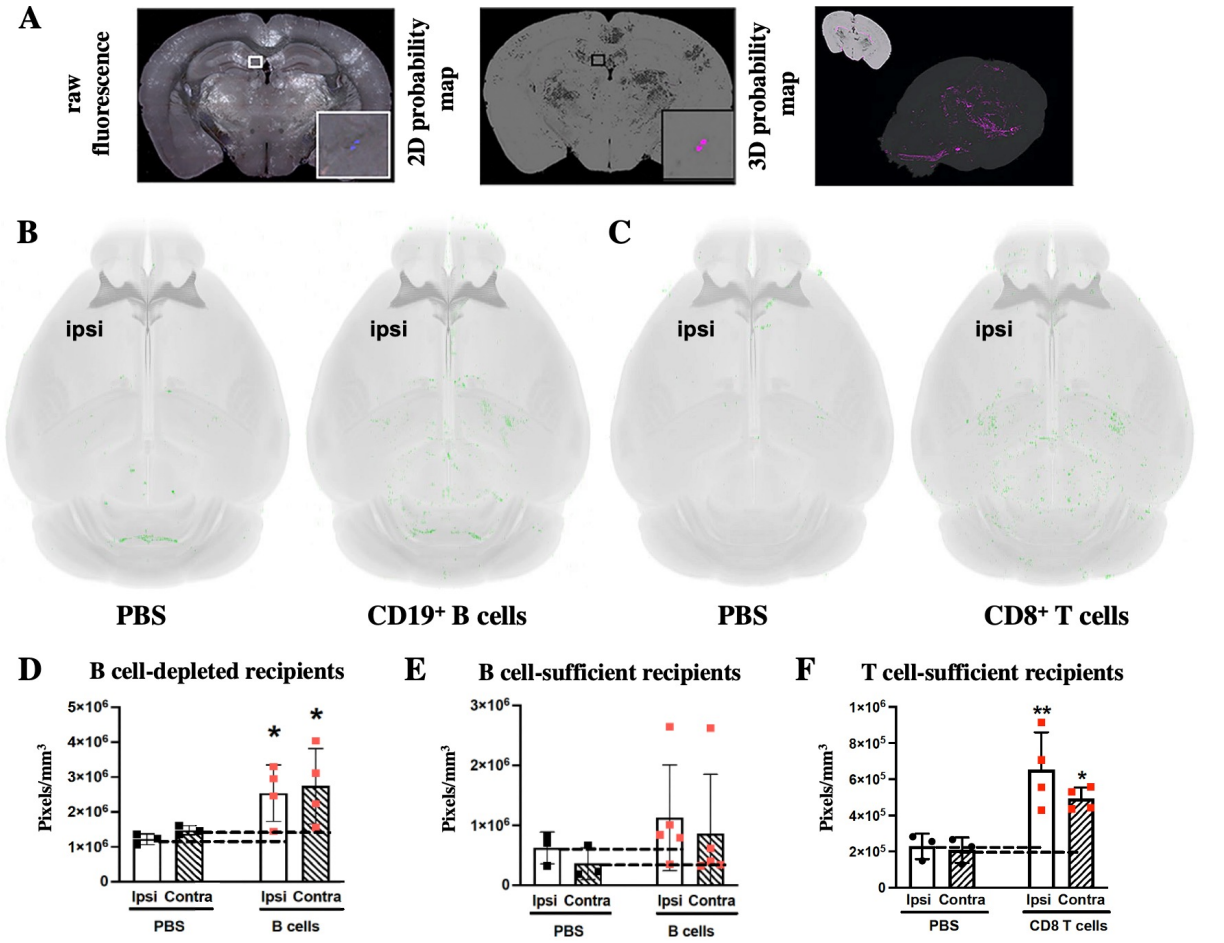

Fig. 23 Establishing whole-brain quantification of neuroinflammation using STPT. (A) Representative coronal section image acquired via STPT shown as a multi-channel raw fluorescence merged image (left panel). Inset shows e450-labeled B cells present in the hippocampus (blue). Middle panel shows the corresponding 2D probability map from the same coronal section in which the trained machine learning algorithm classified pixels likely to represent brain parenchyma (grey) and e450-labeled B cells (magenta). Right panel shows a 3D probability map of the B cell and parenchyma probability maps for each section in the whole brain. (**B** and **C**) The 3D probability maps of e450-labeled cells are shown in green and are overlaid onto the average template from the atlas shown in greyscale. Ipsilesional (ipsi) hemisphere is identified. Whole brain images show a representative brain from **(B)** PBS- (left) and CD19^{+} B cell-recipient (right) or (**C**) PBS- (left) and CD8^{+} T cell-recipient (right) cohorts. **(D)** Whole hemisphere e450^{+} fluorescence (in pixels/mm^{3}) is shown for hCD20^{+}-depleted mice that received PBS (black squares) or B cells (red squares). Dashed lines show mean PBS fluorescence that is used for normalization. **(E** and **F)** Similar to (**D**), showing fluorescence in C57Bl/6J mice that received (**E**) PBS or B cells or (**F**) but without depletion of endogenous lymphocytes. Significance determined by two-way ANOVA (*$p<0.05$, **$p<0.01$ vs. PBS controls*)*. An n=1 experimental replicate was performed totaling an n=3-5 mice per group.

analysis pipeline that utilizes STPT, supervised machine learning-based pixel classification, and image registration to visualize and quantify adoptively transferred e450- labeled B cells throughout the whole mouse brain. The output of our machine learning-based pixel classification step is visualized as a probability map of pixels automatically detected by the trained algorithm as B cells (**Fig. 23A**) [224]. The brighter the area in the probability map, the more likely the trained algorithm identified the fluorescence as a B cell. To account for endogenous post-stroke autofluorescence secondary to ischemic injury and cell death, we included PBS recipient cohorts. STPT detected signal from fluorescent $e450^+$ donor B cells in both the ipsilesional and contralesional hemispheres of B cell-depleted recipient mice ($p<0.05$ for both hemispheres vs. PBS; **Fig. 23B, D**). To determine whether endogenous B cells impact the degree of adoptively transferred B cell detection, we also adoptively transferred naive WT $e450^+$ B cells into post-stroke WT mice that were not B cell depleted. STPT detected $e450^+$ B cells bilaterally throughout the post-stroke brain, however, the $e450^+$ B cell signal was not significantly elevated over PBS controls due to larger within-group fluorescent variation (**Fig. 23E**).

To achieve specific localization of neuroinflammation, raw fluorescent STPT images of every coronal section were registered with the corresponding sections in the CCFv3.0 atlas (**Fig. 24A**) to assess $e450^+$ B cells across brain regions of interest (**Fig. 24B**). Quantification of e450-labeled B cells in whole brain STPT datasets revealed brain regions with significant B cell diapedesis, including ipsilesional cerebral cortex, olfactory areas, and hypothalamus (**Table 6** page 82). Several additional regions exhibited trends (i.e., $p<0.07$) for ipsilesional B cell diapedesis (e.g., striatum, midbrain, cerebellum). Contralesional areas with significant B cell diapedesis included olfactory areas, dentate gyrus, and hypothalamus, revealing a bilateral

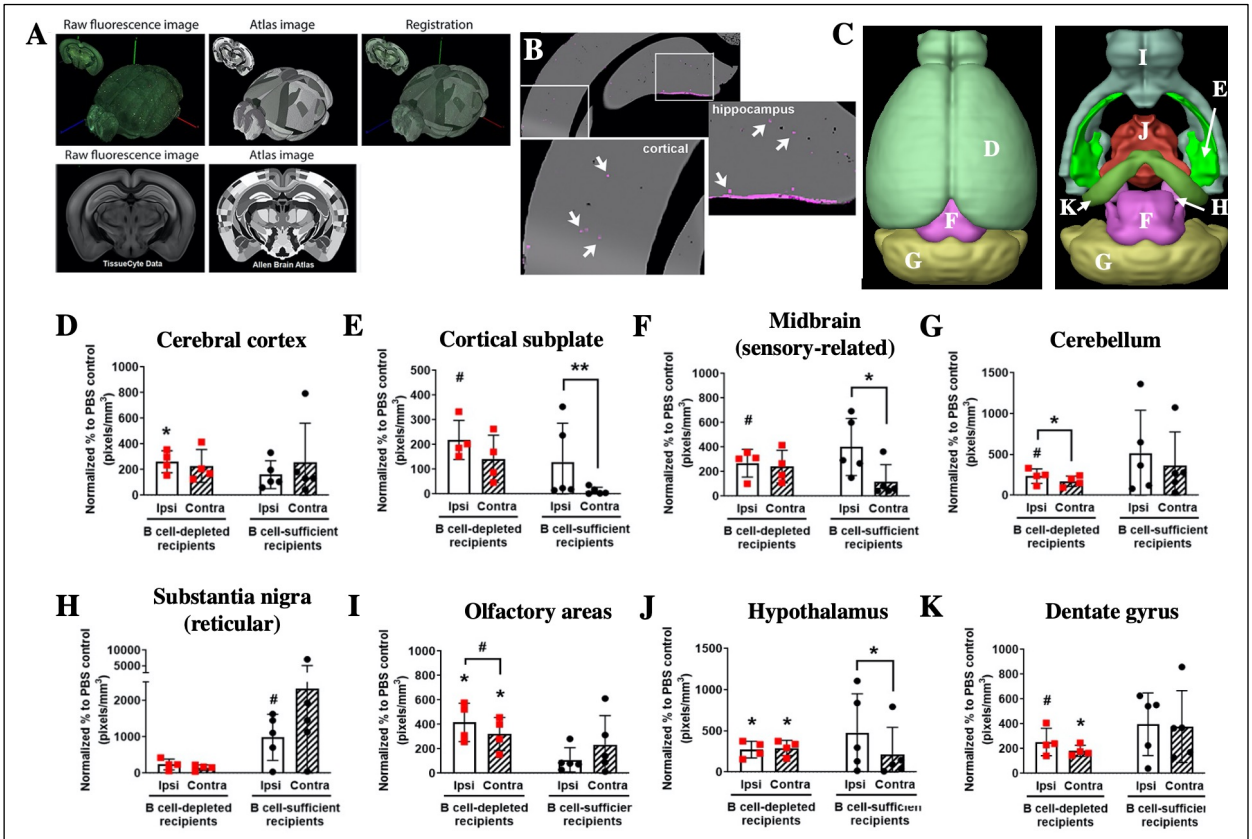

Fig. 24 B cells diapedese into remote motor areas of the brain after stroke. **(A)** Serial two-photon tomography images are co-registered to the Allen Institute CCF3.0 to allow identification of region-specific fluorescence in 3D whole brain probability maps. **(B)** Representative areas classified as e450-labeled B cells via machine learning (punctate magenta dots in the insets, identified by white arrows) that show B cell diapedesis in cortex and hippocampus (enlarged areas indicated by white squares). **(C)** 3D brain renderings created with Brain Explorer (Allen Institute for Brain Science) show regions with bilateral B cell diapedesis after stroke, with areas labeled to the letter corresponding to the data graphs. **(D-K)** Quantification of e450^{+} B cell fluorescence in both B cell-depleted mice (red squares) and mice with endogenous B cells at time of stroke (black circles). Ipsilesional (ipsi, white bars) and contralesional (contra, hatched bars) brain regions show predominantly ipsilesional B cell diapedesis into brain regions related to motor function including **(D)** cerebral cortex, **(E)** cortical subplate, **(F)** midbrain, **(G)** cerebellum and **(H)** substantia nigra. Brain explorer 3D rendering also shows B cell diapedesis in regions related to cognitive function, including **(I)** olfactory areas, **(J)** hypothalamus, and **(K)** dentate gyrus, as indicated by letter in the figure. Both B cell-depleted mice (red squares) and mice with endogenous B cells at time of stroke (black circles) show B cell diapedesis in ipsilesional (ipsi, white bars) and contralesional (contra, hatched bars) brain regions. Fold-change (y-axes) and significance vs. PBS controls unless indicated by brackets. Significance determined by two-way ANOVA (*$^{\#}p<0.06$, *$p<0.05$, **$p<0.01$* vs. PBS controls unless otherwise indicated by brackets). An n=1 experimental replicate was performed totaling an n=4-5 mice per group.

diapedesis pattern of B cells into brain regions typically spared in tMCAo-induced injury but that nonetheless mediate motor and cognitive recovery, as well as active neurogenesis.

B cell diapedesis was elevated in 5 brain regions associated with motor function (i.e., cerebral cortex, cortical sub-plate, midbrain (sensory-related), cerebellum, and substantia nigra pars reticulata – as outlined in the introduction) and 3-4 brain regions associated with cognitive function (i.e., olfactory areas, dentate gyrus, substantia nigra, and hypothalamus [226, 227] – as outlined in the introduction) in B cell-depleted mice. The areas of significant B cell diapedeses are illustrated in 3D renderings created in the Allen Institute for Brain Science Brain Explorer application (**Fig. 24C**). All areas had a similar magnitude of $e450^+$ B cell signal (100-200-fold higher than PBS fluorescence), with either significant (cerebral cortex, $p<0.05$; **Fig. 24D**) or trending (cortical subplate, midbrain, and cerebellum; all $p<0.07$ vs. PBS; **Fig. 24E-G**) ipsilesional signals. Ispilesional B cell diapedesis was only significantly higher compared to the contralesional hemisphere in the cerebellum ($p<0.05$; **Fig. 24G**). In contrast, B cell-sufficient mice exhibited higher laterality for ipsilesional diapedesis, with more $e450^+$ B cell signal localized to the ipsilesional cortical subplate ($p<0.01$; **Fig. 24E**) and midbrain ($p<0.05$; **Fig. 24F**). Interestingly, one motor region, the substantia nigra pars reticulata, had much higher B cell diapedesis (1000-2000-fold vs. PBS) in the mice with endogenous B cells versus B cell-depleted mice (**Fig. 24H**), with highest values in the contralesional hemisphere. On the other hand, all brain regions associated with cognitive function, apart from the substantia nigra, showed high bilateral $e450^+$ B cell signal. Diapedesis of adoptively transferred B cells into the olfactory areas and hypothalamus of B cell-depleted mice was significant for both the ipsi- and contralesional hemispheres (both $p<0.05$ vs. PBS; **Fig. 24I, J**). The dentate gyrus is unique in that $e450^+$ B cell

signal was significant in the *contra*lesional hemisphere ($p<0.05$; **Fig. 24K**), while only trending ($p=0.06$) in the ipsilesional hemisphere. Both the olfactory areas and hypothalamus also exhibited increased signal in ipsi- vs. contralesional hemispheres, though the latter, surprisingly, is in the B cell-sufficient cohort. In summary, these data show that in a mouse devoid of B cells, adoptively transferred B cells migrate to the motor and cognitive areas with a similar magnitude in both the ipsi- and contralesional hemispheres, possibly exerting a supportive role in functional recovery.

3.2C STPT identifies a predominant ipsilesional migration pattern of $CD8^+$ T cells in the post-stroke brain

Several studies confirm the migration of cytotoxic $CD8^+$ T cells into the post-stroke brain and their role in exacerbating pathology [85, 89, 90]. However, these studies performed little-to-no examination of specific brain regions targeted by these cells outside of the area of injury. Therefore, we used our custom analysis pipeline to identify the region-specific migration patterns of $CD8^+$ T cells in the post-stroke brain. As seen with $CD19^+$ B cells, STPT similarly identified $e450^+$ $CD8^+$ T cells throughout the whole brain ($p<0.05$ for both hemispheres vs. PBS; **Fig. 23C, F**) and interestingly, along the meninges (Supplemental Video 9, 10 in reference [181]) of post-stroke recipient mice.

$CD8^+$ T cell diapedesis occurred throughout the brain, including ipsilesional somatosensory cortices (SS; **Fig. 25A-C**) and sensory-related midbrain regions (MBsen). $CD8^+$ T cells migrated with greater diapedesis apparent in the ispilesional hemisphere compared to the contralesional hemisphere. $CD8^+$ T cells targeted the ipsilesional primary and secondary

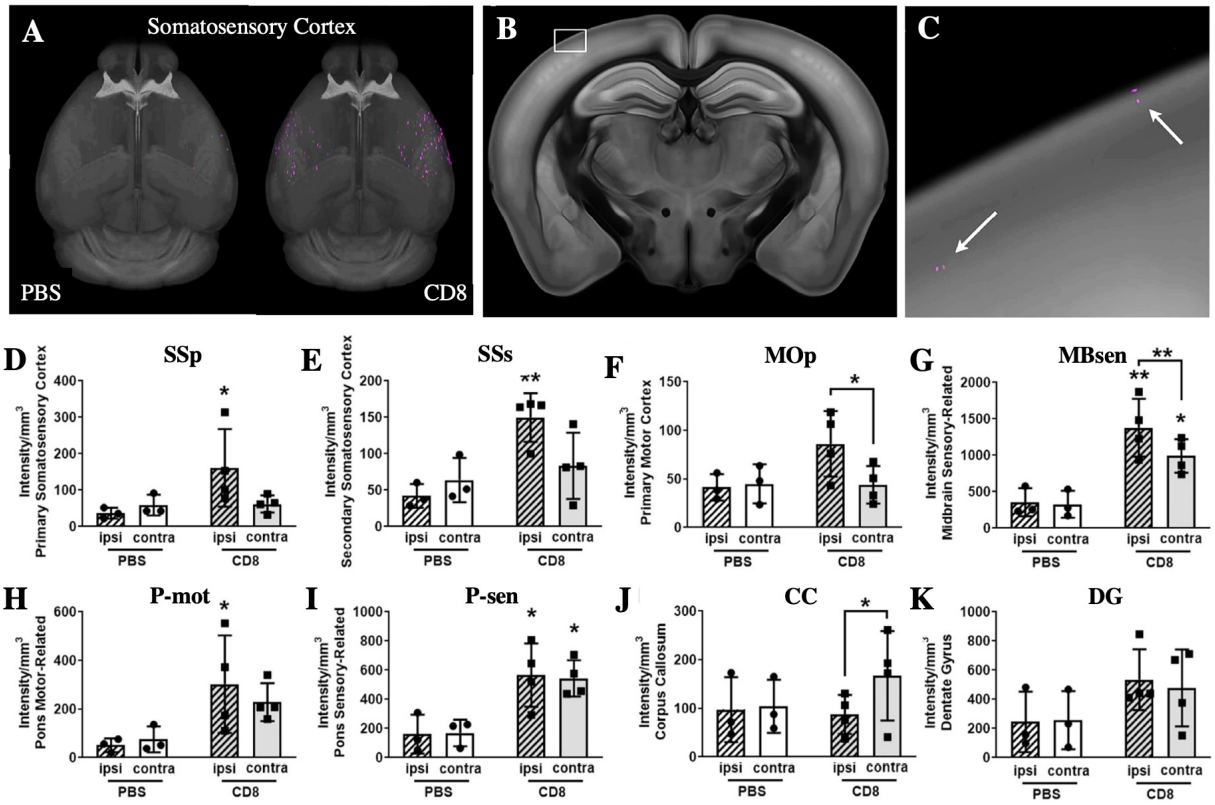

Fig. 25 Visualization of the quantification of CD8$^+$ T cell diapedesis in the whole brain after stroke. (**A**) Masked 3-D probability map images exclusively of somatosensory areas from PBS- (left brain) or CD8-recipient animals (right brain) are overlaid onto the CCFv3.0 average template (grey) to show pixels classified as CD8$^+$ T cell (magenta) that diapedesed into somatasensory areas. (**B**) Coronal section with white box highlighting part of the primary somatosensory area from the brain shown in A, with (**C**) enlargement of white boxed area showing several magenta areas classified as CD8$^+$ T cells (white arrows). (**D-K**) Bar graph shows ipsilesional (hatched bars) and contralesional (plain bars) diapedesis into selected regions in CD8-recipient mice (black squares, right columns) and PBS controls (black circles, left columns). Ipsilesional CD8$^+$ T cell diapedesis also occurs in (**D**) primary somatosensory, (**E**) secondary somatosensory, (**F**) primary motor, (**G**) MBsen, and (**H**) motor-related pons. (**I**) Sensory-related pons exhibits bilateral diapedesis, while (**J**) the corpus callosum is predominantly contralesional. (**K**) There is no significant CD8 T cell diapedesis into the dentate gyrus. Significance was determined by two-way ANOVA (*$p<0.05$, **$p<0.01$ vs. PBS control unless otherwise indicated by brackets). An n=1 experimental replicate was performed totaling an n=3-4 mice per group.

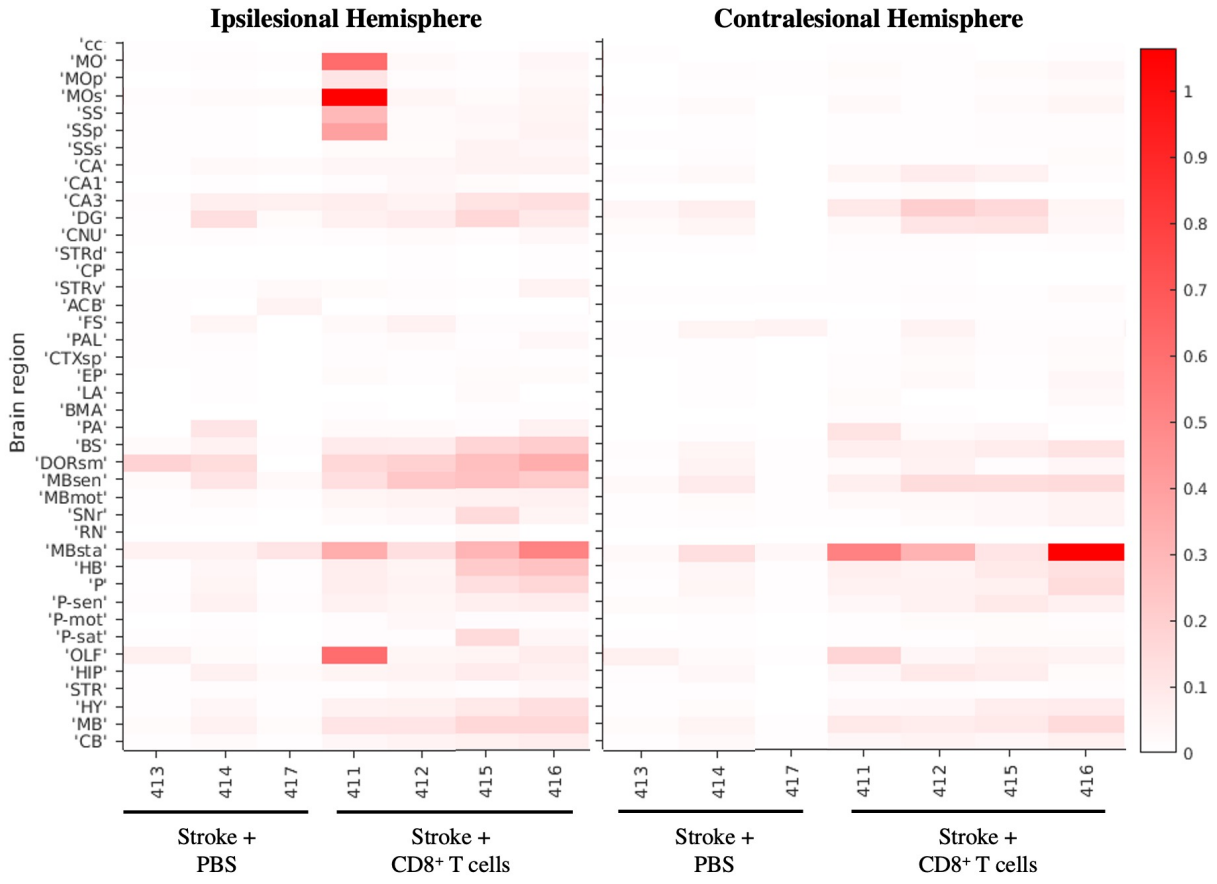

Fig. 26 Heat map of CD8$^+$ T cell diapedesis in cortical and other areas. The signal intensities for pixels classified via machine learning as e450-labeled CD8$^+$ T cells in various cortical and other brain areas are shown for stroke-injured PBS- or CD8$^+$ T cell-recipient mice in both the ipsilesional (left panel) and contralesional hemisphere (right panel). Each brain area analyzed is listed on the left Y-axis according to the nomenclature used in the CCFv3.0 and individual animals (animal ID, x-axis) are grouped by PBS and T cell injected cohorts. The intensity scale is shown on the right Y-axis and corresponds to the number of pixels classified as CD8$^+$ T cells normalized per region volume (pixels/mm^3). (cc – corpus callosum; MO – somatomotor areas; MOp – primary motor cortex; SS – somatosensory areas; SSp – primary somatosensory cortex; SSs – secondary somatosensory cortex; CA – Ammon's horn, CA1 – field CA1; CA3 – field CA3; DG – dentate gyrus; CNU – cerebral nuclei; STRd – striatum, dorsal region; CP – caudate putamen; STRv – striatum, ventral region; ACB – nucleus accumbens; FS – fundus of the striatum; PAL – pallidum; CTXsp – cortical subplate; EP – endopiriform nucleus; LA – lateral amygdalar nucleus; BMA – basomedial amygdalar nucleus; PA – posterior amygdalar nucleus; BS – bed nuclei of stria terminalis; DORsm – thalamus, sensory motor-related; MBsen – midbrain, sensory-related; MBmot – midbrain, motor-related; SNr – substantia nigra, reticular part; RN – red nucleus; MBsta – midbrain, behavioral state-related; HB – hindbrain; P – pons; P-sen – pons, sensory-related; P-mot – pons, motor-related; P-sat – pons, behavioral state-related; OLF – olfactory areas; HIP – hippocampal region; STR – striatum, HY – hypothalamus, MB – midbrain, CB – cerebellum). An n=1 experimental replicate was performed totaling an n=3-4 mice per group.

somatosensory cortex, with significantly more cells detected in the ipsilesional primary somatosensory cortex (SSp; $p<0.05$ compared to PBS controls; **Fig. 25D**) and secondary somatosensory cortex (SSs; $p<0.01$; **Fig. 25E**). The ipsilesional primary motor cortex (MOp) was also infiltrated by $CD8^+$ T cells, with more cells in the ipsilesional MOp than the corresponding contralateral MOp ($p<0.05$; **Fig. 25F**). Given the nature of a tMCAo injury, which encompasses motor and sensory cortices, it is likely these cells were targeting regions damaged by the stroke. In addition to these motor and sensory cortical regions, there was bilateral movement of $CD8^+$ T cells into remote brain regions also associated with motor and sensory function, namely the midbrain (**Fig. 25G**) and the pons (**Fig. 25I**). One region, the corpus callosum (cc), exhibited higher contralesional $CD8^+$ T cell diapedesis compared to ipsilesional cc ($p<0.05$; **Fig. 25J**). $CD8^+$ T cells did not significantly infiltrate behavioral-state related regions in either the midbrain, the pons (*data not shown*), or the hippocampus (**Fig. 25K**). Our custom analysis pipeline allowed us to generate a heat map with 41 brain regions that were pre-selected as regions of interest for immune cell diapedesis (**Fig. 26**). These heat maps allow for the comparison of the fluorescence intensity of e450-labeled $CD8^+$ T cells across multiple brain regions, between groups and animals. As expected, the PBS group showed low fluorescent signal in many of the brain regions, although "background" fluorescence was detected, potentially due to increased autofluoresence in dead or injured ischemic tissue secondary to the tMCAo model [181]. Additionally, some variability was observed in the amount of CD8 diapedesis between animals of the T cell-recipient group, with high diapedesis into two brain regions in particular: the behavioral state-related midbrain (MBsta) and sensory motor-related thalamus (DORsm). Overall, $CD8^+$ T cells migrated into many areas of the brain of all animals four days after stroke,

with greater diapedesis apparent in the ipsilesional hemisphere compared to the contralesional hemisphere.

3.3 Conclusions

It is well-established that immune cells infiltrate the brain and traffic to infarct and peri-infarct areas after stroke. However, the diapedesis of immune cells into remote brain regions supporting post-stroke functional recovery has never been characterized in 3-D, making these **s**tudies the first to quantify whole-brain B cell and $CD8^+$ T cell diapedesis after stroke. Our work establishes STPT as a reliable method to quantify whole brain neuroinflammation after stroke and further understand region-specific mechanisms of injury and repair.

We identified distinct differences in the migration patterns of B cells and $CD8^+$ T cells within the post-stroke brain (**Fig. 27**). The surprising increase of B cells in the contralesional hemisphere 4 days after stroke indicates that B cell diapedesis is not only localized to infarct and peri-infarct areas with high cytokine and chemokine upregulation [97], but also occurs in remote brain regions that support neurogenesis and motor and cognitive recovery after stroke in young male mice. Conversely, $CD8^+$ T cells preferentially diapedese into the ipsilesional hemisphere compared to the corresponding contralesional brain regions, targeting both sensory- and motor-related regions that are negatively impacted by stroke, and potentially further exacerbate injury through their cytotoxic functions. While our STPT data define the migration patterns of B cells and $CD8^+$ T cells in the post-stroke brain, they cannot determine the route of diapedeses (i.e., circulation vs. the ventricles vs. the meninges [179, 180]) into targeted brain regions after stroke. In fact, we discovered B cells (**Fig. 28**) and $CD8^+$ T cells (Supplemental Video 9, 10 from

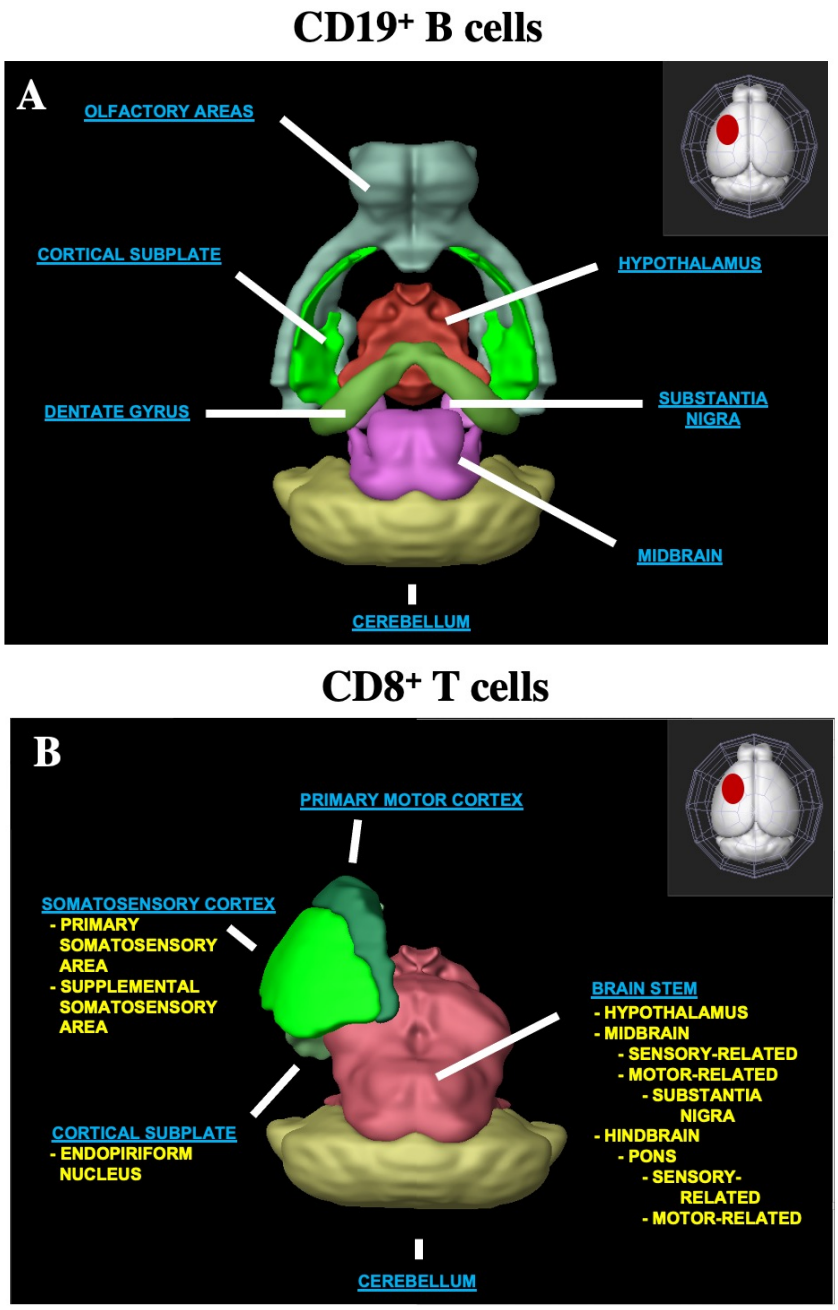

Fig. 27 CD19$^+$ B cells and CD8$^+$ T cells exhibit distinct migration patterns in the brain after stroke. 3D brain renderings created with Brain Explorer (Allen Institute for Brain Science) with insets in the top right corners to denote the ipsilesional hemisphere with a red oval. 3D renderings summarize the regions of (**A**) bilateral CD19$^+$ B cell migration (*Cerebral cortex not shown)* and (**B**) predominantly ipsilesional CD8$^+$ T cell migration in the brain 4 days after stroke. An n=1 experimental replicate was performed totaling an n=3-5 mice per group.

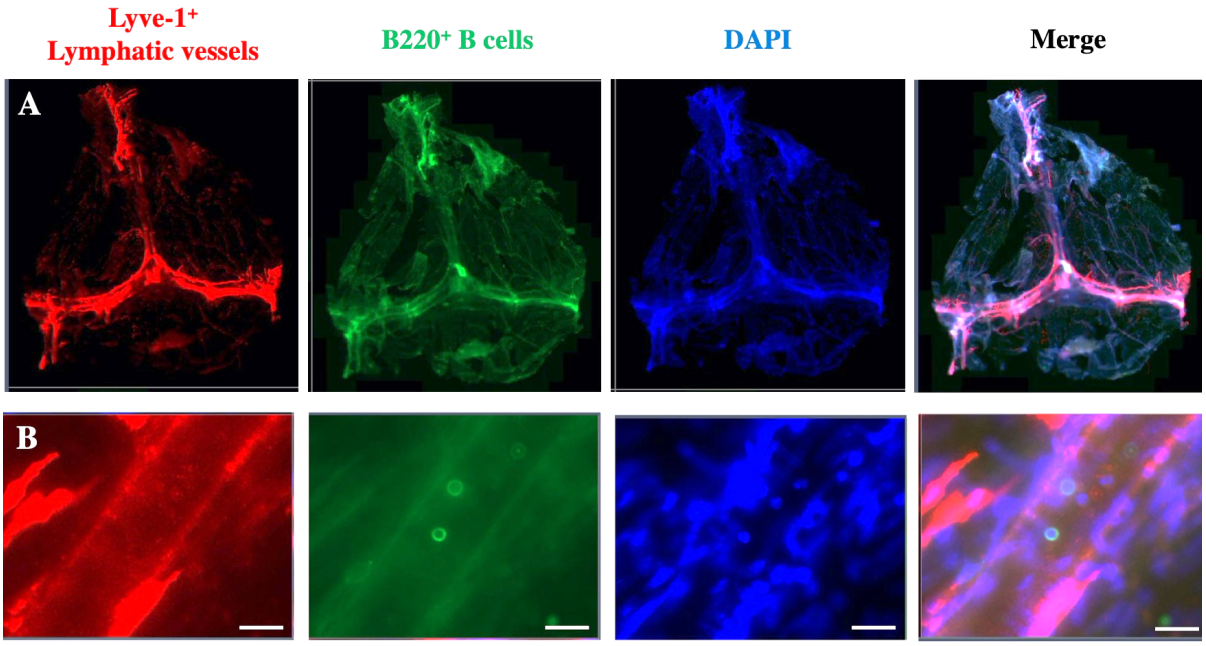

Fig. 28 B220$^+$ B cells are present in the meninges after stroke. Meninges of a mouse 4 days after stroke stained for Lyve-1 (red), B220 (green) and DAPI (blue). Images at (**A**) 20x magnification of the entire brain meninges (top row) with (**B**) zoomed-in inserts (bottom row) to show B220$^+$ B cells within Lyve-1$^+$ meningeal lymphatic vessels. Right column shows a merged composite of all channels. Scale bar 50µm. An n=1 experimental replicates was performed totaling an n=3 mice.

reference [181]) within the meninges, confirming the possibility of various immune cell entry routes into the post-stroke CNS.

Taken together, our unbiased mesoscale whole-brain imaging results reveal important information about region-specific neuroinflammation that may be key to developing long-term therapies to promote functional recovery after stroke. Additionally, several brain regions that exhibit bilateral post-stroke B cell migration undergo significant plasticity, which in turn, can impact the extent of post-stroke functional recovery [228]. Therefore, it may be possible that B cells play a key role in supporting region-specific plasticity and functional recovery after stroke.

Table 6 - STPT data for e450^{+} pixels (of e450-labeled B cells) per brain region

		Ipsilesional, mm^3			Contralesional, mm^3			
Brain region	Allen Brain Atlas abbrev-iation	PBS control (n=3)	B cells (n=4)	*P* value	PBS control (n=3)	B cells (n=4)	*P* value	Later-ality index
Gray matter								
Cerebral cortex	CTX	8.6	22.44	**0.025***	11.64	26.62	0.155	0.9
Olfactory areas	OLF	8.05	33.5	**0.019***	10.1	32.46	**0.041***	1.1
Dentate gyrus	DG	26.55	67.45	0.073	30.3	55	**0.028***	1.2
Cerebral nuclei	CNU	4.25	10.62	**0.061**	8.09	18.78	0.202	0.7
Striatum	STR	3.88	9.27	**0.06**	8.16	18.34	0.227	0.6
Striatum ventricular region	STRv	5.26	13.52	**0.06**	12.18	21.09	0.17	0.6
Cortical subplate	CTXsp	2.5	5.46	**0.066**	6.45	9.15	0.514	0.8
Hypothalamus	HY	11.85	32.21	**0.039***	12.35	36.1	**0.020***	0.9
Midbrain sensory-related	MBsen	28.09	75.47	**0.056**	35.38	85.27	0.136	0.9
Cerebellum	CB	10.32	24.14	**0.061**	12.96	22.32	0.128	1.1
White matter								
Corpus callosum	CC	1.29	4.41	0.313	1.98	6.44	0.242	0.8s

STPT, serial two-photon tomography. Significance between PBS and B cell recipients per hemisphere was analyzed by unpaired, parametric. Student's t test: *$P < 0.05$; bolded text, $P \leq 0.06$.

CHAPTER FOUR

Results

B CELLS PROMOTE FUNCTIONAL AND STRUCTURAL PLASTICITY AFTER ISCHEMIC INJURY

4.1 Introduction

Post-stroke neuroplasticity can both impede and augment recovery, with the degree of functional recovery being highly dependent on the brain regions in which plasticity occurs [228, 229]. The hippocampus, a region that undergoes significant bilateral B cell diapedesis after stroke, regulates neurogenesis and various forms of functional recovery that are negatively impacted in post-stroke B cell-depleted mice. The SGZ of the DG within the hippocampus is one of the two regions where neurogenesis occurs in the healthy brain [25]. Stroke, however, is a potent inducer of neurogenesis [167, 168] and several studies suggest that neuroblasts in the SGZ migrate to ischemic-injured areas with the potential to adapt a neuronal phenotype and integrate into existing circuitry [167, 168, 230] that can support recovery. In fact, the success of post-stroke rehabilitative efforts is highly dependent upon stroke-induced neurogenesis to improve motor and cognitive function [231, 232]. However, both neurogenesis and network reorganization after stroke require significant neurotrophic support, such as that of brain-derived neurotrophic factor (BDNF), to promote functional recovery [233].

Low circulating BDNF in stroke patients negatively impacts various forms of post-stroke plasticity ranging from synaptic transmission to motor and cognitive function [234]. For example, stroke patients with reduced bioavailable BDNF resulting from the BDNF Val66Met

polymorphism who receive transcranial direct current stimulation exhibit reduced motor skill learning when compared to non-BDNF Val66Met carrier stroke patients [235]. When dissected further in animal models of stroke, decreased BDNF signaling significantly impairs hippocampal neurogenesis [236-239] and pre- and post-synaptic transmission [240, 241] at both excitatory and inhibitory synapses [242-245]. Structural plasticity is also compromised by decreased BDNF as neurons exhibit a loss of dendritic complexity and synapses [246-249]. Consistent with the aforementioned role of BDNF in hippocampal neurogenesis and structural/functional plasticity, several behavioral studies have also reported hippocampal-related cognitive deficits resulting from decreased BDNF signaling [250-254]. Collectively, these studies show that decreased BDNF signaling, which can result from age-related decline [11], stroke injury [234], or genetic variation [24], greatly interferes with neuronal plasticity. Therefore, it is important to investigate additional sources of endogenous BDNF within the post-stroke brain so that they may be targeted to enhance plasticity and functional recovery after stroke.

The hippocampal-related cognitive impairment we observed in post-stroke B cell-depleted mice led us investigate whether those functional deficits are attributed to a loss of B cell-induced neuroplasticity. We used electrophysiology to assess synaptic transmission within the DG of B cell-depleted mice 2 weeks after inducing a tMCAo. We also generated conditional BDNF-KO and BDNF-overproducing B cells to further dissect the neurotrophic capacity of B cells to promote neuroplasticity following *in vitro* ischemic injury.

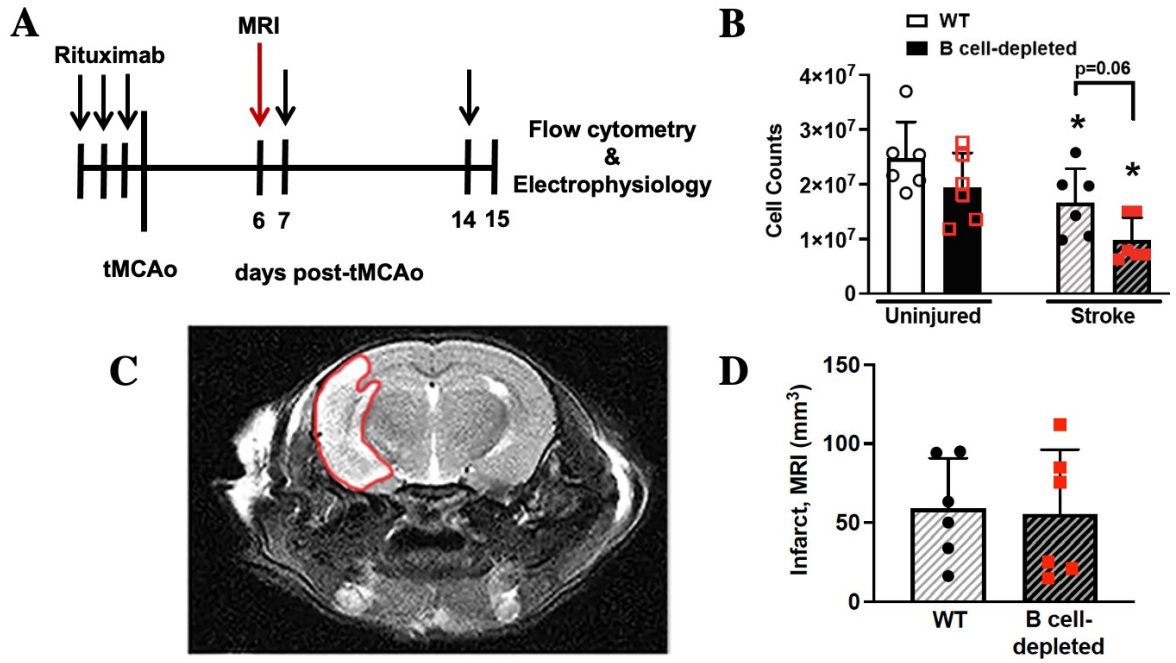

Fig. 29 B cell depletion does not impact infarct size after stroke. (**A**) Experimental timeline for electrophysiology recordings in the dentate gyrus (DG) of B cell-depleted mice after stroke. Uninjured cohorts are solid bar graphs (WT, white; B cell depleted, black) and post-stroke cohorts have hatched bar graphs (**B**) Rituximab ($F_{(1, 20)} = 6.48$, p=0.02) and stroke $F_{(1, 20)} = 13.63$, p=0.001) reduced the number of splenic $CD19^+$ B cells in WT ($hCD20^-$; black closed circles) mice compared to uninjured WT mice (black open circles), with an even greater reduction in post-stroke B cell-depleted mice ($hCD20^+$; red closed squares) compared to uninjured B cell-depleted mice (open red squares). (**C**) Representative MRI image identifying hyper-intense areas (with high water content due to dilated ventricles and edema); the infarcted area is outlined in red within the ipsilesional hemisphere of a mouse brain 6 days after stroke. (**D**) MRI infarct volume quantification of WT and B cell-depleted mice. Significance determined by (B) two-way ANOVA or (D) Student's *t*-test (*$p<0.05$ vs. (B) uninjured or (D) WT control unless indicated by bracket). An n=2 experimental replicated were performed totaling an n=6 mice per group.

4.2 Results

4.2A B cells support long-term synaptic transmission in the dentate gyrus

B cells were recently found to migrate bilaterally into specific remote brain regions after stroke (chapter 3; [166]). Among these regions are highly vascularized areas that are extremely

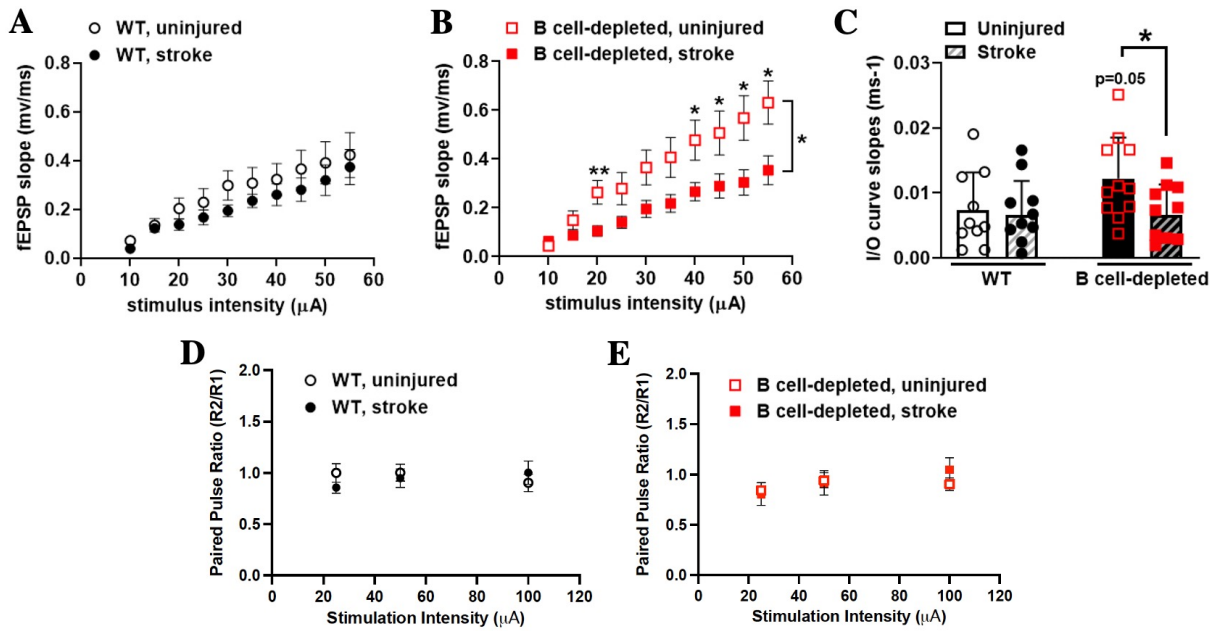

Fig. 30 Stroke reduces synaptic transmission in B cell-depleted mice. Electrophysiology input-output (I-O) curves measuring synaptic transmission at perforant path-DG synapses in uninjured (open symbols) and post-stroke (solid symbols) (**A**) WT and (**B**) B cell-depleted mice. (**C**) Comparison of individual I-O curve slopes (each data point represents slope of the I-O curve from one brain slice). Paired-pulse ratios of perforant path-DG synapses in (**D**) WT and (**E**) B cell-depleted mice. Significance determined by (A, B, D, E) repeated measures or (C) ordinary two-way ANOVA (**p<0.05, **p<0.01* vs. uninjured or WT control unless indicated by bracket). An n=2 experimental replicated were performed totaling an n=6 mice per group with 2-4 slices per mouse.

susceptible to ischemic injury [255] including the hippocampus [256, 257]. While B cells don't impact hippocampal neurogenesis under healthy conditions, stroke-induced neurogenesis is impeded in B cell-depleted young male mice (chapter 3; [166]). Furthermore, under healthy conditions, the absence of B cells negatively impacts hippocampal- and amygdalar-mediated cognitive function, inducing anxiety and memory deficits in mice that are exacerbated after stroke (chapter 3; [166]). These studies suggest B cells support post-stroke neuronal function within remote brain regions involved in regulating cognitive function and neurogenesis after stroke.

To better understand how B cells impact neuronal function, synaptic transmission within the contralesional dentate gyrus (DG) of the hippocampus was assessed in wild-type (WT) and B cell-depleted mice under healthy and 4-days-post-stroke-injured conditions (**Fig. 29A**). Rituximab successfully depleted B cells in the spleens of $hCD20^{+}$ mice when compared to $hCD20^{-}$ (i.e. WT) littermate controls by ~31.5% ($F_{(1, 20)} = 6.48$, p=0.02 (across uninjured and stroke conditions); **Fig. 29B**). T2-weighted magnetic resonance imaging (MRI) scans were performed 6 days after stroke to assess the extent of stroke injury prior to electrophysiological recordings (**Fig. 29C**) and revealed no significant difference in the infarct volume of WT and B cell-depleted mice (**Fig. 29D**). Stroke significantly decreased synaptic transmission in B cell-depleted ($F_{(1, 21)}$=4.96, p=0.37), but not WT mice (**Fig. 30A, B**), consistent with a neuroprotective role of B cells after stroke. Moreover, neither B cell depletion nor stroke affected paired-pulse ratios, suggesting that synaptic release probability is unaffected by these manipulations (**Fig. 30D, E**).

4.2B B cell-derived BDNF provides neuronal protection after *in vitro* ischemic injury

Given that B cells support functional neuroplasticity in the post-stroke brain (Fig. 30), we next assessed the ability of B cells to support structural neuroplasticity following ischemic injury using the *in vitro* oxygen/glucose deprivation (OGD) and NMDA excitotoxicity injury models. Using an *in vitro* approach to determine the direct role of B cells in neuronal protection, mixed cortical cells were subjected to two hours of OGD followed immediately by the addition of naïve B cells at increasing concentrations to the OGD-injured cells for 4 days (**Fig. 31A**). OGD induced significant cell death as the metabolic activity of mixed cortical cell was reduced when compared to uninjured controls (~50%, p<0.001; **Fig. 31B**). Additionally, OGD caused loss of

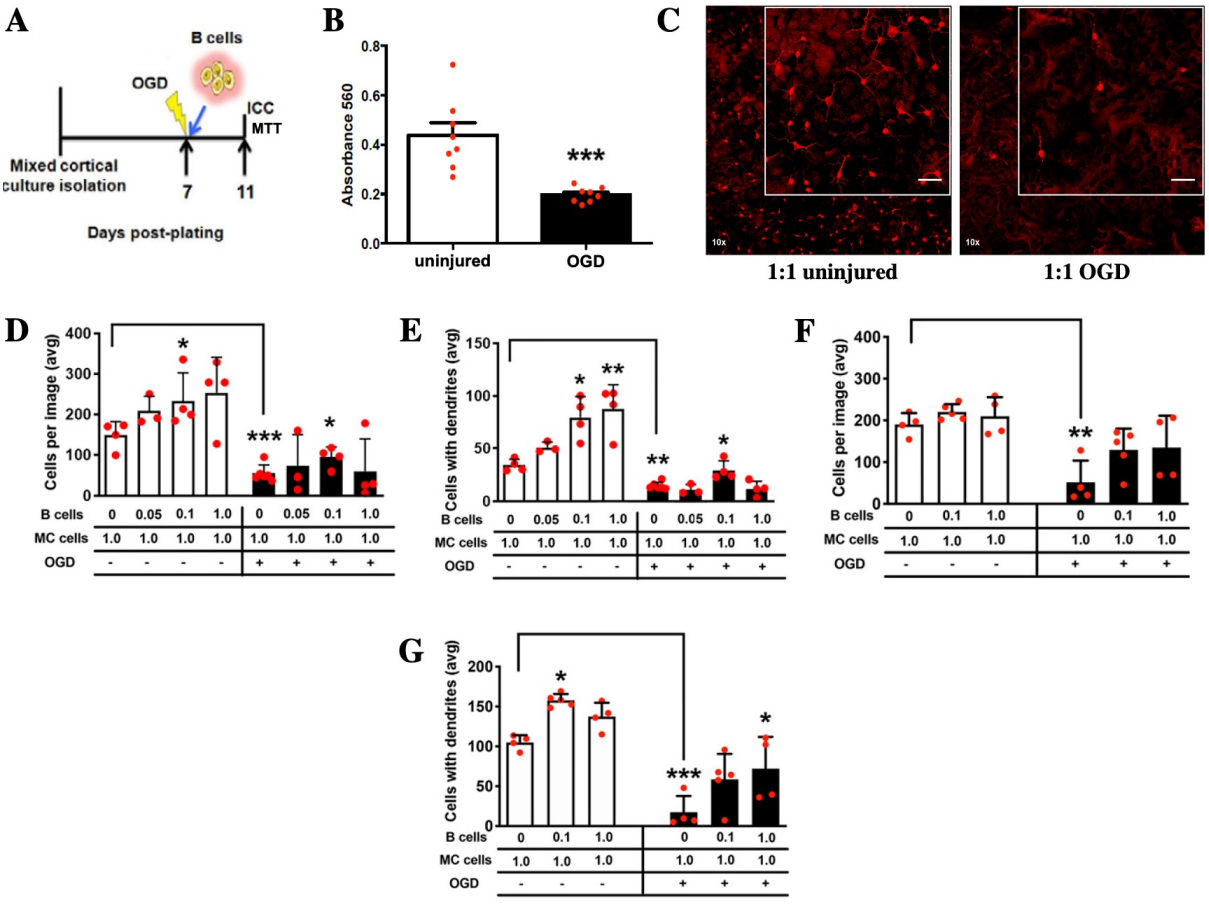

Fig. 31 B cells induce a neurotrophic effect in mixed cortical cultures. (A) Experimental timeline for the co-culture of naïve B cells on oxygen-glucose deprivation (OGD)-injured mixed cortical cells that underwent MTT viability assessment and immunocytochemistry (ICC) after a 4-day co-culture. **(B)** The metabolic activity of viable cells in converting MTT to formazan (absorbance at 560) was reduced in the 'no B cell' OGD-injured mixed cortical cultures **(C)** Images at 10x of microtubule-associated protein $(MAP2)^+$ neurons (red) for treatment groups; higher magnification image is also shown (*inset*) (scale bar = 50µm). **(D)** Increasing ratio of B cells to mixed cortical cells (MC) increased the number of $MAP2^+$ neurons, as well as **(E)** the number of $MAP2^+$ neurons with dendrites in the non-OGD experiments (white bars). OGD (black bars) decreased overall numbers, with only a 0.1:1.0 B cell:mixed cortical cell ratio preserving neuronal survival and dendritic arborization. (**F** and **G**) Experiments were replicated with IL-10-deficitent B cells. IL-10-deficicent B cells (**F**) did not preserve cell survival after OGD, but (**G**) a 1:1 ratio did preserve dendritic arborization after OGD. Replicate, independent experiments (each with interexperimental replicates) are shown by red circles for a total *n*. Data graphed as mean ± SD, and significance determined by nonparametric one-way ANOVA or Student's *t* test (*$p<0.05$, **$p<0.01$, ***$p<0.001$ vs. '0:1.0 no B cell' control unless otherwise indicated by brackets). An n=2-3 experimental replicates were performed.

$MAP2^+$ neurons ($p<0.001$) and loss of arborization in mixed cortical cultures without B cells ($p<0.01$; **Fig. 31D, E**). The co-culture of naïve B cells with cortical cells at a ratio of 1:10 reduced neuronal death and loss of dendritic arborization. In the absence of ischemic injury, naïve B cells promoted the survivability of $MAP2^+$ neurons ($p<0.05$; **Fig. 31D**, white bars) and dendritic arborization ($p<0.05$, 1:10; $p<0.01$, 1:1; **Fig. 31E**) compared to cultures without B cells.

One potential mechanism by which WT B cells exert their neurotrophic effect on uninjured and OGD-injured neurons could be through the production of IL-10. In addition to ameliorating acute post-stroke pathology and inflammation, IL-10 could also induce a direct neurotrophic effect on neurons that are at risk for cell death [86]. Interestingly, the experiments replicated using naïve IL-10-deficient B cells showed no dose-effect response on neuronal survivability with or without OGD. In contrast, IL-10-deficient B cells still preserved dendritic arborization after OGD, albeit at a higher concentration ($p<0.05$; **Fig. 31G**). Increased dendritic arborization also occurred in the absence of OGD with IL-10-deficient B cells ($p<0.05$), suggesting that IL-10 is a redundant mechanism of B cell-mediated neurotrophic support that promotes the maintenance of mature neurons with dendrites. In summary, these data confirm the capacity of naïve B cells to directly exert neuronal protection *in vitro*, in part, by an IL-10-independent mechanism within the context of ischemic neuronal injury.

To further dissect the IL-10-independent mechanism by which WT B cells exert neuroprotection against *in vitro* ischemic injury, we assessed the understudied capacity of B cells to produce neurotrophins, such as BDNF. However, B cells are the only lymphocyte that require BDNF for proper development in the bone marrow as the development of other lymphocytes

(i.e., T cells in the thymus) are unaffected in whole-body BDNF-knock out (BDNF-KO) mice (chapter 1, Table 1; [162]). BDNF also promotes pro-survival B cell functions [162, 163, 165]. In neurons, the GluN2A subunit of the N-methyl-D-aspartate receptor (NMDAR) binds glutamate and initiates downstream pro-survival signaling, including the upregulation of BDNF (**Fig. 32**; [4, 258-260]) BDNF, in turn, initiates autocrine signaling through the BDNF receptor, TrkB, but not $p75^{NTR}$ (i.e., the neurotrophin receptor (NTR) with high affinity for pro-BDNF that promotes cell death signaling [59]). Therefore, conditional BDNF-KO and BDNF-overproducing B cells were created to better assess B cell-derived BDNF in neuroprotection after ischemic injury.

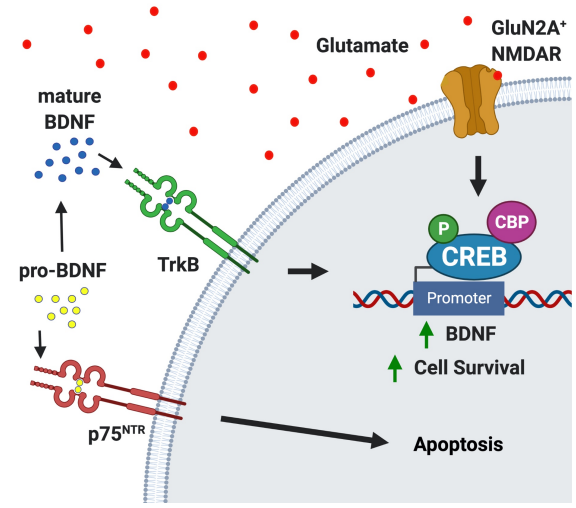

Fig. 32 Schematic depicting NMDAR and BDNF signaling in neurons.

To generate BDNF-KO B cells, BDNF-floxed mice were crossed to hCD20 tamoxifen-inducible cre mice to conditionally knock out BDNF in B cells. Both hCD20-TamCre$^{+/+}$BDNF$^{fl/fl}$ (BDNF-KO) and hCD20-TamCre$^{-/-}$BDNF$^{fl/fl}$ littermate controls received tamoxifen for 3 consecutive days and bone marrow, spleen, and cervical lymph nodes were harvested 48 hours following the final tamoxifen injection (**Fig. 33A**). Flow sorting revealed that ~82% of splenic CD19^{+} B cells co-express hCD20 (**Fig. 33B**) and the cell counts from each organ were similar between BDNF-KO mice and littermate controls (**Fig. 33C-E**). CD19^{+}hCD20^{+} BDNF-KO B cells were sorted by flow cytometry and BDNF deletion was assessed by PCR and sequencing.

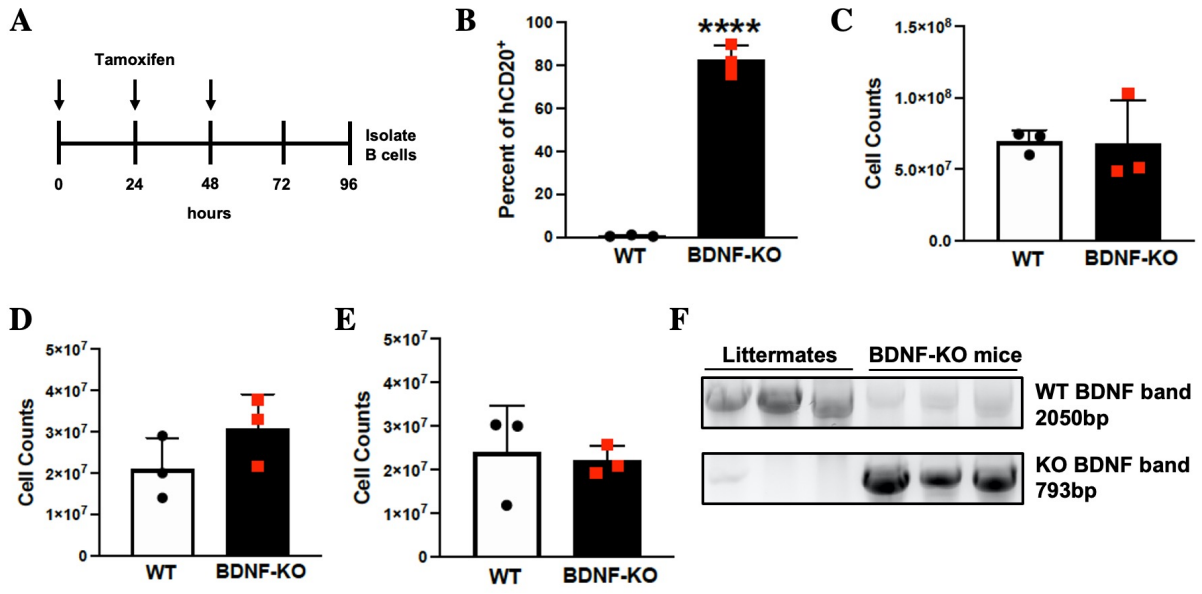

Fig. 33 Development of BDNF knock-out B cells for *in vitro* ischemia assays. (**A**) Experimental timeline for the administration of tamoxifen and B cell isolation. (**B**) The percentage of $hCD20^+$-expressing B cells within the overall $CD19^+$ splenic B cell population of WT (hCD20-TamCre$^{-/-}$BDNF$^{fl/fl}$, white bars) and BDNF-KO (hCD20-TamCre$^{+/+}$BDNF$^{fl/fl}$, black bars) mice. Cell numbers of $CD19^+$ B cells in the (**C**) spleen, (**D**) bone marrow and (**E**) CNS-draining cervical lymph nodes in conditional B cell BDNF-KO (red squares) and littermate control (black circles) mice prior to administering tamoxifen. (**F**) Genotyping results for BDNF and DNA sequencing of tamoxifen-treated conditional B cell-BDNF-KO and littermate control B cells. Significance determined by Student's *t*-test (*****$p<0.0001$* vs. littermate control). An n=2 experimental replicates were performed total an n=3 mice per group.

In tamoxifen-treated mice, the WT BDNF was observed at ~2000bp in littermate control B cells while the knock-out band for BDNF was observed at ~800bp in BDNF-KO B cells (**Fig. 33F**). On the other hand, BDNF-overproducing B cells were generated by transfecting a CMV-BDNF-P2A-mCherry plasmid into LPS-stimulated B cells to drive constitutive overproduction of BDNF (**Fig. 34A**). Flow cytometry confirmed a successful transfection in B cells based on detectable mCherry expression (**Fig. 34B**). The percentage and cell number of $mCherry^+$ B cells was highest 24 hours after transfection and significantly declined by 48 ($p<0.001$ vs. 24 hours) and

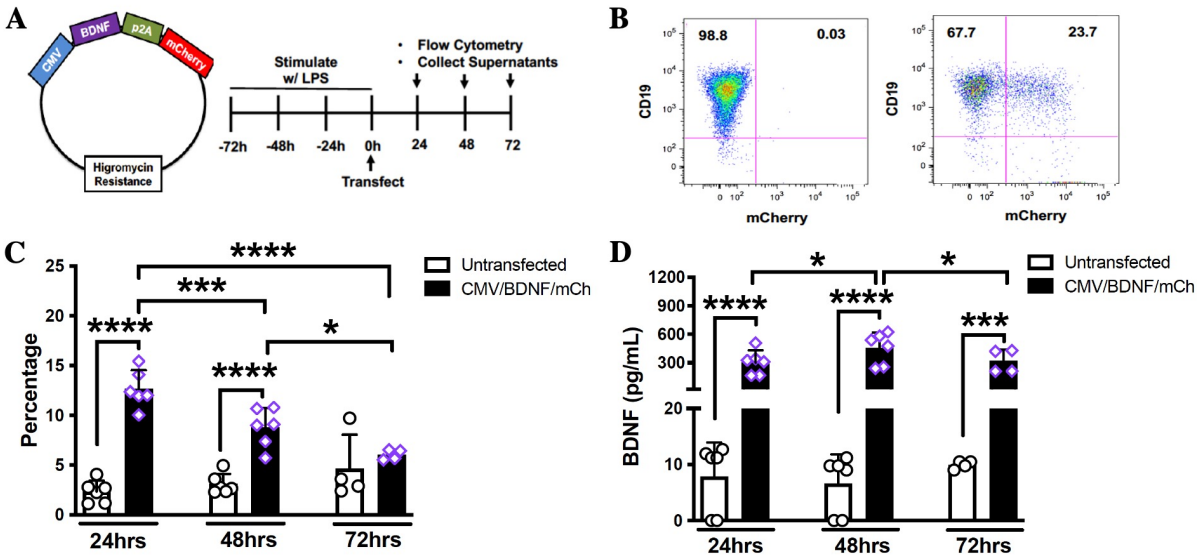

Fig. 34 Development of BDNF-overproducing B cells for *in vitro* ischemia assays. (**A**) Plasmid construct and experimental timeline for B cell stimulation and transfection. (**B**) Dot plots of BDNF-overproducing mCherry$^+$ expression in untransfected (left) or transfected (right) B cells after 24 hours in culture. (**C**) The percent of viable, successfully untransfected (open black circles) or transfected mCherry$^+$ B cells (open purple diamonds) over 72 hours in culture. (**D**) Secreted BDNF detected in the culture supernatants of transfected B cells. Significance determined by one-way ANOVA (**p<0.05, ***p<0.001, ****p<0.00001* vs. untransfected control unless indicated by bracket). An n=3 experimental replicates (inter-experimental replicates shown) were performed.

72 hours (**Fig. 34C**; p<0.0001 vs. 24 hours). Despite this steady decrease (i.e., cell death) of mCherry$^+$ B cells, BDNF secretion remained consistently detectable over 72 hours (**Fig. 34D**). These data suggest that BDNF-overproducing B cells likely induce autocrine BDNF production in the by-stander, untransfected B cells within the culture.

The importance of B cell-derived BDNF in neuroprotection following ischemic injury was investigated by subjecting mixed cortical brain cultures to *in vitro* ischemic injury (i.e., OGD and NMDA-induced excitotoxicity (NE)) followed by a 4-day recovery period in the presence or absence of WT, conditional BDNF-KO, or BDNF-overproducing B cells. When compared to uninjured controls, both OGD (**Fig. 35**) and NE (**Fig. 36**) reduced surviving MAP2$^+$ neurons to

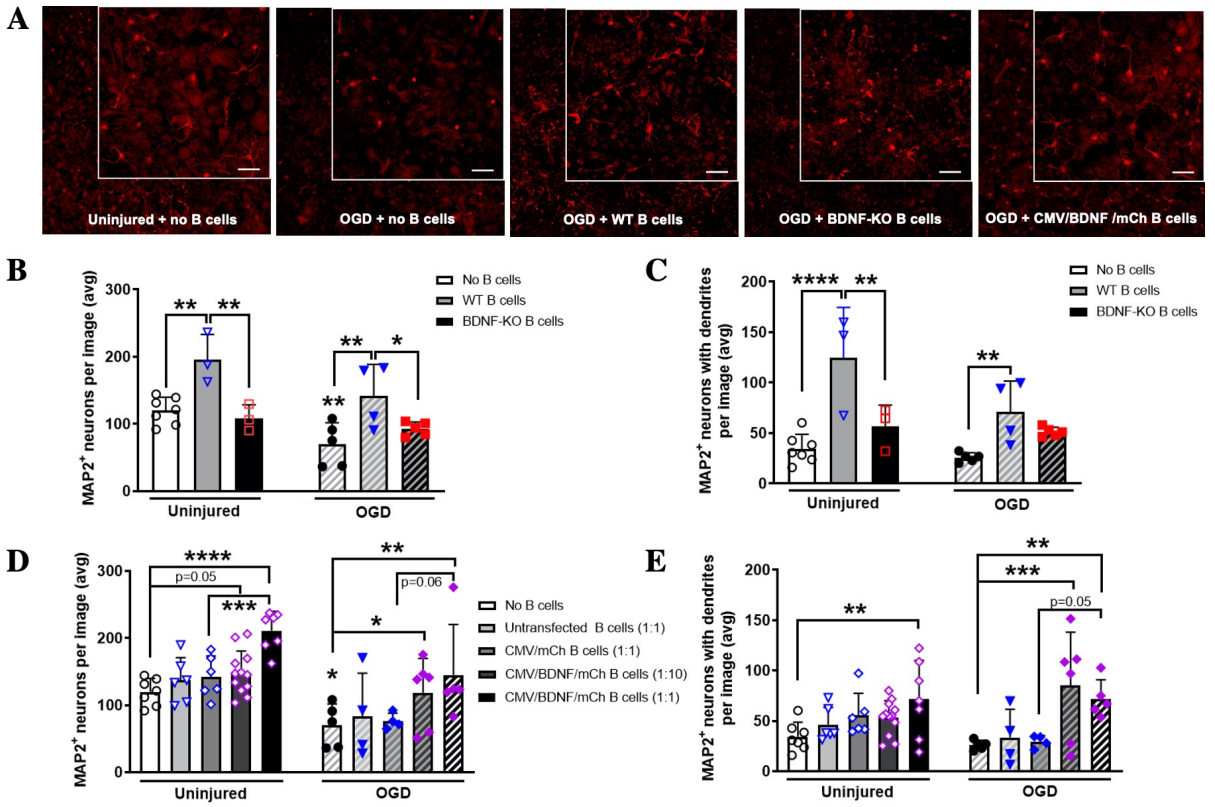

Fig. 35 B cell-derived BDNF provides neuronal protection following oxygen-glucose deprivation. (**A**) Images at 10x magnification of microtubule-associated protein (MAP2) neurons (red) co-cultured with WT (blue triangles), BDNF-KO (red squares) or BDNF-overproducing (i.e., CMV/BDNF/mCh; purple diamonds) B cells in uninjured (open symbols, solid bars) and oxygen glucose deprivation (OGD; filled symbols, hatched bars) conditions; higher magnification inset is also shown (scale bar 50µm). (**B**) Number of MAP2$^+$ neurons or (**C**) neurons with dendrites following a 3-4-day co-culture with (**B** and **C**) BDNF-KO or (**D** and **E**) BDNF-overproducing B cells in the presence or absence of OGD injury. The 'No B cell' controls in (**B** and **C**; black circles) are also represented in (**D** and **E**). Significance determined by one-way ANOVA (**p<0.05, **p<0.01, ***p<0.001, ****p<0.0001* vs. uninjured control unless indicated by bracket). An n=3 experimental replicates (inter-experimental replicates shown) were performed.

~42% (p=0.007) and ~69% (p=0.041) of surviving MAP2$^+$ neurons, respectively. Tamoxifen-treated WT B cells (*in vivo* controls for potential off-target effects in conditional B cell BDNF-KO mice) induced the previously observed (chapter 3; [166]) neurotrophic effect on uninjured neurons (p=0.001; **Fig 35B**) and preserved neuronal dendrites (p<0.0001; **Fig. 35C**) in culture

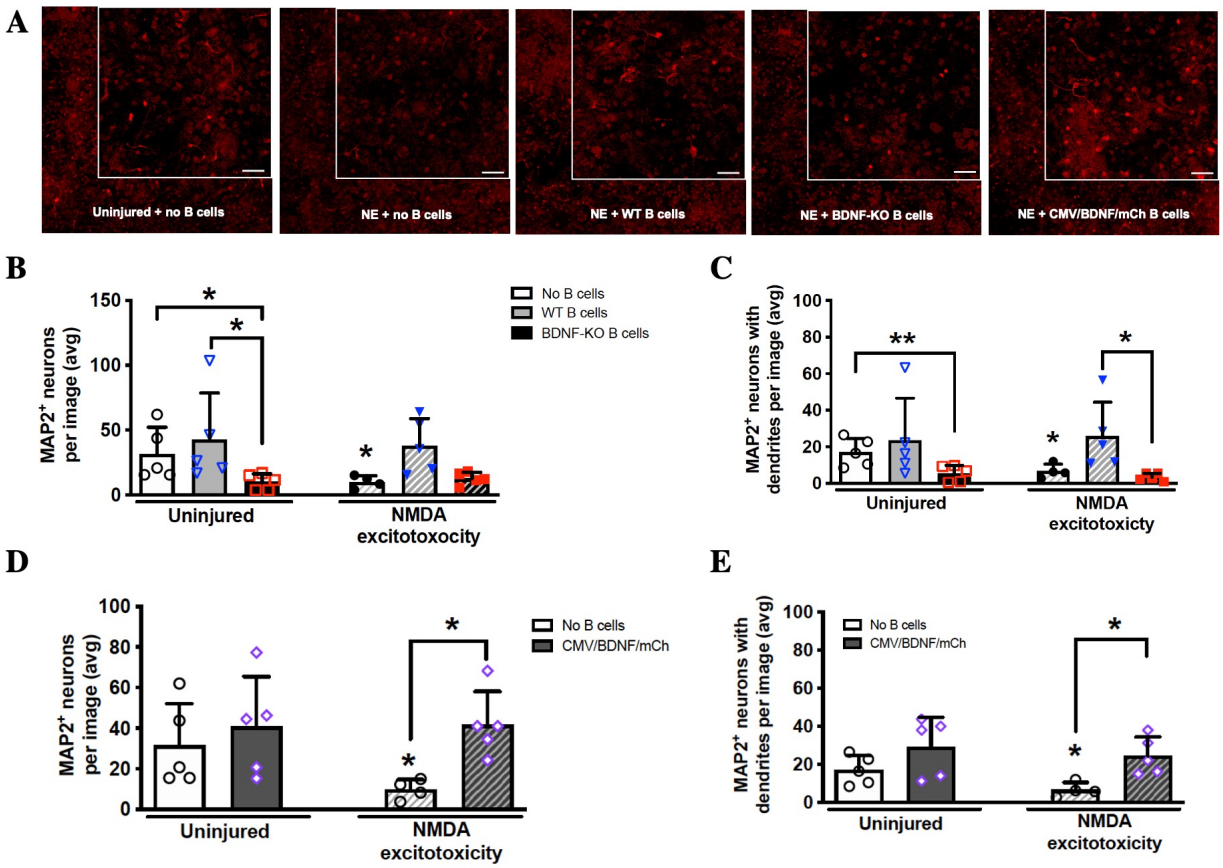

Fig. 36 B cell-derived BDNF provides neuronal protection after NMDA excitotoxicity. (**A**) Images at 10x of MAP2$^+$ neurons (red) co-cultured with WT (blue triangles), BDNF-KO (red squared) or BDNF-overproducing (i.e., (CMV/BDNF/mCh); purple diamonds) B cells in uninjured (solid bars) and NMDA excitotoxicity (NE; hatched bars) conditions; higher magnification inset is also shown (scale bar 50µm). (**B**) Number of MAP2$^+$ neurons or (**C**) neurons with dendrites following a 3-4-day co-culture with (**B** and **C**) BDNF-KO or (**D** and **E**) BDNF-overproducing B cells in the presence or absence of NE injury. The 'No B cell' controls in (**B** and **C**) are also represented in (**D** and **E**). Significance determined by one-way ANOVA (**p<0.05, **p<0.01* vs. uninjured control unless indicated by bracket). An n=3 experimental replicates (inter-experimental replicates shown) were performed.

and protected both neurons and dendritic arborization (p=0.001 and p=0.006, respectively) from OGD injury. Conversely, BDNF-KO B cells failed to exert a neurotrophic effect on uninjured cultures and protect neurons and dendritic arborization from OGD injury (**Fig. 35B, C**). Furthermore, the neuroprotective effects of WT B cells and the inability of BDNF-KO B cells to

protect neurons from ischemic injury were also observed in mixed cortical cultures subjected to NMDA-induced excitotoxicity (**Fig. 36B, C**).

To ensure that neither LPS-stimulation nor plasmid transfection would impact the neuroprotective phenotype of BDNF-overproducing B cells, we co-cultured untransfected or empty vector-transfected (CMV-P2A-mCherry) B cells with OGD-injured mixed cortical cultures. Neither LPS nor plasmid transfection exerted a neurotrophic effect on uninjured neurons or conferred protection following OGD injury. When compared to the 'CMV-P2A-mCherry' controls, a 1:1 ratio of BDNF over-producing B cells to mixed cortical cells promoted neuronal survivability ($p=0.0002$; **Fig. 35D**) in uninjured conditions. Furthermore, BDNF over-producing B cells not only exerted a neurotrophic effect on uninjured neurons, but fully protected neurons and preserved dendritic arborization following OGD injury (**Fig. 35D, E**). BDNF-overproducing B cells also protected against the loss of neurons and neurons with dendrites following NMDA-excitotoxicity (**Fig. 36C, D**). These results suggest that while B cell-derived IL-10 can confer neuroprotection, it is not absolutely required. Conversely, BDNF is a key mediator that *is* required by B cells to exert neuroprotective effects following *in vitro* models of ischemic injury.

4.3 Conclusions

Our previous studies show that B cells migrate to remote areas in the contralesional brain (e.g., the DG; chapter 3) and that systemic long-term B cell-depletion results in hippocampal- and amygdala-related anxiety and memory deficits in uninjured mice that become exacerbated after stroke (**Fig. 10-12**; [166]). In the current chapter, we found that the infarct size between WT

and B cell depleted mice were similar. These data, concomitant with ours and other previous studies [92, 124, 166], suggest that the role B cells play in regulating ischemic injury may occur in remote areas outside the initial infarct as opposed to regulating injury within the infarct itself. The current study finds that synaptic transmission is significantly reduced in the post-stroke contralesional DG of B cell-depleted, but not WT mice. The mechanisms by which B cells regulate synaptic transmission require further investigation. We see a trend towards an increase in synaptic transmission in uninjured B-cell depleted mice, leading us to speculate that the decrease in synaptic transmission in B cell-depleted mice after stroke may result from a compounded effect of ischemic injury- and hyperexcitability-induced neuronal death [261]. Additionally, the similarities in pre-synaptic release probabilities suggest that the impaired function at PP-DG synapses likely occurs in post-synaptic neurons. Lastly, our *in vitro* studies identified an alternative signaling mechanism (e.g., BDNF) to the well-described IL-10-dependent mechanism that Bregs utilize to exert neuroprotection after stroke. We found that B cell-derived BDNF, but not IL-10, is required for B cells to exert neuroprotection and promote structural neuroplasticity following *in vitro* ischemic injury.

Collectively, these studies suggest that B cells exert a neurotrophic effect on structural and functional neuroplasticity following ischemic injury. The novelty of these findings underscores the need to understand the mechanisms potentiating the neurotrophic capacity of B cells in the remote microenvironments they migrate into after stroke.

CHAPTER FIVE

Results

GLUTAMATE ENHANCES THE NEUROTROPHIC CAPACITY OF ACTIVATED B CELLS THROUGH NMDAR SIGNALING

5.1 Introduction

As reviewed in chapter 1, the N-methyl-D-aspartate receptor (NMDAR) is a glutamate-activated cation channel that induces robust synaptic plasticity under physiological conditions. However, due to their high Ca^{2+} permeability, extrasynaptic GluN2B-containing NMDARs are the primary mediators of stroke-induced excitotoxic injury. As a result, neurons interconnected with the area of infarct are negatively impacted by loss of connectivity [43]. Notably, NMDAR antagonists have failed in clinical trials [44-46] which may indicate an additional, beneficial role of NMDARs in promoting plasticity after stroke. In fact, neuronal GluN2A-containing NMDAR activity can upregulate neurotrophins, namely BDNF, promoting neuronal function and stability (**Fig. 32**, [57, 58]). BDNF and its receptor, TrkB, are widely expressed in the adult brain and are required for basal synaptic transmission and memory formation [59, 60]. In the brain, BDNF transcription, which can occur *outside* of the infarct following focal stroke [61], is regulated by neuronal activity [4]. BDNF reduces post-stroke neuronal cell death [57, 58, 61, 62] and excitotoxicity [4], enhances behavioral recovery [57, 58, 63], and promotes neurogenesis [64, 65]. However, the exogenous administration of BDNF has also failed in clinical trials due to the short half-life of BDNF and limited brain permeability [66-68]. Therefore, harnessing

endogenous BDNF production to enhance neurotrophic support within the post-stroke brain is essential.

Both mouse and human B cells express glutamate receptors that could respond to the post-stroke microenvironment and enhance their neurotrophic capacity [141, 145, 146, 148, 150, 152, 172], potentially linking glutamate responses to neurotrophin production in immune cells. While leukocytes have the capacity to produce various neurotrophins, B cells are the primary lymphocytic source of BDNF [164, 165]. In fact, B cells require BDNF for proper development in the bone marrow and BDNF can induce a Ca^{2+} influx into B cells [162], indicating BDNF receptor (i.e., TrkB and/or $p75^{NTR}$) activity in B cells. BDNF can also protect mature B cells from stress-induced apoptosis [163]. These studies suggest that the post-stroke microenvironment could promote the survival of CNS-infiltrating B cells and subsequent autocrine BDNF signaling, thereby enhancing endogenous neurotrophic support for ischemic-injured neurons or neurons requiring additional support for plasticity.

Despite the critical role of BDNF in the development and function of both neurons and B cells under homeostatic and diseased conditions, the regulation of BDNF expression by NMDAR signaling in B cells has never been investigated in the context of stroke. Therefore, functional properties (i.e., the NMDAR subunit assembly, glutamate-induced $Ca2^{+}$ activity and down-stream signaling cascade) of uninjured and post-stroke B cell NMDARs were investigated using microscopy, Ca^{2+} flow cytometry and qPCR. We also assessed glutamate-induced $Ca2^{+}$ activity of B cells from peripheral blood mononuclear cells (PBMCs) of healthy donors to determine the translatability of NMDAR function between mouse and human B cells.

5.2 Results

For clarity, the characterization of NMDAR subunit expression will be presented first (subsection 5.2A), followed by the assessment of NMDAR activity (subsection 5.2B) and concluded with investigation of downstream NMDAR signaling (subsection 5.2C) in B cells.

5.2A B cells express GluN2A- and GluN2B NMDAR subunits

5.2Ai GluN2A is engaged in B cells after stroke and glutamate exposure

Following an ischemic insult, extrasynaptic GluN2B-containing NMDARs are primarily responsible for driving neuronal excitotoxicity after engaging extracellular glutamate [4, 262]. Conversely, synaptic GluN2A-containing NMDARs bind glutamate and initiate downstream pro-survival signaling [4, 258-260]. NMDARs are also expressed in both mouse and human lymphocytes [145, 146, 148, 151, 152, 172, 263-265]. However, the assembly of NMDAR subunits has never been investigated in B cells. Thus, GluN2A and GluN2B NMDAR subunits were first quantified in splenic B cells of uninjured and 4-day-post-stroke mice. To assess expression of B cell NMDARs compared to neurons, methods for identifying extracellular surface expression of NMDARs was first confirmed in DIV 17 mouse hippocampal neurons. Neuronal GluN2A expression was very punctate and highly abundant across the neuron's processes (**Fig. 37A**). Similar to neuronal GluN2A expression, punctate GluN2A (**Fig. 37B**) and GluN2B (**Fig. 37C**) expression was identified on the surface of splenic B cells. When compared to uninjured controls, both the transcript level and surface expression of GluN2A, but not GluN2B, were differentially regulated on splenic B cells after stroke (**Fig. 37D, E**).

B cells migrate to remote brain regions of the post-stroke brain that regulate motor and cognitive function after stroke [166]. The concentration of extracellular glutamate within

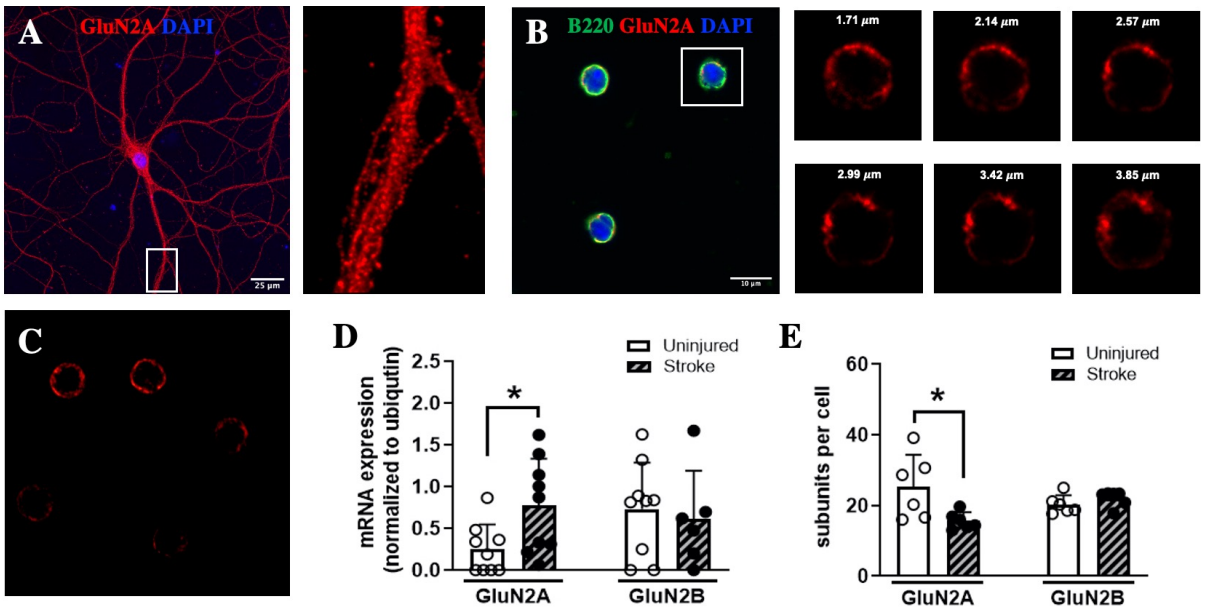

Fig. 37 B cell GluN2A subunits are engaged after stroke. (**A**) Image at 40x magnification of GluN2A subunit expression on DIV17 hippocampal neurons with higher magnification inset also shown to the right (GluN2A (red) and DAPI (blue); scale bar 25μm). (**B**) Image at 120x magnification of (**B**) GluN2A subunit expression in uninjured B220^{+} B cells (left – GluN2A (red), B220 (green), DAPI (blue) merge, right – sequential images at specified μm-depth within a confocal z-stack for the selected B cell; scale bar 10μm) or (**C**) GluN2B. Assessment of (**D**) NMDAR subunit mRNA (n=6-8 mice/group) and (**E**) subunit surface expression (n=3 mice, 2 images/mouse, average of 14.10 ± 0.94 B cells counted per image) in uninjured (open black circles; white bars) and 4-day post-stroke (closed black circles; hatched bars) B220^{+} B cells. Significance determined by two-way ANOVA (*$p<0.05$ vs. uninjured control). An n=3-4 experimental replicates were performed totaling an n=6-10 mice per

these remote brain regions is nearly 100-fold less than what is released into the ischemic core (~100μM in concentration) [266]. Upon glutamate engagement, surface NMDARs internalize to initiate downstream signaling and/or suppress the signaling activity of non-internalized NMDARs [267-269]. To assess the impact of glutamate on B cell NMDARs, particularly the neurotrophic GluN2A subunit, we first needed to identify a concentration of glutamate that would not compromise the viability of isolated B cells after a direct exposure for 24 hours. Using

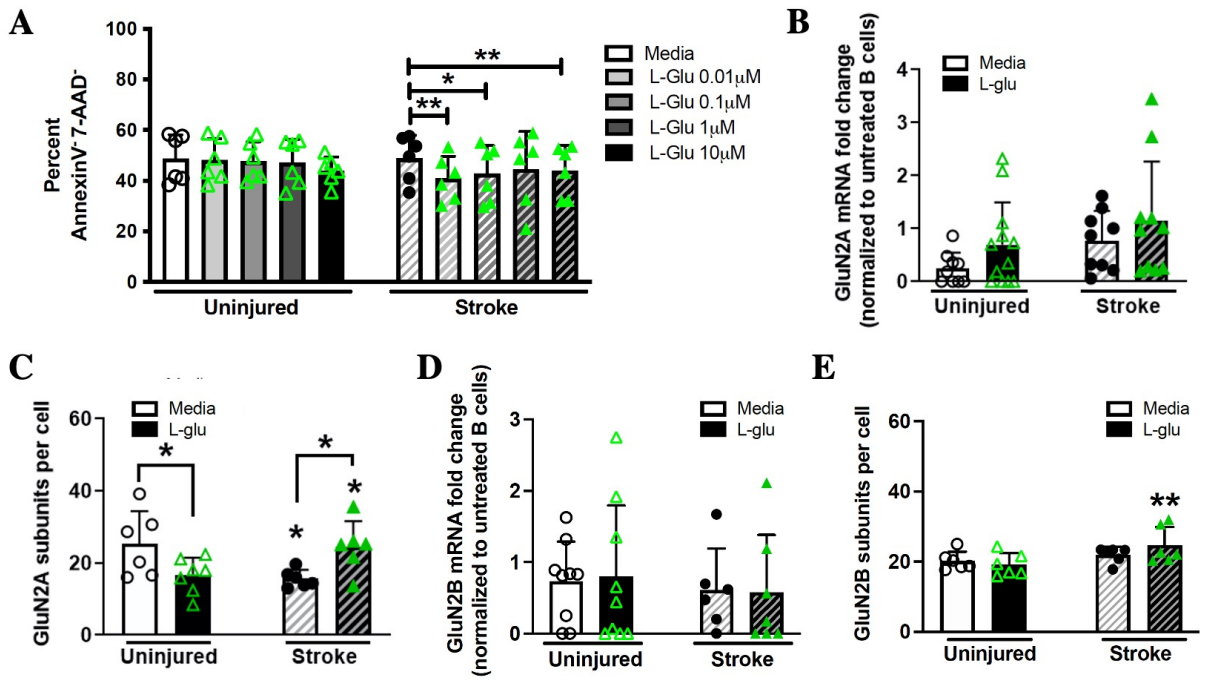

Fig. 38 B cell GluN2A subunits are engaged following glutamate treatment. (**A**) Percentage of live (AnnexinV$^-$7-AAD$^-$) uninjured (solid bard) or 4-day post-stroke (hatched bars) CD19$^+$ B cells following a 24-hour treatment with media (black circles) increasing concentrations of glutamate (L-glu; green triangles). mRNA and surface subunit expression for (**B** and **C**) GluN2A and (**D** and **E**) GluN2B in B220$^+$ B cells following a 24-hour treatment with 1μM L-glu; white bars seen in (**B-E**) reflect the GluN2A and GluN2B groups from Fig. 32 B and C. Significance determined by (**A**) repeated measures one- or (**B-E**) mixed effects two-way ANOVA (*$p<0.05$ vs. uninjured control unless indicated by bracket). An n=3-4 experimental replicates were performed totaling an n=6-10 mice per group.

an apoptosis flow cytometry assay, we identified that 1μM glutamate, a neurophysiological concentration found in remote areas of the brain after stroke, did not reduce the percentage of viable B cells following a 24-hour exposure (**Fig. 38A**). In B cells treated with 1μM glutamate, stroke injury induced an overall increase in Glu2NA mRNA regardless of glutamate exposure ($F_{(1, 36)}$=3.930, p=0.055; **Fig. 38B**). Interestingly, there was an interaction between stroke injury and glutamate treatment on GluN2A subunits ($F_{(1, 10)}$=19.69, p=0.001; **Fig. 38C**) expressed at the surface of B cells. Upon binding glutamate, B cells from uninjured mice expressed fewer surface

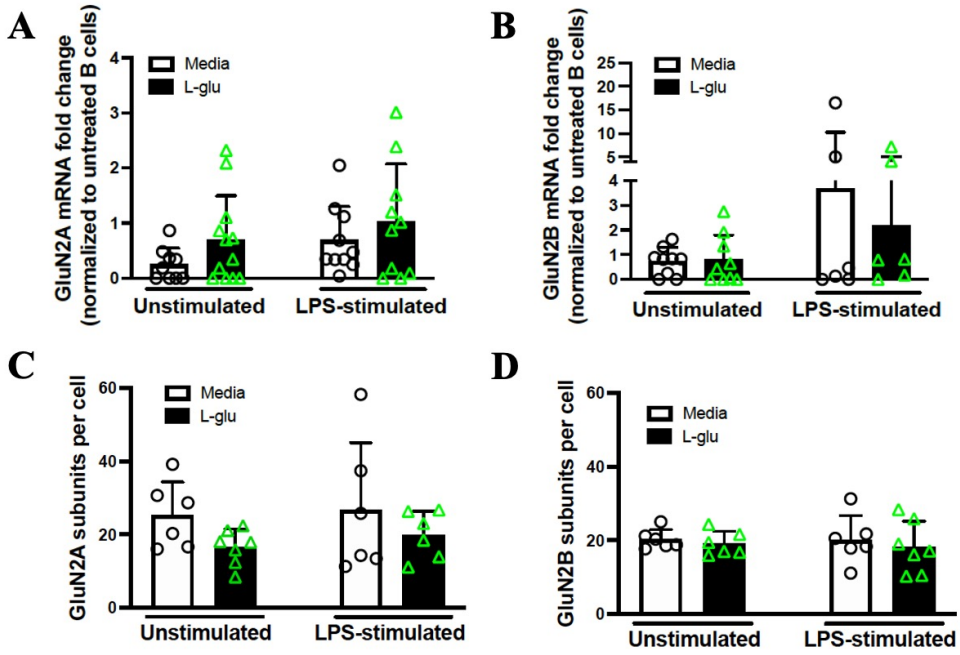

Fig. 39 LPS does not impact NMDAR subunits of glutamate-treated, uninjured B cells. (**A**) Percentage of live (AnnexinV$^-$7-AAD$^-$) uninjured (solid bard) or 4-day post-stroke (hatched bars) CD19$^+$ B cells following a 24-hour treatment with media (black circles) increasing concentrations of glutamate (L-glu; green triangles). mRNA and surface subunit expression for (**B** and **C**) GluN2A and (**D** and **E**) GluN2B in B220$^+$ B cells following a 24-hour treatment with 1μM L-glu; white bars seen in (**B**-**E**) reflect the GluN2A and GluN2B groups from Fig. 32 B and C. Significance determined by (**A**) repeated measures one- or (**B**-**E**) mixed effects two-way ANOVA (*$p<0.05$ vs. uninjured control unless indicated by bracket). An n=3-4 experimental replicates were performed totaling an n=6-10 mice per group

GluN2A subunits than untreated controls (p=0.01; **Fig. 38C**). Glutamate, however, increased GluN2A subunits on the surface of B cells from post-stroke mice (p=0.01; **Fig. 38C**), returning the subunit's expression to within the uninjured, untreated B cell baseline. On the other hand, glutamate does not affect GluN2B mRNA expression in either an up- or down-regulated manner, though stroke injury induced an overall increase in B cell GluN2B subunit expression independent of treatment ($F_{(1, 10)}$=5.024, p=0.049; **Fig. 38**). These results suggest that upon glutamate exposure, GluN2A is preferentially engaged by B cells after stroke. While glutamate generally increases B cell GluN2A mRNA, it is likely that glutamate differentially impacts

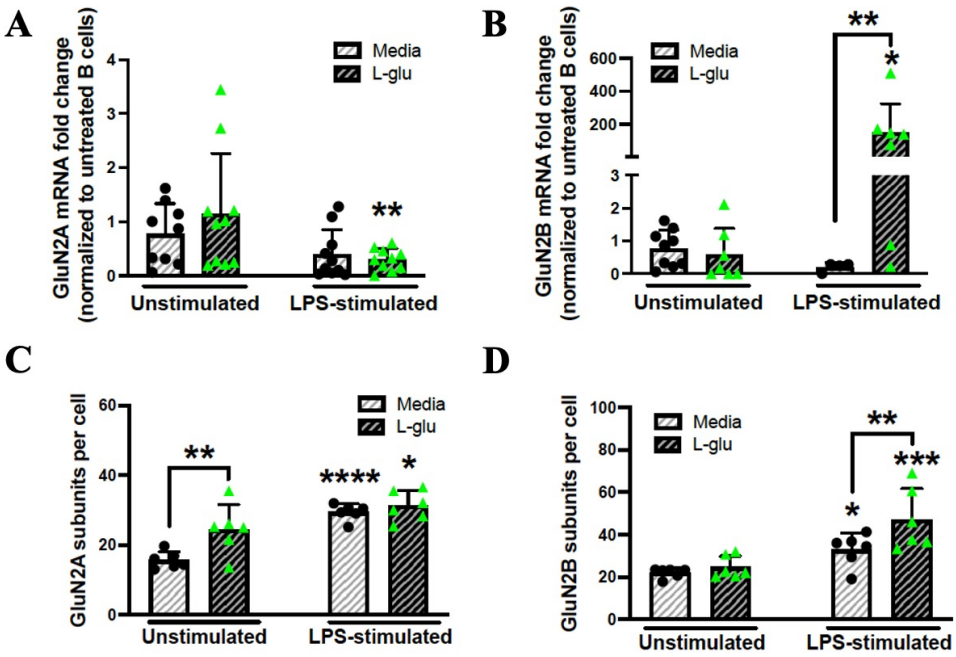

Fig. 40 LPS upregulates surface NMDAR subunit expression in post-stroke B cells (**A**) Percentage of live (AnnexinV$^-$7-AAD$^-$) uninjured (solid bard) or 4-day post-stroke (hatched bars) CD19$^+$ B cells following a 24-hour treatment with media (black circles) increasing concentrations of glutamate (L-glu; green triangles). mRNA and surface subunit expression for (**B** and **C**) GluN2A and (**D** and **E**) GluN2B in B220$^+$ B cells following a 24-hour treatment with 1μM L-glu; white bars seen in (**B**-**E**) reflect the GluN2A and GluN2B groups from Fig. 32 B and C. Significance determined by (**A**) repeated measures one- or (**B-E**) mixed effects two-way ANOVA (*$p<0.05$* vs. uninjured control unless indicated by bracket). An n=3-4 experimental replicates were performed totaling an n=6-10 mice per group.

GluN2A internalization and downstream NMDAR signaling in uninjured and post-stroke B cells as reflected in the surface expression results.

5.2Aii LPS alters NMDAR subunit expression in post-stroke B cells

After stroke, several DAMPs, such as high motility group box 1 (HMGB1), released from ischemic-injured tissue and/or necrotic cells have the potential to activate B cells [270-272] through toll-like receptor (TLR)4 as a key receptor. To test TLR4 activation, mouse splenic B cells were stimulated with LPS to mimic, in part, the stimuli that they may encounter in the post-stroke CNS [86, 92, 93, 273, 274]. While LPS did not impact NMDAR subunit mRNA (**Fig.**

39A, B) or surface expression (**Fig. 39C, D**) in uninjured B cells, it did reduce GluN2A ($F_{(1, 35)}$=7.95, p=0.008; **Fig. 40A**), but not GluN2B mRNA in post-stroke B cells (**Fig. 40B**). Additionally, both glutamate and LPS significantly increased surface protein expression of GluN2A ($F_{(1, 10)}$=7.56, p=0.02 and $F_{(1, 10)}$=36.71, p=0.0001, respectively; **Fig. 40C**) and GluN2B ($F_{(1, 10)}$=10.17, p=0.01 and $F_{(1, 10)}$=15.46, p=0.003, respectively; **Fig. 40D**) in post-stroke B cells. Lastly, the bifurcation of positive- and non-responding mice observed throughout Fig. 38-40 (i.e., glutamate-induced NMDAR subunit mRNA and surface subunit responses) may stem, in part, from the variability in the extent of injury that was induced by the tMCAo stroke model, which in turn, could impact the degree of B cell responsiveness.

5.2B NMDAR activity differs among unstimulated and stimulated B cell subsets

5.2Bi Glutamate induces a Ca^{2+} response in unstimulated mouse B cells

NMDARs are Ca^{2+}-permeable glutamate receptors, however, the functional properties of NMDARs/NMDAR subunits have not been characterized among B cell subsets, which may be critical to understanding previously conflicting studies on the neuroprotective effects of B cells after stroke [127, 166]. To further understand B cell NMDAR activity, the Ca^{2+} response by mouse and human B cell subsets to various stimuli, including glutamate, was measured in the presence or absence of competitive or subunit-specific NMDAR antagonists (**Fig. 41A**). Ionomycin, a potent Ca^{2+} ionophore, induced a strong Ca^{2+} response in mouse $CD19^+$ B cells (**Fig. 41B**), with signature responses in naïve, effector, class-switched and regulatory B cells (Bregs) as well as $B220^+$ and $B220^-$ antibody-secreting cells (ASCs; B220 is expressed on plasmablasts and downregulated on plasma cells; **Fig. 41C**). The response within

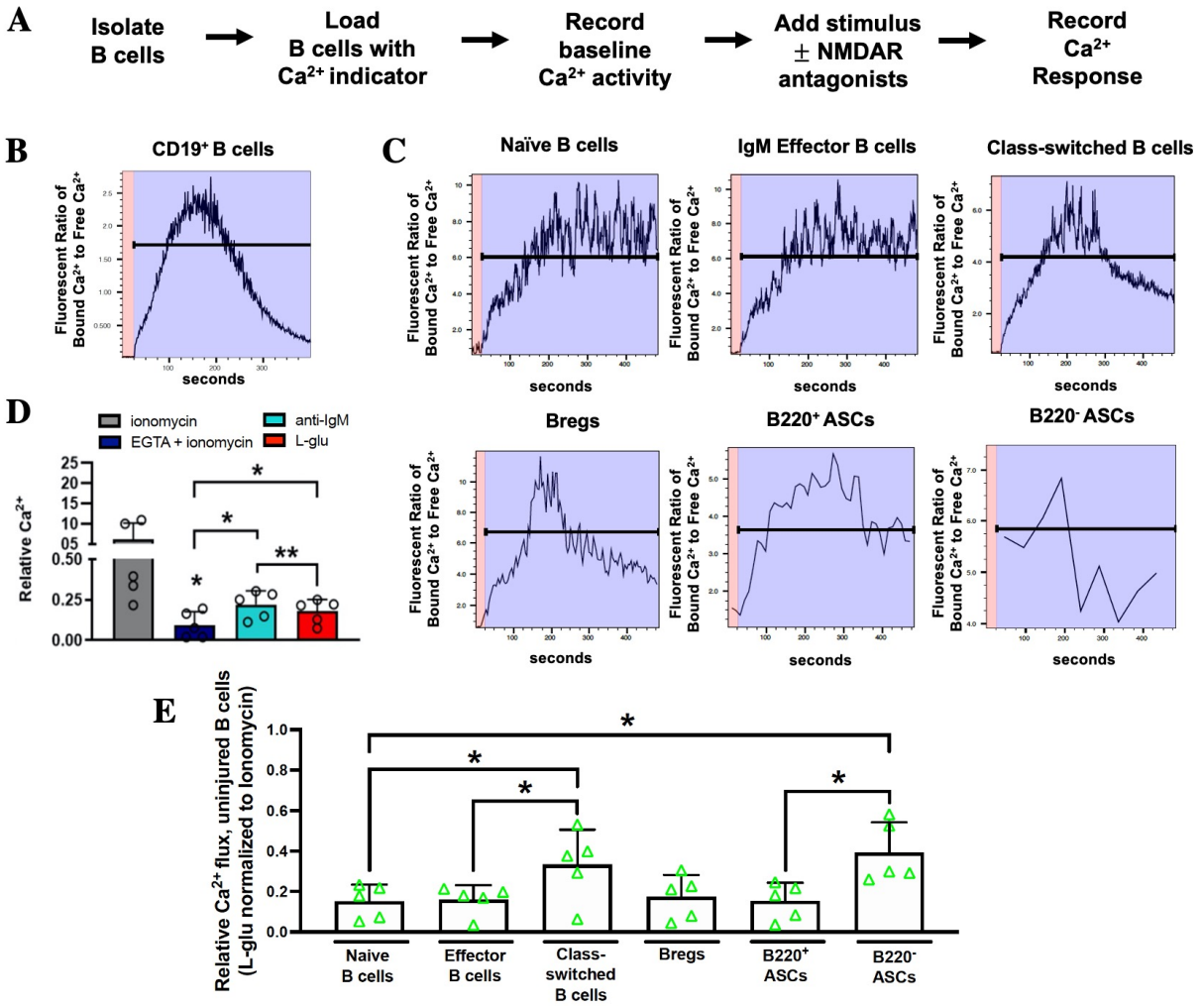

Fig. 41 Mouse B cell subsets exhibit distinct Ca^{2+} responses in unstimulated conditions. (**A**) Experimental design of measuring Ca^{2+} responses in B cells. (**B**) The Ca^{2+} response of $CD19^+$ splenic B cells to ionomycin (peach baseline, purple total response). (**C**) The Ca^{2+} responses of individual B cell subsets to ionomycin. (**D**) The Ca^{2+} responses to various stimuli normalized to ionomycin in $CD19^+$ splenic B cells from uninjured mice (open black circles). (**E**) The individual Ca^{2+} response to 1μM glutamate (L-glu; green triangles) in unstimulated, uninjured B cell subsets. Significance determined by (D) mixed effects or (E) repeated measures one-way ANOVA (*$p<0.05$, **$p<0.01$, vs. ionomycin control unless indicated by bracket). An n=5-6 experimental replicates were performed totaling an n=5-6 mice per group.

all $CD19^+$ B cells was significantly reduced when Ca^{2+} was chelated from the media using EGTA (p=0.025; **Fig. 41D**) which served in every experiment as an internal negative control. While glutamate and anti-IgM (used to engage the BCR) induced a Ca^{2+} response in $CD19^+$ B

cells that was significantly larger than the negative control (p=0.043 and p=0.024, respectively), the response to anti-IgM was larger than the response to glutamate (p=0.008). Unstimulated B cell subsets exhibited distinct Ca^{2+} responses to glutamate (**Fig. 41E;** identification for each mouse B cell subset can be found in chapter 2.11C, Fig. 19), with the strongest responses observed in $B220^-$ ASCs (p=0.038 compared to $B220^+$ ASCs and p=0.045 compared to naïve B cells) and class-switched (p=0.049 compared to naïve B cells and p=0.025 compared to effector B cells) B cells. However, NMDARs are not the primary mediator of glutamate-induced Ca^{2+} entry into unstimulated effector B cells, class-switched B cells or $B220^+$ ASCs, as the Ca^{2+} response to 1μM glutamate was only reduced ~15% by one, but not all NMDAR antagonists (**Table 7-9**, found at the end of chapter 5 on pages 122-123). Additionally, all NMDAR antagonists failed to reduce any of the glutamate-induced Ca^{2+} response in naïve B cells, Bregs or $B220^-$ ASCs (**Table 10-12**, pages 123-124). Given that GluN2A- and GluN2B-expressing NMDARs are indeed present on the surface of B cells (**Fig. 37**), these Ca^{2+} flow data suggest low NMDAR activity in unstimulated B cells. It may be possible that unstimulated B cells require either 1.) A higher concentration of glutamate (resembling what lymphocytes encounter in the periphery [145, 147, 152] or the ischemic core when compared to remote areas of the post-stroke brain [275]); or 2.) Additional stimulation that will activate ion channels to depolarize the resting membrane potential (~59mV [276]) and subsequently activate NMDARs to drive a Ca^{2+} response.

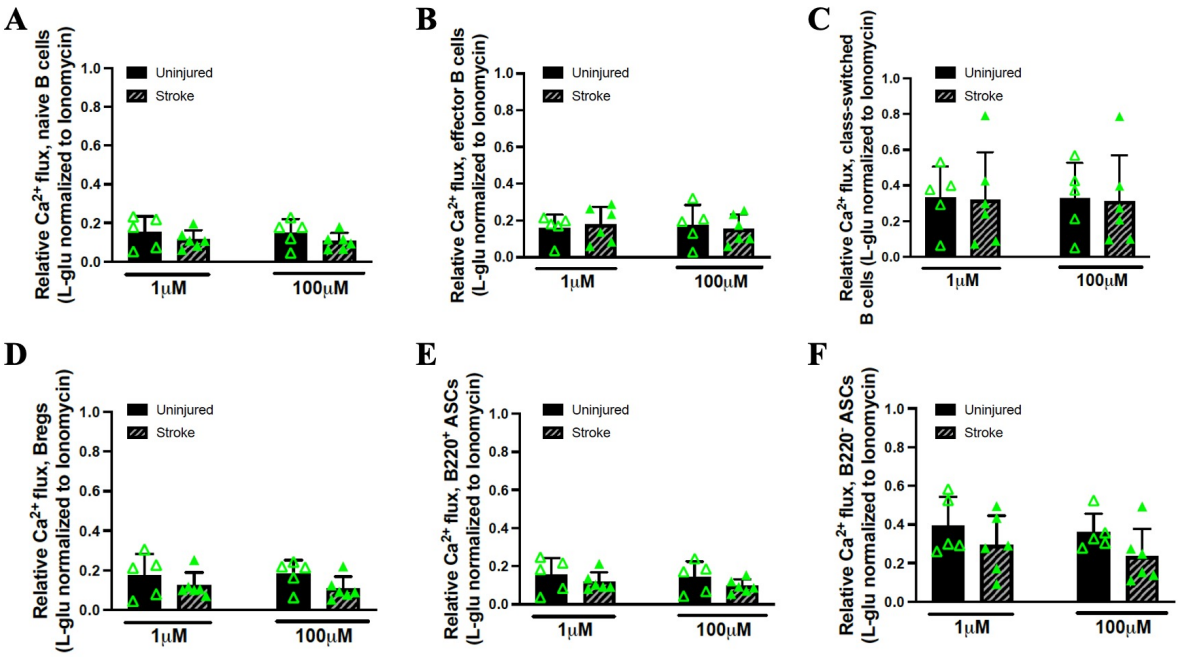

Fig. 42 The Ca^{2+} response to 1- or 100μM glutamate is similar in unstimulated B cells. The Ca^{2+} response of unstimulated (**A**) naïve B cells, (**B**) effector B cells, (**C**) class-switched B cells, (**D**) Bregs, (**E**) $B220^{+}$ ASCs or (**F**) $B220^{-}$ ASCs to 1- or 100μM glutamate (L-glu) in both uninjured (solid bars; open triangles) and post-stroke (hatched bars; closed triangles) mice. Data analyzed by repeated measures two-way ANOVA. An n=11 experimental replicates were performed totaling an n=5-6 mice per group.

5.2Bii Neuropathological glutamate does not increase Ca^{2+} responses in unstimulated B cells

To investigate the first possibility of an impact of glutamate concentration on the magnitude of B cell NMDAR signaling, the Ca^{2+} responses of each B cell subset to a neuropathological level of glutamate (i.e., 100μM; similar to parenchymal levels in regions of post-stroke excitotoxicity [275]) was recorded. When compared to 1μM glutamate, 100μM glutamate had no significant effect on the magnitude of the Ca^{2+} response in any B cell subset (**Fig. 42**). These data may indicate that glutamate binding and its' effect on BDNF transcription is saturated and achieved, respectively, at an exposure of a neurophysiological and not a

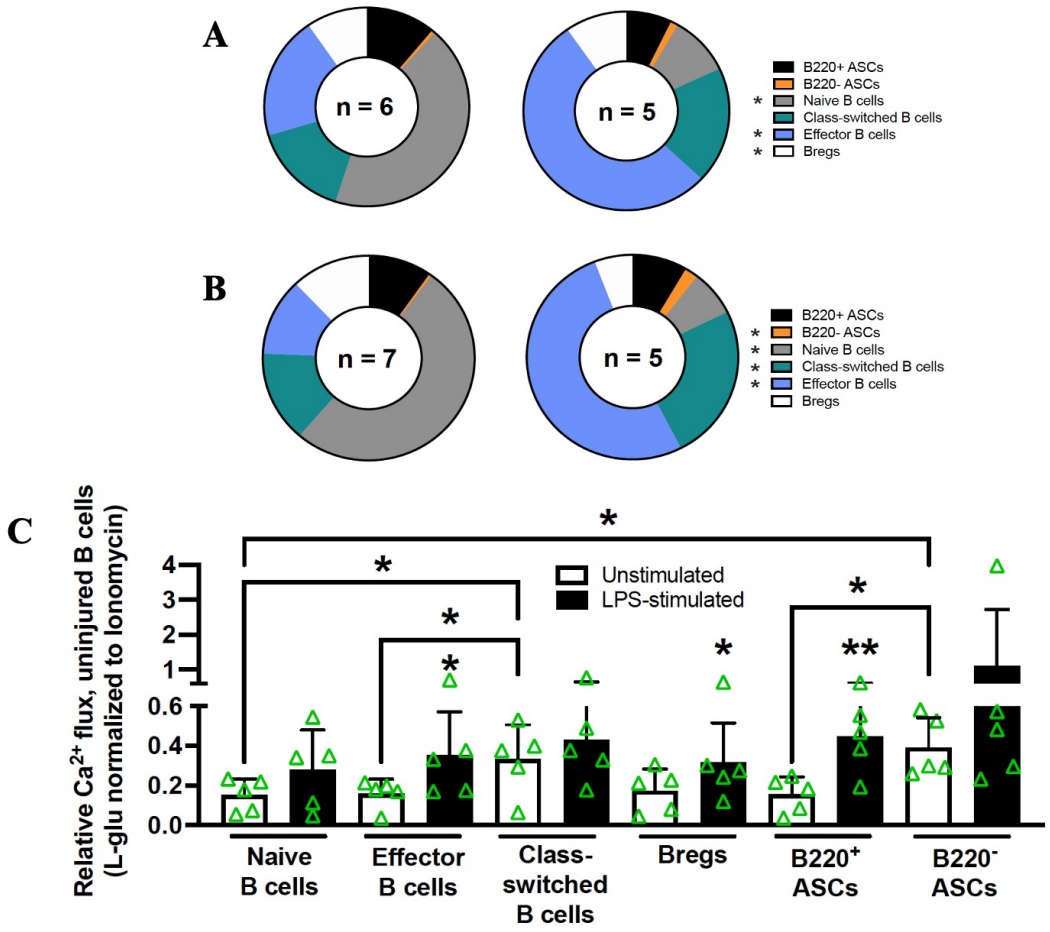

Fig. 43 Mouse B cell subsets exhibit distinct Ca^{2+} responses under stimulated conditions. The distribution of B cell subsets within $CD19^+$ B cells of (**A**) uninjured and (**B**) post-stroke mice in (left) unstimulated and (right) LPS-stimulated conditions. (**C**) The individual Ca^{2+} response to 1μM L-glu (green triangles) in unstimulated (white bars) or LPS-stimulated (black bars) uninjured B cell subsets. Significance determined by (A, B) mixed effects and (C) repeated measures two-way ANOVA (*$p<0.05$, **$p<0.01$ vs. unstimulated unless indicated by brackets). An n=21 experimental replicates were performed totaling an n=5-6 mice per group.

neuropathological glutamate concentration.

5.2Biii Mouse B cell NMDARs become activated upon LPS stimulation

As glutamate concentration did not differentially affect NMDAR responses in B cells, we investigated the second possibility mentioned above regarding the stimulation of B

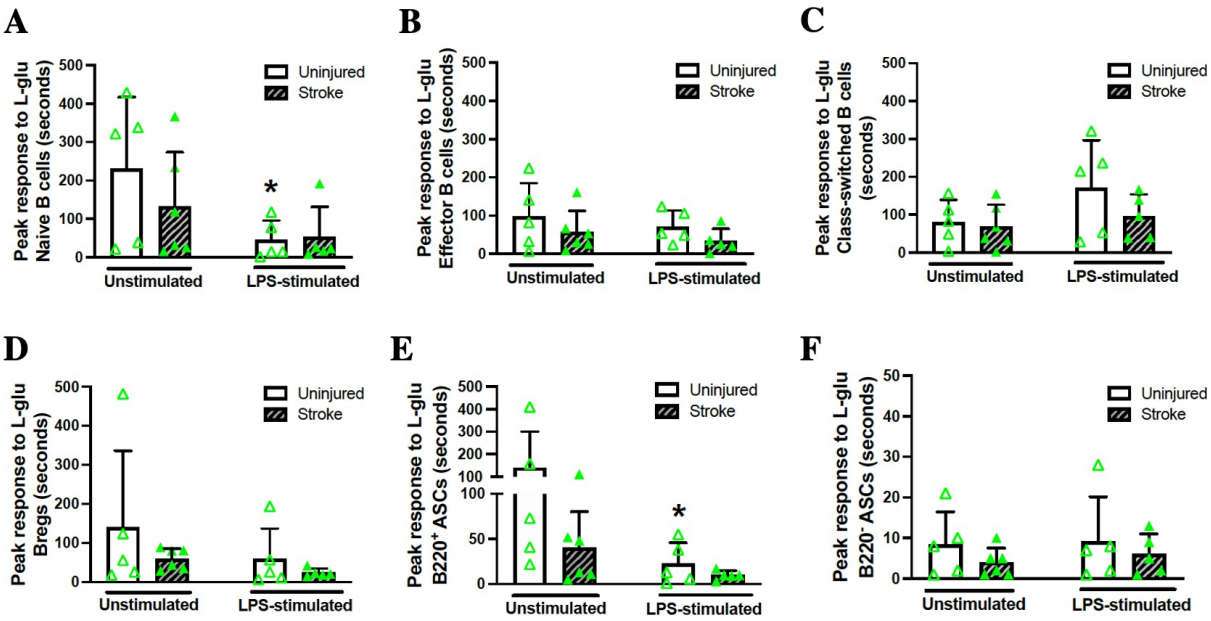

Fig. 44 LPS stimulation reduces the glutamate-induced Ca^{2+} response in select B cell subsets. The time at which the peak Ca^{2+} response to 1μM glutamate (L-glu; green triangles) was achieved in LPS-stimulated (**A**) naïve B cells, (**B**) effector B cells, (**C**) class-switched B cells, (**D**) Bregs, (**E**) $B220^{+}$ or (**F**) $B220^{-}$ antibody secreting cells (ASCs) of uninjured (solid bars, open triangles) or post-stroke (hatched bars, solid triangles) mice. Significance determined by two-way ANOVA (*$p<0.05$, vs. unstimulated control unless indicated by bracket). An n=21 experimental replicates were performed totaling an n=5-6 mice per group.

cells. LPS expanded select B cell subsets in all cohorts of mice (**Fig. 43A, B** and **Table 13**) as well as the magnitude of the Ca^{2+} responses to glutamate in effector B cells, Bregs, and $B220^{+}$ ASCs (both **Fig. 43C** – black bars and Tables 7, 11, 9). Although LPS reduced the time it took for naïve B cells ($F_{(1, 17)}$=5.6, p=0.03) and $B220^{+}$ ASCs ($F_{(1, 17)}$=4.37, p=0.05) to reach their peak response to glutamate (**Fig. 44**), neither stroke nor LPS altered the percent of any Ca^{2+}-responding B cell subset over their respective baseline threshold (**Fig. 45**). In summary, LPS stimulation was predominantly effective in post-stroke B cell populations (**Tables 7-12**), exerting effects on surface NMDAR subunit expression and NMDAR Ca^{2+} responses to glutamate dependent on responding subset without changes to the percent of responding cells within each subset.

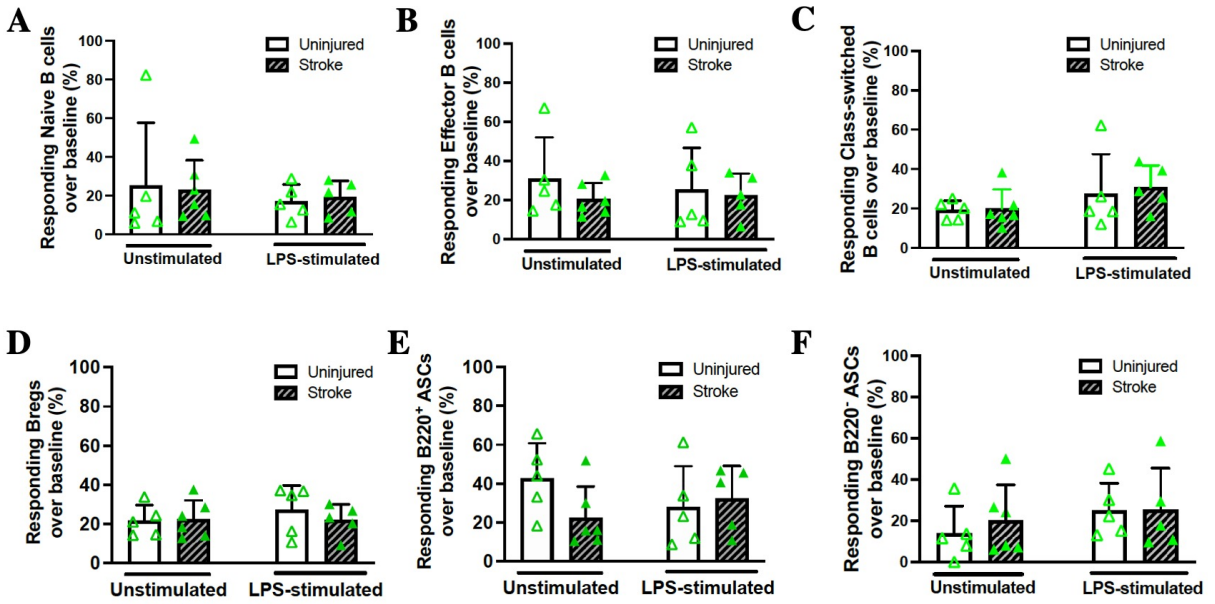

Fig. 45 Neither stroke nor LPS impact the percent of glutamate-responding B cells. The percent of B cells responding 1μM glutamate (L-glu; green triangles) over their respective baseline threshold in LPS-stimulated (**A**) naïve B cells, (**B**) effector B cells, (**C**) class-switched B cells, (**D**) Bregs, (**E**) $B220^+$ or (**F**) $B220^-$ antibody secreting cells (ASCs) of uninjured (solid bars, open triangles) or post-stroke (hatched bars, solid triangles) mice. Data analyzed by two-way ANOVA. An n=21 experimental replicates were performed totaling an n=5-6 mice per group.

As this is the first characterization of B cell NMDAR responses to glutamate, we designed these flow cytometry studies to include 3 NMDAR antagonists: 1) TCN201, a GluN2A-targeting NMDAR antagonist, 2) ifenprodil, a GluN2B-targeting antagonist, and 3) D-APV, a competitive NMDAR antagonist. TCN201 reduced the glutamate-induced Ca^{2+} response of LPS-stimulated naïve B cells ($F_{(1, 7)}$=20.68, p=0.003; **Fig. 46A**), effector B cells ($F_{(1, 7)}$=42.76, p=0.0003; **Fig. 46B**), class-switched B cells ($F_{(1, 7)}$=16, p=0.005; **Fig. 46C**), Bregs ($F_{(1, 7)}$=18.79, p=0.003; **Fig. 46D**), $B220^+$ ASCs ($F_{(1, 7)}$=58.33, p=0.0001; **Fig. 46E**) and $B220^-$ ASCs ($F_{(1, 7)}$=17.19, p=0.004; **Fig. 46F**) regardless of stroke injury. For the exception of $B220^-$ ASCs, D-APV (competitive) and ifenprodil (GluN2B-targeting) also reduced the glutamate-induced Ca^{2+}

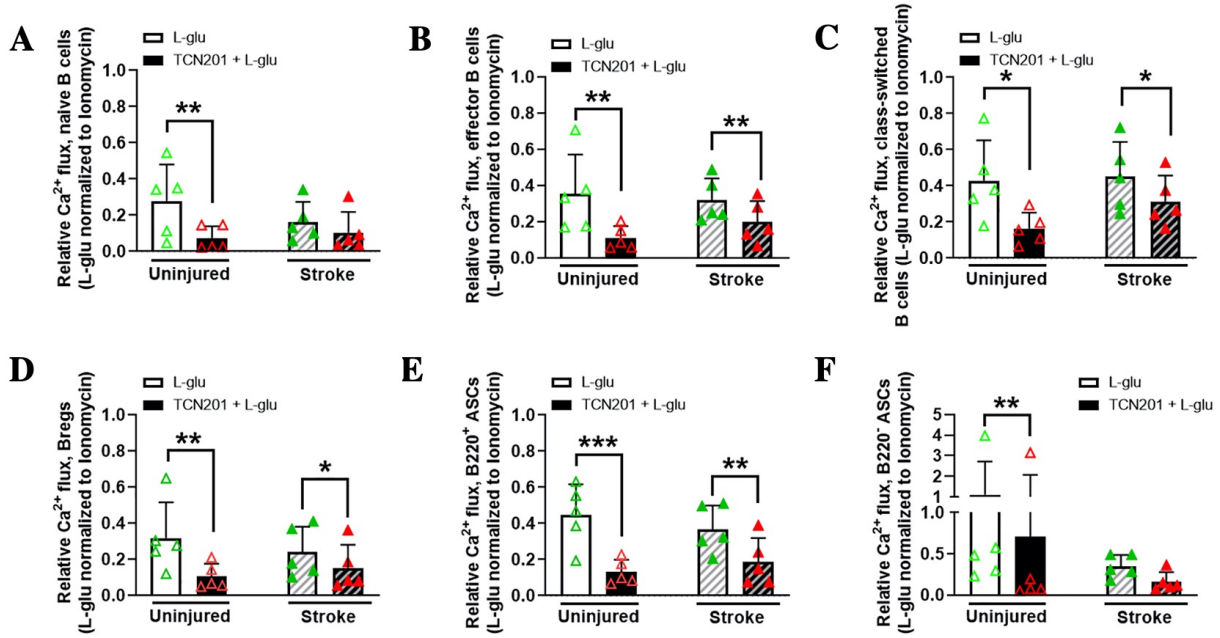

Fig. 46 NMDARs mediate the glutamate-induced Ca^{2+} response in stimulated splenic B cells. The Ca^{2+} response to 1μM glutamate (L-glu; green triangles) in LPS-stimulated (**A**) naïve B cells, (**B**) effector B cells, (**C**) class-switched B cells, (**D**) Bregs, (**E**) $B220^{+}$ or (**F**) $B220^{-}$ antibody secreting cells (ASCs) after antagonizing the GluN2A NMDAR subunit with TCN201 (red triangles) in uninjured (solid bars, open triangles) or post-stroke (hatched bars, solid triangles) mice. Significance determined by two-way ANOVA (*$p<0.05$, **$p<0.01$, ***$p<0.001$ vs. uninjured control unless indicated by bracket). An n=21 experimental replicates were performed totaling an n=5-6 mice per group.

response in all LPS-stimulated uninjured B cell subsets. However, after stroke, all 3 NMDAR antagonists reduced the glutamate-induced Ca^{2+} response in LPS- stimulated $B220^{-}$ ASCs (**Table 12**), suggesting a shift from non-NMDA glutamate receptor activity in $B220^{-}$ ASCs under homeostatic conditions to NMDAR-engagement after stroke. We also observed a stroke-induced shift in NMDAR subunit activity in select LPS-stimulated B cell subsets. In uninjured conditions, both GluN2A and GluN2B mediated the glutamate-induced Ca^{2+} response of LPS-stimulated class-switched B cells (**Table 8**) and Bregs (**Table 11**). However, after stroke, the GluN2B-, but not GluN2A-mediated response was reduced in class switched B cells ($p<0.05$)

and Bregs ($p<0.05$), suggesting a shift from general NMDAR activity to GluN2B-mediated activity within these two subsets after stroke. While the role of $CD138^{-}IgD^{-}IgM^{-}$ class-switched B cells in post-stroke recovery is unclear, it may be possible that Breg NMDARs shift to GluN2B-mediated activity to inhibit GluN2A-BDNF signaling. This may allow Bregs to carry out their IL-10-mediated protective role in stroke recovery and will be further discussed in chapter 6. Collectively, these data suggest that NMDARs mediate up to half of the glutamate-induced Ca^{2+} response in uninjured LPS-stimulated B cells and that NMDAR subunit activity, depending on the B cell subset, may change after stroke.

5.2Biv Glutamate induces a Ca^{2+} response in human B cell subsets

Human B cells, like mouse B cells, express NMDARs and upregulate BDNF after CNS injury [163, 277-279]. To assess the translatability of our mouse studies in human B cell NMDAR function, the glutamate-induced Ca^{2+} response was assessed in B cells from peripheral blood mononuclear cells (PBMCs) of healthy donors (**Table 14**, page 125). However, unlike mice, human B cells do not express TLR4 under healthy conditions [280, 281]. Therefore, healthy donor PBMCs were stimulated with a cocktail of cytokines and TLR agonists (chapter 2, section 2.11C) designed to both mimic post-stroke activation (i.e., DAMPs and pro-inflammatory signals) [272, 282-284] and expand $CD19^{+}$ B cells [285-293]. Naïve, naïve B10, effector, class-switched, memory, memory B10, plasmablasts, and $CD38^{+}$ B10 B cells were identified within the overarching $CD19^{+}$ B cell population of healthy donors (**Fig. 47A**). The overarching $CD19^{+}$ B cell population of each stimulated healthy donor had a positive response to BCR engagement (i.e., anti-IgM/IgG) and glutamate when compared to the within-donor negative controls ($p=0.013$ and $p=0.003$, respectively; **Fig. 47B**). Unlike mouse B cells, there

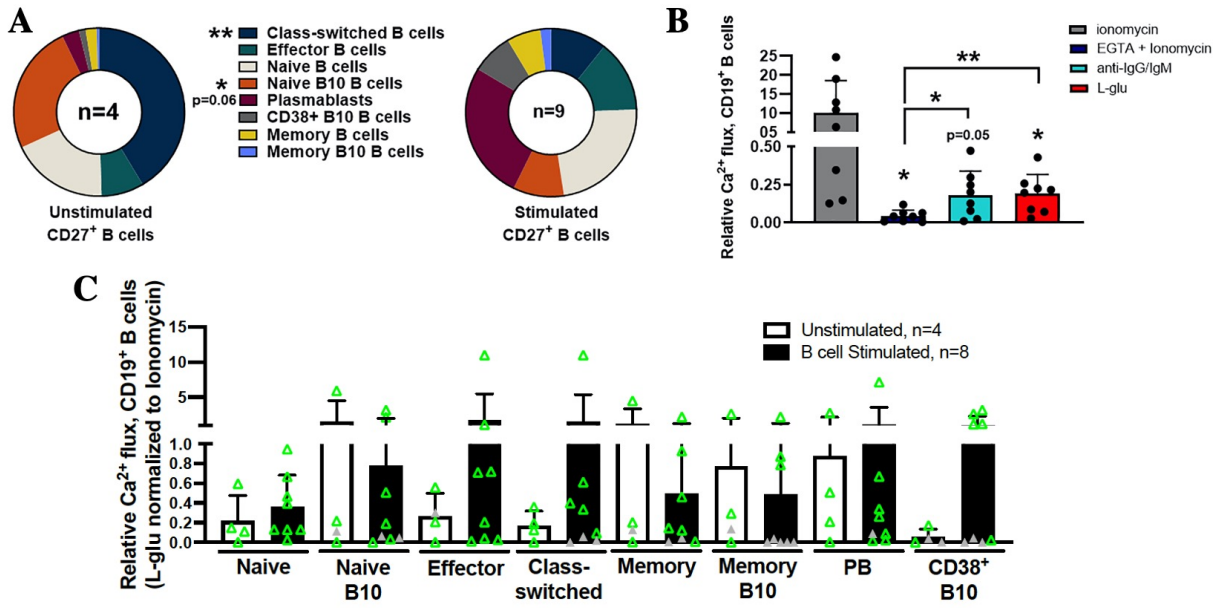

Fig. 47 Glutamate induces a Ca^{2+} response in human peripheral blood B cell subsets. (**A**) The distribution of $CD27^+$ B cell subsets in (left) unstimulated or (right) stimulated healthy donor peripheral blood mononuclear cells (PBMCs), with significant changes in population percentages identified in the legend. (**B**) The Ca^{2+} responses of various stimuli normalized to ionomycin in stimulated $CD19^+$ PBMC B cells; the positive response to glutamate (L-glu) in 8/8 stimulated healthy donor B cells (black circles) is significantly higher than the EGTA control. (**C**) The Ca^{2+} response of positive (open green triangles) and non-responding (closed grey triangles) B cell subsets to 1μM L-glu, the positive responses to L-glu are significantly higher than the EGTA controls. Significance determined by Student's *t* test or mixed-effects one-way (*$p<0.05$, **$p<0.01$ vs. (A, C) unstimulated or (B) ionomycin control unless indicated by bracket). An n=12 experimental replicates were performed totaling an n=4-8 donors per group.

were non-responding donors within each B cell subset of both unstimulated and stimulated healthy control PBMCs (**Fig. 47C** and **Table 15;** identification for each human B cell subset can be found in chapter 2.11C, Fig. 20). This was not dependent on glutamate concentration as 100μM glutamate did not increase Ca^{2+} entry in any B cell subset when compared to 1μM glutamate (**Table 16**, page 127). In fact, 100μM glutamate significantly reduced Ca^{2+} entry in stimulated naïve B cells (p=0.014) when compared to 1μM glutamate. Additionally, with the

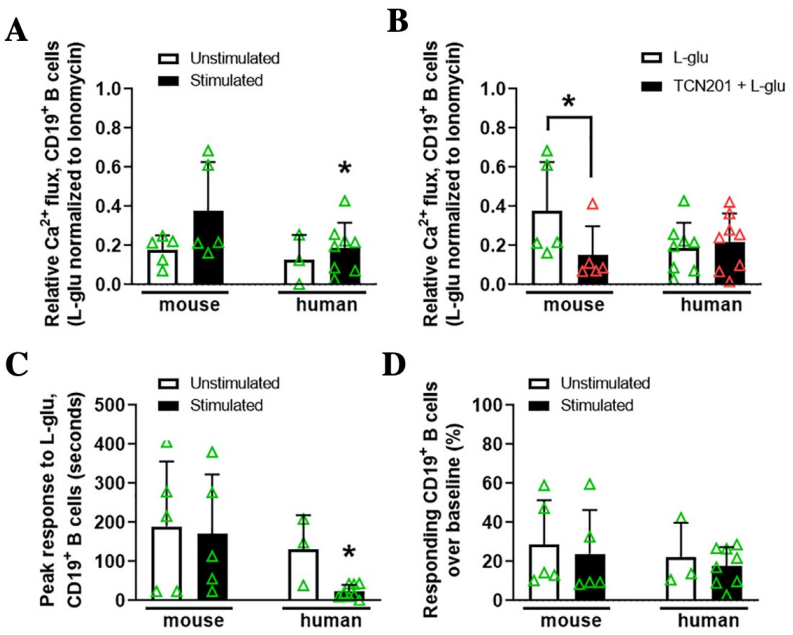

Fig. 48 Stimulated human CD19$^+$ B cells respond more quickly to glutamate than mouse B cells. (**A**) The Ca^{2+} response to 1μM glutamate (L-glu) in uninjured mouse and positive-responding human CD19$^+$ B cells (3 of 4 unstimulated healthy donor B cells responded over baseline; open green triangles). (**B**) The Ca^{2+} response to 1μM L-glu in stimulated CD19$^+$ B cells after antagonizing the GluN2A NMDAR subunit with TCN201 (red open triangles). (**C**) The time at which the peak response to 1μM L-glu was reached in mouse and positive-responding human CD19$^+$ B cells. (**D**) The percent of 1μM L-glu-responding CD19$^+$ B cells over baseline Ca^{2+} threshold in mice and positive-responding human donors. Significance determined by two-way ANOVA (*$p<0.05$ vs. mouse unless indicated by bracket). An n=10-11 experimental replicates were performed totaling an n=3-8 mice or donors per group.

exception of CD38$^+$ B10 B cells, none of NMDAR antagonists (D-APV, ifenprodil, or TCN201) reduced the Ca2$^+$ response to glutamate in any positive-responding B cell subset (**Table 16**). The failure to reduce the Ca^{2+} responses in human B cell subsets following NMDAR antagonism could, in part, be a result of an insufficient pre-incubation or an ineffective concentration of NMDAR antagonist required to achieve the effect observed in purified stimulated mouse B cells. Lastly, when comparing the kinetics of the overarching CD19$^+$ B cell population between mice and humans (**Fig. 48**), the glutamate-induced Ca2$^+$ response of stimulated human B cells are

quicker to respond to glutamate than stimulated mouse B cells, which may similarly be attributed to NMDAR activity.

5.2C Glutamate upregulates BDNF in B cells

In neurons, synaptic GluN2A-NMDAR signaling activates the transcription factor CREB to induce pro-survival signaling [4, 46, 258, 294, 295] and upregulate BDNF [4, 296]. BDNF also initiates autocrine signaling through the BDNF receptor, TrkB, but not through $p75^{NTR}$ (please refer to Fig. 32 for a visual schematic) [59]. To better understand the NMDAR-neurotrophin signaling cascade that may occur in B cells upon glutamate binding, key NMDAR-signaling neurotrophins, transcription factors and neurotrophin receptor transcripts were assessed in uninjured and post-stroke B cells. For clarity, the effect of stroke and glutamate on neurotrophin and neurotrophin receptor gene expression will be presented first, followed by changes in the respective gene expression that occur after LPS stimulation.

5.2Ci Autocrine BDNF signaling is upregulated in unstimulated B cells

Stroke injury significantly increased the low basal level of BDNF mRNA expression in B cells ($p=0.01$; **Fig. 49A**) whereas IL-10 expression, though more abundant than BDNF, was unaffected (**Fig. 49A**). Interestingly, stroke ($F_{(1, 26)}=11.13$, $p=0.003$) and glutamate ($F_{(1, 26)}=4.37$, $p=0.046$) individually increased BDNF mRNA expression (both **Fig. 49B** and **Table 17**, page 128) in B cells, with a 6.5-fold increase observed in post-stroke B cells when compared to untreated controls ($p=0.005$; **Fig. 49B**). Conversely, IL-10 expression was neither affected by stroke nor glutamate treatment (both **Fig. 49F** and **Table 17**), suggesting that IL-10 is not a key neurotrophin associated with the GluN2A signaling cascade in B cells. To confirm our BDNF

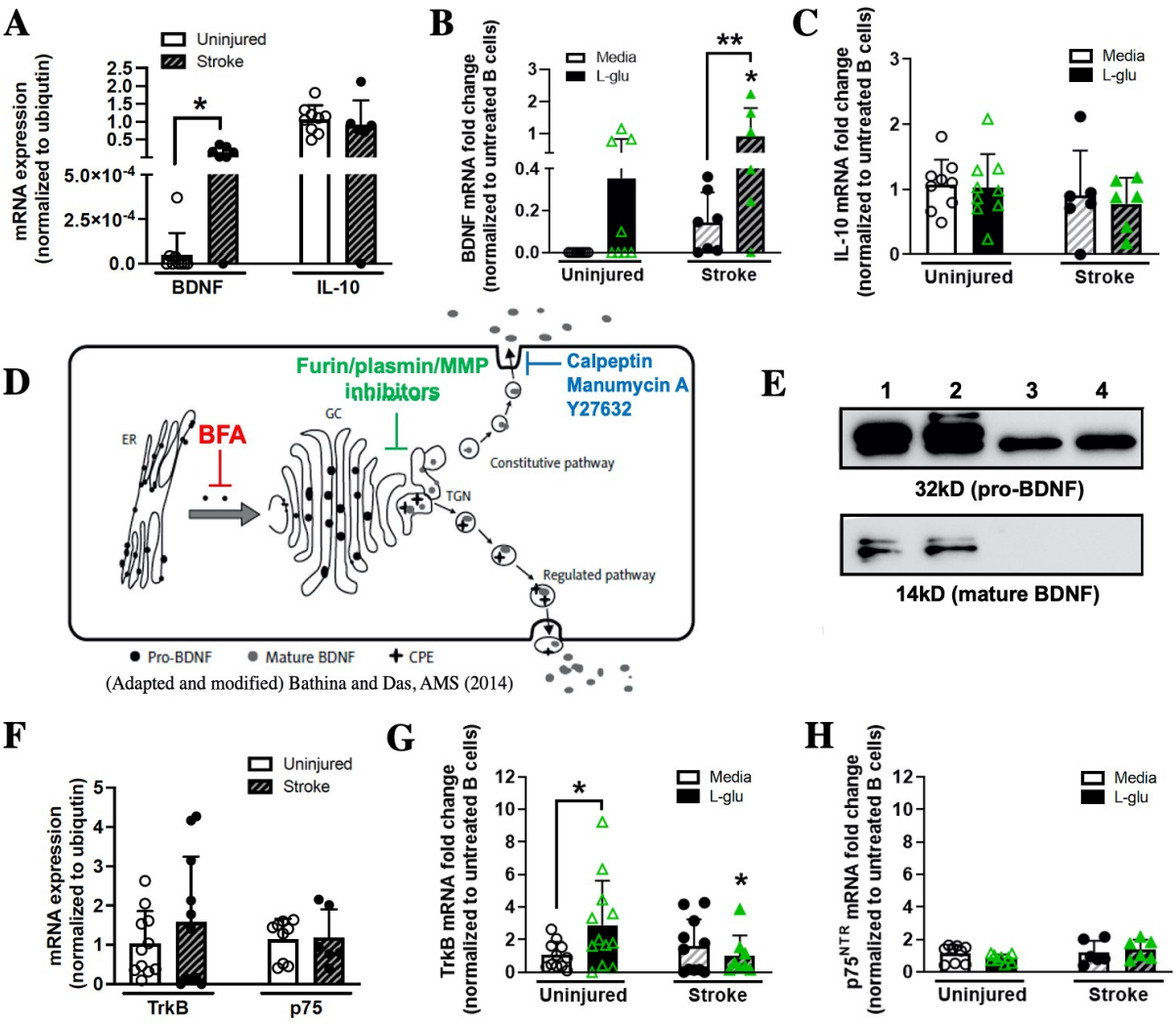

Fig. 49 Stroke injury and glutamate treatment upregulate BDNF signaling in B cells. Basal (**A**) neurotrophin mRNA expression in uninjured (open symbols; solid bars) and post-stroke (closed symbols; hatched bars) B cells. (**B**) BDNF and (**C**) IL-10 mRNA expression in uninjured and post-stroke B cells following a 24-hour treatment of 1μM glutamate (L-glu; green triangles; black bars) or media control (black circles). (**D**) Schematic showing pro-to-mature BDNF cleavage within the endoplasmic reticulum (ER), Golgi complex (GC) and trans-Golgi network (TGN). Inhibitors of ER-GC transport (brefeldin-A (BFA); red), GC-TGN packing and transport (green) or the formation and release of extracellular vesicles (blue) are shown. (**E**) Western blot analysis of pro-BDNF (32kD) and mature BDNF (14kD) expression in lysates of L-glu-treated B cells; Lane 1- CMV/BDNF/mCh-transfected HEK293-T cells, Lane 2 - brefeldin-treated CMV/BDNF/mCh-transfected HEK293-T cells, Lanes 3,4 brefeldin-treated B cells from 2 uninjured mice after a 24-hour treatment with 1μM L-glu. BDNF and (**F**) BDNF receptor in uninjured and post-stroke B cells. 1μM L-glu induced a fold change in mRNA expression of (**G**) TrkB, but not (**H**) $p75^{NTR}$ in uninjured and post-stroke B cells. Significance determined by Student's *t*-test or two-way ANOVA (*$p<0.05$, **$p<0.01$ vs. uninjured control unless indicated by bracket). An n=3-4 experimental replicates were performed totaling an n=6-9 mice per group.

mRNA data, we isolated protein from 5-10x10^6 B cells for western blot analysis of BDNF. However, B cells were pre-incubated with brefeldin-A (BFA), a endoplasmic reticulum to Golgi complex transport inhibitor [297], to ensure a sufficient amount of protein could be obtained. In neurons, however, pro-BDNF is cleaved to its' mature isoform by proteases (e.g., furin proteases [298], plasmin [299] and MMPs [300]) at the n-terminus of the trans-Golgi network and subsequently becomes transported in vesicles to be released through the regulated secretory pathway (**Fig. 49D**) [298]. Thus, the BFA-treatment prevented us from detecting the mature isoform of BDNF in glutamate-treated B cells (**Fig. 49E**). Nonetheless, our BDNF ELISA (Fig. 34) and *in vitro* ischemic injury (Fig. 35, 36) studies confirm that pro-BDNF is cleaved to the functional, mature BDNF isoform in B cells.

With respect to NMDAR-relevant transcription factor mRNA in B cells, neither stroke nor glutamate impacted CREB (or CREM, a CREB family transcription factor [296]) mRNA expression in either uninjured or post-stroke B cells (**Table 17**). Our data suggest that CREB/CREM may, instead, be undergoing post-translational modifications, such as phosphorylation, known to induce BDNF production [301]. With respect to BDNF receptors, neither of the two receptors were impacted by stroke injury (**Fig. 49F**). Glutamate did however, increase TrkB in uninjured B cells and had a significant interaction with stroke injury ($F_{(1, 38)}$=4.53, p=0.04; **Fig. 49G**) as a 2.9-fold decrease was observed in glutamate-treated post-stroke B cells (p=0.029). The differential regulation of TrkB may also reflect the extent and impact of mature BDNF-signaling in post-stroke B cells, as neither stroke nor glutamate impacted B cell $p75^{NTR}$ expression (**Fig. 49H**).

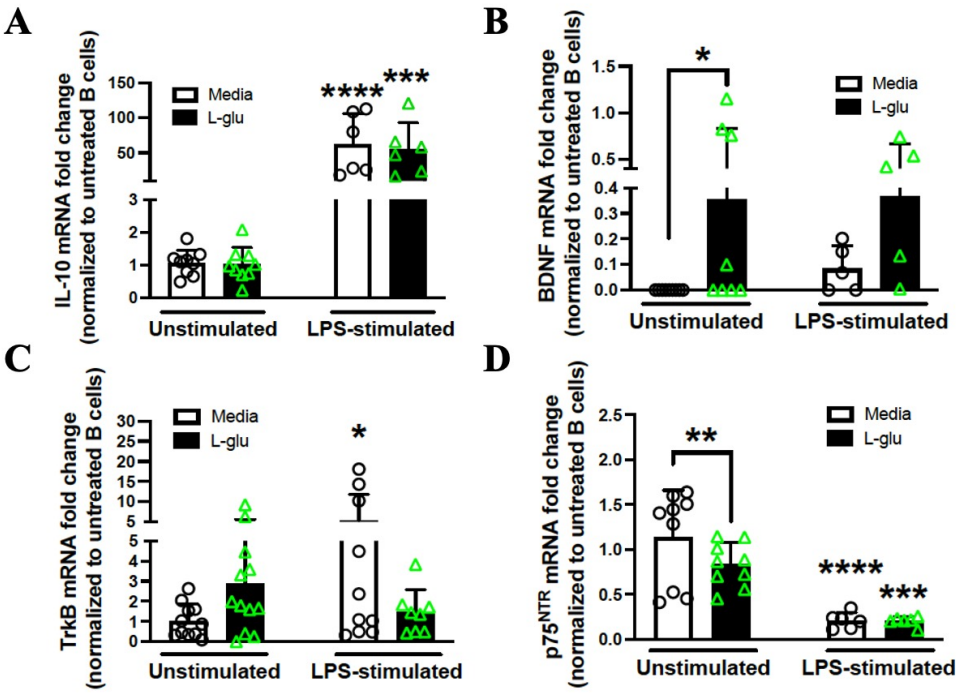

Fig. 50 LPS differentially regulates BDNF receptors in uninjured B cells. LPS upregulates the pro-survival BDNF receptor in uninjured B cells. Uninjured splenic B cells were stimulated with LPS for 24 hours followed by a subsequent treatment of glutamate (L-glu; green triangles) for 24 hours. Fold change in mRNA expression of (**A**) IL-10, (**B**) BDNF, (**C**) TrkB and (**D**) $p75^{NTR}$ in LPS-stimulated B cells treated with or without L-glu. Significance determined by mixed-effects two-way ANOVA (*$p<0.05$, **$p<0.01$, ***$p<0.001$, ****$p<0.0001$ vs. unstimulated control unless indicated by bracket). An n=3-4 experimental replicates were performed totaling an n=6-11 mice per group.

Collectively, these data, along with those discussed in 5.2Bi, suggest that neurophysiological levels of glutamate promote an autocrine BDNF signaling cascade in B cells much like the autocrine neuronal Glu2NA-BDNF signaling.

5.2Cii LPS supports autocrine BDNF signaling in B cells

Given that B cells require stimulation to enable NMDAR activity (as seen in 5.2Biii), we also assessed the NMDAR signaling cascade in LPS-stimulated B cells. LPS significantly increased IL-10 mRNA in uninjured ($F_{(1,13)}$=21.11, p=0.001; **Fig. 50A**) and post-

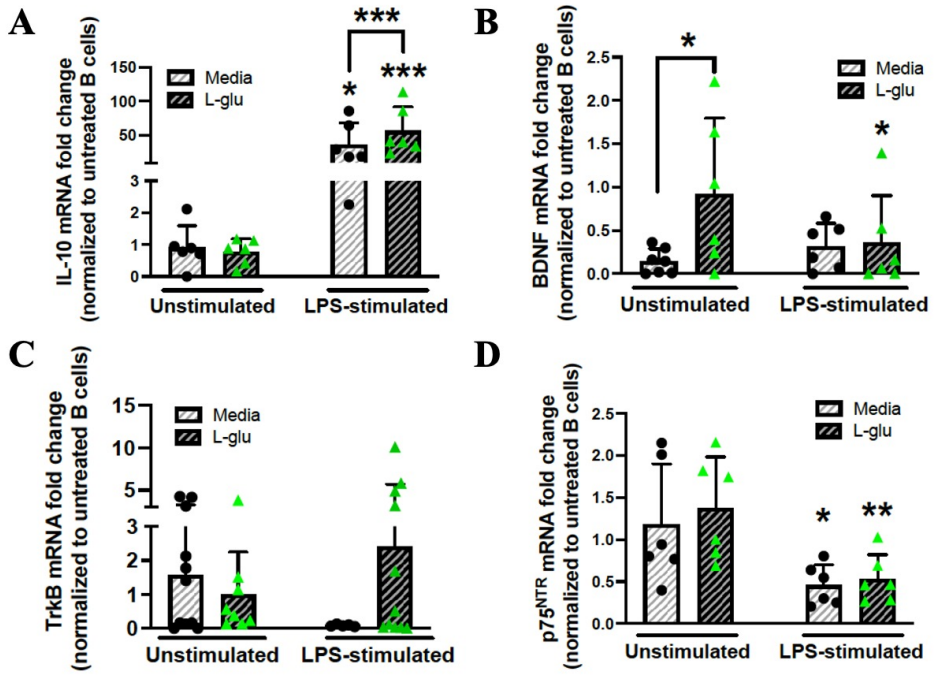

Fig. 51 LPS reduces the pro-death BDNF receptor in post-stroke B cells. Post-stroke splenic B cells were stimulated with LPS for 24 hours followed by a subsequent treatment of 1μM glutamate (L-glu; green triangles) for 24 hours. Fold change in mRNA expression of (**A**) IL-10, (**B**) BDNF, (**C**) TrkB and (**D**) $p75^{NTR}$ in LPS-stimulated B cells treated with or without L-glu. Significance determined by mixed-effects two-way ANOVA (*$p<0.05$, **$p<0.01$, ***$p<0.001$, vs. unstimulated control unless indicated by bracket). An n=3-4 experimental replicates were performed totaling an n=6-11 mice per group.

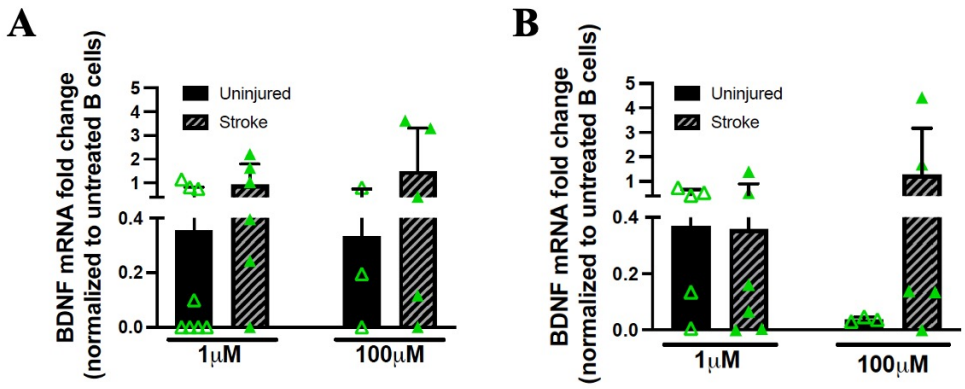

Fig. 52 100μM glutamate does not impact BDNF expression in LPS-stimulated B cells. BDNF mRNA expression in (**A**) unstimulated or (**B**) LPS-stimulated B cells. Data analyzed by mixed-effects two-way ANOVA. An n=3-4 experimental replicates were performed totaling an n=5-10 mice per group

stroke ($F_{(1,10)}$=11.69, p=0.007; **Fig. 51A**) B cells, as expected [191]. Although LPS exerted no impact on BDNF expression, glutamate did significantly increase BDNF expression in both unstimulated and stimulated, uninjured B cells ($F_{(1,23)}$=7.45, p=0.01; **Fig. 50B**). Additionally, treatment with the neuropathological concentration glutamate (i.e., 100μM) for 24 hours had no effect on BDNF mRNA expression in either unstimulated or stimulated B cells (**Fig. 52**). With respect to BDNF receptors, LPS significantly increased TrkB in uninjured B cells (p=0.01; **Fig. 50C**) and reduced $p75^{NTR}$ in uninjured ($F_{(1,13)}$=27.45, p=0.0002; **Fig. 50D**) and post-stroke ($F_{(1,20)}$=14.28, p=0.001; **Fig. 51D**) B cells. These studies suggest that both unstimulated and stimulated B cells have the capacity to initiate autocrine BDNF signaling in response to glutamate.

5.3 Conclusion

Lymphocyte NMDARs primarily regulate Ca^{2+} entry into the cell and, as a result, impact lymphocyte activation [153, 302], proliferation [146, 149, 302], cytokine production [152, 303], and cell survival [145, 148] under homeostatic and disease conditions. GluN2A signaling drives BDNF-induced neuroplasticity after stroke[4], but the role of NMDAR subunit signaling in B cells is not clear. In fact, studies investigating lymphocyte NMDAR functions have only focused on: 1.) GluN1 or GluN2 without A-D subunit specificity [148, 263, 265]; or 2.) PBMCs or T cells [152, 153], and never B cells. We show that B cell GluN2A becomes preferentially engaged after glutamate exposure or stroke injury in most B cell subsets and coincides with an upregulation of BDNF in B cells. Thus, GluN2A-BDNF signaling could be a potential mechanism by which B cells exert neurotrophic effects to support structural and functional

plasticity after stroke in contralesional areas not undergoing excitotoxicity and ostensibly, without inflammation (e.g., cytokines, danger-associated-molecular patterns (DAMPs), etc.).

Table 7 – Relative L-glu-induced $Ca2^+$ response of effector B cells in the presence or absence of NMDAR antagonists

	Uninjured B cells			Post-stroke B cells			2-way ANOVA Results		
	Unstim.	LPS	p value	Unstim.	LPS	p value	Stimulation	Stroke	Interaction
L-glu 1μM	0.16	0.35	**0.04**	0.2	0.32	0.11	**F = 7.786, p = 0.01**	F = 0.02, p = 0.88	F = 0.19, p = 0.67
L-glu 100μM	0.18	0.3†	0.15	0.16	0.28	0.12	**F = 4.93, p = 0.04**	F = 0.13, p = 0.72	F = 0.0004, p = 0.98
D-APV + L-glu 1μM	0.15	0.23†	0.36	0.16†	0.25†	0.25	F = 2.28, p = 0.15	F = 0.005, p = 0.95	F = 0.02, p = 0.88
Ifenprodil + L-glu 1μM	0.16	0.21††	0.5	0.14#	0.21†	0.37	F = 1.28, p = 0.27	F = 0.04, p = 0.84	F = 0.02, p = 0.89
TCN201 + L-glu 1μM	0.1†	0.11†	0.89	0.16	0.2†	0.47	F = 0.39, p = 0.54	F = 3.06, p = 0.1	F = 0.18, p = 0.68

Significant effects of LPS stimulation, stroke, and an interaction between the two are bolded in the right-most column. † $p<0.05$, †† $p<0.01$ vs. 1μM L-glu of the respective inter-column group.

Table 8 - Relative L-glu-induced $Ca2^+$ response of class-switched B cells in the presence or absence of NMDAR antagonists

	Uninjured B cells			Post-stroke B cells			2-way ANOVA Results		
	Unstim.	LPS	p value	Unstim.	LPS	p value	Stimulation	Stroke	Interaction
L-glu 1μM	0.33	0.43	0.5	0.37	0.45	0.35	F = 1.4, p = 0.25	F = 0.001, p = 0.97	F = 0.03, p = 0.86
L-glu 100μM	0.33	0.36†	0.821	0.35	0.41	0.445	F = 0.5, p = 0.49	F = 0.04, p = 0.85	F = 0.14, p = 0.71
D-APV + L-glu 1μM	0.29	0.28†	0.94	0.35	0.37	0.63	F = 0.08, p = 0.79	F = 0.22, p = 0.65	F = 0.15, p = 0.7
Ifenprodil + L-glu 1μM	0.28†	0.28†	0.99	0.33	0.36†	0.59	F = 0.14, p = 0.72	F = 0.22, p = 0.64	F = 0.15, p = 0.7
TCN201 + L-glu 1μM	0.22	0.16†	0.65	0.35	0.31	0.78	F = 0.27, p = 0.61	F = 2.42, p = 0.14	F = 0.02, p = 0.9

Significant effects of LPS stimulation, stroke, and an interaction between the two are bolded in the right-most column. † $p<0.05$, †† $p<0.01$ vs. 1μM L-glu of the respective inter-column group.

Table 9 - Relative L-glu-induced $Ca2^+$ response of $B220^+$ ASCs in the presence or absence of NMDAR antagonists									
	Uninjured B cells			**Post-stroke B cells**			**2-way ANOVA Results**		
	Unstim.	LPS	p value	Unstim.	LPS	p value	Stimulation	Stroke	Interaction
L-glu 1μM	0.15	0.45	**0.001**	0.12	0.37	**0.002**	**F = 28.70, p <0.0001**	F = 1.28, p = 0.27	F = 0.19, p = 0.67
L-glu 100μM	0.14	0.31†	**0.03**	0.09	0.29†	**0.01**	**F = 14.81, p = 0.001**	F = 0.46, p = 0.51	F = 0.10, p = 0.76
D-APV + L-glu 1μM	0.13	0.24†	0.1	0.09†	0.24†	**0.02**	**F = 9.24, p = 0.01**	F = 0.16, p = 0.7	F = 0.26, p = 0.62
Ifenprodil + L-glu 1μM	0.12†	0.2††	0.24	0.09	0.22††	**0.04**	**F = 5.94, p = 0.03**	F = 0.004, p = 0.95	F = 0.46, p = 0.51
TCN201 + L-glu 1μM	0.13	0.13†	1	0.08	0.19††	0.08	F = 1.78, p = 0.20	F = 0.004, p = 0.95	F = 1.8, p = 0.20
Significant effects of LPS stimulation, stroke, and an interaction between the two are bolded in the right-most column. † p<0.05, †† p<0.01 vs. 1μM L-glu of the respective inter-column group.									

Table 10 - Relative L-glu-induced $Ca2^+$ response of naïve B cells in the presence or absence of NMDAR antagonists									
	Uninjured B cells			**Post-stroke B cells**			**2-way ANOVA Results**		
	Unstim.	LPS	p value	Unstim.	LPS	p value	Stimulation	Stroke	Interaction
L-glu 1μM	0.15	0.28	0.11	0.12	0.16	0.51	F = 2.8, p = 0.11	F = 2.07, p = 0.17	F = 0.56, p = 0.47
L-glu 100μM	0.15	0.2†	0.54	0.11	0.15	0.55	F = 0.76, p = 0.39	F = 0.85, p = 0.37	F = 0.002, p = 0.97
D-APV + L-glu 1μM	0.13	0.16†	0.71	0.12	0.14	0.7	F = 0.3, p = 0.59	F = 0.24, p = 0.63	F = 2.13e-005, p = 1.0
Ifenprodil + L-glu 1μM	0.14	0.15†	0.81	0.1	0.14†	0.6	F = 0.3, p = 0.59	F = 0.33, p = 0.57	F = 0.04, p = 0.85
TCN201 + L-glu 1μM	0.12	0.07†	0.46	0.11	0.1†	0.96	F = 0.32, p = 0.58	F = 0.09, p = 0. 77	F = 0.25, p = 0.62
Significant effects of LPS stimulation, stroke, and an interaction between the two are bolded in the right-most column. † p<0.05, †† p<0.01 vs. 1μM L-glu of the respective inter-column group.									

Table 11 - Relative L-glu-induced $Ca2^+$ response of Bregs in the presence or absence of NMDAR antagonists									
	Uninjured B cells			**Stroke-injured B cells**			**2-way ANOVA Results**		
	Unstim.	LPS	p value	Unstim.	LPS	p value	Stimulation	Stroke	Interaction
L-glu 1μM	0.17	0.32	0.12	0.13	0.24	0.18	**F = 4.88, p = 0.04**	F = 1.23, p = 0.28	F = 0.06, p = 0.80
L-glu 100μM	0.18	0.25††	0.37	0.11	0.22	0.15	F = 2.91, p = 0.11	F = 0.89, p = 0.36	F = 0.14, p = 0.71
D-APV + L-glu 1μM	0.14	0.19††	0.53	0.11	0.19	0.30	F = 1.45, p = 0.24	F = 0.09, p = 0.77	F = 0.07, p = 0.79
Ifenprodil + L-glu 1μM	0.13	0.2††	0.42	0.1	0.17†	0.39	F = 1.45, p = 0.25	F = 0.25, p = 0.62	F = 2.64e-005, p = 0.1
TCN201 + L-glu 1μM	0.13	0.1†	0.63	0.11	0.15	0.43	F = 0.05, p = 0.83	F = 0.07, p = 0.79	F = 0.86, p = 0.37

Significant effects of LPS stimulation, stroke, and an interaction between the two are bolded in the right-most column. † $p<0.05$, †† $p<0.01$ vs. 1μM L-glu of the respective inter-column group.

Table 12 - Relative L-glu-induced $Ca2^+$ response of $B220^-$ ASCs in the presence or absence of NMDAR antagonists									
	Uninjured B cells			**Post-stroke B cells**			**2-way ANOVA Results**		
	Unstim.	LPS	p value	Unstim.	LPS	p value	Stimulation	Stroke	Interaction
L-glu 1μM	0.39	1.11	0.17	0.25	0.35	0.91	F = 1.26, p = 0.28	F = 1.56, p = 0.23	F = 0.92, p = 0.35
L-glu 100μM	0.36	0.4	0.73	0.23	0.27†	0.79	F = 0.2, p =0.66	F = 2.12, p = 0.16	F = 0.004, p = 0.95
D-APV + L-glu 1μM	0.29	0.76	0.25	0.16#	0.22††	0.91	F = 0.88, p = 0.36	F = 1.37, p = 0.26	F = 0.61, p = 0.44
Ifenprodil + L-glu 1μM	0.3	0.64	0.31	0.16	0.2††	0.92	F = 0.67, p = 0.43	F = 1.59, p = 0.22	F = 0.47, p = 0.50
TCN201 + L-glu 1μM	0.28#	0.71#	0.34	0.19	0.16†	0.94	F = 0.41, p = 0.53	F = 1.02, p = 0.33	F = 0.56, p = 0.47

Significant effects of LPS stimulation, stroke, and an interaction between the two are bolded in the right-most column. † $p<0.05$, †† $p<0.01$ vs. 1μM L-glu of the respective inter-column group.

Table 13 – The effect of LPS stimulation on mouse B cell subset percentages within $CD19^+$ B cells

	Uninjured B cells			**Post-stroke B cells**			**2-way ANOVA Results**		
	Unstim.	LPS	p value	Unstim.	LPS	p value	Stimulation	Stroke	Interaction
Naive B cells	19.14	7.24	0.009	21.81	4.85	**0.0004**	**F = 25.78, p<0.0001**	F = 0.002, p = 0.96	F = 0.79, p = 0.38
Effector B cells	8.83	39.88	**<0.0001**	5.21	34.63	**<0.0001**	F = 59.43, **p<0.0001**	F = 1.28, p = 0.27	F = 0.04, p = 0.84
Class-switched B cells	6.79	14.16	0.108	6.11	16.52	**0.02**	**F = 8.58, p = 0.009**	F = 0.08, p = 0.79	F = 0.25, p = 0.62
Bregs	4.23	7.24	**0.005**	5.14	3.89	0.19	F = 1.78, p = 0.20	F = 3.44, p = 0.08	**F = 10.37, p = 0.005**
$B220^+$ ASCs	4.86	5.36	0.81	4.14	5.65	0.46	F = 0.49, p = 0.49	F = 0.02, p = 0.88	F = 0.12, p = 0.73
$B220^-$ ASCs	0.24	0.87	0.1	0.16	1.37	**0.003**	**F = 13.16, p = 0.002**	F = 0.69, p = 0.41	F = 1.23, p = 0.27

Significant effects of LPS stimulation, stroke, and an interaction between the two are bolded in the right-most column.

Table 14 – Sex & Age of Peripheral Blood Mononuclear Cell Healthy Donors

Treatment	**Sex**	**Age**
unstimulated	F	61 years
unstimulated	M	28 years
unstimulated	F	21 years
unstimulated	F	26 years
stimulated	F	53 years
stimulated	M	27 years
stimulated	M	30 years
stimulated	M	29 years
stimulated	F	41 years
stimulated	M	25 years
stimulated	F	33 years
stimulated	M	30 years

Table 15 – The effect of stimulation on human B cell subset percentages within CD19$^+$ B cells			
	Treatment		**Student's *t*-test Results**
B cell subset	Unstimulated	Stimulated	p value
Class-switched B cells	14.17	2.36	**0.01**
Effector B cells	2.76	3.05	0.80
Naïve B cells	6.34	5.14	0.79
Naïve B10 B cells	8.48	2.13	**0.03**
Memory B cells	0.72	1.42	0.25
Memory B10 B cells	0.15	0.45	0.55
Plasmablasts	1.11	5.86	**0.059**
CD38$^+$ B10 B cells	0.43	1.74	0.44
Significant effects of stimulation are shown in the right-most column ($^{\#}p<0.06$ vs. unstimulated controls).			

Table 16 – Relative L-glu-induced $Ca2^+$ response of stimulated, positive-responding human PBMC B cells subsets in the presence or absence of NMDAR antagonists						
	Treatment					**One-way ANOVA Results**
B cell subset (positive responders/total)	L-glu 1μM	L-glu 100μM	D-APV + L-glu 1μM	Ifenprodil + L-glu 1μM	TCN201 + L-glu 1μM	p value
Class-switched B cells (5/8)	2.49	11.2	1.6	1.67	5.46	F = 0.85, p = 0.43
Effector B cells (8/8)	1.73	1.02	0.73	1.88	0.91	F = 1.03, p = 0.34
Naïve B cells (8/8)	0.36	0.28†	0.29	0.25#	0.28	F = 1.55, p = 0.24
Naïve B10 B cells (5/8)	1.22	2.55	0.84	0.54	0.5	F = 0.83, p = 0.42
Memory B cells (4/8)	0.91	3.04	0.77	0.66	0.45	F = 0.87, p = 0.42
Memory B10 B cells (2/8)	1.55	13.16	1.31	0.14	8.73	F = 2.77, p = 0.34
Plasmablasts (7/8)	1.22	2.78	1.1	1.8	1.5	F = 0.88, p = 0.37
$CD38^+$ B10 B cells (5/8)	1.65	3.06	0.96*	0.73#	0.76	F = 1.26, p = 0.33
One-way ANOVA results shown in the right-most column. #p<0.06, †p<0.05 vs. 1μM L-glu for the respective B cell subset						

Table 17 - mRNA Fold Change vs. untreated B cells									
	Uninjured B cells			**Post-stroke B cells**			**2-way ANOVA Results**		
	Untre-ated	L-glu 1μM	p value	Untre-ated	L-glu 1μM	p value	L-glu	Stroke	Interaction
BDNF	5.03 E-05	0.35	0.13	0.14	0.92†	**0.005**	**F = 11.13, p = 0.003**	**F = 4.370, p = 0.05**	F = 1.57, p = 0.22
IL-10	1.07	1.02	0.88	0.91	0.78	0.65	F = 0.21, p = 0.65	F = 1.21, p = 0.28	F = 0.06, p = 0.80
TrkB	1.03	2.89	**0.02**	1.58	1†	0.5	F = 1.24, p = 0.27	F = 1.38, p = 0.25	**F = 4.53, p = 0.04**
$p75^{NTR}$	1.14	0.83	0.22	1.18	$1.38^{\#}$	0.52	F = 0.08, p = 0.78	F = 2.26, p = 0.14	F = 1.7, p = 0.20
GluN2A	0.25	0.7	0.2	0.77	1.15	0.29	F = 2.81, p = 0.10	**F = 3.93, p = 0.06**	F = 0.02, p = 0.89
GluN2B	0.73	0.8	0.85	0.61	0.58	0.94	F = 0.004, p = 0.95	F = 0.37, p = 0.55	F = 0.03, p = 0.86
CREB	1.09	1.13	0.84	1.06	1.4	0.07	F = 2.30, p = 0.14	F = 0.96, p = 0.33	F = 1.52, p = 0.22
CREM	1.05	1.17	0.55	1.07	1.37	0.16	F = 2.16, p = 0.15	F = 0.63, p = 0.43	F = 0.42, p = 0.52

Significant effects of glutamate, stroke, and/or an interaction between the two were determined by two-way ANOVA are bolded in the right-most column. $^{\#}p<0.06$, † $p<0.05$ vs. the respective uninjured control.

CHAPTER SIX

Conclusions and Discussion

DICUSSION

6.1 The implications of BDNF-producing B cells in stroke recovery

The loss of blood flow during ischemic stroke triggers cascades of reactions including neurotransmitter and ion dysregulation, excitotoxicity, BBB disruption, metabolic stress, release of ROS, and necrotic tissue/cell death [304]. In addition to the initial ischemic insult, activated immune cells, including B cells, infiltrate the brain in response to local chemokine gradients upregulated after stroke [68, 69, 93, 97], including the B cell-specific chemokine CXCL13, which we previously showed was upregulated by the post-stroke endothelium [182]. B cells can produce CNS-reactive antibodies that impair cognition [92, 127, 219] or secrete IL-10 that ameliorates stroke pathology [120, 121, 123]. However, our studies show that B cells also play a protective role by promoting post-stroke plasticity and functional recovery [166]. In continuance of these studies, we wanted to know whether B cell-mediated neuroprotection is attributed to neuroplasticity induced locally by B cells within specific brain regions after stroke. In chapter 3, we utilized STPT to identify significant bilateral migration of B cells to select brain regions, including regions undergoing post-stroke plasticity that are outside of the area of infarction and thus, distant to the epicenter of post-stroke neuroinflammation. In chapter 4, we also observed that B cells regulate synaptic transmission within one of the contralesional regions that B cells migrate to after stroke. In chapter 5, we confirmed the capacity of physiologic levels of glutamate, found in remote brain areas, as capable of eliciting pro-neurotrophic signaling

mechanisms in B cells. Thus, our studies suggest that the neuroprotective effect B cells exert on post-stroke plasticity and functional recovery may stem, in part, from their ability to migrate into specific brain regions and support proper synaptic function. This chapter will discuss the implications of the neuroimmune interactions of BDNF-producing B cells in stroke recovery as well as their potential implications in other CNS and non-CNS diseases.

6.1A B cells migrate to remote brain regions to support functional recovery after stroke

The spontaneous and regenerative mechanisms that occur in the ipsi- and contralesional hemispheres begin immediately after stroke onset and continue progressively over time to counteract ischemic injury and reorganize network connectivity during functional recovery [213, 305]. The degree of structural neuroplasticity (i.e., dendritic remodeling, synaptogenesis and axonal sprouting) in both injured and uninjured regions [228], such as the hippocampus [306], can significantly impact synaptic transmission that in turn, mediates motor and cognitive function after stroke. Moreover, the location of plasticity after stroke is of particular interest given that patient recovery is dependent on functional plasticity in areas outside of the infarct to restore and/or rehabilitate lost function [9]. Therefore, harnessing the migration pattern of B cells within the post-stroke brain to gain access to specific regions that regulate motor and cognitive function may prove to be a promising therapeutic to modulate functional plasticity and recovery after stroke.

6.1B B cells upregulate BDNF in response to glutamate via NMDAR signaling

The bilateral migration pattern of B cells into specific remote regions known to undergo significant reorganization after stroke [213], along with the regulation of post-stroke synaptic

transmission, raised a critical question in our studies: if B cells migrate into areas of the post-stroke brain (e.g., into the contralesional DG and cerebellum) that are not "pro-inflammatory" microenvironments capable of driving canonical B cell responses, what signal(s) might B cells encounter in the parenchyma that induce a neuroprotective response? Glutamate, a neurotransmitter that becomes highly dysregulated after stroke, drives neuronal excitotoxicity through extrasynaptic GluN2B-containing NMDARs [4, 262]. Conversely, synaptic GluN2A-containing NMDARs bind glutamate and initiate downstream pro-survival signaling, including the upregulation of BDNF [4, 258-260]. B cells, like neurons, also require BDNF for development [162] and survival [163]. Although lymphocytes express NDMARs [145, 146, 148, 151, 152, 172, 263-265], neither the subunit assembly of NMDARs nor the upregulation of BDNF following glutamate exposure have ever been investigated in B cells in the context of stroke. Thus, we investigated the NMDAR subunit assembly, glutamate-induced NMDAR activity and signaling cascade in B cells to delineate a potential mechanism by which B cells provide neurotrophic support in the post-stroke brain, particularly in "at-risk" brain regions that could benefit from enhanced and long-lasting support.

6.1Bi NMDAR subunit activity

Our studies in chapter 5 revealed that both stroke and glutamate differentially regulate gene and surface expression of the NMDAR subunit, GluN2A, but not GluN2B. While NMDAR subunit-specific roles in B cell function are yet to be defined, GluN2A and GluN2B likely mediate different signaling mechanisms much like GluN2A and GluN2B neuronal signaling after stroke [4]. It may be possible that GluN2A-NMDAR signaling is preferentially engaged over GluN2B in splenic B cells in efforts to upregulate pro-survival signaling. In

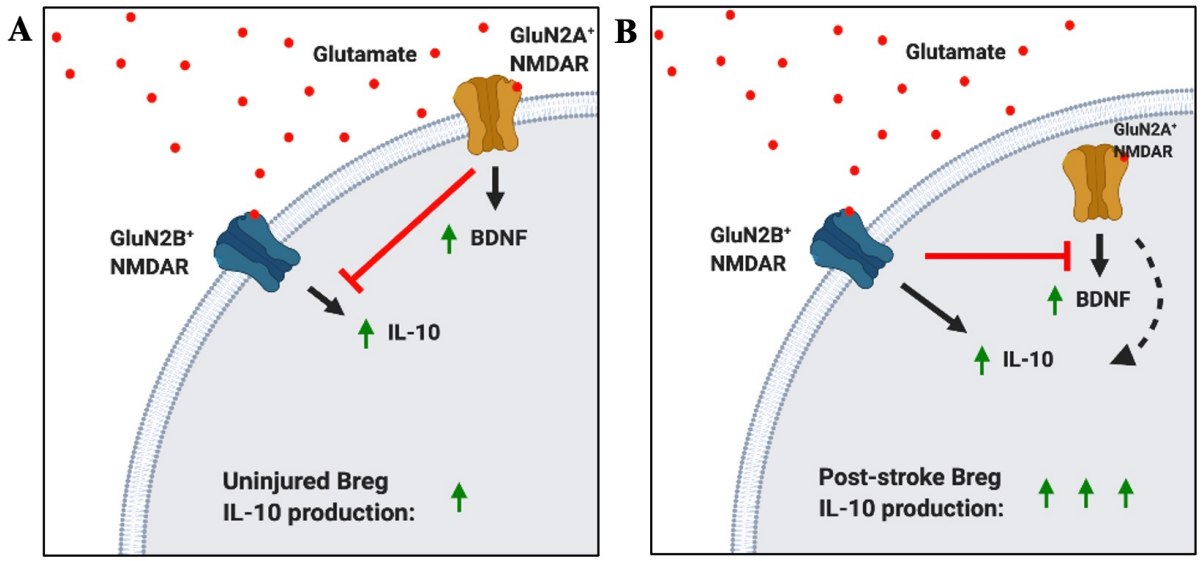

Fig. 53 Proposed model for NMDAR subunit-mediated IL-10 production in Bregs. (A) GluN2A-NMDARs elicit a glutamate-induced Ca2+ response uninjured Bregs, but not **(B)** post-stroke Bregs.

chapter 5, we also discovered that glutamate induces a Ca^{2+} response in mouse and human B cell subsets, with higher Ca^{2+} responses in class-switched B cells and $B220^{-}$ ASCs subsets. This observation may be associated with differences in the amounts of Ca^{2+} required to support the primary functionality of B cell subsets as they carry out their specific effector functions such antibody secretion [307-309]. Additionally, NMDARs mediate up to half of the glutamate-induced Ca^{2+} response in stimulated B cells with a shift toward GluN2B-activity in specific B cell subsets after stroke. This observation may provide insight into which post-stroke B subset(s) produces BDNF for future studies. The shift to GluN2B activity in specific subsets (e.g., Bregs) could indicate that all GluN2A subunits have been internalized as a way to reduce BDNF production and upregulate IL-10 (**Fig. 53**). In fact, lymphocytes with internalized GluN2A secrete more IL-10 in comparison to lymphocytes with non-internalized GluN2A [152]. Nonetheless, our data are the first to show that the glutamate-induced Ca^{2+} response differs

among human and mouse B cell subsets, which may reflect the magnitude of their overall neurotrophic capacity after stroke.

6.1Bii NMDAR upregulation of neurotrophin and neurotrophin receptors

Although BDNF is required for B cell development and function throughout life, the role of BDNF splice variants in B cell function has not yet been investigated. BDNF splice variants are spatially diverse and found in specific patterns throughout the brain (even at subcellular neuronal specificity) to enable localized BDNF production and support synaptic transmission [310]. As seen in chapter 5, glutamate upregulates a BDNF splice variant (mBDNF4 [310, 311], originating from BDNF exonIV in both mice and rats) in unstimulated and stimulated B cells that is abundantly expressed in hippocampal neurons [312-314]. Contrary to previous reports [163, 315, 316], LPS did not increase BDNF gene expression in B cells. However, unlike previous reports, our studies specifically assessed gene expression of the mBDNF4 splice variant which can be found in the spleen, but is specifically not expressed in T cells [275]. The increased Ca^{2+} activity of B cell NMDARs in stimulated B cells and the upregulation of mBDNF4 in both unstimulated and stimulated B cells following glutamate treatment suggests a shift from non-NMDAR-BDNF signaling towards NMDAR-BDNF signaling upon stimulation. Interestingly, IL-10 is unaffected by glutamate exposure and instead increases upon LPS stimulation. Additionally, increased mBDNF4 coincides with an increase in the TrkB BDNF receptor, but not $p75^{NTR}$ activity, suggesting active mature BDNF-TrkB signaling in B cells.

The studies performed in chapter 5 identify a novel NMDAR-BDNF signaling mechanism by which B cells may exert their neuroprotective phenotype to promote

neuroplasticity following ischemic injury. However, here are other neuroprotective factors that can be upregulated following NMDAR engagement. For example, lymphocytes have been reported to upregulate IL-10 and IL-8 downstream of the NMDAR [147, 152, 303], while downregulating IL-2, IL-6, and Th1 (i.e., IFNγ and TNFα) cytokines [147, 265, 317]. Therefore, it may be possible that BDNF, along with other potential anti-inflammatory and neuroprotective mediators produced downstream of the B cell NMDAR, not only support local neuroplasticity, but promote the survival of CNS-infiltrating B cells and enhance local B cell-derived BDNF production. Collectively, the migration of B cells to specific brain regions after stroke, the induction of NMDAR signaling, and upregulation of the mBDNF4 splice variant suggest that B cells could mediate region-specific neuroprotection in the recovering brain after stroke.

6.1C B cell-derived BDNF protects neurons from ischemic injury

Neuroplasticity occurs throughout life in healthy cortical, subcortical, and cerebellar brain regions that are responsible for brain development, neurogenesis, learning, and memory formation. However, after stroke, neuronal survival and functional plasticity requires significant neurotrophic support, particularly in regions experiencing extensive primary ischemic injury (e.g., oxygen-glucose deprivation and glutamate-induced excitotoxicity) [4]. BDNF, the most abundantly-produced neurotrophin in the CNS [318], has been a neurotrophin of long-standing interest for treatment of stroke [66, 67]. Given that neurons and glia are primary sources of BDNF within the CNS [319], we wanted to determine whether B cells could respond to signals released by ischemic-injured neurons and confer protection despite the already-existing levels of neuronal- and glial-derived BDNF. In chapter 4, we discovered that neuroprotection exerted by B

cells against the loss of neurons and neuronal dendrites following *in vitro* ischemic injury, is completely dependent on their secretion of BDNF.

As discussed in 6.1A, functional recovery after stroke is completely dependent on plasticity in remote areas of the brain and required significant neurotrophic support [9]. Thus, investigating mechanisms that can enhance endogenous neurotrophic support could allow for the development of novel neurotherapeutics that support long-term stroke recovery lasting for years after the ischemic insult. While our studies investigate NMDAR signaling as a potential mechanism upregulating BDNF in B cells, there are alternative mechanisms that could also potentially activate both mouse and human B cells to upregulate BDNF in the post-stroke brain. Some of those mechanisms include, but are not limited to, ionotropic and metabotropic glutamate receptor activity, TLR engagement [163, 315, 320], CD40/CD40L interactions [321], MyD88/NF-κB signaling [322], and autocrine BDNF signaling [163, 323]. There are also several clinical factors (including age, sex and genetics) that impact BDNF and are believed to significantly influence stroke recovery. Age, one of the biggest risk factors for stroke, drastically impacts the severity of stroke and degree of recovery [324, 325]. Circulating levels of BDNF decline with age [11] and are significantly lower in women [12]. In fact, post-stroke depression has been linked to low levels of BDNF [13], with an overall lower quality of life in women [16-18]. Additionally, genetic variations of BDNF (e.g., Val66Met BDNF polymorphism), expressed in up to 50% of the population [19, 20], reduce BDNF production and subsequently hinder post-stroke plasticity [21-24] and functional recovery. Although further studies are needed to determine the role of B cell-derived BDNF in age-, sex- and genetic-related plasticity after stroke, our studies highlight the therapeutic potential of harnessing the migration

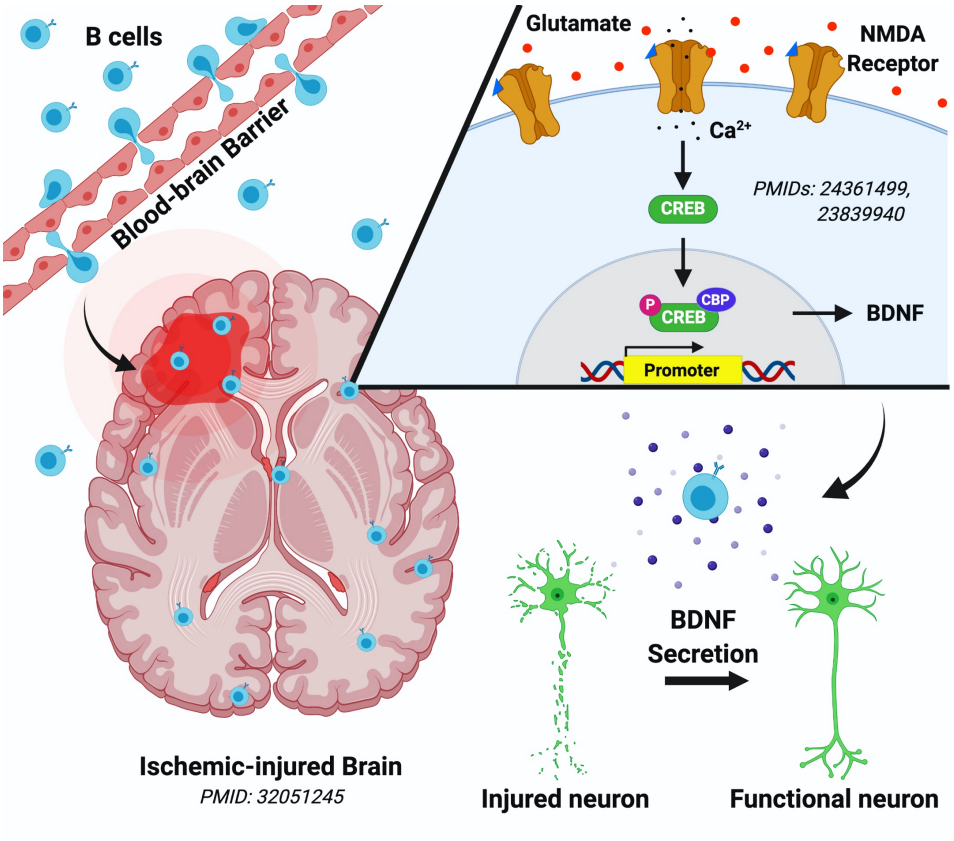

Fig. 54 A proposed model for the neurotrophic role of B cells in stroke recovery.

of B cells into the post stroke CNS to deliver enhanced, brain region-specific neurotrophic support to counter ischemic injury and clinical factors that can compromise stroke recovery. Our studies are the first to show that B cells bilaterally migrate to non-ischemic, remote brain regions outside the area of infarct and can respond to glutamate in a neurotrophic manner that promotes structural and functional neuroplasticity after stroke (**Fig. 54**).

6.2 Technical limitations

Following the completion of our studies, we assessed the limitations within our methodologies and wish to address them in the order of the data presented throughout chapters 3-

5, along with future studies that could improve our understanding of these neuro-immune mechanisms.

6.2A Brain warping, meningeal and ventricular analyses within STPT data

The automated quantification of STPT provides many advantages over traditional methods of mesoscale brain imaging. However, our machine learning algorithm was not trained to detect ischemic tissue in stroke-injured animals. Therefore, the automated quantification in STPT of stroke-injured brains could be impaired by improper tissue warping and atlas registration due to abnormal presentation of the brain tissue. An additional limitation of our STPT analysis of B cells and $CD8^+$ T cells stems from their ability to diapedese from the ventricles and the meninges into their targeted brain tissue after stroke [179, 180]. Not all of the meningeal lymphatics are removed during sample preparation, and the ventricles are adjacent to several analyzed brain regions. Thus, it is possible that these areas could be warped and registered into the atlas, giving the false positive impression of parenchymal penetration of B or $CD8^+$ T cells when in actuality, they are traveling through the meningeal lymphatics or ventricles to another location. Therefore, it may be necessary to visually inspect coronal sections on a case-by-case basis, particularly if larger immune cell populations are quantified in a similar manner.

6.2B Limited structural analysis of neurons in mixed cortical cultures

We initially designed our *in vitro* ischemic injury assays in pure neuronal cultures so that we could obtain high-resolution neuronal images for Sholl analysis to perform sophisticated analysis of dendritic arborization and dendritic spines [326]. However, it was not technically possible to co-culture pure neurons (requiring serum-free media) and B cells (requiring serum-rich media) together. Thus, we reverted to using our mixed cortical culture system that is grown

in 6-well polystyrene tissue culture plates. In addition, the image resolution of cells in the tissue culture plates becomes compromised at magnifications higher than 10x due to the optical resolution of polystyrene. Therefore, our *in vitro* analyses of structural plasticity in ischemic-injured neurons were limited to an assessment of total neuronal cells and neurons that had dendrites associated to their cell body. It may be possible that the neurotrophic effect of BDNF-producing B cells impacts the degree of dendritic arborization and spine density. Future studies should establish mixed cortical cultures on coverslips or glass-chamber slides for higher resolution analysis.

6.2C Physiological relevance of the glutamate-induced Ca^{2+} response in B cells

The glutamate-induced Ca^{2+} response downstream of the NMDAR in neurons occurs on the scale of milliseconds and has been determined through use of electrophysiological assays such as patch-clamp recordings or confocal live cell-imaging [327]. However, patch-clamp recordings are limited in the number of neurons that can be assessed at any given time. Ca^{2+} flow cytometry circumvents this limitation as the glutamate-induced Ca^{2+}response is continuously recorded in thousands of B cells over the course of 8 minutes. Unfortunately, the flow cytometer cannot record the glutamate-induced Ca^{2+}response response within the same B cell over the 8-minute recording. Additionally, the responses seen in Fig. 40C represent a shift in fluorescence once Ca^{2+} has bound to the intracellular Ca^{2+} indicator. Thus, it could be possible that the physiological time of glutamate uptake and Ca^{2+} entry occurs much sooner than the time it took the flow cytometer to detect a significant shift in fluorescence. Future studies should utilize an assay with higher sensitivity, such as patch-clamp recordings or confocal imaging, to determine the physiological time for glutamate uptake and Ca^{2+} entry in B cells on a per cell basis.

6.3 General implications of BDNF-producing B cells in other CNS diseases

The neurotrophic capacity of B cells has clinical implications in other CNS diseases (e.g., neurodegenerative, neuropsychiatric and neuroinflammatory diseases of the CNS) that are similarly affected by BDNF polymorphisms, sexual dimorphism, and age. The potential role for BDNF-producing B cells in each of those disease settings are discussed below.

6.3A Neurodegenerative diseases

The manifestation of neurodegenerative diseases, including vascular cognitive impairment and dementia (VCID), Alzheimer's (AD), Parkinson's (PD) and Huntington's disease (HD), is commonly associated with motor and/or cognitive impairment that progressively transitions toward dementia [328]. The aging process, hallmarked in part by genomic instability, cellular senescence, inflammation, and dysregulated cellular function [329], renders elderly adults most susceptible to developing neurodegenerative diseases, with varying sexual dimorphism depending on the specific disease [330]. For example, the production of BDNF is reduced in pre-clinical models and patients [331] with VCID [332, 333], AD [334-336], PD [337, 338] and HD; [339-341]. These BDNF deficiencies impair memory, language, and thinking – all cognitive deficits that progress toward dementia. BDNF polymorphisms (i.e., Val66Met) also increase the susceptibility of developing AD [342-344], PD [345] and HD [346, 347]. The circulating level of BDNF has also proven to be a useful biomarker for identifying neurodegenerative disease states and predicting cognitive decline [334-336]. As a result, therapeutic interventions designed to increase BDNF, such as exercise [348, 349] and deep brain stimulation [350-352], show promise in improving cognitive function. Interestingly, an increased frequency of circulating B cells after exercise [353, 354] correlates with improved cognitive function in individuals with amnestic

mild cognitive impairment [225]. However, none of the aforementioned therapeutic studies have investigated whether circulating or tissue-specific levels of BDNF are secondary to an upregulation and secretion (or lack thereof) of BDNF by B cells.

The current understanding of the role B cells play in neurodegenerative disease pathology, though still in its infancy, primarily stems from investigations in AD and PD [355]. As discussed in chapter 1.4B, B cells are implicated in the disease progression of AD given that B cells migrate into CNS regions where they secrete antibodies associated amyloid burden that ultimately contributed to the formation of behavioral and cognitive deficits [113]. In PD, however, the downregulation of B cell-related genes correlates with increased disease severity and duration [114], suggesting a potentially protective role of B cells in neurodegenerative pathology. These studies suggest that B cells, depending on the neurodegenerative disease, could either ameliorate or mediate pathology, possibly as a result of eliciting a subset-specific response like those seen in stroke recovery. In addition to the potentially contrasting role of B cells in neurodegenerative disease, the chronic glutamate release associated with AD and HD pathologies [356] also presents an opportunity for CNS-infiltrating B cells to engage NMDAR-BDNF signaling and potentially promote neurotrophic support to neuronal networks interconnected to the affected brain regions, though this has also not been studied.

6.3B Neuropsychiatric disease

Neuropsychiatric diseases, also known as mental illnesses, are sub-categorized based on how thoughts, mood, and behavior are impacted [357]. Anxiety (e.g., obsessive-compulsive disorder (OCD) and post-traumatic stress disorder (PTSD)), mood (e.g., major depressive disorder (MDD) and bipolar disorder (BD)), and psychotic (e.g., the psychosis of epilepsy and

schizophrenia) disorders are just a few sub-categories of neuropsychiatric disease. While anxiety and mood disorders exhibit higher incidence rates in women than men [358], psychotic disorders tend to occur equally between both sexes [359]. While the neurobiology underlying each of the aforementioned disorders is very complex, there is substantial evidence demonstrating the importance of BDNF signaling in development and progression of neuropsychiatric disease. An interest in understanding the role of B cells in neuropsychiatric disease has also emerged, with particular focus on mood and psychotic disorders.

BDNF is significantly modulated in specific brain regions of various neuropsychiatric diseases, and BDNF polymorphisms (such as Val66Met) strongly correlate with the susceptibility of anxiety- [360, 361], mood- [362] and psychotic disorders[318]. The reduction in hippocampal [363] and prefrontal cortex [364] volume observed in patients with mood disorders is strongly associated with decreased BDNF and TrkB expression in the serum [365-367] or post-mortem brain tissue [368, 369]. Antidepressants, lithium, and valproic acid (BD treatments) upregulate BDNF expression and TrkB signaling in hippocampus, prefrontal cortex, and serum of MDD [318, 370] or BD patients [366, 371], respectively. With respect to psychotic disorders, BDNF is reduced in the serum [367], but increased in the brain [318] of patients suffering from psychotic disorders. This observation may stem from imbalances of BDNF at the neuronal circuit-level. This is further supported by the ability of anti-psychotic drugs to either reduce (i.e., haloperidol and risperidone [372]) or increase (i.e., clozapine and olanzapine [373]) hippocampal BDNF expression in animal models of schizophrenia. The dysregulation of BDNF signaling observed in psychotic disorders may also result from reduced NMDAR activity in inhibitory neurons that subsequently drives glutamate hyperactivity in glutamatergic neurons [374, 375].

In addition to the critical role of BDNF in neuropsychiatric disease, there is increasing evidence suggesting the involvement of the immune system in modulating disease. The infiltration of B cells into the hippocampus, thalamus, temporal and frontal cortex, cingulate gyrus, and even areas of white matter have been observed in post-mortem brain tissues from patients who suffered from mood- and psychotic disorders [376, 377]. However, the role of the brain-infiltrating B cells in these disorders is not clearly understood. Notably, the increase in circulating IL-10 observed in patients treated with anti-depressants [116] or in the remission phase of BD [115] is associated with an increase in circulating B cells and/or Bregs [115, 117]. These studies suggest a potentially protective effect of peripheral B cells in mood disorders, which may be exerted locally within the CNS. The brain-region-specific infiltration of B cells along with their ability to potentially initiate NMDAR-BDNF signaling in response to glutamate particularly in areas with impaired inhibitory signaling, highlight the therapeutic potential of B cell-derived BDNF in affected brain regions of neuropsychiatric diseases.

6.3C Neuroinflammatory disease

B cells are key mediators of pathology in autoimmune neuroinflammatory diseases of the CNS, including neuromyelitis optica (NMO), multiple sclerosis (MS), and NMDA-encephalitis. Despite contrasting evidence highlighting the importance of B cells in ameliorating or mediating neuroinflammatory pathology, the role of B cell-derived BDNF in NMO, MS or NMDA-encephalitis is not clearly understood.

The neuropathologies associated with NMO and MS, diseases with higher female incidence rates [378, 379], are driven by strong humoral responses [101, 102]. Typically, the onset of NMO occurs in middle-aged adults [380], where ~75% express autoantibodies with

reactivity toward the astrocyte water channel, aquaporin 4 [326], resulting in astrocyte injury and inflammation that impacts the optic nerves and spinal cord. MS is a debilitating demyelinating disease of the CNS that primarily affects young adults and presents with oligoclonal immunoglobulin bands in the CSF, indicating abnormal antibody production within the CNS [381]. Although the targets of autoantibodies in MS are more elusive than NMO, reactivity toward white- (i.e., myelin antigens [382, 383]) and grey matter (i.e., neuronal and astrocytic [384]) antigens has been suggested. In addition to plasmablast expansion and autoantibody production, dysregulated functions of B cells such as enhanced antigen presentation [103], pro-inflammatory activity [104-106], reduced regulatory/immunosuppressive function [107, 108], and a potential loss of B cell anergic maintenance (i.e., B cells that have received signals to inhibit their ability to elicit significant BCR signaling, activation, proliferation or immunoglobulin production in response to stimulation [385]), have also been associated with exacerbating NMO [109] and MS pathologies [102].

A reduction in autoantibodies and improved pathology has been reported as a result of B cell depletion in both NMO [112] and MS [110, 111]. However, there are studies that show Rituximab-induced B cell depletion fails to reduce autoantibody titers and/or ameliorate NMO [386, 387] and MS pathology [388], suggesting that not all B cells/B cell functions are detrimental to NMO or MS pathology. Although the neurotrophic capacity of B cells has never been investigated in NMO, the therapeutic potential of BDNF-producing B cells is intriguing given that the optic neuritis attacks (i.e., severe optic nerve fiber layer damage and axonal loss) NMO patients experience are associated with reduced BDNF resulting from the BDNF Val66Met polymorphism [389]. With respect to MS, BDNF-producing B cells have been found

in demyelinating areas of MS lesions [277], and animal models reveal a neuroprotective role for B cell-derived BDNF in reducing CNS inflammation [390]. Some clinical studies also report an association of the inactive and acute recovery phases of relapsing-remitting MS with increased levels of circulating BDNF [391, 392]. Additionally, therapeutic interventions, such as exercise, have shown to increase circulating levels of BDNF in MS patients [393] which may improve disease outcome. Nonetheless, there are studies that challenge the beneficial role of BDNF in MS recovery [394]. Specifically, the BDNF Val66Met polymorphism has been reported to protect MS patients from loss of grey matter and cognitive decline [395, 396]. Given the protective role of BDNF in MS, it may be possible that MS patients with BDNF polymorphisms have developed an alternative mechanism of promoting neuroprotection and recovery in MS that does not require much BDNF. In turn, this may cause a hypersensitivity to BDNF in MS patients with BDNF polymorphisms where an increase in BDNF could mediate autoreactive neuroinflammation or induce neurotoxicity in neurons that would normally require low BDNF to function. Therefore, harnessing BDNF-producing B cells in MS patients to augment recovery might only be effective in NMO and MS patients that lack any genetic variation of BDNF.

NMDA encephalitis is an autoimmune disease of the CNS that primarily affects children and young adults and has higher prevalence in females [397, 398]. This disease is widely characterized by CSF autoantibodies with reactivity against the GluN1 subunit of the NMDAR [133, 134, 399]. The subsequent reduction in neuronal NMDARs and synaptic transmission [400, 401] drive the hallmark behavioral and psychiatric symptoms exhibited by NMDA encephalitis patients [399]. The likelihood that neuronal BDNF is also reduced as a result of NMDAR dysfunction is a reasonable notion, however, neuronal BDNF signaling in NMDA encephalitis is

unclear. Nonetheless, the clinical implication of BDNF-producing B cells in NMDA encephalitis pathology is a potentially double-edged sword. On one hand, the ability for BDNF-producing B cells to augment neurotrophic support to neurons with impaired NMDAR signaling presents an intriguing therapeutic avenue. On the other, it is quite possible that B cell-derived BDNF could support the survival of autoreactive B cells that exacerbate disease. However, the impact of NMDAR autoantibodies may benefit other NMDAR-mediated CNS diseases such as stroke. For example, circulating GluN1 autoantibodies are associated with reduced lesion size in stroke patients who have a healthy BBB prior to the ischemic insult [402], possibly through reduced NMDAR-mediated excitotoxicity following the ischemic event. Conversely, GluN1 antibodies in stroke patients that have pre-existing conditions of compromised BBB integrity [402] are associated with larger lesions and neurological deficits [403]. This may result from long-term NMDAR inhibition by GluN1 antibodies with continuous access to post-stroke CNS as a result of genetically dysregulated BBB permeability. Although more studies are needed to understand the role of BDNF in NMDA encephalitis, B cell-derived BDNF could potentially promote the survival and function of GluN1-autoreactive B cells within the acute phase of stroke recovery that in turn, could help reduce NMDAR-mediated excitotoxicity.

6.4 General implications of BDNF-producing B cells in autoimmune disease

In addition to its' role in the healthy and diseased CNS, BDNF is also implicated in several B cell-mediated autoimmune diseases that primarily target non-CNS organs, including systemic lupus erythematosus (SLE), rheumatoid arthritis (RA), and autoimmune diabetes. Although the role of BDNF-producing B cells has not been investigated within peripheral autoimmune

disease, the potential implications of BDNF-producing B cells in the pathologies of SLE, RA and autoimmune diabetes are discussed below.

6.4A Systemic lupus erythematosus and rheumatoid arthritis

SLE and RA are autoimmune diseases characterized by autoantibodies that target peripheral organs (e.g., DNA antibodies that target the kidneys and brain [404]) or joints (e.g., rheumatoid factors and anticitrullinated protein antibodies [405]), respectively, and the ensuing inflammation causes significant damage. While the prevalence of SLE [406] and RA [407] is much higher in women than men, SLE typically occurs in women of child-bearing age whereas RA primarily targets aged women. In addition to their hallmarked autoantibody production, B cells also carry out other functions that mediate SLE and RA pathology which are thought to result from defective B cell tolerance [408, 409]. In both SLE and RA, B cells can act as antigen presenting cells to efficiently activate T cells [404, 405, 410], and B cells can also produce chemokines and cytokines [405, 411] that recruit leukocytes to the site of inflammation to further exacerbate pathology. Apart from tissue damage in the kidneys of SLE patients, many patients also present with impaired cognitive function and neuropsychiatric complications, leading to a form of SLE more commonly known as neuropsychiatric SLE (NPSLE) [412].

Although the role of glutamate release is not well characterized in SLE, there is significant evidence demonstrating a pathological role of GluN2A antibodies in driving SLE neuropathology [413-415]. Interestingly, BDNF is considered a biomarker associated with the severity of the cognitive and psychiatric symptoms in NPSLE patients, though the impact of BDNF concentration is still debatable [416-419]. The Val66Met BDNF polymorphism, however, protects SLE patients from motor and cognitive decline [412], suggesting a detrimental role for

BDNF in NPSLE pathology. With respect to RA, patients exhibit elevated levels of circulating BDNF that are strongly associated with inflammation (e.g., TNFα, IL-2 and IFNγ secretion) in synovial fluid [420-422] and can be reduced in response to anti-TNF treatments [420, 421]. There are reports also suggesting a disconnect between levels of BDNF in the serum and brain in preclinical models of RA [423]. Unlike SLE, the role of BDNF polymorphisms in RA pathology has not yet been investigated. However, glutamate, found in excess within RA synovial fluid [424], is a key mediator of RA-induced inflammation as it can upregulate TNFα expression and contribute to bone resorption [425, 426]. While there are no studies assessing the role of B cell-derived BDNF in SLE or RA, the depletion of B cells as a treatment for SLE [427, 428] and RA [429, 430] has proven successful by interfering with the known mechanisms of B cell-mediated autoimmune inflammation. Given that B cells can upregulate BDNF in response to glutamate and that BDNF and glutamate mediate SLE and RA pathology, it may also be possible that B cell depletion targets BDNF-producing B cells to ameliorate an additional mechanism of B cell-mediated pathology.

6.4B Autoimmune diabetes

Type-1 diabetes, primarily expressed in children and adolescents [431], and the adult subgroup of type-1 diabetes, late autoimmune diabetes in adults, are autoimmune forms of diabetes with higher prevalence in men than women [432, 433]. Autoimmune diabetes is characterized by autoantibodies against neuroendocrine islet-cell proteins such as insulin, glutamic acid decarboxylase and the tyrosine phosphatase IA-2 [434]. Unlike SLE and RA, autoantibodies in autoimmune diabetes are not believed to be pathogenic [435], and instead are used as predictive and diagnostic biomarkers [433, 436, 437]. In fact, the pathogenic role of B

cells in mediating autoimmune diabetes stems from the antigen presenting capacity of autoreactive B cells. [435, 438] On the other hand, unlike the detrimental role of BDNF in SLE and RA, BDNF is thought play a beneficial role in autoimmune diabetes based on the positive impact BDNF exerts on glucose metabolism [439] and insulin resistance [440] in type-2 diabetes [441]. Exercise has been reported to increase the low circulating level of BDNF observed in autoimmune diabetic patients and improve cognitive function [442]. While there is no clear link between BDNF polymorphisms (e.g., Val66Met) and autoimmune diabetes, the Val66Met polymorphism has been associated with depression in type-2 diabetic patients [443]. Furthermore, elevated extracellular glutamate and hyperglycemia in autoimmune diabetes is suggested to induce excess activation of NMDARs on islet cells and subsequently, induce excitotoxic cell death [444, 445]. Therefore, harnessing B cells and a therapeutic to enhance BDNF availability in autoimmune diabetic patients might improve glucose metabolism and/or insulin resistance by potentially inducing insulin secretion downstream of TrkB receptors in pancreatic β-islet cells [439].

6.5 General implications of BDNF-producing B cells in cancer

Glutamate and BDNF, factors that our studies show can upregulate [autocrine] BDNF signaling in B cells, play a critical role in tumor survival within the CNS and periphery [446, 447]. The potential relevance of BDNF-producing B cells in cancer treatment, with respect to glutamate and BDNF, are discussed below.

6.5A The role of BDNF in cancer progression

BDNF can exert either oncogenic or tumor suppressive effects depending on the BDNF isoform (see Fig. 32) and organ in which it is produced. Mature BDNF and its receptor TrkB, are highly expressed across several cancer types [447], including B cell-related malignancies such as acute leukemia, multiple myeloma, and Burkitt's lymphoma [165]. BDNF-TrkB signaling protects tumor cells from apoptosis [448], and signaling downstream of PI3 kinase and AKT phosphorylation [449], pathways that upregulate BDNF, significantly promotes tumor cell proliferation, survival, and migration [447]. B cell-related malignant tumors can also respond to stress by altering their neurotrophin-to-neurotrophin receptor ratio [165], likely in an effort to evade chemotherapeutics and thrive within the tumor microenvironment. Furthermore, BDNF-TrkB signaling plays a critical role in promoting the growth and survival of CNS cancers, including gliomas [450] and neuroblastomas [451, 452].

Interestingly, the tumor-suppressing effects of BDNF in CNS cancer are mediated, in part, by pro-BDNF-p75^{NTR} signaling that subsequently inhibits malignant tumor cell growth, survivability, and migration [450]. Other studies show that the upregulation of BDNF within the hypothalamus (a brain region of significant B cell migration after stroke; **Fig. 24J** and **Table 6**) enhances the anti-tumor inflammatory response elicited by cytotoxic CD8^{+} T cells to target gliomas [453] and non-CNS, orthotopic melanomas [454]. Moreover, antigen presentation by B cells in CNS cancers is critical for the tumor antigen-specific response of T cells [455]. Collectively, these studies suggest that BDNF-TrkB signaling outside of the CNS will likely always promote tumor progression and aggressiveness. However, the upregulation of BDNF within the CNS can impact hypothalamic function to initiate oncolytic, rather than oncogenic

mechanisms. Thus, it is reasonable to speculate that within the CNS, BDNF-producing B cells could enhance the anti-tumor immune response and increase the efficacy of current cancer treatments.

6.5B The role of glutamate in cancer progression

Glutamate metabolism fuels the development of peripheral and brain tumors [446] by acting as an autocrine and paracrine growth factor and signal mediator [456], and thus, has been the target for various anti-cancer therapeutics [457]. Astrocytes, a major glial population in the brain, scavenge extracellular glutamate and protect neurons from glutamate toxicity [83]. Glioma cells, however, fail to prevent an excitotoxic environment due to impaired glutamate uptake. Additionally, glioma cells release copious amounts of glutamate into the extracellular space, thereby rendering neurons, particularly hippocampal neurons, susceptible to wide-spread excitotoxic death [458]. Therefore, one potential mechanism by which gliomas earn their title of being ‘the most lethal brain tumor’ stems from their ability to induce excitotoxic neuronal cell death within the affected brain region. Much like neurons that are impacted by stroke-induced excitotoxicity, neuronal networks interconnected to the glioma tumor are likely in need of enhanced neurotrophic support for functional plasticity. Given that B cells infiltrate the CNS to drive anti-glioma immune responses [455], it is possible that extracellular glutamate in remote areas of the tumor could induce NMDAR-BDNF signaling in B cells that, as previously described [453], would promote anti-tumor mechanisms. Thus, glutamate release in the CNS-tumor microenvironment, along with the ability of BDNF to exert anti-tumor effects, highlight the therapeutic potential for utilizing BDNF-producing B cells in the CNS as a novel cancer immunotherapeutic.

6.6 Remaining questions and concluding remarks

6.6A What B cell subset(s) produce BDNF after stroke?

The studies conducted in this thesis, specifically those described in chapter 5, demonstrate the ability of B cells to upregulate BDNF, but not IL-10 mRNA, in response to glutamate. While we did not directly confirm *in vivo* upregulated secretion of BDNF from glutamate-treated B cells, our *in vitro* studies, discussed in chapter 4, suggest that the secretion of functional BDNF by B cells is required for B cells to exert neuroprotective effects in two different *in vitro* models of ischemic injury. Nonetheless, the identified neurotrophic capacity of BDNF-producing B cells was amongst a *general* population of $CD19^+$ B cells as opposed to the individual B cell subsets assessed in the Ca^{2+} response assays. Given that 1.) IL-10-KO B cells protect neurons from *in vitro* ischemic injury [166], 2.) glutamate does not impact B cell IL-10 expression, and 3.) NMDAR subunit activity in Bregs shifts to a GluN2B-NMDAR dominant phenotype after stroke, it may be possible that BDNF-producing B cells are a subset(s) of B cells distinctly different than IL-10-producing B cells. Interestingly, IL-10-producing B cells are not confined to one specific B cell subset [459-461], including the traditional $CD5^+$ $CD1d^{hi}$ Bregs and even ASCs. Unlike Tregs [95], however, IL-10-producing B cells are not distinguishable by a specific transcription factor or surface marker and instead, are defined by their sole ability to produce IL-10. In fact, the neuroprotective population of IL-10-producing B cells in stroke is comprised of traditional Bregs, B1-a B cells and T2 marginal zone B cells [462]. Because our studies revealed GluN2A-NMDAR activity in most uninjured and post-stroke B cell subsets, it may be possible that BDNF-producing B cells are a functionally defined population of B cells, rather than a specific subset. Thus, future studies should assess BDNF protein in B cells (through use of trans-

Golgi network or extracellular vesicle inhibitors; **Fig. 49D**) to determine the frequency and magnitude of BDNF-producing B cells within individual B cell subsets.

6.6B How might the migration and neurotrophic capacity of B cells evolve over the course of stroke recovery?

Our STPT studies revealed that B cells bilaterally diapedese into specific remote brain regions within 96 hours of stroke. However, we did not conduct long-term studies to assess the migration and production of BDNF by B cells at later time points in stroke recovery. There are several factors that could impact long-term migration pattern and function of B cells within the post-stroke brain based upon potential changes in brain region-specific B cell chemokine expression [97], neuronal plasticity and reorganization after stroke [213], CNS barriers (i.e., BBB [463], meninges [179, 464] and choroid plexus [464]) and the formation of ectopic lymphoid structures (ELS) [465].

CXCL13, a B cell-specific chemokine, is predominantly expressed in cortical and subcortical endothelium in the acute post-stroke brain [97], coinciding with an acute, region-specific migration pattern elicited by B cells. Additionally, B cells upregulate a BDNF splice variant after stroke that is specifically expressed within some of the brain regions into which B cells migrate. Moreover, the long-term motor and cognitive deficits observed in post-stroke B cell-depleted mice are also regulated by the brain regions that B cells acutely migrate into [166]. Our studies might suggest that BDNF-producing B cells could remain in those areas of acute migration throughout recovery. However, the regenerative process the brain undergoes after stroke can result in either reinnervation and restoration of neuronal function within the ipsilesional hemisphere, or complete reorganization of neuronal networks within the

contralesional hemisphere [213]. Therefore, it may also be conceivable that B cells follow newly established networks to the brain regions they may innervate in efforts to continue providing neurotrophic support during long-term stroke recovery.

As stroke-induced injury affecting the currently known routes of leukocyte entry into the post-stroke CNS begins to subside, it may be possible that the route of B cell infiltration might change or selectively recruit specific B cell subsets. Several studies show that the choroid plexus is a significant route of entry for pro-inflammatory T cells to infiltrate the post-stroke brain, migrate into the ipsilesional hemisphere and exacerbate pathology [179, 464]. While the route of B cell entry into the post-stroke CNS is poorly understood, it would be interesting to know whether pathological B cells, namely, ASCs, enter the post-stroke CNS through a specific route that could subsequently be targeted to prevent antibody-mediated cognitive decline after stroke. Conversely, pathological ASCs have been suggested to arise in the post-stroke CNS, in part, as a result of the formation of local ELS within the post-stroke brain [92, 465]. In MS patients, the overexpression of CXCL13 has been observed in ELS within the CNS [466]. Although the formation of post-stroke ELS are completely dependent upon $CD4^+$ T cells [92], the signals that recruit B cells to ELS are not well understood and CXCL13 is not yet implicated in the generation of pathological ASCs within post-stroke ELS. Nonetheless, the potential recruitment of BDNF-producing B cells to ELS in the post-stroke brain could promote the generation and longevity of pathological ASCs. Thus, to further understand the neurotrophic capacity of B cells in long-term stroke recovery, future studies should assess region-specific CXCL13 expression and the migration pattern of B cells in the post-stroke brain beyond the acute window of injury.

6.6C What role might BDNF-producing B cells play in stroke-induced immunosuppression?

There is a compensatory peripheral immunosuppressive period that follows the acute robust CNS inflammatory response after stroke, rendering recovering stroke patients susceptible to infections including urinary tract infections [14, 467] and pneumonia [14, 468]. Additionally, peripheral glutamate (i.e., blood/plasma levels typically ranging from 50-100μM under homeostatic conditions [469, 470]) increases acutely after stroke [145] and stabilizes within 15 days of the ischemic insult [471]. The concentration of peripheral glutamate inversely correlates with neurological function in stroke patients within the 15-day window [471]. While the studies in this thesis identified a neurotrophic response of B cells to neurophysiological concentrations of glutamate in the post-stroke CNS, the response elicited by B cells exposed to post-stroke peripheral glutamate was not assessed. It may be possible that in the periphery, BDNF-producing B cells mediate peripheral immune suppression through B cell $p75^{NTR}$-induced apoptosis, thereby contributing to the previously characterized reduction of splenic and circulating B cells after stroke [472]. On the other hand, mature BDNF could induce autocrine pro-survival signaling in B cells through TrkB and potentially promote the increase of post-stroke peripheral Tregs [473, 474] previously reported in preclinical and clinical studies [472]. Thus, the neurotrophic role of B cells in peripheral stroke recovery may differ around the stroke-induced immunosuppressive window. Future studies should assess the response of B cells to peripheral concentrations of post-stroke glutamate and determine if and/or when B cells in the periphery become activated to produce BDNF.

6.6D How might sex and age impact BDNF production from B cells after stroke?

In male animal models of stroke, we previously observed that B cell depletion prior to stroke in young male mice impedes motor recovery and stroke-induced neurogenesis and increases hippocampal-dependent cognitive deficits including anxiety and memory loss. The studies in this thesis further identified B cell NMDAR-BDNF signaling as a potential mechanism by which B cells exert neuroprotective effects in long-term stroke recovery. However, given that the incidence of stroke is reduced in pre-menopausal, estrogen-producing women which, in part, is believed to be a neuroprotective effect of estrogen in stroke recovery [475, 476], we also conducted pilot studies in which we investigated the role of B cells in post-stroke recovery of young female mice (**Fig. 7-9, 11, 12**). Although our stroke model requires modification to assess the role of B cells in long-term cognitive function in females after stroke, we observed long-term motor deficits in young B cell-depleted females that male mice did not exhibit. These data suggest a potentially greater neuroprotective role of B cells in supporting long-term motor recovery in young females after stroke. Nonetheless, the question of age still remains. Thus, future studies should assess the role of BDNF-producing B cells in long-term functional recovery in aged female mice as they are the population most susceptible to stroke [477, 478].

Aged, post-menopausal women experience a significantly lower quality of life (i.e., mobility, self-care, daily activities, depression/anxiety, and pain) after stroke when compared to men [16] that may, in part, stem from age-related co-morbidities, immunosuppression, and immune senescence. Post-stroke comorbidities, such as coronary heart disease and diabetes, also greatly impact women's recovery, with an increasing risk relative to age [479]. Additionally, women possess higher levels of immunosuppressive factors in their circulating blood after stroke

than men [14, 15], but whether those immunosuppressive factors contribute to a more challenging recovery, and thus, poorer outcomes, remains unknown. Both mice [480] and humans [481] experience immune senescence, resulting in an age-related decline in B cell development and responsiveness, where aged B cells produce fewer growth factors in response to stimuli [481]. Given that B cell-derived secretory factors are lost in post-menopausal women [482], it is a considerable notion that low circulating levels of BDNF observed in elderly women with advanced cognitive decline [12] may partly be attributed to impaired BDNF production by aged B cells. Interestingly, therapeutic stroke interventions known individually to increase both BDNF [349, 483] and B cell responsiveness [484-486], warrant further investigation as they may impact B cell-derived BDNF production after stroke.

6.6E How might BDNF-producing B cells be therapeutically increased?

The studies in this thesis demonstrate the therapeutic potential of BDNF-producing B cells in enhancing plasticity in the recovering brain after stroke to promote functional recovery. We also discuss the general implications of BDNF producing B cells in other CNS diseases, autoimmune diseases and cancer. While the pathology underlying specific diseases (e.g., SLE and RA) indicate that BDNF-producing B cells could potentially exacerbate pathology, most diseases discussed in this chapter stand to theoretically benefit from an increase of BDNF-producing B cells.

Our studies preliminarily explore the use of viral nucleofection to induce constitutive BDNF production in B cells. While our studies demonstrate a successful upregulated secretion of BDNF from viable B cells (**Fig. 34**) that is functionally neuroprotective *in vitro* (**Fig. 35, 36**), the therapeutic efficacy of these virally-induced BDNF-overproducing B cells ought to be assessed

in vivo. On the other hand, there are less invasive "natural regimens", such as exercise, that upregulate BDNF in stroke patients [487, 488] and can increase the frequency of circulating B cells [353, 354]. It may be possible that circulating or tissue-specific levels of BDNF after exercise are secondary to an upregulation and secretion of BDNF by B cells. Lastly, it may be possible to redirect the use of FDA-approved treatments for MS (e.g., glatiramer acetate) and depression (e.g., selective serotonin reuptake inhibitors (SSRIs)) as a way of increasing BDNF-producing B cells in stroke patients. Glatiramer acetate upregulates BDNF in the brain and increases Bregs and anti-inflammatory cytokines in animal models of MS [489, 490] and SLE [491]. In an animal model of stroke, glatiramer acetate promoted neurogenesis in the acute and chronic phases of stroke recovery, reduced infarction and improved neurological deficits [492]. Despite glatiramer acetate's ability to increase BDNF in the brain [489], this study observed no change in BDNF within the infarct 7 days after stroke [492]. However, our studies suggest that BDNF-producing B cells likely exert their neurotrophic effect in remote brain regions outside the infarct. Thus, glatiramer acetate could potentially promote BDNF-producing B cells after stroke. Conversely, SSRIs, commonly used to manage depression in MDD, enhance BDNF expression [493] and increase B cell frequencies [494] in MDD patients that are in long-term remission of depressive episodes. SSRIs also reduce anxiety and depression in stroke patients and are thought to improve cognitive function after stroke[495], potentially as a result of promoting BDNF-producing B cells. Therefore, therapeutic avenues that can upregulate BDNF and/or increase B cell frequencies should also be considered to maximize the therapeutic potential of BDNF-producing B cells.

Our studies, taken together with these remaining questions, underscore the need to understand neuroimmune interactions after stroke, as with the advent of new patient-specific immunotherapies, we are now in the era of harnessing the immune system as adjunctive therapy to stroke rehabilitation.

6.7 Thesis Summary: The major findings of this work and their implications in this field

Neuronal survival and functional plasticity after stroke require significant neurotrophic support, particularly in brain regions experiencing glutamate-induced excitotoxicity [4]. However, the delivery of neurotrophins (e.g., BDNF) into the CNS has failed primarily due to restricted BBB permeability [66-68]. Therefore, identifying endogenous mechanisms that could augment neurotrophic support and promote long-term plasticity, could allow for the development of novel neurotherapeutics that could improve recovery months to years after stroke onset.

Our previous studies revealed that depleting endogenous B cells after stroke induces long-term motor and cognitive deficits mediated by specific brain regions (e.g., hippocampus, cerebellum) outside the area of infarct [166]. Given that B cells infiltrate the post-stroke brain and can produce neurotrophins such as BDNF, we hypothesized that stroke enhances the neurotrophic capacities of B cells to support recovery after stroke. We discovered that B cells migrate bilaterally to specific, remote brain regions that are found outside the initial ischemic infarct. We also found that B cells support neuronal synaptic transmission in an identified B cell-specific remote brain region. Additionally, we discovered that B cells require BDNF to protect neurons from ischemic injury. Lastly, our studies revealed that glutamate can induce B cell NMDAR signaling and upregulate a brain region-specific splice variant of BDNF in B cells. These data are the first to demonstrate a glutamate-induced neurotrophic role of B cells after stroke to promote functional and structural neuroplasticity. This might be a potential mechanism by which B cells in remote, non-ischemic regions of the brain, elicit an immune response to neurotransmitters (independent of canonical pro-inflammatory stimuli) to support functional recovery.

Our studies highlight the therapeutic potential of harnessing the migration pattern of B cells into the post stroke CNS to deliver enhanced, brain region-specific neurotrophic support to counter ischemic injury and clinical factors that can compromise stroke recovery. Future studies might consider 1.) identifying the B cell subset(s) that produce BDNF, 2.) assessing how B cell-derived BDNF impacts post-stroke plasticity and functional recovery relative to age-, sex- and/or genetic risk factors, and 3.) investigating therapeutic avenues to upregulate B cell-derived BDNF and/or increase BDNF-producing B cell frequencies. Nonetheless, the studies conducted in this thesis underscore the importance of furthering our understanding of neuro-immune mechanisms as a critical component to the development of immune-based therapeutics for stroke.

BIBLIOGRAPHY

1. Virani, S.S., et al., *Heart Disease and Stroke Statistics-2020 Update: A Report From the American Heart Association.* Circulation, 2020. **141**(9): p. e139-e596.
2. Virani, S.S., et al., *Heart Disease and Stroke Statistics-2021 Update: A Report From the American Heart Association.* Circulation, 2021. **143**(8): p. e254-e743.
3. Sun, M.S., et al., *Free Radical Damage in Ischemia-Reperfusion Injury: An Obstacle in Acute Ischemic Stroke after Revascularization Therapy.* Oxid Med Cell Longev, 2018. **2018**: p. 3804979.
4. Lai, T.W., S. Zhang, and Y.T. Wang, *Excitotoxicity and stroke: identifying novel targets for neuroprotection.* Prog Neurobiol, 2014. **115**: p. 157-88.
5. Liaw, N. and D. Liebeskind, *Emerging therapies in acute ischemic stroke.* F1000Res, 2020. **9**.
6. Sacco, R.L., et al., *Survival and recurrence following stroke. The Framingham study.* Stroke, 1982. **13**(3): p. 290-5.
7. Nudo, R.J., *Functional and structural plasticity in motor cortex: implications for stroke recovery.* Phys Med Rehabil Clin N Am, 2003. **14**(1 Suppl): p. S57-76.
8. Hendricks, H.T., et al., *Motor recovery after stroke: a systematic review of the literature.* Arch Phys Med Rehabil, 2002. **83**(11): p. 1629-37.
9. Dancause, N. and R.J. Nudo, *Shaping plasticity to enhance recovery after injury.* Prog Brain Res, 2011. **192**: p. 273-95.
10. Duncan, P.W., et al., *Measurement of motor recovery after stroke. Outcome assessment and sample size requirements.* Stroke, 1992. **23**(8): p. 1084-9.
11. Erickson, K.I., et al., *Brain-derived neurotrophic factor is associated with age-related decline in hippocampal volume.* J Neurosci, 2010. **30**(15): p. 5368-75.
12. Lejri, I., A. Grimm, and A. Eckert, *Mitochondria, Estrogen and Female Brain Aging.* Front Aging Neurosci, 2018. **10**: p. 124.
13. Zhou, Z., et al., *Decreased serum brain-derived neurotrophic factor (BDNF) is associated with post-stroke depression but not with BDNF gene Val66Met polymorphism.* Clin Chem Lab Med, 2011. **49**(2): p. 185-9.
14. Worthmann, H., et al., *Lipopolysaccharide binding protein, interleukin-10, interleukin-6 and C-reactive protein blood levels in acute ischemic stroke patients with post-stroke infection.* J Neuroinflammation, 2015. **12**: p. 13.
15. Conway, S.E., et al., *Sex differences and the role of IL-10 in ischemic stroke recovery.* Biol Sex Differ, 2015. **6**: p. 17.
16. Bushnell, C.D., et al., *Sex differences in quality of life after ischemic stroke.* Neurology, 2014. **82**(11): p. 922-31.
17. Paradiso, S. and R.G. Robinson, *Gender differences in poststroke depression.* J Neuropsychiatry Clin Neurosci, 1998. **10**(1): p. 41-7.
18. Alajbegovic, A., et al., *Post stroke depression.* Med Arch, 2014. **68**(1): p. 47-50.
19. Balkaya, M. and S. Cho, *Genetics of stroke recovery: BDNF val66met polymorphism in stroke recovery and its interaction with aging.* Neurobiol Dis, 2019. **126**: p. 36-46.
20. Shen, T., et al., *BDNF Polymorphism: A Review of Its Diagnostic and Clinical Relevance in Neurodegenerative Disorders.* Aging Dis, 2018. **9**(3): p. 523-536.

21. Siironen, J., et al., *The Met allele of the BDNF Val66Met polymorphism predicts poor outcome among survivors of aneurysmal subarachnoid hemorrhage.* Stroke, 2007. **38**(10): p. 2858-60.
22. Di Lazzaro, V., et al., *Val66Met BDNF gene polymorphism influences human motor cortex plasticity in acute stroke.* Brain Stimul, 2015. **8**(1): p. 92-6.
23. Chang, W.H., et al., *BDNF polymorphism and differential rTMS effects on motor recovery of stroke patients.* Brain Stimul, 2014. **7**(4): p. 553-8.
24. Stanne, T.M., et al., *Genetic variation at the BDNF locus: evidence for association with long-term outcome after ischemic stroke.* PLoS One, 2014. **9**(12): p. e114156.
25. Ming, G.L. and H. Song, *Adult neurogenesis in the mammalian brain: significant answers and significant questions.* Neuron, 2011. **70**(4): p. 687-702.
26. Taupin, P., *Adult neurogenesis and neuroplasticity.* Restor Neurol Neurosci, 2006. **24**(1): p. 9-15.
27. Sanes, J.N. and J.P. Donoghue, *Plasticity and primary motor cortex.* Annu Rev Neurosci, 2000. **23**: p. 393-415.
28. Clark, T.A., et al., *Preferential stabilization of newly formed dendritic spines in motor cortex during manual skill learning predicts performance gains, but not memory endurance.* Neurobiol Learn Mem, 2018. **152**: p. 50-60.
29. Gu, Y., S. Janoschka, and S. Ge, *Neurogenesis and hippocampal plasticity in adult brain.* Curr Top Behav Neurosci, 2013. **15**: p. 31-48.
30. Carrillo, J., et al., *The long-term structural plasticity of cerebellar parallel fiber axons and its modulation by motor learning.* J Neurosci, 2013. **33**(19): p. 8301-7.
31. D'Angelo, E., *The organization of plasticity in the cerebellar cortex: from synapses to control.* Prog Brain Res, 2014. **210**: p. 31-58.
32. Kew, J.N. and J.A. Kemp, *Ionotropic and metabotropic glutamate receptor structure and pharmacology.* Psychopharmacology (Berl), 2005. **179**(1): p. 4-29.
33. Dawson, L.A., et al., *Characterization of transient focal ischemia-induced increases in extracellular glutamate and aspartate in spontaneously hypertensive rats.* Brain Res Bull, 2000. **53**(6): p. 767-76.
34. Drejer, J., et al., *Cellular origin of ischemia-induced glutamate release from brain tissue in vivo and in vitro.* J Neurochem, 1985. **45**(1): p. 145-51.
35. Bosley, T.M., et al., *Effects of anoxia on the stimulated release of amino acid neurotransmitters in the cerebellum in vitro.* J Neurochem, 1983. **40**(1): p. 189-201.
36. Phillis, J.W., J. Ren, and M.H. O'Regan, *Transporter reversal as a mechanism of glutamate release from the ischemic rat cerebral cortex: studies with DL-threo-beta-benzyloxyaspartate.* Brain Res, 2000. **868**(1): p. 105-12.
37. Rossi, D.J., T. Oshima, and D. Attwell, *Glutamate release in severe brain ischaemia is mainly by reversed uptake.* Nature, 2000. **403**(6767): p. 316-21.
38. Sanchez-Prieto, J. and P. Gonzalez, *Occurrence of a large Ca2+-independent release of glutamate during anoxia in isolated nerve terminals (synaptosomes).* J Neurochem, 1988. **50**(4): p. 1322-4.
39. Silverstein, F.S., K. Buchanan, and M.V. Johnston, *Perinatal hypoxia-ischemia disrupts striatal high-affinity [3H]glutamate uptake into synaptosomes.* J Neurochem, 1986. **47**(5): p. 1614-9.

40. Castilho, R.F., M.W. Ward, and D.G. Nicholls, *Oxidative stress, mitochondrial function, and acute glutamate excitotoxicity in cultured cerebellar granule cells.* J Neurochem, 1999. **72**(4): p. 1394-401.
41. Reynolds, I.J. and T.G. Hastings, *Glutamate induces the production of reactive oxygen species in cultured forebrain neurons following NMDA receptor activation.* J Neurosci, 1995. **15**(5 Pt 1): p. 3318-27.
42. Stout, A.K., et al., *Glutamate-induced neuron death requires mitochondrial calcium uptake.* Nat Neurosci, 1998. **1**(5): p. 366-73.
43. Murphy, T.H. and D. Corbett, *Plasticity during stroke recovery: from synapse to behaviour.* Nat Rev Neurosci, 2009. **10**(12): p. 861-72.
44. Hoyte, L., et al., *The rise and fall of NMDA antagonists for ischemic stroke.* Curr Mol Med, 2004. **4**(2): p. 131-6.
45. Ikonomidou, C. and L. Turski, *Why did NMDA receptor antagonists fail clinical trials for stroke and traumatic brain injury?* Lancet Neurol, 2002. **1**(6): p. 383-6.
46. Wu, Q.J. and M. Tymianski, *Targeting NMDA receptors in stroke: new hope in neuroprotection.* Mol Brain, 2018. **11**(1): p. 15.
47. Ishii, T., et al., *Molecular characterization of the family of the N-methyl-D-aspartate receptor subunits.* J Biol Chem, 1993. **268**(4): p. 2836-43.
48. Kutsuwada, T., et al., *Molecular diversity of the NMDA receptor channel.* Nature, 1992. **358**(6381): p. 36-41.
49. Meguro, H., et al., *Functional characterization of a heteromeric NMDA receptor channel expressed from cloned cDNAs.* Nature, 1992. **357**(6373): p. 70-4.
50. Monyer, H., et al., *Heteromeric NMDA receptors: molecular and functional distinction of subtypes.* Science, 1992. **256**(5060): p. 1217-21.
51. Watanabe, M., et al., *Developmental changes in distribution of NMDA receptor channel subunit mRNAs.* Neuroreport, 1992. **3**(12): p. 1138-40.
52. Harney, S.C., D.E. Jane, and R. Anwyl, *Extrasynaptic NR2D-containing NMDARs are recruited to the synapse during LTP of NMDAR-EPSCs.* J Neurosci, 2008. **28**(45): p. 11685-94.
53. Liu, Y., et al., *NMDA receptor subunits have differential roles in mediating excitotoxic neuronal death both in vitro and in vivo.* J Neurosci, 2007. **27**(11): p. 2846-57.
54. Stocca, G. and S. Vicini, *Increased contribution of NR2A subunit to synaptic NMDA receptors in developing rat cortical neurons.* J Physiol, 1998. **507 (Pt 1)**: p. 13-24.
55. Thomas, C.G., A.J. Miller, and G.L. Westbrook, *Synaptic and extrasynaptic NMDA receptor NR2 subunits in cultured hippocampal neurons.* J Neurophysiol, 2006. **95**(3): p. 1727-34.
56. Tovar, K.R. and G.L. Westbrook, *The incorporation of NMDA receptors with a distinct subunit composition at nascent hippocampal synapses in vitro.* J Neurosci, 1999. **19**(10): p. 4180-8.
57. Ding, Y., et al., *Exercise pre-conditioning reduces brain damage in ischemic rats that may be associated with regional angiogenesis and cellular overexpression of neurotrophin.* Neuroscience, 2004. **124**(3): p. 583-91.

58. Yanamoto, H., et al., *Spreading depression induces long-lasting brain protection against infarcted lesion development via BDNF gene-dependent mechanism.* Brain Res, 2004. **1019**(1-2): p. 178-88.
59. Chen, A., et al., *The neuroprotective roles of BDNF in hypoxic ischemic brain injury.* Biomed Rep, 2013. **1**(2): p. 167-176.
60. Ninan, I., *Synaptic regulation of affective behaviors; role of BDNF.* Neuropharmacology, 2014. **76 Pt C**: p. 684-95.
61. Ferrer, I., et al., *Brain-derived neurotrophic factor reduces cortical cell death by ischemia after middle cerebral artery occlusion in the rat.* Acta Neuropathol, 2001. **101**(3): p. 229-38.
62. Zhang, Y. and W.M. Pardridge, *Neuroprotection in transient focal brain ischemia after delayed intravenous administration of brain-derived neurotrophic factor conjugated to a blood-brain barrier drug targeting system.* Stroke, 2001. **32**(6): p. 1378-84.
63. Qin, L., et al., *Genetic variant of BDNF (Val66Met) polymorphism attenuates stroke-induced angiogenic responses by enhancing anti-angiogenic mediator CD36 expression.* J Neurosci, 2011. **31**(2): p. 775-83.
64. Keiner, S., O.W. Witte, and C. Redecker, *Immunocytochemical detection of newly generated neurons in the perilesional area of cortical infarcts after intraventricular application of brain-derived neurotrophic factor.* J Neuropathol Exp Neurol, 2009. **68**(1): p. 83-93.
65. Schabitz, W.R., et al., *Intravenous brain-derived neurotrophic factor enhances poststroke sensorimotor recovery and stimulates neurogenesis.* Stroke, 2007. **38**(7): p. 2165-72.
66. *A controlled trial of recombinant methionyl human BDNF in ALS: The BDNF Study Group (Phase III).* Neurology, 1999. **52**(7): p. 1427-33.
67. Ochs, G., et al., *A phase I/II trial of recombinant methionyl human brain derived neurotrophic factor administered by intrathecal infusion to patients with amyotrophic lateral sclerosis.* Amyotroph Lateral Scler Other Motor Neuron Disord, 2000. **1**(3): p. 201-6.
68. Sandoval, K.E. and K.A. Witt, *Blood-brain barrier tight junction permeability and ischemic stroke.* Neurobiol Dis, 2008. **32**(2): p. 200-19.
69. Iadecola, C. and J. Anrather, *The immunology of stroke: from mechanisms to translation.* Nat Med, 2011. **17**(7): p. 796-808.
70. Carden, D.L. and D.N. Granger, *Pathophysiology of ischaemia-reperfusion injury.* J Pathol, 2000. **190**(3): p. 255-66.
71. Peerschke, E.I., W. Yin, and B. Ghebrehiwet, *Complement activation on platelets: implications for vascular inflammation and thrombosis.* Mol Immunol, 2010. **47**(13): p. 2170-5.
72. Pinsky, D.J., et al., *Hypoxia-induced exocytosis of endothelial cell Weibel-Palade bodies. A mechanism for rapid neutrophil recruitment after cardiac preservation.* J Clin Invest, 1996. **97**(2): p. 493-500.
73. Pelvig, D.P., et al., *Neocortical glial cell numbers in human brains.* Neurobiol Aging, 2008. **29**(11): p. 1754-62.
74. Neumann, J., et al., *Microglia provide neuroprotection after ischemia.* FASEB J, 2006. **20**(6): p. 714-6.

75. Denes, A., et al., *Proliferating resident microglia after focal cerebral ischaemia in mice.* J Cereb Blood Flow Metab, 2007. **27**(12): p. 1941-53.
76. Ma, M.W., et al., *NADPH oxidase in brain injury and neurodegenerative disorders.* Mol Neurodegener, 2017. **12**(1): p. 7.
77. Zhou, M., et al., *Microglial CD14 activated by iNOS contributes to neuroinflammation in cerebral ischemia.* Brain Res, 2013. **1506**: p. 105-14.
78. Facci, L., et al., *Toll-like receptors 2, -3 and -4 prime microglia but not astrocytes across central nervous system regions for ATP-dependent interleukin-1beta release.* Sci Rep, 2014. **4**: p. 6824.
79. Dudvarski Stankovic, N., et al., *Microglia-blood vessel interactions: a double-edged sword in brain pathologies.* Acta Neuropathol, 2016. **131**(3): p. 347-63.
80. da Fonseca, A.C., et al., *The impact of microglial activation on blood-brain barrier in brain diseases.* Front Cell Neurosci, 2014. **8**: p. 362.
81. Xu, S., et al., *Glial Cells: Role of the Immune Response in Ischemic Stroke.* Front Immunol, 2020. **11**: p. 294.
82. Lalancette-Hebert, M., et al., *Galectin-3 is required for resident microglia activation and proliferation in response to ischemic injury.* J Neurosci, 2012. **32**(30): p. 10383-95.
83. Bylicky, M.A., G.P. Mueller, and R.M. Day, *Mechanisms of Endogenous Neuroprotective Effects of Astrocytes in Brain Injury.* Oxid Med Cell Longev, 2018. **2018**: p. 6501031.
84. Jayaraj, R.L., et al., *Neuroinflammation: friend and foe for ischemic stroke.* J Neuroinflammation, 2019. **16**(1): p. 142.
85. Gelderblom, M., et al., *Temporal and spatial dynamics of cerebral immune cell accumulation in stroke.* Stroke, 2009. **40**(5): p. 1849-57.
86. Selvaraj, U.M., et al., *Heterogeneity of B Cell Functions in Stroke-Related Risk, Prevention, Injury, and Repair.* Neurotherapeutics, 2016. **13**(4): p. 729-747.
87. del Zoppo, G.J., K.J. Becker, and J.M. Hallenbeck, *Inflammation after stroke: is it harmful?* Arch Neurol, 2001. **58**(4): p. 669-72.
88. Selvaraj, U.M. and A.M. Stowe, *Long-term T cell responses in the brain after an ischemic stroke.* Discov Med, 2017. **24**(134): p. 323-333.
89. Xie, L., et al., *Experimental ischemic stroke induces long-term T cell activation in the brain.* J Cereb Blood Flow Metab, 2019. **39**(11): p. 2268-2276.
90. Selvaraj, U.M., et al., *Delayed diapedesis of CD8 T cells contributes to long-term pathology after ischemic stroke in male mice.* Brain Behav Immun, 2021. **95**: p. 502-513.
91. Vindegaard, N., et al., *T-cells and macrophages peak weeks after experimental stroke: Spatial and temporal characteristics.* Neuropathology, 2017. **37**(5): p. 407-414.
92. Weitbrecht, L., et al., *CD4(+) T cells promote delayed B cell responses in the ischemic brain after experimental stroke.* Brain Behav Immun, 2021. **91**: p. 601-614.
93. Chamorro, A., et al., *The immunology of acute stroke.* Nat Rev Neurol, 2012. **8**(7): p. 401-10.
94. Macrez, R., et al., *Stroke and the immune system: from pathophysiology to new therapeutic strategies.* Lancet Neurol, 2011. **10**(5): p. 471-80.
95. Liesz, A., et al., *Regulatory T cells are key cerebroprotective immunomodulators in acute experimental stroke.* Nat Med, 2009. **15**(2): p. 192-9.

96. Tsubata, T., *B-cell tolerance and autoimmunity.* F1000Res, 2017. **6**: p. 391.
97. Monson, N.L., et al., *Repetitive hypoxic preconditioning induces an immunosuppressed B cell phenotype during endogenous protection from stroke.* J Neuroinflammation, 2014. **11**: p. 22.
98. Aoki, M., et al., *Sphingosine-1-Phosphate Signaling in Immune Cells and Inflammation: Roles and Therapeutic Potential.* Mediators Inflamm, 2016. **2016**: p. 8606878.
99. Webb, M., et al., *Sphingosine 1-phosphate receptor agonists attenuate relapsing-remitting experimental autoimmune encephalitis in SJL mice.* J Neuroimmunol, 2004. **153**(1-2): p. 108-21.
100. Tanabe, S. and T. Yamashita, *B-1a lymphocytes promote oligodendrogenesis during brain development.* Nat Neurosci, 2018. **21**(4): p. 506-516.
101. Lucchinetti, C.F., et al., *A role for humoral mechanisms in the pathogenesis of Devic's neuromyelitis optica.* Brain, 2002. **125**(Pt 7): p. 1450-61.
102. Li, R., K.R. Patterson, and A. Bar-Or, *Reassessing B cell contributions in multiple sclerosis.* Nat Immunol, 2018. **19**(7): p. 696-707.
103. Barnett, L.G., et al., *B cell antigen presentation in the initiation of follicular helper T cell and germinal center differentiation.* J Immunol, 2014. **192**(8): p. 3607-17.
104. Uzawa, A., et al., *Cytokine and chemokine profiles in neuromyelitis optica: significance of interleukin-6.* Mult Scler, 2010. **16**(12): p. 1443-52.
105. Li, R., et al., *Cytokine-Defined B Cell Responses as Therapeutic Targets in Multiple Sclerosis.* Front Immunol, 2015. **6**: p. 626.
106. Li, R., et al., *Proinflammatory GM-CSF-producing B cells in multiple sclerosis and B cell depletion therapy.* Sci Transl Med, 2015. **7**(310): p. 310ra166.
107. Quan, C., et al., *Impaired regulatory function and enhanced intrathecal activation of B cells in neuromyelitis optica: distinct from multiple sclerosis.* Mult Scler, 2013. **19**(3): p. 289-98.
108. Matsushita, T., et al., *Regulatory B cells inhibit EAE initiation in mice while other B cells promote disease progression.* J Clin Invest, 2008. **118**(10): p. 3420-30.
109. Bennett, J.L., et al., *B lymphocytes in neuromyelitis optica.* Neurol Neuroimmunol Neuroinflamm, 2015. **2**(3): p. e104.
110. Hauser, S.L., et al., *B-cell depletion with rituximab in relapsing-remitting multiple sclerosis.* N Engl J Med, 2008. **358**(7): p. 676-88.
111. Bar-Or, A., et al., *Rituximab in relapsing-remitting multiple sclerosis: a 72-week, open-label, phase I trial.* Ann Neurol, 2008. **63**(3): p. 395-400.
112. Nakashima, I., et al., *Transient increases in anti-aquaporin-4 antibody titers following rituximab treatment in neuromyelitis optica, in association with elevated serum BAFF levels.* J Clin Neurosci, 2011. **18**(7): p. 997-8.
113. Kim, K., et al., *Therapeutic B-cell depletion reverses progression of Alzheimer's disease.* Nat Commun, 2021. **12**(1): p. 2185.
114. Kobo, H., et al., *Down-regulation of B cell-related genes in peripheral blood leukocytes of Parkinson's disease patients with and without GBA mutations.* Mol Genet Metab, 2016. **117**(2): p. 179-85.
115. Pietruczuk, K., et al., *Peripheral blood lymphocyte subpopulations in patients with bipolar disorder type II.* Sci Rep, 2019. **9**(1): p. 5869.

116. Maes, M., et al., *Negative immunoregulatory effects of antidepressants: inhibition of interferon-gamma and stimulation of interleukin-10 secretion.* Neuropsychopharmacology, 1999. **20**(4): p. 370-9.
117. Ahmetspahic, D., et al., *Altered B Cell Homeostasis in Patients with Major Depressive Disorder and Normalization of CD5 Surface Expression on Regulatory B Cells in Treatment Responders.* J Neuroimmune Pharmacol, 2018. **13**(1): p. 90-99.
118. Liesz, A., et al., *Inhibition of lymphocyte trafficking shields the brain against deleterious neuroinflammation after stroke.* Brain, 2011. **134**(Pt 3): p. 704-20.
119. An, C., et al., *Molecular dialogs between the ischemic brain and the peripheral immune system: dualistic roles in injury and repair.* Prog Neurobiol, 2014. **115**: p. 6-24.
120. Ren, X., et al., *Regulatory B cells limit CNS inflammation and neurologic deficits in murine experimental stroke.* J Neurosci, 2011. **31**(23): p. 8556-63.
121. Bodhankar, S., et al., *IL-10-producing B-cells limit CNS inflammation and infarct volume in experimental stroke.* Metab Brain Dis, 2013. **28**(3): p. 375-86.
122. Chen, Y., et al., *Intrastriatal B-cell administration limits infarct size after stroke in B-cell deficient mice.* Metab Brain Dis, 2012. **27**(4): p. 487-93.
123. Bodhankar, S., et al., *Treatment of experimental stroke with IL-10-producing B-cells reduces infarct size and peripheral and CNS inflammation in wild-type B-cell-sufficient mice.* Metab Brain Dis, 2014. **29**(1): p. 59-73.
124. Schuhmann, M.K., et al., *B cells do not have a major pathophysiologic role in acute ischemic stroke in mice.* J Neuroinflammation, 2017. **14**(1): p. 112.
125. Leys, D., et al., *Poststroke dementia.* Lancet Neurol, 2005. **4**(11): p. 752-9.
126. Pruss, H., et al., *Evidence of intrathecal immunoglobulin synthesis in stroke: a cohort study.* Arch Neurol, 2012. **69**(6): p. 714-7.
127. Doyle, K.P., et al., *B-lymphocyte-mediated delayed cognitive impairment following stroke.* J Neurosci, 2015. **35**(5): p. 2133-45.
128. Bunker, J.J., et al., *Natural polyreactive IgA antibodies coat the intestinal microbiota.* Science, 2017. **358**(6361).
129. Zbesko, J.C., et al., *IgA natural antibodies are produced following T-cell independent B-cell activation following stroke.* Brain Behav Immun, 2021. **91**: p. 578-586.
130. Planas, A.M., et al., *Brain-derived antigens in lymphoid tissue of patients with acute stroke.* J Immunol, 2012. **188**(5): p. 2156-63.
131. Becker, K.J., et al., *Autoimmune responses to the brain after stroke are associated with worse outcome.* Stroke, 2011. **42**(10): p. 2763-9.
132. Ortega, S.B., et al., *Stroke induces a rapid adaptive autoimmune response to novel neuronal antigens.* Discov Med, 2015. **19**(106): p. 381-92.
133. Barry, H., et al., *Anti-N-methyl-d-aspartate receptor encephalitis: review of clinical presentation, diagnosis and treatment.* BJPsych Bull, 2015. **39**(1): p. 19-23.
134. Lazar-Molnar, E. and A.E. Tebo, *Autoimmune NMDA receptor encephalitis.* Clin Chim Acta, 2015. **438**: p. 90-7.
135. Gronwall, C. and G.J. Silverman, *Natural IgM: beneficial autoantibodies for the control of inflammatory and autoimmune disease.* J Clin Immunol, 2014. **34 Suppl 1**: p. S12-21.
136. Wootla, B., et al., *Naturally Occurring Monoclonal Antibodies and Their Therapeutic Potential for Neurologic Diseases.* JAMA Neurol, 2015. **72**(11): p. 1346-53.

137. Traynelis, S.F., et al., *Glutamate receptor ion channels: structure, regulation, and function.* Pharmacol Rev, 2010. **62**(3): p. 405-96.
138. Jane, D.E., D. Lodge, and G.L. Collingridge, *Kainate receptors: pharmacology, function and therapeutic potential.* Neuropharmacology, 2009. **56**(1): p. 90-113.
139. Platt, S.R., *The role of glutamate in central nervous system health and disease--a review.* Vet J, 2007. **173**(2): p. 278-86.
140. Niswender, C.M. and P.J. Conn, *Metabotropic glutamate receptors: physiology, pharmacology, and disease.* Annu Rev Pharmacol Toxicol, 2010. **50**: p. 295-322.
141. Ganor, Y. and M. Levite, *Glutamate in the Immune System: Glutamate Receptors in Immune Cells, Potent Effects, Endogenous Production and Involvement in Disease*, in *Nerve-Driven Immunity: Neurotransmitters and Neuropeptides in the Immune System*, M. Levite, Editor. 2012, Springer Vienna: Vienna. p. 121-161.
142. Jourdi, H., et al., *Positive AMPA receptor modulation rapidly stimulates BDNF release and increases dendritic mRNA translation.* J Neurosci, 2009. **29**(27): p. 8688-97.
143. Jean, Y.Y., L.D. Lercher, and C.F. Dreyfus, *Glutamate elicits release of BDNF from basal forebrain astrocytes in a process dependent on metabotropic receptors and the PLC pathway.* Neuron Glia Biol, 2008. **4**(1): p. 35-42.
144. Mitsukawa, K., et al., *Metabotropic glutamate receptor subtype 7 ablation causes dysregulation of the HPA axis and increases hippocampal BDNF protein levels: implications for stress-related psychiatric disorders.* Neuropsychopharmacology, 2006. **31**(6): p. 1112-22.
145. Boldyrev, A.A., D.O. Carpenter, and P. Johnson, *Emerging evidence for a similar role of glutamate receptors in the nervous and immune systems.* J Neurochem, 2005. **95**(4): p. 913-8.
146. Lombardi, G., et al., *Characterization of ionotropic glutamate receptors in human lymphocytes.* Br J Pharmacol, 2001. **133**(6): p. 936-44.
147. Pacheco, R., et al., *Glutamate released by dendritic cells as a novel modulator of T cell activation.* J Immunol, 2006. **177**(10): p. 6695-704.
148. Boldyrev, A.A., et al., *Rodent lymphocytes express functionally active glutamate receptors.* Biochem Biophys Res Commun, 2004. **324**(1): p. 133-9.
149. Lombardi, G., et al., *Glutamate modulation of human lymphocyte growth: in vitro studies.* Biochem Biophys Res Commun, 2004. **318**(2): p. 496-502.
150. Sturgill, J.L., et al., *Glutamate signaling through the kainate receptor enhances human immunoglobulin production.* J Neuroimmunol, 2011. **233**(1-2): p. 80-9.
151. Jovic, Z., et al., *Monosodium glutamate induces apoptosis in naive and memory human B cells.* Bratisl Lek Listy, 2009. **110**(10): p. 636-40.
152. Kvaratskhelia, E., et al., *N-methyl-D-aspartate and sigma-ligands change the production of interleukins 8 and 10 in lymphocytes through modulation of the NMDA glutamate receptor.* Neuroimmunomodulation, 2009. **16**(3): p. 201-7.
153. Kahlfuss, S., et al., *Immunosuppression by N-methyl-D-aspartate receptor antagonists is mediated through inhibition of Kv1.3 and KCa3.1 channels in T cells.* Mol Cell Biol, 2014. **34**(5): p. 820-31.

154. Poyhonen, S., et al., *Effects of Neurotrophic Factors in Glial Cells in the Central Nervous System: Expression and Properties in Neurodegeneration and Injury.* Front Physiol, 2019. **10**: p. 486.
155. Aloe, L., et al., *Nerve Growth Factor: A Focus on Neuroscience and Therapy.* Curr Neuropharmacol, 2015. **13**(3): p. 294-303.
156. Brodie, C. and E.W. Gelfand, *Functional nerve growth factor receptors on human B lymphocytes. Interaction with IL-2.* J Immunol, 1992. **148**(11): p. 3492-7.
157. Thorpe, L.W. and J.R. Perez-Polo, *The influence of nerve growth factor on the in vitro proliferative response of rat spleen lymphocytes.* J Neurosci Res, 1987. **18**(1): p. 134-9.
158. Otten, U., P. Ehrhard, and R. Peck, *Nerve growth factor induces growth and differentiation of human B lymphocytes.* Proc Natl Acad Sci U S A, 1989. **86**(24): p. 10059-63.
159. Torcia, M., et al., *Nerve growth factor is an autocrine survival factor for memory B lymphocytes.* Cell, 1996. **85**(3): p. 345-56.
160. Kimata, H., et al., *Stimulation of Ig production and growth of human lymphoblastoid B-cell lines by nerve growth factor.* Immunology, 1991. **72**(3): p. 451-2.
161. Kimata, H., et al., *Nerve growth factor specifically induces human IgG4 production.* Eur J Immunol, 1991. **21**(1): p. 137-41.
162. Schuhmann, B., et al., *A role for brain-derived neurotrophic factor in B cell development.* J Neuroimmunol, 2005. **163**(1-2): p. 15-23.
163. Fauchais, A.L., et al., *Role of endogenous brain-derived neurotrophic factor and sortilin in B cell survival.* J Immunol, 2008. **181**(5): p. 3027-38.
164. Vega, J.A., et al., *Neurotrophins and the immune system.* J Anat, 2003. **203**(1): p. 1-19.
165. Hillis, J., M. O'Dwyer, and A.M. Gorman, *Neurotrophins and B-cell malignancies.* Cell Mol Life Sci, 2016. **73**(1): p. 41-56.
166. Ortega, S.B., et al., *B cells migrate into remote brain areas and support neurogenesis and functional recovery after focal stroke in mice.* Proc Natl Acad Sci U S A, 2020. **117**(9): p. 4983-4993.
167. Jiang, W., et al., *Cortical neurogenesis in adult rats after transient middle cerebral artery occlusion.* Stroke, 2001. **32**(5): p. 1201-7.
168. Parent, J.M., et al., *Rat forebrain neurogenesis and striatal neuron replacement after focal stroke.* Ann Neurol, 2002. **52**(6): p. 802-13.
169. Gould, E., et al., *Neurogenesis in the dentate gyrus of the adult tree shrew is regulated by psychosocial stress and NMDA receptor activation.* J Neurosci, 1997. **17**(7): p. 2492-8.
170. Liu, J., et al., *Increased neurogenesis in the dentate gyrus after transient global ischemia in gerbils.* J Neurosci, 1998. **18**(19): p. 7768-78.
171. Cho, K.O., et al., *Aberrant hippocampal neurogenesis contributes to epilepsy and associated cognitive decline.* Nat Commun, 2015. **6**: p. 6606.
172. Mashkina, A.P., et al., *NMDA receptors are expressed in lymphocytes activated both in vitro and in vivo.* Cell Mol Neurobiol, 2010. **30**(6): p. 901-7.
173. Khalil, A.M., J.C. Cambier, and M.J. Shlomchik, *B cell receptor signal transduction in the GC is short-circuited by high phosphatase activity.* Science, 2012. **336**(6085): p. 1178-81.

174. Jellusova, J., et al., *Context-specific BAFF-R signaling by the NF-kappaB and PI3K pathways.* Cell Rep, 2013. **5**(4): p. 1022-35.
175. Lin, P.Y., E.T. Kavalali, and L.M. Monteggia, *Genetic Dissection of Presynaptic and Postsynaptic BDNF-TrkB Signaling in Synaptic Efficacy of CA3-CA1 Synapses.* Cell Rep, 2018. **24**(6): p. 1550-1561.
176. Rios, M., et al., *Conditional deletion of brain-derived neurotrophic factor in the postnatal brain leads to obesity and hyperactivity.* Mol Endocrinol, 2001. **15**(10): p. 1748-57.
177. Monson, N.L., et al., *Rituximab therapy reduces organ-specific T cell responses and ameliorates experimental autoimmune encephalomyelitis.* PLoS One, 2011. **6**(2): p. e17103.
178. Gidday, J.M., et al., *Leukocyte-derived matrix metalloproteinase-9 mediates blood-brain barrier breakdown and is proinflammatory after transient focal cerebral ischemia.* Am J Physiol Heart Circ Physiol, 2005. **289**(2): p. H558-68.
179. Benakis, C., G. Llovera, and A. Liesz, *The meningeal and choroidal infiltration routes for leukocytes in stroke.* Ther Adv Neurol Disord, 2018. **11**: p. 1756286418783708.
180. Yanev, P., et al., *Impaired meningeal lymphatic vessel development worsens stroke outcome.* J Cereb Blood Flow Metab, 2020. **40**(2): p. 263-275.
181. Poinsatte, K., et al., *Visualization and Quantification of Post-stroke Neural Connectivity and Neuroinflammation Using Serial Two-Photon Tomography in the Whole Mouse Brain.* Front Neurosci, 2019. **13**: p. 1055.
182. Selvaraj, U.M., et al., *Preconditioning-induced CXCL12 upregulation minimizes leukocyte infiltration after stroke in ischemia-tolerant mice.* J Cereb Blood Flow Metab, 2017. **37**(3): p. 801-813.
183. Ragan, T., et al., *Serial two-photon tomography for automated ex vivo mouse brain imaging.* Nat Methods, 2012. **9**(3): p. 255-8.
184. Peng, H., et al., *V3D enables real-time 3D visualization and quantitative analysis of large-scale biological image data sets.* Nat Biotechnol, 2010. **28**(4): p. 348-53.
185. Schindelin, J., et al., *Fiji: an open-source platform for biological-image analysis.* Nat Methods, 2012. **9**(7): p. 676-82.
186. Royer, L.A., et al., *ClearVolume: open-source live 3D visualization for light-sheet microscopy.* Nat Methods, 2015. **12**(6): p. 480-1.
187. Oh, S.W., et al., *A mesoscale connectome of the mouse brain.* Nature, 2014. **508**(7495): p. 207-14.
188. Modat, M., et al., *Global image registration using a symmetric block-matching approach.* J Med Imaging (Bellingham), 2014. **1**(2): p. 024003.
189. Modat, M., et al., *Fast free-form deformation using graphics processing units.* Comput Methods Programs Biomed, 2010. **98**(3): p. 278-84.
190. Niedworok, C.J., et al., *aMAP is a validated pipeline for registration and segmentation of high-resolution mouse brain data.* Nat Commun, 2016. **7**: p. 11879.
191. Yanaba, K., et al., *The development and function of regulatory B cells expressing IL-10 (B10 cells) requires antigen receptor diversity and TLR signals.* J Immunol, 2009. **182**(12): p. 7459-72.

192. Patterson, G.A., *Surgical techniques in the diagnosis of lung cancer.* Chest, 1991. **100**(2): p. 523-6.
193. Lu, M. and R. Munford, *LPS stimulates IgM production in vivo without help from non-B cells.* Innate Immun, 2016. **22**(5): p. 307-15.
194. Ireland, S.J., et al., *The effect of glatiramer acetate therapy on functional properties of B cells from patients with relapsing-remitting multiple sclerosis.* JAMA Neurol, 2014. **71**(11): p. 1421-8.
195. Ireland, S.J., N.L. Monson, and L.S. Davis, *Seeking balance: Potentiation and inhibition of multiple sclerosis autoimmune responses by IL-6 and IL-10.* Cytokine, 2015. **73**(2): p. 236-44.
196. Kaech, S. and G. Banker, *Culturing hippocampal neurons.* Nat Protoc, 2006. **1**(5): p. 2406-15.
197. van Meerloo, J., G.J. Kaspers, and J. Cloos, *Cell sensitivity assays: the MTT assay.* Methods Mol Biol, 2011. **731**: p. 237-45.
198. McNeill, T.H., et al., *Synapse replacement in the striatum of the adult rat following unilateral cortex ablation.* J Comp Neurol, 2003. **467**(1): p. 32-43.
199. Latchney, S.E., et al., *Inducible knockout of Mef2a, -c, and -d from nestin-expressing stem/progenitor cells and their progeny unexpectedly uncouples neurogenesis and dendritogenesis in vivo.* FASEB J, 2015. **29**(12): p. 5059-71.
200. Latchney, S.E., et al., *Chronic P7C3 treatment restores hippocampal neurogenesis in the Ts65Dn mouse model of Down Syndrome [Corrected].* Neurosci Lett, 2015. **591**: p. 86-92.
201. Latchney, S.E., et al., *Developmental and adult GAP-43 deficiency in mice dynamically alters hippocampal neurogenesis and mossy fiber volume.* Dev Neurosci, 2014. **36**(1): p. 44-63.
202. Rao, X., et al., *An improvement of the 2^(-delta delta CT) method for quantitative real-time polymerase chain reaction data analysis.* Biostat Bioinforma Biomath, 2013. **3**(3): p. 71-85.
203. Gibbons, J., *Western blot: protein transfer overview.* N Am J Med Sci, 2014. **6**(3): p. 158-9.
204. Altman, J. and G.D. Das, *Autoradiographic and histological evidence of postnatal hippocampal neurogenesis in rats.* J Comp Neurol, 1965. **124**(3): p. 319-35.
205. Adkins, D.L., J.E. Hsu, and T.A. Jones, *Motor cortical stimulation promotes synaptic plasticity and behavioral improvements following sensorimotor cortex lesions.* Exp Neurol, 2008. **212**(1): p. 14-28.
206. Benowitz, L.I. and S.T. Carmichael, *Promoting axonal rewiring to improve outcome after stroke.* Neurobiol Dis, 2010. **37**(2): p. 259-66.
207. Biernaskie, J., et al., *Bi-hemispheric contribution to functional motor recovery of the affected forelimb following focal ischemic brain injury in rats.* Eur J Neurosci, 2005. **21**(4): p. 989-99.
208. Riley, J.D., et al., *Anatomy of stroke injury predicts gains from therapy.* Stroke, 2011. **42**(2): p. 421-6.
209. Perederiy, J.V. and G.L. Westbrook, *Structural plasticity in the dentate gyrus- revisiting a classic injury model.* Front Neural Circuits, 2013. **7**: p. 17.

210. Luft, A.R., et al., *Brain activation of lower extremity movement in chronically impaired stroke survivors.* Neuroimage, 2005. **26**(1): p. 184-94.
211. Starkey, M.L., et al., *Back seat driving: hindlimb corticospinal neurons assume forelimb control following ischaemic stroke.* Brain, 2012. **135**(Pt 11): p. 3265-81.
212. Wang, L., et al., *Rehabilitation drives enhancement of neuronal structure in functionally relevant neuronal subsets.* Proc Natl Acad Sci U S A, 2016. **113**(10): p. 2750-5.
213. Jones, T.A. and D.L. Adkins, *Motor System Reorganization After Stroke: Stimulating and Training Toward Perfection.* Physiology (Bethesda), 2015. **30**(5): p. 358-70.
214. Lindau, N.T., et al., *Rewiring of the corticospinal tract in the adult rat after unilateral stroke and anti-Nogo-A therapy.* Brain, 2014. **137**(Pt 3): p. 739-56.
215. Hsu, J.E. and T.A. Jones, *Contralesional neural plasticity and functional changes in the less-affected forelimb after large and small cortical infarcts in rats.* Exp Neurol, 2006. **201**(2): p. 479-94.
216. Lapash Daniels, C.M., et al., *Axon sprouting in adult mouse spinal cord after motor cortex stroke.* Neurosci Lett, 2009. **450**(2): p. 191-5.
217. Liu, Z., et al., *Remodeling of the corticospinal innervation and spontaneous behavioral recovery after ischemic stroke in adult mice.* Stroke, 2009. **40**(7): p. 2546-51.
218. Chopp, M., Z.G. Zhang, and Q. Jiang, *Neurogenesis, angiogenesis, and MRI indices of functional recovery from stroke.* Stroke, 2007. **38**(2 Suppl): p. 827-31.
219. Becker, K.J., et al., *Antibodies to myelin basic protein are associated with cognitive decline after stroke.* J Neuroimmunol, 2016. **295-296**: p. 9-11.
220. Wang, X., et al., *The evolving role of neuro-immune interaction in brain repair after cerebral ischemic stroke.* CNS Neurosci Ther, 2018. **24**(12): p. 1100-1114.
221. Amato, S.P., et al., *Whole Brain Imaging with Serial Two-Photon Tomography.* Front Neuroanat, 2016. **10**: p. 31.
222. Kim, Y., et al., *Whole-Brain Mapping of Neuronal Activity in the Learned Helplessness Model of Depression.* Front Neural Circuits, 2016. **10**: p. 3.
223. Whitesell, J.D., et al., *Whole brain imaging reveals distinct spatial patterns of amyloid beta deposition in three mouse models of Alzheimer's disease.* J Comp Neurol, 2019. **527**(13): p. 2122-2145.
224. Ramirez, D.M.O., et al., *Serial Multiphoton Tomography and Analysis of Volumetric Images of the Mouse Brain*, in *Multiphoton Microscopy*, E. Hartveit, Editor. 2019, Springer New York: New York, NY. p. 195-224.
225. Poinsatte, K., et al., *T and B cell subsets differentially correlate with amyloid deposition and neurocognitive function in patients with amnestic mild cognitive impairment after one year of physical activity.* Exerc Immunol Rev, 2019. **25**: p. 34-49.
226. Duval, E.R., A. Javanbakht, and I. Liberzon, *Neural circuits in anxiety and stress disorders: a focused review.* Ther Clin Risk Manag, 2015. **11**: p. 115-26.
227. Shin, L.M. and I. Liberzon, *The neurocircuitry of fear, stress, and anxiety disorders.* Neuropsychopharmacology, 2010. **35**(1): p. 169-91.
228. Dancause, N., et al., *Extensive cortical rewiring after brain injury.* J Neurosci, 2005. **25**(44): p. 10167-79.
229. Kim, Y.R., et al., *Measurements of BOLD/CBV ratio show altered fMRI hemodynamics during stroke recovery in rats.* J Cereb Blood Flow Metab, 2005. **25**(7): p. 820-9.

230. Arvidsson, A., Z. Kokaia, and O. Lindvall, *N-methyl-D-aspartate receptor-mediated increase of neurogenesis in adult rat dentate gyrus following stroke.* Eur J Neurosci, 2001. **14**(1): p. 10-8.
231. Shiromoto, T., et al., *The Role of Endogenous Neurogenesis in Functional Recovery and Motor Map Reorganization Induced by Rehabilitative Therapy after Stroke in Rats.* J Stroke Cerebrovasc Dis, 2017. **26**(2): p. 260-272.
232. Jelenova, I., *[The effect of temperature and relative humidity on survival of eggs of the cestode, Monieza expansa (Rudolphi, 1810)].* Vet Med (Praha), 1991. **36**(5): p. 291-6.
233. Liu, W., et al., *Brain-Derived Neurotrophic Factor and Its Potential Therapeutic Role in Stroke Comorbidities.* Neural Plast, 2020. **2020**: p. 1969482.
234. Stanne, T.M., et al., *Low Circulating Acute Brain-Derived Neurotrophic Factor Levels Are Associated With Poor Long-Term Functional Outcome After Ischemic Stroke.* Stroke, 2016. **47**(7): p. 1943-5.
235. van der Vliet, R., et al., *BDNF Val66Met but not transcranial direct current stimulation affects motor learning after stroke.* Brain Stimul, 2017. **10**(5): p. 882-892.
236. Chen, S.J., et al., *Brain-derived neurotrophic factor-transfected and nontransfected 3T3 fibroblasts enhance migratory neuroblasts and functional restoration in mice with intracerebral hemorrhage.* J Neuropathol Exp Neurol, 2012. **71**(12): p. 1123-36.
237. Li, Y., et al., *TrkB regulates hippocampal neurogenesis and governs sensitivity to antidepressive treatment.* Neuron, 2008. **59**(3): p. 399-412.
238. Sairanen, M., et al., *Brain-derived neurotrophic factor and antidepressant drugs have different but coordinated effects on neuronal turnover, proliferation, and survival in the adult dentate gyrus.* J Neurosci, 2005. **25**(5): p. 1089-94.
239. Taliaz, D., et al., *Knockdown of brain-derived neurotrophic factor in specific brain sites precipitates behaviors associated with depression and reduces neurogenesis.* Mol Psychiatry, 2010. **15**(1): p. 80-92.
240. Fortin, D.A., et al., *Brain-derived neurotrophic factor activation of CaM-kinase kinase via transient receptor potential canonical channels induces the translation and synaptic incorporation of GluA1-containing calcium-permeable AMPA receptors.* J Neurosci, 2012. **32**(24): p. 8127-37.
241. Minichiello, L., *TrkB signalling pathways in LTP and learning.* Nat Rev Neurosci, 2009. **10**(12): p. 850-60.
242. Figurov, A., et al., *Regulation of synaptic responses to high-frequency stimulation and LTP by neurotrophins in the hippocampus.* Nature, 1996. **381**(6584): p. 706-9.
243. Gottschalk, W., et al., *Presynaptic modulation of synaptic transmission and plasticity by brain-derived neurotrophic factor in the developing hippocampus.* J Neurosci, 1998. **18**(17): p. 6830-9.
244. Kang, H. and E.M. Schuman, *Long-lasting neurotrophin-induced enhancement of synaptic transmission in the adult hippocampus.* Science, 1995. **267**(5204): p. 1658-62.
245. Korte, M., et al., *Hippocampal long-term potentiation is impaired in mice lacking brain-derived neurotrophic factor.* Proc Natl Acad Sci U S A, 1995. **92**(19): p. 8856-60.
246. Tanaka, J., et al., *Protein synthesis and neurotrophin-dependent structural plasticity of single dendritic spines.* Science, 2008. **319**(5870): p. 1683-7.

247. Mamounas, L.A., et al., *Brain-derived neurotrophic factor promotes the survival and sprouting of serotonergic axons in rat brain.* J Neurosci, 1995. **15**(12): p. 7929-39.
248. Studer, L., et al., *Comparison of the effects of the neurotrophins on the morphological structure of dopaminergic neurons in cultures of rat substantia nigra.* Eur J Neurosci, 1995. **7**(2): p. 223-33.
249. Yamada, M.K., et al., *Brain-derived neurotrophic factor promotes the maturation of GABAergic mechanisms in cultured hippocampal neurons.* J Neurosci, 2002. **22**(17): p. 7580-5.
250. Mizuno, M., et al., *Involvement of brain-derived neurotrophic factor in spatial memory formation and maintenance in a radial arm maze test in rats.* J Neurosci, 2000. **20**(18): p. 7116-21.
251. Mu, J.S., et al., *Deprivation of endogenous brain-derived neurotrophic factor results in impairment of spatial learning and memory in adult rats.* Brain Res, 1999. **835**(2): p. 259-65.
252. Ma, Y.L., et al., *Brain-derived neurotrophic factor antisense oligonucleotide impairs memory retention and inhibits long-term potentiation in rats.* Neuroscience, 1998. **82**(4): p. 957-67.
253. Hall, J., K.L. Thomas, and B.J. Everitt, *Rapid and selective induction of BDNF expression in the hippocampus during contextual learning.* Nat Neurosci, 2000. **3**(6): p. 533-5.
254. Chen, Z.Y., et al., *Genetic variant BDNF (Val66Met) polymorphism alters anxiety-related behavior.* Science, 2006. **314**(5796): p. 140-3.
255. Nikonenko, A.G., et al., *Structural features of ischemic damage in the hippocampus.* Anat Rec (Hoboken), 2009. **292**(12): p. 1914-21.
256. Kirino, T., A. Tamura, and K. Sano, *Selective vulnerability of the hippocampus to ischemia--reversible and irreversible types of ischemic cell damage.* Prog Brain Res, 1985. **63**: p. 39-58.
257. Kreisman, N.R., S. Soliman, and D. Gozal, *Regional differences in hypoxic depolarization and swelling in hippocampal slices.* J Neurophysiol, 2000. **83**(2): p. 1031-8.
258. Sun, Y., L. Wang, and Z. Gao, *Identifying the Role of GluN2A in Cerebral Ischemia.* Front Mol Neurosci, 2017. **10**: p. 12.
259. Sun, Y., et al., *The Role of GluN2A in Cerebral Ischemia: Promoting Neuron Death and Survival in the Early Stage and Thereafter.* Mol Neurobiol, 2018. **55**(2): p. 1208-1216.
260. Mattson, M.P., *Glutamate and neurotrophic factors in neuronal plasticity and disease.* Ann N Y Acad Sci, 2008. **1144**: p. 97-112.
261. Pasantes-Morales, H. and K. Tuz, *Volume changes in neurons: hyperexcitability and neuronal death.* Contrib Nephrol, 2006. **152**: p. 221-240.
262. Zhou, X., et al., *Involvement of the GluN2A and GluN2B subunits in synaptic and extrasynaptic N-methyl-D-aspartate receptor function and neuronal excitotoxicity.* J Biol Chem, 2013. **288**(33): p. 24151-9.
263. Boldyrev, A.A., E.A. Bryushkova, and E.A. Vladychenskaya, *NMDA receptors in immune competent cells.* Biochemistry (Mosc), 2012. **77**(2): p. 128-34.

264. Vladychenskaya, E., et al., *Rat lymphocytes express NMDA receptors that take part in regulation of cytokine production.* Cell Biochem Funct, 2011. **29**(7): p. 527-33.
265. Mashkina, A.P., et al., *The excitotoxic effect of NMDA on human lymphocyte immune function.* Neurochem Int, 2007. **51**(6-7): p. 356-60.
266. Herman, M.A. and C.E. Jahr, *Extracellular glutamate concentration in hippocampal slice.* J Neurosci, 2007. **27**(36): p. 9736-41.
267. Fang, X.Q., et al., *Regulated internalization of NMDA receptors drives PKD1-mediated suppression of the activity of residual cell-surface NMDA receptors.* Mol Brain, 2015. **8**(1): p. 75.
268. Scott, D.B., et al., *Endocytosis and degradative sorting of NMDA receptors by conserved membrane-proximal signals.* J Neurosci, 2004. **24**(32): p. 7096-109.
269. Nong, Y., et al., *Glycine binding primes NMDA receptor internalization.* Nature, 2003. **422**(6929): p. 302-7.
270. Li, Y., et al., *The peripheral immune response after stroke-A double edge sword for blood-brain barrier integrity.* CNS Neurosci Ther, 2018. **24**(12): p. 1115-1128.
271. Liesz, A., et al., *DAMP signaling is a key pathway inducing immune modulation after brain injury.* J Neurosci, 2015. **35**(2): p. 583-98.
272. Shichita, T., M. Ito, and A. Yoshimura, *Post-ischemic inflammation regulates neural damage and protection.* Front Cell Neurosci, 2014. **8**: p. 319.
273. McCulloch, L., C.J. Smith, and B.W. McColl, *Adrenergic-mediated loss of splenic marginal zone B cells contributes to infection susceptibility after stroke.* Nat Commun, 2017. **8**: p. 15051.
274. Offner, H., et al., *Splenic atrophy in experimental stroke is accompanied by increased regulatory T cells and circulating macrophages.* J Immunol, 2006. **176**(11): p. 6523-31.
275. Davalos, A., A. Shuaib, and N.G. Wahlgren, *Neurotransmitters and pathophysiology of stroke: evidence for the release of glutamate and other transmitters/mediators in animals and humans.* J Stroke Cerebrovasc Dis, 2000. **9**(6 Pt 2): p. 2-8.
276. Feske, S., H. Wulff, and E.Y. Skolnik, *Ion channels in innate and adaptive immunity.* Annu Rev Immunol, 2015. **33**: p. 291-353.
277. Kerschensteiner, M., et al., *Activated human T cells, B cells, and monocytes produce brain-derived neurotrophic factor in vitro and in inflammatory brain lesions: a neuroprotective role of inflammation?* J Exp Med, 1999. **189**(5): p. 865-70.
278. Edling, A.E., et al., *Human and murine lymphocyte neurotrophin expression is confined to B cells.* J Neurosci Res, 2004. **77**(5): p. 709-17.
279. Barouch, R. and M. Schwartz, *Autoreactive T cells induce neurotrophin production by immune and neural cells in injured rat optic nerve: implications for protective autoimmunity.* FASEB J, 2002. **16**(10): p. 1304-6.
280. Ganley-Leal, L.M., et al., *Differential regulation of TLR4 expression in human B cells and monocytes.* Mol Immunol, 2010. **48**(1-3): p. 82-8.
281. Bekeredjian-Ding, I. and G. Jego, *Toll-like receptors--sentries in the B-cell response.* Immunology, 2009. **128**(3): p. 311-23.
282. Offner, H., et al., *Experimental stroke induces massive, rapid activation of the peripheral immune system.* J Cereb Blood Flow Metab, 2006. **26**(5): p. 654-65.

283. Nayak, A.R., et al., *Time course of inflammatory cytokines in acute ischemic stroke patients and their relation to inter-alfa trypsin inhibitor heavy chain 4 and outcome.* Ann Indian Acad Neurol, 2012. **15**(3): p. 181-5.
284. Clarkson, B.D., et al., *T cell-derived interleukin (IL)-21 promotes brain injury following stroke in mice.* J Exp Med, 2014. **211**(4): p. 595-604.
285. Mingari, M.C., et al., *Human interleukin-2 promotes proliferation of activated B cells via surface receptors similar to those of activated T cells.* Nature, 1984. **312**(5995): p. 641-3.
286. Le Gallou, S., et al., *IL-2 requirement for human plasma cell generation: coupling differentiation and proliferation by enhancing MAPK-ERK signaling.* J Immunol, 2012. **189**(1): p. 161-73.
287. Dienz, O., et al., *The induction of antibody production by IL-6 is indirectly mediated by IL-21 produced by CD4+ T cells.* J Exp Med, 2009. **206**(1): p. 69-78.
288. Eto, D., et al., *IL-21 and IL-6 are critical for different aspects of B cell immunity and redundantly induce optimal follicular helper CD4 T cell (Tfh) differentiation.* PLoS One, 2011. **6**(3): p. e17739.
289. Konforte, D., N. Simard, and C.J. Paige, *IL-21: an executor of B cell fate.* J Immunol, 2009. **182**(4): p. 1781-7.
290. Poovassery, J.S., T.J. Vanden Bush, and G.A. Bishop, *Antigen receptor signals rescue B cells from TLR tolerance.* J Immunol, 2009. **183**(5): p. 2974-83.
291. Jahnmatz, M., et al., *Optimization of a human IgG B-cell ELISpot assay for the analysis of vaccine-induced B-cell responses.* J Immunol Methods, 2013. **391**(1-2): p. 50-9.
292. Marasco, E., et al., *B-cell activation with CD40L or CpG measures the function of B-cell subsets and identifies specific defects in immunodeficient patients.* Eur J Immunol, 2017. **47**(1): p. 131-143.
293. Henn, A.D., et al., *Functionally Distinct Subpopulations of CpG-Activated Memory B Cells.* Sci Rep, 2012. **2**: p. 345.
294. Caracciolo, L., et al., *CREB controls cortical circuit plasticity and functional recovery after stroke.* Nat Commun, 2018. **9**(1): p. 2250.
295. Lujan, B., X. Liu, and Q. Wan, *Differential roles of GluN2A- and GluN2B-containing NMDA receptors in neuronal survival and death.* Int J Physiol Pathophysiol Pharmacol, 2012. **4**(4): p. 211-8.
296. Esvald, E.E., et al., *CREB Family Transcription Factors Are Major Mediators of BDNF Transcriptional Autoregulation in Cortical Neurons.* J Neurosci, 2020. **40**(7): p. 1405-1426.
297. Bathina, S. and U.N. Das, *Brain-derived neurotrophic factor and its clinical implications.* Arch Med Sci, 2015. **11**(6): p. 1164-78.
298. Mowla, S.J., et al., *Biosynthesis and post-translational processing of the precursor to brain-derived neurotrophic factor.* J Biol Chem, 2001. **276**(16): p. 12660-6.
299. Pang, P.T., et al., *Cleavage of proBDNF by tPA/plasmin is essential for long-term hippocampal plasticity.* Science, 2004. **306**(5695): p. 487-91.
300. Mizoguchi, H., et al., *Matrix metalloproteinase-9 contributes to kindled seizure development in pentylenetetrazole-treated mice by converting pro-BDNF to mature BDNF in the hippocampus.* J Neurosci, 2011. **31**(36): p. 12963-71.

301. Finkbeiner, S., et al., *CREB: a major mediator of neuronal neurotrophin responses.* Neuron, 1997. **19**(5): p. 1031-47.
302. Miglio, G., F. Varsaldi, and G. Lombardi, *Human T lymphocytes express N-methyl-D-aspartate receptors functionally active in controlling T cell activation.* Biochem Biophys Res Commun, 2005. **338**(4): p. 1875-83.
303. Simma, N., et al., *NMDA-receptor antagonists block B-cell function but foster IL-10 production in BCR/CD40-activated B cells.* Cell Commun Signal, 2014. **12**: p. 75.
304. Doyle, K.P., R.P. Simon, and M.P. Stenzel-Poore, *Mechanisms of ischemic brain damage.* Neuropharmacology, 2008. **55**(3): p. 310-8.
305. Allred, R.P., S.Y. Kim, and T.A. Jones, *Use it and/or lose it-experience effects on brain remodeling across time after stroke.* Front Hum Neurosci, 2014. **8**: p. 379.
306. Kovalenko, T., et al., *Ischemia-induced modifications in hippocampal CA1 stratum radiatum excitatory synapses.* Hippocampus, 2006. **16**(10): p. 814-25.
307. Baba, Y. and T. Kurosaki, *Role of Calcium Signaling in B Cell Activation and Biology.* Curr Top Microbiol Immunol, 2016. **393**: p. 143-174.
308. Scharenberg, A.M., L.A. Humphries, and D.J. Rawlings, *Calcium signalling and cell-fate choice in B cells.* Nat Rev Immunol, 2007. **7**(10): p. 778-89.
309. Baba, Y. and T. Kurosaki, *Impact of Ca2+ signaling on B cell function.* Trends Immunol, 2011. **32**(12): p. 589-94.
310. Liu, Q.R., et al., *Rodent BDNF genes, novel promoters, novel splice variants, and regulation by cocaine.* Brain Res, 2006. **1067**(1): p. 1-12.
311. Kruse, N., et al., *Differential expression of BDNF mRNA splice variants in mouse brain and immune cells.* J Neuroimmunol, 2007. **182**(1-2): p. 13-21.
312. Chiaruttini, C., et al., *BDNF mRNA splice variants display activity-dependent targeting to distinct hippocampal laminae.* Mol Cell Neurosci, 2008. **37**(1): p. 11-9.
313. Pattabiraman, P.P., et al., *Neuronal activity regulates the developmental expression and subcellular localization of cortical BDNF mRNA isoforms in vivo.* Mol Cell Neurosci, 2005. **28**(3): p. 556-70.
314. Timmusk, T., et al., *Multiple promoters direct tissue-specific expression of the rat BDNF gene.* Neuron, 1993. **10**(3): p. 475-89.
315. Barouch, R., et al., *Differential regulation of neurotrophin expression by mitogens and neurotransmitters in mouse lymphocytes.* J Neuroimmunol, 2000. **103**(2): p. 112-21.
316. Moretto, G., et al., *Co-expression of mRNA for neurotrophic factors in human neurons and glial cells in culture.* J Neuropathol Exp Neurol, 1994. **53**(1): p. 78-85.
317. Orihara, K., et al., *Neurotransmitter signalling via NMDA receptors leads to decreased T helper type 1-like and enhanced T helper type 2-like immune balance in humans.* Immunology, 2018. **153**(3): p. 368-379.
318. Autry, A.E. and L.M. Monteggia, *Brain-derived neurotrophic factor and neuropsychiatric disorders.* Pharmacol Rev, 2012. **64**(2): p. 238-58.
319. Miranda, M., et al., *Brain-Derived Neurotrophic Factor: A Key Molecule for Memory in the Healthy and the Pathological Brain.* Front Cell Neurosci, 2019. **13**: p. 363.
320. Brea, D., et al., *Toll-like receptors 2 and 4 in ischemic stroke: outcome and therapeutic values.* J Cereb Blood Flow Metab, 2011. **31**(6): p. 1424-31.

321. Shibata, A., et al., *Peripheral nerve induces macrophage neurotrophic activities: regulation of neuronal process outgrowth, intracellular signaling and synaptic function.* J Neuroimmunol, 2003. **142**(1-2): p. 112-29.
322. Xu, D., et al., *Brain-derived neurotrophic factor is regulated via MyD88/NF-kappaB signaling in experimental Streptococcus pneumoniae meningitis.* Sci Rep, 2017. **7**(1): p. 3545.
323. Carvalho, A.L., et al., *Role of the brain-derived neurotrophic factor at glutamatergic synapses.* Br J Pharmacol, 2008. **153 Suppl 1**: p. S310-24.
324. Kelly-Hayes, M., *Influence of age and health behaviors on stroke risk: lessons from longitudinal studies.* J Am Geriatr Soc, 2010. **58 Suppl 2**: p. S325-8.
325. Roy-O'Reilly, M. and L.D. McCullough, *Age and Sex Are Critical Factors in Ischemic Stroke Pathology.* Endocrinology, 2018. **159**(8): p. 3120-3131.
326. Waters, P.J., et al., *Evaluation of aquaporin-4 antibody assays.* Clin Exp Neuroimmunol, 2014. **5**(3): p. 290-303.
327. Kovalchuk, Y., et al., *NMDA receptor-mediated subthreshold Ca(2+) signals in spines of hippocampal neurons.* J Neurosci, 2000. **20**(5): p. 1791-9.
328. Duraes, F., M. Pinto, and E. Sousa, *Old Drugs as New Treatments for Neurodegenerative Diseases.* Pharmaceuticals (Basel), 2018. **11**(2).
329. Carmona, J.J. and S. Michan, *Biology of Healthy Aging and Longevity.* Rev Invest Clin, 2016. **68**(1): p. 7-16.
330. Hanamsagar, R. and S.D. Bilbo, *Sex differences in neurodevelopmental and neurodegenerative disorders: Focus on microglial function and neuroinflammation during development.* J Steroid Biochem Mol Biol, 2016. **160**: p. 127-33.
331. Zuccato, C. and E. Cattaneo, *Brain-derived neurotrophic factor in neurodegenerative diseases.* Nat Rev Neurol, 2009. **5**(6): p. 311-22.
332. Levada, O.A., et al., *Plasma Brain-Derived Neurotrophic Factor as a Biomarker for the Main Types of Mild Neurocognitive Disorders and Treatment Efficacy: A Preliminary Study.* Dis Markers, 2016. **2016**: p. 4095723.
333. Yasutake, C., et al., *Serum BDNF, TNF-alpha and IL-1beta levels in dementia patients: comparison between Alzheimer's disease and vascular dementia.* Eur Arch Psychiatry Clin Neurosci, 2006. **256**(7): p. 402-6.
334. Weinstein, G., et al., *Serum brain-derived neurotrophic factor and the risk for dementia: the Framingham Heart Study.* JAMA Neurol, 2014. **71**(1): p. 55-61.
335. Ng, T.K.S., et al., *Decreased Serum Brain-Derived Neurotrophic Factor (BDNF) Levels in Patients with Alzheimer's Disease (AD): A Systematic Review and Meta-Analysis.* Int J Mol Sci, 2019. **20**(2).
336. Laske, C., et al., *Higher BDNF serum levels predict slower cognitive decline in Alzheimer's disease patients.* Int J Neuropsychopharmacol, 2011. **14**(3): p. 399-404.
337. Palasz, E., et al., *BDNF as a Promising Therapeutic Agent in Parkinson's Disease.* Int J Mol Sci, 2020. **21**(3).
338. Jiang, L., et al., *Serum level of brain-derived neurotrophic factor in Parkinson's disease: a meta-analysis.* Prog Neuropsychopharmacol Biol Psychiatry, 2019. **88**: p. 168-174.
339. Zuccato, C., et al., *Loss of huntingtin-mediated BDNF gene transcription in Huntington's disease.* Science, 2001. **293**(5529): p. 493-8.

340. Zuccato, C. and E. Cattaneo, *Role of brain-derived neurotrophic factor in Huntington's disease.* Prog Neurobiol, 2007. **81**(5-6): p. 294-330.
341. Zuccato, C., et al., *Systematic assessment of BDNF and its receptor levels in human cortices affected by Huntington's disease.* Brain Pathol, 2008. **18**(2): p. 225-38.
342. Tsai, S.J., et al., *Association analysis of brain-derived neurotrophic factor Val66Met polymorphisms with Alzheimer's disease and age of onset.* Neuropsychobiology, 2004. **49**(1): p. 10-2.
343. Desai, P., et al., *Investigation of the effect of brain-derived neurotrophic factor (BDNF) polymorphisms on the risk of late-onset Alzheimer's disease (AD) and quantitative measures of AD progression.* Neurosci Lett, 2005. **379**(3): p. 229-34.
344. Akatsu, H., et al., *Variations in the BDNF gene in autopsy-confirmed Alzheimer's disease and dementia with Lewy bodies in Japan.* Dement Geriatr Cogn Disord, 2006. **22**(3): p. 216-22.
345. Karamohamed, S., et al., *BDNF genetic variants are associated with onset age of familial Parkinson disease: GenePD Study.* Neurology, 2005. **65**(11): p. 1823-5.
346. Alberch, J., et al., *Association between BDNF Val66Met polymorphism and age at onset in Huntington disease.* Neurology, 2005. **65**(6): p. 964-5.
347. Nishimura, M., et al., *Brain-derived neurotrophic factor gene polymorphisms in Japanese patients with sporadic Alzheimer's disease, Parkinson's disease, and multiple system atrophy.* Mov Disord, 2005. **20**(8): p. 1031-3.
348. Trigiani, L.J. and E. Hamel, *An endothelial link between the benefits of physical exercise in dementia.* J Cereb Blood Flow Metab, 2017. **37**(8): p. 2649-2664.
349. Uysal, N., et al., *Effects of voluntary and involuntary exercise on cognitive functions, and VEGF and BDNF levels in adolescent rats.* Biotech Histochem, 2015. **90**(1): p. 55-68.
350. Fischer, D.L. and C.E. Sortwell, *BDNF provides many routes toward STN DBS-mediated disease modification.* Mov Disord, 2019. **34**(1): p. 22-34.
351. McKinnon, C., et al., *Deep brain stimulation: potential for neuroprotection.* Ann Clin Transl Neurol, 2019. **6**(1): p. 174-185.
352. Luo, Y., et al., *Deep Brain Stimulation for Alzheimer's Disease: Stimulation Parameters and Potential Mechanisms of Action.* Front Aging Neurosci, 2021. **13**: p. 619543.
353. Turner, J.E., et al., *Exercise-induced B cell mobilisation: Preliminary evidence for an influx of immature cells into the bloodstream.* Physiol Behav, 2016. **164**(Pt A): p. 376-82.
354. Duggal, N.A., et al., *Major features of immunesenescence, including reduced thymic output, are ameliorated by high levels of physical activity in adulthood.* Aging Cell, 2018. **17**(2).
355. Sabatino, J.J., Jr., A.K. Probstel, and S.S. Zamvil, *Publisher Correction: B cells in autoimmune and neurodegenerative central nervous system diseases.* Nat Rev Neurosci, 2020. **21**(1): p. 56.
356. Lewerenz, J. and P. Maher, *Chronic Glutamate Toxicity in Neurodegenerative Diseases-What is the Evidence?* Front Neurosci, 2015. **9**: p. 469.
357. Nestler, E.J. and S.E. Hyman, *Animal models of neuropsychiatric disorders.* Nat Neurosci, 2010. **13**(10): p. 1161-9.
358. Becker, J.B., et al., *Stress and disease: is being female a predisposing factor?* J Neurosci, 2007. **27**(44): p. 11851-5.

359. Ochoa, S., et al., *Gender differences in schizophrenia and first-episode psychosis: a comprehensive literature review.* Schizophr Res Treatment, 2012. **2012**: p. 916198.
360. Hall, D., et al., *Sequence variants of the brain-derived neurotrophic factor (BDNF) gene are strongly associated with obsessive-compulsive disorder.* Am J Hum Genet, 2003. **73**(2): p. 370-6.
361. Gatt, J.M., et al., *Interactions between BDNF Val66Met polymorphism and early life stress predict brain and arousal pathways to syndromal depression and anxiety.* Mol Psychiatry, 2009. **14**(7): p. 681-95.
362. Lohoff, F.W., et al., *Confirmation of association between the Val66Met polymorphism in the brain-derived neurotrophic factor (BDNF) gene and bipolar I disorder.* Am J Med Genet B Neuropsychiatr Genet, 2005. **139B**(1): p. 51-3.
363. Bremner, J.D., et al., *Hippocampal volume reduction in major depression.* Am J Psychiatry, 2000. **157**(1): p. 115-8.
364. Dwivedi, Y., et al., *Altered gene expression of brain-derived neurotrophic factor and receptor tyrosine kinase B in postmortem brain of suicide subjects.* Arch Gen Psychiatry, 2003. **60**(8): p. 804-15.
365. Castren, E. and T. Rantamaki, *The role of BDNF and its receptors in depression and antidepressant drug action: Reactivation of developmental plasticity.* Dev Neurobiol, 2010. **70**(5): p. 289-97.
366. Sanacora, G., *New understanding of mechanisms of action of bipolar medications.* J Clin Psychiatry, 2008. **69 Suppl 5**: p. 22-7.
367. Green, M.J., et al., *Brain-derived neurotrophic factor levels in schizophrenia: a systematic review with meta-analysis.* Mol Psychiatry, 2011. **16**(9): p. 960-72.
368. Thompson Ray, M., et al., *Decreased BDNF, trkB-TK+ and GAD67 mRNA expression in the hippocampus of individuals with schizophrenia and mood disorders.* J Psychiatry Neurosci, 2011. **36**(3): p. 195-203.
369. Knable, M.B., et al., *Molecular abnormalities of the hippocampus in severe psychiatric illness: postmortem findings from the Stanley Neuropathology Consortium.* Mol Psychiatry, 2004. **9**(6): p. 609-20, 544.
370. Duman, R.S. and L.M. Monteggia, *A neurotrophic model for stress-related mood disorders.* Biol Psychiatry, 2006. **59**(12): p. 1116-27.
371. Hashimoto, R., et al., *Lithium induces brain-derived neurotrophic factor and activates TrkB in rodent cortical neurons: an essential step for neuroprotection against glutamate excitotoxicity.* Neuropharmacology, 2002. **43**(7): p. 1173-9.
372. Angelucci, F., A.A. Mathe, and L. Aloe, *Brain-derived neurotrophic factor and tyrosine kinase receptor TrkB in rat brain are significantly altered after haloperidol and risperidone administration.* J Neurosci Res, 2000. **60**(6): p. 783-94.
373. Terry, A.V., Jr., et al., *Differential effects of haloperidol, risperidone, and clozapine exposure on cholinergic markers and spatial learning performance in rats.* Neuropsychopharmacology, 2003. **28**(2): p. 300-9.
374. Moghaddam, B. and D. Javitt, *From revolution to evolution: the glutamate hypothesis of schizophrenia and its implication for treatment.* Neuropsychopharmacology, 2012. **37**(1): p. 4-15.

375. Javitt, D.C., *Glutamatergic theories of schizophrenia.* Isr J Psychiatry Relat Sci, 2010. **47**(1): p. 4-16.
376. Schlaaff, K., et al., *Increased densities of T and B lymphocytes indicate neuroinflammation in subgroups of schizophrenia and mood disorder patients.* Brain Behav Immun, 2020. **88**: p. 497-506.
377. Busse, S., et al., *Different distribution patterns of lymphocytes and microglia in the hippocampus of patients with residual versus paranoid schizophrenia: further evidence for disease course-related immune alterations?* Brain Behav Immun, 2012. **26**(8): p. 1273-9.
378. Papp, V., et al., *Worldwide Incidence and Prevalence of Neuromyelitis Optica: A Systematic Review.* Neurology, 2021. **96**(2): p. 59-77.
379. Harbo, H.F., R. Gold, and M. Tintore, *Sex and gender issues in multiple sclerosis.* Ther Adv Neurol Disord, 2013. **6**(4): p. 237-48.
380. Mealy, M.A., et al., *Epidemiology of neuromyelitis optica in the United States: a multicenter analysis.* Arch Neurol, 2012. **69**(9): p. 1176-80.
381. Villar, L.M., et al., *Early differential diagnosis of multiple sclerosis using a new oligoclonal band test.* Arch Neurol, 2005. **62**(4): p. 574-7.
382. Berger, T., et al., *Antimyelin antibodies as a predictor of clinically definite multiple sclerosis after a first demyelinating event.* N Engl J Med, 2003. **349**(2): p. 139-45.
383. Weber, M.S., B. Hemmer, and S. Cepok, *The role of antibodies in multiple sclerosis.* Biochim Biophys Acta, 2011. **1812**(2): p. 239-45.
384. Rivas, J.R., et al., *Peripheral VH4+ plasmablasts demonstrate autoreactive B cell expansion toward brain antigens in early multiple sclerosis patients.* Acta Neuropathol, 2017. **133**(1): p. 43-60.
385. Quach, T.D., et al., *Anergic responses characterize a large fraction of human autoreactive naive B cells expressing low levels of surface IgM.* J Immunol, 2011. **186**(8): p. 4640-8.
386. Kim, S.H., et al., *Repeated treatment with rituximab based on the assessment of peripheral circulating memory B cells in patients with relapsing neuromyelitis optica over 2 years.* Arch Neurol, 2011. **68**(11): p. 1412-20.
387. Pellkofer, H.L., et al., *Long-term follow-up of patients with neuromyelitis optica after repeated therapy with rituximab.* Neurology, 2011. **76**(15): p. 1310-5.
388. Sefia, E., et al., *Depletion of CD20 B cells fails to inhibit relapsing mouse experimental autoimmune encephalomyelitis.* Mult Scler Relat Disord, 2017. **14**: p. 46-50.
389. Shen, T., et al., *Association Between BDNF Val66Met Polymorphism and Optic Neuritis Damage in Neuromyelitis Optica Spectrum Disorder.* Front Neurosci, 2019. **13**: p. 1236.
390. Begum-Haque, S., et al., *Augmentation of regulatory B cell activity in experimental allergic encephalomyelitis by glatiramer acetate.* J Neuroimmunol, 2011. **232**(1-2): p. 136-44.
391. Liguori, M., et al., *A longitudinal observation of brain-derived neurotrophic factor mRNA levels in patients with relapsing-remitting multiple sclerosis.* Brain Res, 2009. **1256**: p. 123-8.
392. Frota, E.R., et al., *Increased plasma levels of brain derived neurotrophic factor (BDNF) after multiple sclerosis relapse.* Neurosci Lett, 2009. **460**(2): p. 130-2.

393. Gold, S.M., et al., *Basal serum levels and reactivity of nerve growth factor and brain-derived neurotrophic factor to standardized acute exercise in multiple sclerosis and controls.* J Neuroimmunol, 2003. **138**(1-2): p. 99-105.
394. Luhder, F., et al., *Brain-derived neurotrophic factor in neuroimmunology: lessons learned from multiple sclerosis patients and experimental autoimmune encephalomyelitis models.* Arch Immunol Ther Exp (Warsz), 2013. **61**(2): p. 95-105.
395. Zivadinov, R., et al., *Preservation of gray matter volume in multiple sclerosis patients with the Met allele of the rs6265 (Val66Met) SNP of brain-derived neurotrophic factor.* Hum Mol Genet, 2007. **16**(22): p. 2659-68.
396. Portaccio, E., et al., *The Brain-Derived Neurotrophic Factor Val66Met Polymorphism Can Protect Against Cognitive Impairment in Multiple Sclerosis.* Front Neurol, 2021. **12**: p. 645220.
397. Dalmau, J., et al., *Paraneoplastic anti-N-methyl-D-aspartate receptor encephalitis associated with ovarian teratoma.* Ann Neurol, 2007. **61**(1): p. 25-36.
398. Liu, C.Y., et al., *Anti-N-Methyl-D-aspartate Receptor Encephalitis: A Severe, Potentially Reversible Autoimmune Encephalitis.* Mediators Inflamm, 2017. **2017**: p. 6361479.
399. Dalmau, J., et al., *An update on anti-NMDA receptor encephalitis for neurologists and psychiatrists: mechanisms and models.* Lancet Neurol, 2019. **18**(11): p. 1045-1057.
400. Wenke, N.K., et al., *N-methyl-D-aspartate receptor dysfunction by unmutated human antibodies against the NR1 subunit.* Ann Neurol, 2019. **85**(5): p. 771-776.
401. Hughes, E.G., et al., *Cellular and synaptic mechanisms of anti-NMDA receptor encephalitis.* J Neurosci, 2010. **30**(17): p. 5866-75.
402. Zerche, M., et al., *Preexisting Serum Autoantibodies Against the NMDAR Subunit NR1 Modulate Evolution of Lesion Size in Acute Ischemic Stroke.* Stroke, 2015. **46**(5): p. 1180-6.
403. Kalev-Zylinska, M.L., et al., *Stroke patients develop antibodies that react with components of N-methyl-D-aspartate receptor subunit 1 in proportion to lesion size.* Stroke, 2013. **44**(8): p. 2212-9.
404. Nashi, E., Y. Wang, and B. Diamond, *The role of B cells in lupus pathogenesis.* Int J Biochem Cell Biol, 2010. **42**(4): p. 543-50.
405. Silverman, G.J. and D.A. Carson, *Roles of B cells in rheumatoid arthritis.* Arthritis Res Ther, 2003. **5 Suppl 4**: p. S1-6.
406. Weckerle, C.E. and T.B. Niewold, *The unexplained female predominance of systemic lupus erythematosus: clues from genetic and cytokine studies.* Clin Rev Allergy Immunol, 2011. **40**(1): p. 42-9.
407. Goronzy, J.J., L. Shao, and C.M. Weyand, *Immune aging and rheumatoid arthritis.* Rheum Dis Clin North Am, 2010. **36**(2): p. 297-310.
408. Yurasov, S., et al., *Defective B cell tolerance checkpoints in systemic lupus erythematosus.* J Exp Med, 2005. **201**(5): p. 703-11.
409. Samuels, J., et al., *Impaired early B cell tolerance in patients with rheumatoid arthritis.* J Exp Med, 2005. **201**(10): p. 1659-67.
410. Chan, O.T., et al., *A novel mouse with B cells but lacking serum antibody reveals an antibody-independent role for B cells in murine lupus.* J Exp Med, 1999. **189**(10): p. 1639-48.

411. Anolik, J.H., *B cell biology and dysfunction in SLE.* Bull NYU Hosp Jt Dis, 2007. **65**(3): p. 182-6.
412. Oroszi, G., et al., *The Met66 allele of the functional Val66Met polymorphism in the brain-derived neurotrophic factor gene confers protection against neurocognitive dysfunction in systemic lupus erythematosus.* Ann Rheum Dis, 2006. **65**(10): p. 1330-5.
413. Chan, K., et al., *Lupus autoantibodies act as positive allosteric modulators at GluN2A-containing NMDA receptors and impair spatial memory.* Nat Commun, 2020. **11**(1): p. 1403.
414. Faust, T.W., et al., *Neurotoxic lupus autoantibodies alter brain function through two distinct mechanisms.* Proc Natl Acad Sci U S A, 2010. **107**(43): p. 18569-74.
415. Husebye, E.S., et al., *Autoantibodies to a NR2A peptide of the glutamate/NMDA receptor in sera of patients with systemic lupus erythematosus.* Ann Rheum Dis, 2005. **64**(8): p. 1210-3.
416. Zheng, Q., et al., *Serum levels of brain-derived neurotrophic factor are associated with depressive symptoms in patients with systemic lupus erythematosus.* Psychoneuroendocrinology, 2017. **78**: p. 246-252.
417. Tian, B., et al., *Peripheral blood brain-derived neurotrophic factor level and tyrosine kinase B expression on T lymphocytes in systemic lupus erythematosus: Implications for systemic involvement.* Cytokine, 2019. **123**: p. 154764.
418. Ikenouchi-Sugita, A., et al., *Serum brain-derived neurotrophic factor levels as a novel biological marker for the activities of psychiatric symptoms in systemic lupus erythematosus.* World J Biol Psychiatry, 2010. **11**(2): p. 121-8.
419. Tamashiro, L.F., et al., *Participation of the neutrophin brain-derived neurotrophic factor in neuropsychiatric systemic lupus erythematosus.* Rheumatology (Oxford), 2014. **53**(12): p. 2182-90.
420. Grimsholm, O., et al., *BDNF in RA: downregulated in plasma following anti-TNF treatment but no correlation with inflammatory parameters.* Clin Rheumatol, 2008. **27**(10): p. 1289-97.
421. del Porto, F., et al., *Nerve growth factor and brain-derived neurotrophic factor levels in patients with rheumatoid arthritis treated with TNF-alpha blockers.* Ann N Y Acad Sci, 2006. **1069**: p. 438-43.
422. Lai, N.S., et al., *Increased Serum Levels of Brain-Derived Neurotrophic Factor Contribute to Inflammatory Responses in Patients with Rheumatoid Arthritis.* Int J Mol Sci, 2021. **22**(4).
423. Pedard, M., et al., *Brain-derived neurotrophic factor in adjuvant-induced arthritis in rats. Relationship with inflammation and endothelial dysfunction.* Prog Neuropsychopharmacol Biol Psychiatry, 2018. **82**: p. 249-254.
424. McNearney, T., et al., *Excitatory amino acids, TNF-alpha, and chemokine levels in synovial fluids of patients with active arthropathies.* Clin Exp Immunol, 2004. **137**(3): p. 621-7.
425. Hajati, A.K., et al., *Endogenous glutamate in association with inflammatory and hormonal factors modulates bone tissue resorption of the temporomandibular joint in patients with early rheumatoid arthritis.* J Oral Maxillofac Surg, 2009. **67**(9): p. 1895-903.

426. Hajati, A.K., et al., *Temporomandibular joint bone tissue resorption in patients with early rheumatoid arthritis can be predicted by joint crepitus and plasma glutamate level.* Mediators Inflamm, 2010. **2010**: p. 627803.
427. Looney, R.J., et al., *B cell depletion as a novel treatment for systemic lupus erythematosus: a phase I/II dose-escalation trial of rituximab.* Arthritis Rheum, 2004. **50**(8): p. 2580-9.
428. Parodis, I., M. Stockfelt, and C. Sjowall, *B Cell Therapy in Systemic Lupus Erythematosus: From Rationale to Clinical Practice.* Front Med (Lausanne), 2020. **7**: p. 316.
429. Finckh, A., et al., *B cell depletion may be more effective than switching to an alternative anti-tumor necrosis factor agent in rheumatoid arthritis patients with inadequate response to anti-tumor necrosis factor agents.* Arthritis Rheum, 2007. **56**(5): p. 1417-23.
430. Lee, D.S.W., O.L. Rojas, and J.L. Gommerman, *B cell depletion therapies in autoimmune disease: advances and mechanistic insights.* Nat Rev Drug Discov, 2021. **20**(3): p. 179-199.
431. Leete, P., et al., *The Effect of Age on the Progression and Severity of Type 1 Diabetes: Potential Effects on Disease Mechanisms.* Curr Diab Rep, 2018. **18**(11): p. 115.
432. Bullard, K.M., et al., *Prevalence of Diagnosed Diabetes in Adults by Diabetes Type - United States, 2016.* MMWR Morb Mortal Wkly Rep, 2018. **67**(12): p. 359-361.
433. Qi, X., et al., *Prevalence and correlates of latent autoimmune diabetes in adults in Tianjin, China: a population-based cross-sectional study.* Diabetes Care, 2011. **34**(1): p. 66-70.
434. Taplin, C.E. and J.M. Barker, *Autoantibodies in type 1 diabetes.* Autoimmunity, 2008. **41**(1): p. 11-8.
435. Wong, F.S. and L. Wen, *B cells in autoimmune diabetes.* Rev Diabet Stud, 2005. **2**(3): p. 121-35.
436. Wasserfall, C.H. and M.A. Atkinson, *Autoantibody markers for the diagnosis and prediction of type 1 diabetes.* Autoimmun Rev, 2006. **5**(6): p. 424-8.
437. Zimmet, P.Z., et al., *Latent autoimmune diabetes mellitus in adults (LADA): the role of antibodies to glutamic acid decarboxylase in diagnosis and prediction of insulin dependency.* Diabet Med, 1994. **11**(3): p. 299-303.
438. Smith, M.J., K.M. Simmons, and J.C. Cambier, *B cells in type 1 diabetes mellitus and diabetic kidney disease.* Nat Rev Nephrol, 2017. **13**(11): p. 712-720.
439. Fulgenzi, G., et al., *Novel metabolic role for BDNF in pancreatic beta-cell insulin secretion.* Nat Commun, 2020. **11**(1): p. 1950.
440. Duan, W., et al., *Reversal of behavioral and metabolic abnormalities, and insulin resistance syndrome, by dietary restriction in mice deficient in brain-derived neurotrophic factor.* Endocrinology, 2003. **144**(6): p. 2446-53.
441. Rozanska, O., A. Uruska, and D. Zozulinska-Ziolkiewicz, *Brain-Derived Neurotrophic Factor and Diabetes.* Int J Mol Sci, 2020. **21**(3).
442. Tonoli, C., et al., *Neurotrophins and cognitive functions in T1D compared with healthy controls: effects of a high-intensity exercise.* Appl Physiol Nutr Metab, 2015. **40**(1): p. 20-7.

443. Zhou, J.X., et al., *Functional Val66Met polymorphism of Brain-derived neurotrophic factor in type 2 diabetes with depression in Han Chinese subjects.* Behav Brain Funct, 2013. **9**: p. 34.
444. Huang, X.T., et al., *An excessive increase in glutamate contributes to glucose-toxicity in beta-cells via activation of pancreatic NMDA receptors in rodent diabetes.* Sci Rep, 2017. **7**: p. 44120.
445. Davalli, A.M., C. Perego, and F.B. Folli, *The potential role of glutamate in the current diabetes epidemic.* Acta Diabetol, 2012. **49**(3): p. 167-83.
446. Stepulak, A., et al., *Glutamate and its receptors in cancer.* J Neural Transm (Vienna), 2014. **121**(8): p. 933-44.
447. Radin, D.P. and P. Patel, *BDNF: An Oncogene or Tumor Suppressor?* Anticancer Res, 2017. **37**(8): p. 3983-3990.
448. Sniderhan, L.F., et al., *Neurotrophin signaling through tropomyosin receptor kinases contributes to survival and proliferation of non-Hodgkin lymphoma.* Exp Hematol, 2009. **37**(11): p. 1295-309.
449. Pearse, R.N., et al., *A neurotrophin axis in myeloma: TrkB and BDNF promote tumor-cell survival.* Blood, 2005. **105**(11): p. 4429-36.
450. Xiong, J., et al., *Mature BDNF promotes the growth of glioma cells in vitro.* Oncol Rep, 2013. **30**(6): p. 2719-24.
451. Jaboin, J., et al., *Brain-derived neurotrophic factor activation of TrkB protects neuroblastoma cells from chemotherapy-induced apoptosis via phosphatidylinositol 3'-kinase pathway.* Cancer Res, 2002. **62**(22): p. 6756-63.
452. Jaboin, J., et al., *Cisplatin-induced cytotoxicity is blocked by brain-derived neurotrophic factor activation of TrkB signal transduction path in neuroblastoma.* Cancer Lett, 2003. **193**(1): p. 109-14.
453. Garofalo, S., et al., *Enriched environment reduces glioma growth through immune and non-immune mechanisms in mice.* Nat Commun, 2015. **6**: p. 6623.
454. Xiao, R., et al., *Environmental and Genetic Activation of Hypothalamic BDNF Modulates T-cell Immunity to Exert an Anticancer Phenotype.* Cancer Immunol Res, 2016. **4**(6): p. 488-497.
455. Candolfi, M., et al., *B cells are critical to T-cell-mediated antitumor immunity induced by a combined immune-stimulatory/conditionally cytotoxic therapy for glioblastoma.* Neoplasia, 2011. **13**(10): p. 947-60.
456. Takano, T., et al., *Glutamate release promotes growth of malignant gliomas.* Nat Med, 2001. **7**(9): p. 1010-5.
457. Choi, Y.K. and K.G. Park, *Targeting Glutamine Metabolism for Cancer Treatment.* Biomol Ther (Seoul), 2018. **26**(1): p. 19-28.
458. Ye, Z.C. and H. Sontheimer, *Glioma cells release excitotoxic concentrations of glutamate.* Cancer Res, 1999. **59**(17): p. 4383-91.
459. Tedder, T.F., *B10 cells: a functionally defined regulatory B cell subset.* J Immunol, 2015. **194**(4): p. 1395-401.
460. Matsushita, T. and T.F. Tedder, *Identifying regulatory B cells (B10 cells) that produce IL-10 in mice.* Methods Mol Biol, 2011. **677**: p. 99-111.

461. Kalampokis, I., A. Yoshizaki, and T.F. Tedder, *IL-10-producing regulatory B cells (B10 cells) in autoimmune disease.* Arthritis Res Ther, 2013. **15 Suppl 1**: p. S1.
462. Seifert, H.A., A.A. Vandenbark, and H. Offner, *Regulatory B cells in experimental stroke.* Immunology, 2018. **154**(2): p. 169-177.
463. Jiang, X., et al., *Blood-brain barrier dysfunction and recovery after ischemic stroke.* Prog Neurobiol, 2018. **163-164**: p. 144-171.
464. Llovera, G., et al., *The choroid plexus is a key cerebral invasion route for T cells after stroke.* Acta Neuropathol, 2017. **134**(6): p. 851-868.
465. Doyle, K.P. and M.S. Buckwalter, *Does B lymphocyte-mediated autoimmunity contribute to post-stroke dementia?* Brain Behav Immun, 2017. **64**: p. 1-8.
466. Serafini, B., et al., *Detection of ectopic B-cell follicles with germinal centers in the meninges of patients with secondary progressive multiple sclerosis.* Brain Pathol, 2004. **14**(2): p. 164-74.
467. Poisson, S.N., S.C. Johnston, and S.A. Josephson, *Urinary tract infections complicating stroke: mechanisms, consequences, and possible solutions.* Stroke, 2010. **41**(4): p. e180-4.
468. Katzan, I.L., et al., *The effect of pneumonia on mortality among patients hospitalized for acute stroke.* Neurology, 2003. **60**(4): p. 620-5.
469. Leibowitz, A., et al., *Blood glutamate scavenging: insight into neuroprotection.* Int J Mol Sci, 2012. **13**(8): p. 10041-66.
470. Castillo, J., et al., *A novel mechanism of neuroprotection: Blood glutamate grabber.* J Cereb Blood Flow Metab, 2016. **36**(2): p. 292-301.
471. Aliprandi, A., et al., *Increased plasma glutamate in stroke patients might be linked to altered platelet release and uptake.* J Cereb Blood Flow Metab, 2005. **25**(4): p. 513-9.
472. Ross, A.M., et al., *Evidence of the peripheral inflammatory response in patients with transient ischemic attack.* J Stroke Cerebrovasc Dis, 2007. **16**(5): p. 203-7.
473. Chan, A., et al., *Circulating brain derived neurotrophic factor (BDNF) and frequency of BDNF positive T cells in peripheral blood in human ischemic stroke: Effect on outcome.* J Neuroimmunol, 2015. **286**: p. 42-7.
474. Yu, X., et al., *Brain-derived neurotrophic factor modulates immune reaction in mice with peripheral nerve xenotransplantation.* Neuropsychiatr Dis Treat, 2016. **12**: p. 685-94.
475. Suzuki, S., C.M. Brown, and P.M. Wise, *Neuroprotective effects of estrogens following ischemic stroke.* Front Neuroendocrinol, 2009. **30**(2): p. 201-11.
476. Bushnell, C.D., *Stroke and the female brain.* Nat Clin Pract Neurol, 2008. **4**(1): p. 22-33.
477. Sun, M., et al., *The need to incorporate aged animals into the preclinical modeling of neurological conditions.* Neurosci Biobehav Rev, 2020. **109**: p. 114-128.
478. Choleris, E., et al., *Sex differences in the brain: Implications for behavioral and biomedical research.* Neurosci Biobehav Rev, 2018. **85**: p. 126-145.
479. Bushnell, C.D., et al., *Impact of comorbidities on ischemic stroke outcomes in women.* Stroke, 2008. **39**(7): p. 2138-40.
480. Riley, R.L., K. Khomtchouk, and B.B. Blomberg, *Inflammatory immune cells may impair the preBCR checkpoint, reduce new B cell production, and alter the antibody repertoire in old age.* Exp Gerontol, 2018. **105**: p. 87-93.

481. Duggal, N.A., et al., *An age-related numerical and functional deficit in CD19(+) CD24(hi) CD38(hi) B cells is associated with an increase in systemic autoimmunity.* Aging Cell, 2013. **12**(5): p. 873-81.
482. Xiao, P., et al., *In vivo genome-wide expression study on human circulating B cells suggests a novel ESR1 and MAPK3 network for postmenopausal osteoporosis.* J Bone Miner Res, 2008. **23**(5): p. 644-54.
483. Ke, Z., et al., *The effects of voluntary, involuntary, and forced exercises on brain-derived neurotrophic factor and motor function recovery: a rat brain ischemia model.* PLoS One, 2011. **6**(2): p. e16643.
484. Ding, Y.H., et al., *Exercise preconditioning ameliorates inflammatory injury in ischemic rats during reperfusion.* Acta Neuropathol, 2005. **109**(3): p. 237-46.
485. Elphick, G.F., et al., *B-1 cell (CD5+/CD11b+) numbers and nIgM levels are elevated in physically active vs. sedentary rats.* J Appl Physiol (1985), 2003. **95**(1): p. 199-206.
486. Suzuki, K. and K. Tagami, *Voluntary wheel-running exercise enhances antigen-specific antibody-producing splenic B cell response and prolongs IgG half-life in the blood.* Eur J Appl Physiol, 2005. **94**(5-6): p. 514-9.
487. Morais, V.A.C., et al., *A single session of moderate intensity walking increases brain-derived neurotrophic factor (BDNF) in the chronic post-stroke patients.* Top Stroke Rehabil, 2018. **25**(1): p. 1-5.
488. Alcantara, C.C., et al., *Post-stroke BDNF Concentration Changes Following Physical Exercise: A Systematic Review.* Front Neurol, 2018. **9**: p. 637.
489. Aharoni, R., et al., *The immunomodulator glatiramer acetate augments the expression of neurotrophic factors in brains of experimental autoimmune encephalomyelitis mice.* Proc Natl Acad Sci U S A, 2005. **102**(52): p. 19045-50.
490. Van Kaer, L., *Glatiramer acetate for treatment of MS: regulatory B cells join the cast of players.* Exp Neurol, 2011. **227**(1): p. 19-23.
491. Amrouche, K., J.O. Pers, and C. Jamin, *Glatiramer Acetate Stimulates Regulatory B Cell Functions.* J Immunol, 2019. **202**(7): p. 1970-1980.
492. Cruz, Y., et al., *Copolymer-1 promotes neurogenesis and improves functional recovery after acute ischemic stroke in rats.* PLoS One, 2015. **10**(3): p. e0121854.
493. Martinowich, K. and B. Lu, *Interaction between BDNF and serotonin: role in mood disorders.* Neuropsychopharmacology, 2008. **33**(1): p. 73-83.
494. Hernandez, M.E., et al., *Evaluation of the effect of selective serotonin-reuptake inhibitors on lymphocyte subsets in patients with a major depressive disorder.* Eur Neuropsychopharmacol, 2010. **20**(2): p. 88-95.
495. Mead, G.E., et al., *Selective serotonin reuptake inhibitors (SSRIs) for stroke recovery.* Cochrane Database Syst Rev, 2012. **11**: p. CD009286.